Lecture Notes on

QUANTUM COMPUTING

STEFANO OLIVARES
Quantum Technology Lab
Dipartimento di Fisica "Aldo Pontremoli"
Università degli Studi di Milano

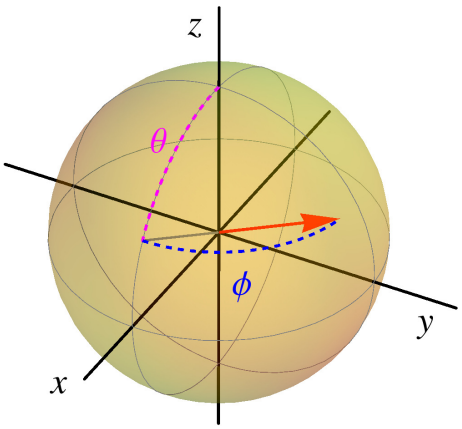

— Ver. 5.0 —

Preface

"Quantum computation is a new conceptual arena
for trying to come to a better understanding of quantum weirdness."
— N. D. Mermin

THERE ARE MANY BOOKS on the subject of quantum information and, in particular, quantum computation. The student or the researcher can find the one he/she prefers according to his/her own interests, ranging from the quantum algorithms to the physical implementations of quantum information processing and computation. In the "Suggested bibliography" reported at the end of this preface, the reader can find the list of references I considered to prepare the lectures on quantum computing I have been holding at the Department of Physics of the University of Milan: each book has particular aspects that I appreciated and, therefore, I wanted to communicate to my students. However, when the bibliography is always growing, it is sometimes necessary to provide some useful tools to help the students to follow the lectures and not to get lost into the flow of information coming from the suggested readings.

Motivated also by the requests of my students, I wrote these lecture notes that, year by year, will be corrected (*sic!*), enhanced and improved with further comments to the old material and by adding new topics concerning quantum computation. Nevertheless, the notes may contain imprecisions and misprints: comments and suggestions are always welcome!

In order to further help the students, at the end of each chapter I put the references to the corresponding chapters of the books or to the research articles that inspired my lectures and should be considered the main resource to begin the advanced study in the field of quantum computation.

I hope these pages will bring the reader to better understand and appreciate some aspects of our world as described by quantum mechanics.

— Stefano Olivares

Suggested bibliography

- M. A. Nielsen and I. L. Chuang
  Quantum Computation and Quantum Information
  (Cambridge University Press)

- N. D. Mermin
  Quantum Computer Science
  (Cambridge University Press)

- S. Stenholm and K.-A. Suominen
  Quantum Approach to Informatics
  (Wiley-Interscience)

- S. Haroche and J.-M. Raimond
  Exploring the Quantum: Atoms, Cavities, and Photons
  (Oxford Graduate Texts)

- J. A. Jones and D. Jaksch
  Quantum Information, Computation and Communication
  (Cambridge University Press)

- J. Stolze and D. Suter
  Quantum Computing: A Short Course from Theory to Experiment
  (Wiley-VCH)

Contents

Chapter 1

Basic concepts of classical logic

CLASSICAL INFORMATION is carried by numerical variables and it is extremely useful to use the binary representation $\{0,1\}$ in order to encode it. If we consider four binary variables $x_k \in \{0,1\}$, $k = 0,\ldots,3$, an integer number x can be written in binary notation as follows:

$$\begin{aligned} x &\to x_3\, x_2\, x_1\, x_0, \\ &= x_3 \times 2^3 + x_2 \times 2^2 + x_1 \times 2^1 + x_0 \times 2^0 \,. \end{aligned} \tag{1.1}$$

For instance, $1001 \to 1 \times 2^3 + 0 \times 2^2 + 0 \times 2^1 + 1 \times 2^0 = 9$.

The *amount of information* carried by the binary variable is called *bit*. Each binary variable can take only two values, thus a sequence of n binary variables can be actually used to name $N = 2^n$ different numbers. The length of a string tells us the space required to hold the number. We can consider $\log_2 N = \log_2 2^n = n$ a measure of the information. Note that a single bit carries $\log_2 2 = 1$ bit of information.

1.1 Abstract representation of bits

Instead of using the symbols "0" and "1", we will use the *abstract* symbols $|0\rangle$ and $|1\rangle$, respectively. By using this formalism, the binary string "1001" rewrites as[1]:

$$1001 \to |1\rangle|0\rangle|0\rangle|1\rangle, \tag{1.2}$$

which represents the *state* of the four classical bit carrying the information. It is worth noting that, in reality, each symbol $|x\rangle$, $x = 0,1$, is associated with a *physical* entity. Therefore, we can identify the numerical value of the classical bit with the bit itself. For the sake of simplicity, we

[1] We will se later on the mathematical framework of this formalism.

can also use the following notation:

$$|1001\rangle \equiv |1\rangle|0\rangle|0\rangle|1\rangle \tag{1.3}$$

or also write:

$$|1001\rangle \equiv |9\rangle_4 \tag{1.4}$$

where we used the decimal notation "9" to represent the binary value "1001" and the subscript "4" refers to the four bits we used to encode the number (indeed, mathematically, the two binary strings "1001" and "0000001001" represent the same digital number "9", but, physically, the first involves only four bits, the second emploies ten bits!!).

It is possible to associate with $|0\rangle$ and $|1\rangle$ two column vectors as follows:

$$|0\rangle \to \begin{pmatrix} 1 \\ 0 \end{pmatrix}, \quad \text{and} \quad |1\rangle \to \begin{pmatrix} 0 \\ 1 \end{pmatrix}. \tag{1.5}$$

We clearly see that the two vectors are orthonormal. Now, we note that the symbol $|1\rangle|0\rangle|0\rangle|1\rangle$ is a short-hand for the tensor product of four single-bit 2-dimensional vector, namely:

$$|1\rangle|0\rangle|0\rangle|1\rangle \equiv |1\rangle \otimes |0\rangle \otimes |0\rangle \otimes |1\rangle. \tag{1.6}$$

Let's focus on a 4-dimensional space, with orthonormal basis:

$$|0\rangle_2 = |00\rangle \to \begin{pmatrix} 1 \\ 0 \\ 0 \\ 0 \end{pmatrix}, |1\rangle_2 = |01\rangle \to \begin{pmatrix} 0 \\ 1 \\ 0 \\ 0 \end{pmatrix}, |2\rangle_2 = |10\rangle \to \begin{pmatrix} 0 \\ 0 \\ 1 \\ 0 \end{pmatrix}, |3\rangle_2 = |11\rangle \to \begin{pmatrix} 0 \\ 0 \\ 0 \\ 1 \end{pmatrix}, \tag{1.7}$$

where we explicitly evaluated the tensor product[2]. In this way it is possible to obtain the 2^n-dimensional column vector representing any of the 2^n possible states of n bits. If $x = (x_0, x_1, \ldots, x_{n-1})^T$, $x_k \in \{0,1\}$, $k = 0, \ldots, n-1$, is a column vector associated with the binary representation of an integer $0 \leq x < 2^n$, then $x = \sum_{k=0}^{n-1} x_k 2^k$ and we have[3]:

$$|x\rangle_n = |x_{n-1}\rangle \otimes \cdots \otimes |x_0\rangle = |x_{n-1} \cdots x_1\, x_0\rangle, \tag{1.8}$$

i.e., $|x\rangle_n$ is the tensor product of the single-bit states $|x_k\rangle$.

1.2 Classical logical operations

Any logical or arithmetical operation can be obtained by the composition of three elementary logical operations: "NOT", "AND" and "OR". The NOT operation acts on a single bit, while AND and OR are two-bit operations. Their actions are summarized in the truth tables 1.1, 1.2 and 1.3.

$\|x\rangle$	$\|\overline{x}\rangle$
$\|0\rangle$	$\|1\rangle$
$\|1\rangle$	$\|0\rangle$

Table 1.1: NOT operation. We used the alternative notation NOT$|x\rangle = |\overline{x}\rangle$.

$\|x\rangle\|y\rangle$	$\|x \wedge y\rangle$
$\|0\rangle\|0\rangle$	$\|0\rangle$
$\|0\rangle\|1\rangle$	$\|0\rangle$
$\|1\rangle\|0\rangle$	$\|0\rangle$
$\|1\rangle\|1\rangle$	$\|1\rangle$

Table 1.2: AND operation. We used the alternative notation AND$|x\rangle|y\rangle = |x \wedge y\rangle$.

It is worth noting that the three logical operations introduced above are not independent: given NOT and OR it is possible to obtain the operation AND; analogously, given NOT and AND it is possible to obtain the operation OR. Thus, we can introduce the two *universal* operators "NOR" (i.e., NOT OR) and "NAND" (i.e., NOT AND):

$$\text{NOR}|x\rangle|y\rangle \equiv |\overline{x \vee y}\rangle = |\overline{x} \wedge \overline{y}\rangle, \tag{1.9a}$$

$$\text{NAND}|x\rangle|y\rangle \equiv |\overline{x \wedge y}\rangle = |\overline{x} \vee \overline{y}\rangle. \tag{1.9b}$$

Another useful operator is the XOR, or *exclusive* OR operator, which corresponds to the modulo-2 sum. Its action is summarized in table 1.4. Note that $|\overline{x}\rangle = |x \oplus 1\rangle$. As a matter of fact the XOR can be reduced to more elementary operations as:

$$|x \oplus y\rangle = \Big|(x \vee y) \wedge \overline{(x \wedge y)}\Big\rangle. \tag{1.10}$$

1.2.1 Reversible logical operations and permutations

A logical function is reversible if each output arises from a unique input: it is possible to show that a reversible function should be a *permutation* of the input bit states. The inspection of the tables 1.1–1.4 shows that among the presented operations, only NOT is reversible. Reversibility plays a relevant role in quantum computation, since, as we will see, the general computational process can be modeled with a unitary operation that is indeed reversible.

[2]The tensor product of the two column vectors $(a_1, \ldots, a_N)^T$ and $(b_1, \ldots, b_M)^T$ is a NM-component vector with components indexed by all the MN possible pairs of indices (ν, μ), whose $(\nu, \mu)^{\text{th}}$ component is just the product $a_\nu b_\mu$.

[3]Note that the binary expansion of the column vector $x = (x_0, x_1, \ldots, x_{n-1})^T$ is $x \to x_{n-1} \cdots x_1 x_0$.

$\|x\rangle\|y\rangle$	$\|x \vee y\rangle$
$\|0\rangle\|0\rangle$	$\|0\rangle$
$\|0\rangle\|1\rangle$	$\|1\rangle$
$\|1\rangle\|0\rangle$	$\|1\rangle$
$\|1\rangle\|1\rangle$	$\|1\rangle$

Table 1.3: OR operation. We used the alternative notation $\mathrm{OR}|x\rangle|y\rangle = |x \vee y\rangle$.

$\|x\rangle\|y\rangle$	$\|x \oplus y\rangle$
$\|0\rangle\|0\rangle$	$\|0\rangle$
$\|0\rangle\|1\rangle$	$\|1\rangle$
$\|1\rangle\|0\rangle$	$\|1\rangle$
$\|1\rangle\|1\rangle$	$\|0\rangle$

Table 1.4: XOR operation. We used the alternative notation $\mathrm{XOR}|x\rangle|y\rangle = |x \oplus y\rangle$.

□ **– Exercise 1.1** *Prove that NOR and NAND are universal.*

1.3 Single-bit reversible operations

The NOT is the only reversible (classical) operation acting on single bits (excluding the identity operator $\hat{\mathbb{I}}$, which is a trivial operation). By using the matrix formalism, we can represent NOT with the 2×2 matrix:

$$\mathbf{X} \to \begin{pmatrix} 0 & 1 \\ 1 & 0 \end{pmatrix}. \tag{1.11}$$

Since $\mathbf{X}^2 = \hat{\mathbb{I}} \to \mathbb{1}_2 = \mathrm{diag}(1,1)$ is the 2×2 identity matrix, it follows that $\mathbf{X}$ is invertible and $\mathbf{X} = \mathbf{X}^{-1}$.

It is also instructive to introduce the operators $\mathbf{N}$, the number operator, and $\overline{\mathbf{N}} = \hat{\mathbb{I}} - \mathbf{N}$:

$$\mathbf{N}|x\rangle = x|x\rangle, \quad \text{and} \quad \overline{\mathbf{N}}|x\rangle = \overline{x}|x\rangle, \quad x \in \{0,1\}. \tag{1.12}$$

The corresponding matrices are:

$$\mathbf{N} \to \begin{pmatrix} 0 & 0 \\ 0 & 1 \end{pmatrix}, \quad \text{and} \quad \overline{\mathbf{N}} \to \begin{pmatrix} 1 & 0 \\ 0 & 0 \end{pmatrix}. \tag{1.13}$$

Classically, $\mathbf{N}$ and $\overline{\mathbf{N}}$ are just mathematical operators and do not correspond to a physical operation, e.g. we cannot imagine the meaning of multiplying by 0 the *state* – not the *numerical value* – of a bit... However, they could be useful from the formal point of view.

□ – **Exercise 1.2** *Verify that* $\mathbf{X}|x\rangle = |\overline{x}\rangle$.

□ – **Exercise 1.3** *Verify that* $\overline{\mathbf{N}}^2 = \mathbf{N}$ *and* $\mathbf{N}\overline{\mathbf{N}} = \overline{\mathbf{N}}\mathbf{N} = \mathbf{0}$.

1.4 Two-bit reversible operations

1.4.1 SWAP

The SWAP operation exchanges the *values* x and y of the two bits $|x\rangle|y\rangle$:

$$\mathbf{S}|x\rangle|y\rangle = |y\rangle|x\rangle. \tag{1.14}$$

If we consider the n-bit state $|x\rangle_n$, then we can define the operator $\mathbf{S}_{hk}$ which acts on the bits h and k, namely:

$$\begin{aligned}\mathbf{S}_{hk}|x\rangle_n &= \mathbf{S}_{hk}|x_{n-1}\rangle\cdots|x_h\rangle\cdots|x_k\rangle\cdots|x_0\rangle,\\ &= |x_{n-1}\rangle\cdots|x_k\rangle\cdots|x_h\rangle\cdots|x_0\rangle.\end{aligned} \tag{1.15}$$

Since $\mathbf{S}_{hk}\mathbf{S}_{hk} = \hat{\mathbb{I}}$, the SWAP is indeed unitary. It is also possible to represent the SWAP as follows:

$$\mathbf{S}_{hk} = \mathbf{N}_h \otimes \mathbf{N}_k + \overline{\mathbf{N}}_h \otimes \overline{\mathbf{N}}_k + (\mathbf{X}_h \otimes \mathbf{X}_k)\left(\mathbf{N}_h \otimes \overline{\mathbf{N}}_k + \overline{\mathbf{N}}_h \otimes \mathbf{N}_k\right), \tag{1.16}$$

where $\mathbf{N}_k$, $\overline{\mathbf{N}}_k$ and $\mathbf{X}_k$ have been introduced in section 1.3 and act on the k-th bits. Sometimes, we will drop the tensor product symbol and we will write:

$$\mathbf{S}_{hk} = \mathbf{N}_h\mathbf{N}_k + \overline{\mathbf{N}}_h\overline{\mathbf{N}}_k + \mathbf{X}_h\mathbf{X}_k\left(\mathbf{N}_h\overline{\mathbf{N}}_k + \overline{\mathbf{N}}_h\mathbf{N}_k\right), \tag{1.17}$$

The reader can verify the action of the left-hand-side member of Eq. (1.16) by exploiting the properties of the tensor product and recalling that: (i) given two operators $\mathbf{A}_h$ and $\mathbf{B}_k$, acting on the h-th and k-th bits, respectively, one has $\mathbf{A}_h \otimes \mathbf{B}_k|x_h\rangle \otimes |x_k\rangle = \mathbf{A}_h|x_h\rangle \otimes \mathbf{B}_k|x_k\rangle$; (ii) $(\mathbf{A}_h \otimes \mathbf{B}_k)(\mathbf{C}_h \otimes \mathbf{D}_k) = (\mathbf{A}_h\mathbf{C}_h) \otimes (\mathbf{B}_k\mathbf{D}_k)$.

The matrix representation of $\mathbf{S}_{hk}$ is just a single permutation matrix[4].

[4] The explicit form of the permutation matrix associated with $\mathbf{S}_{hk}$ can be obtained starting from the identity matrix and exchanging the h-th and k-th columns.

$\|x\rangle\|y\rangle$	$\mathbf{C}_{10}$	$\mathbf{C}_{01}$
$\|0\rangle\|0\rangle$	$\|0\rangle\|0\rangle$	$\|0\rangle\|0\rangle$
$\|0\rangle\|1\rangle$	$\|0\rangle\|1\rangle$	$\|1\rangle\|1\rangle$
$\|1\rangle\|0\rangle$	$\|1\rangle\|1\rangle$	$\|1\rangle\|0\rangle$
$\|1\rangle\|1\rangle$	$\|1\rangle\|0\rangle$	$\|0\rangle\|1\rangle$

Table 1.5: CNOT operation.

1.4.2 Controlled NOT

The controlled NOT, CNOT, is a "workhorse for quantum computation". This operation acts on a *target* bit according to the value of a *control* bit. By definition, $\mathbf{C}_{hk}$ flips the state of the k-th bit (target state) only if the state of the h-th bit (control state) is $|1\rangle$. The action of $\mathbf{C}_{10}$ and $\mathbf{C}_{01}$ is summarized in table 1.5: we can easily see that they act as permutations on the input basis in which only two elements are exchanged.

The matrix representations of $\mathbf{C}_{01}$ and $\mathbf{C}_{10}$ are:

$$\mathbf{C}_{10} \to \begin{pmatrix} 1 & 0 & 0 & 0 \\ 0 & 1 & 0 & 0 \\ 0 & 0 & 0 & 1 \\ 0 & 0 & 1 & 0 \end{pmatrix}, \quad \mathbf{C}_{01} \to \begin{pmatrix} 1 & 0 & 0 & 0 \\ 0 & 0 & 0 & 1 \\ 0 & 0 & 1 & 0 \\ 0 & 1 & 0 & 0 \end{pmatrix}, \tag{1.18}$$

respectively.

Note that, in general, we can summarize the action of CNOT as follows:

$$\begin{aligned} \mathbf{C}_{hk}|x\rangle_n = \mathbf{C}_{hk}|x_{n-1}\rangle \cdots |x_h\rangle \cdots |x_k\rangle \cdots |x_0\rangle, \\ = |x_{n-1}\rangle \cdots |x_h\rangle \cdots |x_k \oplus x_h\rangle \cdots |x_0\rangle, \end{aligned} \tag{1.19}$$

where we used $|x_k \oplus x_h\rangle = |\overline{x}_k\rangle$ if and only if $|x_h\rangle = |1\rangle$. It is clear that CNOT acts as a generalized XOR.

Now, we introduce the operator:

$$\mathbf{Z} = \overline{\mathbf{N}} - \mathbf{N} \to \begin{pmatrix} 1 & 0 \\ 0 & -1 \end{pmatrix}, \tag{1.20}$$

and $\mathbf{XZ} = -\mathbf{ZX}$. It is straightforward to see that:

$$\mathbf{Z}|x\rangle = (-1)^x|x\rangle, \quad x \in \{0,1\}. \tag{1.21}$$

From a classical point of view the action of $\mathbf{Z}$ is meaningless: it multiplies by -1 the state $|1\rangle$ – note that the *state* of the bit is multiplied by -1 and not its numerical value!

Since, $\mathbf{N} = \frac{1}{2}(\hat{\mathbb{I}} - \mathbf{Z})$ and $\overline{\mathbf{N}} = \frac{1}{2}(\hat{\mathbb{I}} + \mathbf{Z})$ which directly follows from Eq. (1.21), we can write[5]:

$$\mathbf{C}_{hk} = \frac{1}{2}(\hat{\mathbb{I}} + \mathbf{Z}_h) + \frac{1}{2}(\hat{\mathbb{I}} - \mathbf{Z}_h)\mathbf{X}_k, \tag{1.22a}$$

$$= \frac{1}{2}(\hat{\mathbb{I}} + \mathbf{X}_k) + \frac{1}{2}\mathbf{Z}_h(\hat{\mathbb{I}} - \mathbf{X}_k), \tag{1.22b}$$

where we dropped the tensor product.

□ **– Exercise 1.4** *Verify that* $\mathbf{C}_{hk} = \overline{\mathbf{N}}_h + \mathbf{N}_h\mathbf{X}_k$, *where the subscripts refere to the bit affected by the operation.*

□ **– Exercise 1.5** *Show that the same action of the SWAP can be obtained by the application of three CNOT operations, namely:*

$$\mathbf{S}_{hk} = \mathbf{C}_{hk}\mathbf{C}_{kh}\mathbf{C}_{hk}. \tag{1.23}$$

1.4.3 SWAP operator and Pauli matrices

Substituting Eqs. (1.22) into Eq. (1.23), one find the following interesting identity for the SWAP operator:

$$\mathbf{S}_{hk} = \frac{1}{2}(\hat{\mathbb{I}} + \mathbf{Z}_h\mathbf{Z}_k) + \frac{1}{2}\mathbf{X}_h\mathbf{X}_k(\hat{\mathbb{I}} - \mathbf{Z}_h\mathbf{Z}_k), \tag{1.24}$$

which may be also written as:

$$\mathbf{S}_{hk} = \frac{1}{2}(\hat{\mathbb{I}} + \mathbf{X}_h\mathbf{X}_k - \mathbf{Y}_h\mathbf{Y}_k + \mathbf{Z}_h\mathbf{Z}_k), \tag{1.25}$$

where[6]:

$$\mathbf{Y}_k = \mathbf{Z}_k\mathbf{X}_k \to \begin{pmatrix} 0 & 1 \\ -1 & 0 \end{pmatrix}. \tag{1.26}$$

If, however, we introduce the Pauli operators (and the corresponding 2×2 Pauli matrices):

$$\hat{\sigma}_x \to \sigma_x = \begin{pmatrix} 0 & 1 \\ 1 & 0 \end{pmatrix}, \quad \hat{\sigma}_y \to \sigma_y = \begin{pmatrix} 0 & -i \\ i & 0 \end{pmatrix}, \quad \hat{\sigma}_z \to \sigma_z = \begin{pmatrix} 1 & 0 \\ 0 & -1 \end{pmatrix} \tag{1.27}$$

[5] In order to simplify the formalism, we use the following convention:

$$\mathbf{A}_h \otimes \hat{\mathbb{I}}(|x_h\rangle \otimes |x_k\rangle) \equiv \mathbf{A}_h(|x_h\rangle \otimes |x_k\rangle),$$

i.e. $\mathbf{A}_h \otimes \hat{\mathbb{I}} \equiv \mathbf{A}_h$.

[6] It is worth noting that in our formalism if $k \neq h$ we have $\mathbf{A}_k\mathbf{B}_h = \mathbf{A}_k \otimes \mathbf{B}_h$, since the two operators refer to different physical entities; the symbol $\mathbf{A}_k\mathbf{B}_k$ represents the composition of the two operators.

we have:

$$\mathbf{S}_{hk} = \frac{1}{2}\left(\hat{\mathbb{I}} + \hat{\sigma}_x^{(h)}\hat{\sigma}_x^{(k)} + \hat{\sigma}_y^{(h)}\hat{\sigma}_y^{(k)} + \hat{\sigma}_z^{(h)}\hat{\sigma}_z^{(k)}\right), \tag{1.28}$$

where the superscripts refere to the target bits.

Pauli matrices, together with the identity matrix, form a bais for the 2×2 matrices and have the following properties:

$$[\hat{\sigma}_x, \hat{\sigma}_y] = \hat{\sigma}_x\hat{\sigma}_y - \hat{\sigma}_y\hat{\sigma}_x = 2i\hat{\sigma}_z, \tag{1.29a}$$

$$[\hat{\sigma}_y, \hat{\sigma}_z] = \hat{\sigma}_y\hat{\sigma}_z - \hat{\sigma}_z\hat{\sigma}_y = 2i\hat{\sigma}_x, \tag{1.29b}$$

$$[\hat{\sigma}_z, \hat{\sigma}_x] = \hat{\sigma}_z\hat{\sigma}_x - \hat{\sigma}_x\hat{\sigma}_z = 2i\hat{\sigma}_y, \tag{1.29c}$$

or, by introducing the totally antisymmetric tensor ε_{hkl}, $[\hat{\sigma}_h, \hat{\sigma}_k] = 2i\varepsilon_{hkl}\hat{\sigma}_l$.

1.4.4 The Hadamard transformation

The Hadamard transformation is defined as:

$$\mathbf{H} = \frac{1}{\sqrt{2}}(\mathbf{X} + \mathbf{Z}) \to \frac{1}{\sqrt{2}}\begin{pmatrix} 1 & 1 \\ 1 & -1 \end{pmatrix}. \tag{1.30}$$

Though, classically speaking, the action of $\mathbf{H}$ on $|x\rangle$ is meaningless, since $\mathbf{H}$ transforms a single-bit state into a linear combination of states, namely:

$$\mathbf{H}|x\rangle = \frac{|0\rangle + (-1)^x|1\rangle}{\sqrt{2}},$$

or, explicitly:

$$\mathbf{H}|0\rangle = \frac{|0\rangle + |1\rangle}{\sqrt{2}}, \quad \text{and} \quad \mathbf{H}|1\rangle = \frac{|0\rangle - |1\rangle}{\sqrt{2}}, \tag{1.31}$$

this transformation is useful when applied recursively to other operators, as the reader can see from the exercises 1.6 and 1.7.

□ **– Exercise 1.6** *Show that* $\mathbf{HXH} = \mathbf{Z}$ *and* $\mathbf{HZH} = \mathbf{X}$*, that is, the Hadamard transformation allows to transform* $\mathbf{X}$ *into* $\mathbf{Z}$ *and vice versa.*

□ **– Exercise 1.7** *Show that:*

$$\mathbf{C}_{hk} = \mathbf{H}_h\mathbf{H}_k\mathbf{C}_{kh}\mathbf{H}_h\mathbf{H}_k, \tag{1.32}$$

where the subscripts have the usual meaning – the Hadamard transformation allows to exchange the roles of the target bit and of the control bit of a CNOT, i.e., $\mathbf{C}_{hk} \to \mathbf{C}_{kh}$.

Bibliography

- M. A. Nielsen and I. L. Chuang, *Quantum Computation and Quantum Information* (Cambridge University Press, 2010) – Chapter 1.
- N. D. Mermin, *Quantum Computer Science* (Cambridge University Press, 2007) – Chapter 1.

Chapter 2

Elements of quantum mechanics

IN THIS CHAPTER we briefly review the structure of quantum mechanics. In particular, the reader can find the postulates of quantum mechanics and the description of the measurement through the positive operator-valued measures (POVMs). The quantum operation will be discussed in chapter 7.

2.1 Dirac notation (in brief)

Throughout this chapter we use the Dirac braket notation. An n-dimensional complex vector (or state) is represented with the symbol $|\psi\rangle_n$, that is called "ket". Given two vectors $|\psi\rangle_n$ and $|\phi\rangle_n$, we use the following symbol for the *inner product* (we drop the subscript n): $\langle\psi|(|\phi\rangle) \equiv \langle\psi|\phi\rangle \in \mathbb{C}$. Indeed, $\langle\psi|\phi\rangle$ can be seen as a linear functional associated with the vector $|\psi\rangle$ that takes $|\phi\rangle$ into a complex number. This functional is $(|\psi\rangle)^\dagger = \langle\psi|$, where the symbol $(\cdots)^\dagger$ represents the adjoint operator, and $\langle\psi|$ is called "bra". As usual, the inner product satisfies the following properties:

(i) $\langle\psi|\phi\rangle = \langle\phi|\psi\rangle^*$;
(ii) $\langle\psi|(\alpha|\phi\rangle + \beta|\gamma\rangle) = \alpha\langle\psi|\phi\rangle + \beta\langle\psi|\gamma\rangle, \forall\alpha,\beta \in \mathbb{C}$;
(iii) $\langle\psi|\psi\rangle = 0 \Leftrightarrow |\psi\rangle = 0$.

We can expand the (2^n-dimensional) vector $|\psi\rangle$ as follows:

$$|\psi\rangle = \sum_{x=0}^{2^n-1} \alpha_x |x\rangle, \tag{2.1}$$

where $\langle x|y\rangle = \delta_{xy}$ and δ_{xy} is the Kronecker delta. By using the same association between kets

and vectors introduced in section 1.1, we have:

$$|\psi\rangle \to \begin{pmatrix} \alpha_0 \\ \alpha_1 \\ \vdots \\ \alpha_{2^n-1} \end{pmatrix}, \quad \text{and} \quad \langle\psi| \to \left(\alpha_0^*, \alpha_1^*, \ldots, \alpha_{2^n-1}^*\right), \tag{2.2}$$

where $\langle x|\psi\rangle = \alpha_x$ and the basis the vectors $|x\rangle$, $0 \leq x < 2^n$, have been introduced in section 1.1. It is now clear that, with this association, the inner product between bras and kets corresponds to the standard inner product between the corresponding vectors.

Let us now consider the linear operator $\hat{A}$ which acts on a ket $|\psi\rangle$ leading to a new vector, namely $\hat{A}|\psi\rangle = |\psi'\rangle$. We have $(\hat{A}|\psi\rangle)^\dagger = \langle\psi|\hat{A}^\dagger$ and:

$$\langle\phi|\hat{A}|\psi\rangle = \underbrace{\left(\langle\phi|\hat{A}\right)}_{\left(\hat{A}^\dagger|\phi\rangle\right)^\dagger} |\psi\rangle = \langle\phi|\left(\hat{A}|\psi\rangle\right). \tag{2.3}$$

The *outer product* between $|\psi\rangle$ and $|\phi\rangle$ is an operator $|\psi\rangle\langle\phi|$ whose action on $|\gamma\rangle$ reads:

$$|\psi\rangle\langle\phi|(|\gamma\rangle) = |\psi\rangle\langle\phi|\gamma\rangle \equiv \langle\phi|\gamma\rangle|\psi\rangle. \tag{2.4}$$

Furthermore, we have:

$$|\psi\rangle\langle\phi| \to \begin{pmatrix} \alpha_0 \\ \alpha_1 \\ \vdots \\ \alpha_{2^n-1} \end{pmatrix} \cdot \left(\beta_0^*, \beta_1^*, \ldots, \beta_{2^n-1}^*\right) \equiv \mathbf{M}, \tag{2.5}$$

where $\mathbf{M}$ is a $2^n \times 2^n$ matrix with entries $[\mathbf{M}]_{xy} = \alpha_x\beta_y^*$, and we wrote $|\psi\rangle = \sum_x \alpha_x|x\rangle$ and $|\phi\rangle = \sum_y \beta_y|y\rangle$.

The operator $\hat{P}_x = |x\rangle\langle x|$, $0 \leq x < 2^n$, is called *projector* onto the vector $|x\rangle$ (indeed, one can define a projector $\hat{P}_\psi = |\psi\rangle\langle\psi|$ onto the state $|\psi\rangle$). Since $\{|x\rangle\}$ is an orthonormal basis for the 2^n-dimensional vector space, we have the following *completeness* relation: $\sum_x |x\rangle\langle x| = \hat{\mathbb{I}}$, that is we have a resolution of the identity operator. The completeness relation may be used to express vectors and operators in a particular orthonormal basis.

□ **– Exercise 2.1** *Exploiting the completeness relation* $\sum_x |x\rangle\langle x| = \hat{\mathbb{I}}$*, write the expansion of* $|\psi\rangle$ *in the basis* $\{|x\rangle\}$*.*

□ **– Exercise 2.2** *Exploiting the completeness relation* $\sum_x |x\rangle\langle x| = \hat{\mathbb{I}}$*, write the expansion of a linear operator* $\hat{A}$ *in the basis* $\{|x\rangle\}$*.*

2.2 Quantum bits - qubits

We consider the complex vector space generated by the two column vectors associated with the bit states $|0\rangle$ and $|1\rangle$ (that is a 2-dimensional complex Hilbert space). Since the two states form a basis for this space, any linear combination, or *superposition*:

$$|\psi\rangle = \alpha|0\rangle + \beta|1\rangle \rightarrow \begin{pmatrix} \alpha \\ \beta \end{pmatrix}, \tag{2.6}$$

where $\alpha, \beta \in \mathbb{C}$, belongs to the space. If $|\alpha|^2 + |\beta|^2 = 1$, i.e., if $|\psi\rangle$ is *normalized*, we will refer to the state (2.6) as *quantum bit* or simply *qubit*. Of course, if $\alpha = 0$ or $\beta = 0$, then $|\psi\rangle = |1\rangle$ or $|\psi\rangle = |0\rangle$, respectively[1] The basis $\{|0\rangle, |1\rangle\}$ is called *computational basis* and the information is stored in complex numbers α and β: it follows that in a single qubit it is possible to encode an infinite amount of information. At least potentially... In fact, in order to extract the information we should perform a *measurement* on the qubit: as we will see in the next sections, it is a fundamental aspect of Nature that when we observe a system in the superposition state (2.6), we find it[2] either in the state $|0\rangle$ or $|1\rangle$ with a probabilities $p(0) = |\alpha|^2$ and $p(0) = |\beta|^2$, that's why $|\alpha|^2 + |\beta|^2 = 1$.

Since $|\alpha|^2 + |\beta|^2 = 1$, we can use the following useful parameterization for the amplitudes of the qubit sate[3]:

$$\alpha = \cos\frac{\theta}{2}, \quad \text{and} \quad \beta = e^{i\phi}\sin\frac{\theta}{2}, \tag{2.7}$$

obtaining:

$$|\psi\rangle = \cos\frac{\theta}{2}|0\rangle + e^{i\phi}\sin\frac{\theta}{2}|1\rangle. \tag{2.8}$$

We will address in the chapters 9 and 11 some examples of the physical realization of qubits.

2.2.1 The Bloch sphere

We can associate with the qubit the following three real numbers:

$$r_x = \sin\theta\,\cos\phi, \quad r_y = \sin\theta\,\sin\phi, \quad r_z = \cos\theta, \tag{2.9}$$

which can be seen as the components of a 3-dimensional vector, i.e.:

$$\boldsymbol{r} = \begin{pmatrix} r_x \\ r_y \\ r_z \end{pmatrix} = \begin{pmatrix} \sin\theta\,\cos\phi \\ \sin\theta\,\sin\phi \\ \cos\theta \end{pmatrix}. \tag{2.10}$$

[1] The reader may observe that one should write $|\psi\rangle = e^{i\phi}|1\rangle$ or $|\psi\rangle = e^{i\phi}|0\rangle$, but we will see in section 2.3 that a *global* phase, as $e^{i\phi}$, does not have a physical meaning.

[2] Here we are assuming that the measurement allows to observe as outcomes the state $|0\rangle$ or $|1\rangle$, i.e., the computational basis; of course one may choose a different basis for the measurement, for instance one can also use other computational basis, e.g., $\{|+\rangle, |-\rangle\}$, where $|\pm\rangle = 2^{-1/2}(|0\rangle + |1\rangle)$.

[3] More in general one should have $\alpha = e^{i\delta}\cos\frac{\theta}{2}$ and $\beta = e^{i\phi}\sin\frac{\theta}{2}$, but this is equivalent to add a global phase to the state and, thus, we can set $\delta = 0$.

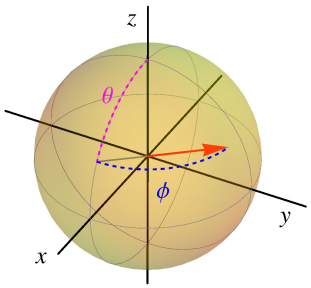

Figure 2.1: The Bloch sphere is represented by the yellow unit sphere, while the red vector represents a pure state, i.e., a state belonging to the surface of the sphere). We also show the two angles θ (magenta) and ϕ (blue) which identify the quantum state.

Furthermore, since $\sqrt{r_x^2 + r_y^2 + r_z^2} = 1$, $\boldsymbol{r}$ represents a point on the surface of the unit sphere, that is the so-called Bloch sphere. In figure 2.1 we show the Bloch sphere and the vectorial representation of a quantum state (the red vector).

In particular we have:

$$|0\rangle \Rightarrow \begin{pmatrix} 0 \\ 0 \\ 1 \end{pmatrix}, \quad \text{and} \quad |1\rangle \Rightarrow \begin{pmatrix} 0 \\ 0 \\ -1 \end{pmatrix}, \tag{2.11}$$

namely, $|0\rangle$ corresponds to the north pole of the Bloch sphere, whereas $|1\rangle$ to its south pole. The state $|\psi\rangle = 2^{-1/2}(|0\rangle + e^{i\phi}|1\rangle)$, with $\phi \in [0, 2\pi)$, corresponds to equatorial states.

2.2.2 Multiple qubit states

A n-qubit state reads:

$$|\Psi\rangle_n = \sum_{x=0}^{2^n-1} \alpha_x |x\rangle_n, \quad \text{with} \quad \sum_{x=0}^{2^n-1} |\alpha_x|^2 = 1, \tag{2.12}$$

as usual, the subscript n refers to the number of physical entities (qubits) used to encode the information. In particular, the state of two qubits can be written as:

$$|\Psi\rangle_2 = \alpha_{00}|00\rangle + \alpha_{01}|01\rangle + \alpha_{10}|10\rangle + \alpha_{11}|11\rangle, \tag{2.13}$$

with $|\alpha_{00}|^2 + |\alpha_{10}|^2 + |\alpha_{01}|^2 + |\alpha_{11}|^2 = 1$. In this case, each $|\alpha_{xy}|^2$ corresponds to the *joint* probability to find the two qubits of the state (2.13) in the state $|x\, y\rangle$.

2.3 Postulates of quantum mechanics

In this section we introduce quantum mechanics more formally. The postulates of quantum mechanics are a list of prescription to summarize: (1) how to describe the *state* of a physical

system; (2) how to describe the *measurement* performed on a physical system; (3) how to describe the *evolution* of a physical system.

Postulate 1 – States of a quantum system. Each physical system is associated with a complex Hilbert space $\mathcal{H}$ with inner product. The possible states of the physical system correspond to normalized vectors $|\psi\rangle$, $\langle\psi|\psi\rangle = 1$, which contain all the information about the system. For a composite system we have $|\psi\rangle = |\psi\rangle_1 \otimes \ldots \otimes |\psi\rangle_N \in \mathcal{H}$, where $\mathcal{H} = \mathcal{H}_1 \otimes \ldots \otimes \mathcal{H}_N$ is the tensor product of the Hilbert spaces $\mathcal{H}_k$ associated with the k-th subsystem. If $|\psi\rangle$ and $|\phi\rangle$ are possible states of a quantum system, then any normalized linear superposition $|\Psi\rangle = \alpha|\psi\rangle + \beta|\phi\rangle$, $\langle\Psi|\Psi\rangle = 1$, is an admissible state of the system (note that, in general, $\langle\psi|\phi\rangle \neq 0$, therefore one may have $\langle\Psi|\Psi\rangle = 1$ but $|\alpha|^2 + |\beta|^2 \neq 1$).

Postulate 2 – Quantum measurements. Observable quantities are described by Hermitian operators $\hat{A}$, that is $\hat{A} = \hat{A}^\dagger$. The operator $\hat{A}$ admits a spectral decomposition $\hat{A} = \sum_x a_x \hat{P}(a_x)$ in terms of the real eigenvalues a_x, which are the possible values of the observable, where $\hat{P}(a_x) = |u_x\rangle\langle u_x|$ and $\hat{A}|u_x\rangle = a_x|u_x\rangle$. Note that the orthonormal eigenstates $\{|u_x\rangle\}$ form a basis for the Hilbert space. The probability of obtaining the outcome a_x from the measurement of $\hat{A}$ given the state $|\psi\rangle$ is:

$$p(a_x) = \langle\psi|\hat{P}(a_x)|\psi\rangle = |\langle u_x|\psi\rangle|^2, \tag{2.14}$$

and the overall expectation value is:

$$\langle\hat{A}\rangle = \langle\psi|\hat{A}|\psi\rangle = \mathrm{Tr}\left[|\psi\rangle\langle\psi|\,\hat{A}\right]. \tag{2.15}$$

This is the *Born rule*, the fundamental recipe to connect the mathematical description of a quantum state $|\psi\rangle$ to the prediction of quantum theory about the results of an experiment. It is now clear that an overall phase has not a physical meaning: the two states $|\psi\rangle$ and $e^{i\varphi}|\psi\rangle$, when inserted in Eqs. (2.14) and (2.15), lead to the same results and, thus, represent the same physical state!

Postulate 3 – Dynamics of a quantum system. The dynamical evolution of a physical system from an initial time t_0 to a time $t \geq t_0$ is described by a unitary operator $\hat{U}(t, t_0)$, with $\hat{U}(t, t_0)\,\hat{U}^\dagger(t, t_0) = \hat{U}^\dagger(t, t_0)\,\hat{U}(t, t_0) = \hat{\mathbb{1}}$. If $|\psi_{t_0}\rangle$ is the state of the system at time t_0, then at time t we have $|\psi_t\rangle = \hat{U}(t, t_0)|\psi_{t_0}\rangle$. Furthermore, given $\hat{U}(t, t_0)$ there exists a unique Hermitian operator $\hat{H}$ such that (Stone theorem):

$$\hat{U}(t, t_0) = \exp\left[-i\hat{H}(t - t_0)\right], \tag{2.16}$$

and the form of $\hat{H}$ can be obtained from its identification with the expression for the classical energy of the system, that is the *Hamiltonian* of the system.

□ – **Exercise 2.3** *(Two-level system) Given the (quantum) Hamiltonian:*

$$\hat{H} = \hbar[\omega_0|0\rangle\langle 0| + \omega_1|1\rangle\langle 1| + \gamma(|1\rangle\langle 0| + |0\rangle\langle 1|)], \tag{2.17}$$

where we used the computational basis $\{|0\rangle, |1\rangle\}$*, find the eigenvalues and the eigenstates of* $\hat{H}$ *and calculate:*

$$\hat{U}(t)|1\rangle = \exp\left(-i\hat{H}t/\hbar\right)|1\rangle. \tag{2.18}$$

(Hint: express the Hamiltonian in its matrix form...)

2.4 Quantum two-level system: explicit analysis

Since two-level systems are of extreme interest for quantum mechanics and, in particular, for quantum computation, in this section we explicitly solve exercise 2.3 (however, we suggest the reader to study and solve it before reading what follows!).

The 2×2 matrix associated with the Hamiltonian of Eq. (2.17) is (without loss of generality we assume the coupling constant $\gamma \in \mathbb{R}$):

$$\hat{H} \to \begin{pmatrix} E_0 & g \\ g & E_1 \end{pmatrix} \tag{2.19}$$

where $E_k = \hbar\omega_k$, $k = 0, 1$, and $g = \hbar\gamma$. The eigenvalues are:

$$E_\pm = \frac{(E_0 + E_1) \pm \sqrt{(\Delta E)^2 + 4g^2}}{2}, \tag{2.20}$$

with $\Delta E = E_1 - E_0$, and the corresponding eigenvectors $|\psi_\pm\rangle$, $\hat{H}|\psi_\pm\rangle = E_\pm|\psi_\pm\rangle$, can be written as:

$$|\psi_\pm\rangle = c_{0,\pm}|0\rangle + c_{1,\pm}|1\rangle\,, \tag{2.21}$$

whose coefficients $c_{k,\pm}$, $k = 0, 1$, satisfy the conditions:

$$\left(\frac{c_{0,\pm}}{c_{1,\pm}}\right) = \frac{g}{E_\pm - E_0} \quad \text{and} \quad |c_{0,\pm}|^2 + |c_{1,\pm}|^2 = 1\,. \tag{2.22}$$

After few calculations we find:

$$c_{0,\pm} = \frac{g}{\sqrt{(E_\pm - E_0)^2 + g^2}} \quad \text{and} \quad c_{1,\pm} = \frac{E_\pm - E_0}{\sqrt{(E_\pm - E_0)^2 + g^2}}\,. \tag{2.23}$$

Since $\hat{U}(t)|\psi_\pm\rangle = \exp(-i\omega_\pm t)|\psi_\pm\rangle$, where $\hbar\omega_\pm = E_\pm$, it is straightforward to calculate the time evolution of the computational basis $\{|0\rangle, |1\rangle\}$. The time evolution of the generic state

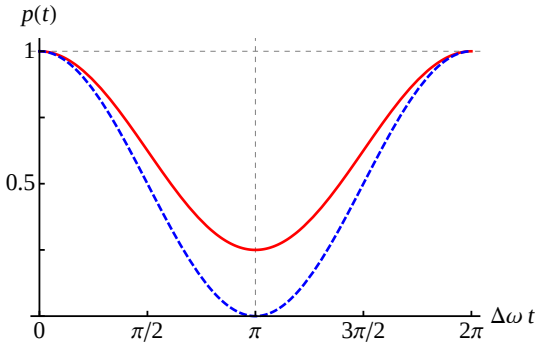

Figure 2.2: Probability $p(t)$ given in Eq. (2.25) to find an evolved state in the corresponding initial state as a function of $\Delta\omega t$ for $|c_+|^2 = 1/4$ (red, solid line) and $|c_+|^2 = 1/2$ (blue, dashed line). The minimum value of $p(t)$ at $\Delta\omega\, t = \pi$ is given by $(\Delta E)^2/[4g^2 + (\Delta E)^2]$.

$|\phi_0\rangle = c_+|\psi_+\rangle + c_-|\psi_-\rangle$, $|c_+|^2 + |c_-|^2 = 1$, reads:

$$|\phi_t\rangle \equiv \hat{U}(t)|\psi_0\rangle = \mathrm{e}^{-i\omega_+ t} c_+|\psi_+\rangle + \mathrm{e}^{-i\omega_- t} c_-|\psi_-\rangle. \tag{2.24}$$

The probability $p(t) = |\langle\phi_0|\phi_t\rangle|^2 = |\langle\phi_0|\hat{U}(t)|\phi_0\rangle|^2$ to find the evolved state in the initial state $|\phi_0\rangle$ at the time t is given by:

$$p(t) = 1 - 4|c_+|^2 \underbrace{\left(1 - |c_+|^2\right)}_{|c_-|^2} \sin^2\left(\frac{\Delta\omega\, t}{2}\right), \tag{2.25}$$

where we introduced $\Delta\omega = \omega_+ - \omega_- = \hbar^{-1}\sqrt{(\Delta E)^2 + 4g^2}$ and we used $|c_+|^2 + |c_-|^2 = 1$. In figure 2.2 we plot $p(t)$ for two different choices of the coefficient c_+ as a function of $\Delta\omega\, t$.

The last term of Eq. (2.25) represents the interference of the probability amplitudes, whose visibility is:

$$\mathcal{V} = \frac{p_{\max} - p_{\min}}{p_{\max} + p_{\min}}, \tag{2.26a}$$

$$= \frac{2|c_+|^2\left(1 - |c_+|^2\right)}{1 - 2|c_+|^2\left(1 - |c_+|^2\right)}, \tag{2.26b}$$

where, clearly, $p_{\max} = 1$ and $p_{\min} = 1 - 4|c_+|^2\left(1 - |c_+|^2\right)$. It is worth noting that the $\mathcal{V}$ reaches its maximum 1 if $|c_+|^2 = |c_-|^2 = 1/2$ (see the blue dashed line in figure 2.2): the initial state should be a balanced superposition of the eigenstates $|\psi_\pm\rangle$ of the Hamiltonian (2.17), namely:

$$|\phi_0\rangle = \frac{|\psi_+\rangle + \mathrm{e}^{i\varphi}|\psi_-\rangle}{\sqrt{2}}, \tag{2.27}$$

in this case at times t_n such that $\Delta\omega\, t_n = 2n\pi$, $n \in \mathbb{N}$, one has $p(t_n) = 0$ and the evolved system is in the state:

$$|\phi_{t_n}\rangle \equiv \left|\phi_0^\perp\right\rangle = \frac{|\psi_+\rangle - \mathrm{e}^{i\varphi}|\psi_-\rangle}{\sqrt{2}} \tag{2.28}$$

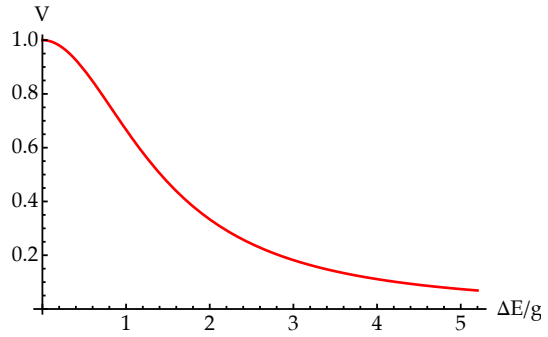

Figure 2.3: Visibility $\mathcal{V} = \mathcal{V}_0 = \mathcal{V}_1$ of Eq. (2.33) as a function of the ratio $\Delta E/g$.

where $\langle \phi_0^{\perp} | \phi_0 \rangle = 0$.

In order to calculate the time evolution of the states $|0\rangle$ and $|1\rangle$, we rewrite them as functions of $|\psi_\pm\rangle$, namely:

$$|0\rangle = \frac{(E_+ - E_0)\sqrt{(E_- - E_0)^2 + g^2}\,|\psi_-\rangle - (E_- - E_0)\sqrt{(E_+ - E_0)^2 + g^2}\,|\psi_+\rangle}{g(E_+ - E_-)}, \tag{2.29a}$$

$$|1\rangle = \frac{\sqrt{(E_+ - E_0)^2 + g^2}\,|\psi_+\rangle - \sqrt{(E_- - E_0)^2 + g^2}\,|\psi_-\rangle}{E_+ - E_-}, \tag{2.29b}$$

or, in a more compact form:

$$|0\rangle = a_+ |\psi_+\rangle + a_- |\psi_-\rangle \quad \text{and} \quad |1\rangle = b_+ |\psi_+\rangle + b_- |\psi_-\rangle, \tag{2.30}$$

where:

$$a_\pm = \pm \frac{(E_\pm - E_0)\sqrt{(E_\pm - E_0)^2 + g^2}}{g(E_+ - E_-)} \quad \text{and} \quad b_\pm = \pm \frac{g\, a_\pm}{E_\pm - E_0}\,. \tag{2.31}$$

Exploiting Eq. (2.26) we can easily calculate the corresponding visibilities of the probability amplitudes due to the time evolution:

$$\mathcal{V}_0 = \frac{2|a_+|^2\,|a_-|^2}{1 - 2|a_+|^2\,|a_-|^2} \quad \text{and} \quad \mathcal{V}_1 = \frac{2|b_+|^2\,|b_-|^2}{1 - 2|b_+|^2\,|b_-|^2}, \tag{2.32}$$

which are the same for both the computational basis states, namely:

$$\mathcal{V}_0 = \mathcal{V}_1 = \left[1 + \frac{1}{2}\left(\frac{\Delta E}{g}\right)^2\right]^{-1}, \tag{2.33}$$

and they are reported in figure 2.3 as a function of $\Delta E/g$.

□ **– Exercise 2.4** *Prove Eq. (2.33) and plot the probabilities* $p_k(t) = |\langle k|\hat{U}(t)|k\rangle|^2$, $k = 0, 1$, *as functions of time.*

2.5 Structure of 1-qubit unitary transformations

Any 2×2 complex matrix $\mathbf{M}$ can be written as:

$$\mathbf{M} = r_0 \mathbb{1} + \boldsymbol{r} \cdot \boldsymbol{\sigma}, \tag{2.34}$$

where $\boldsymbol{r} = (r_x, r_y, r_z)$, with $r_0, r_k \in \mathbb{C}$, $\boldsymbol{\sigma} = (\sigma_x, \sigma_y, \sigma_x)^T$, σ_k are the Pauli matrices introduced in Eqs. (1.27), $k = x, y, z$, and $\boldsymbol{r} \cdot \boldsymbol{\sigma} = \sum_k r_k \sigma_k$. Here we are interested in unitary transformations, namely, $\mathbf{M}^\dagger \mathbf{M} = \mathbf{M}\mathbf{M}^\dagger = \mathbb{1}$, where $\mathbf{M}^\dagger = r_0^* \mathbb{1} + \boldsymbol{r}^* \cdot \boldsymbol{\sigma}$. Since $\mathbf{M}$ is unitary, also $e^{i\theta}\mathbf{M}$ is unitary, thus we can assume $r_0 \in \mathbb{R}$ without loss of generality.

We have:

$$\mathbf{M}^\dagger \mathbf{M} = (r_0 \mathbb{1} + \boldsymbol{r}^* \cdot \boldsymbol{\sigma})(r_0 \mathbb{1} + \boldsymbol{r} \cdot \boldsymbol{\sigma}) \tag{2.35}$$

that is equivalent to write:

$$\mathbb{1} = r_0^2 \mathbb{1} + r_0(\boldsymbol{r}^* + \boldsymbol{r}) \cdot \boldsymbol{\sigma} + (\boldsymbol{r}^* \cdot \boldsymbol{\sigma})(\boldsymbol{r} \cdot \boldsymbol{\sigma}). \tag{2.36}$$

By using the identity $(\boldsymbol{a} \cdot \boldsymbol{\sigma})(\boldsymbol{b} \cdot \boldsymbol{\sigma}) = \boldsymbol{a} \cdot \boldsymbol{b}\, \mathbb{1} + i(\boldsymbol{a} \times \boldsymbol{b}) \cdot \boldsymbol{\sigma}$, $\forall \boldsymbol{a}, \boldsymbol{b} \in \mathbb{C}^3$, we obtain the following two conditions:

$$r_0^2 + \boldsymbol{r}^* \cdot \boldsymbol{r} = 1, \tag{2.37a}$$

$$r_0(\boldsymbol{r}^* + \boldsymbol{r}) + i(\boldsymbol{r}^* \times \boldsymbol{r}) = 0. \tag{2.37b}$$

Since we can write $\boldsymbol{r}^* + \boldsymbol{r} = 2\Re\mathrm{e}[\boldsymbol{r}]$ and $i(\boldsymbol{r}^* \times \boldsymbol{r}) = -2\Re\mathrm{e}[\boldsymbol{r}] \times \Im\mathrm{m}[\boldsymbol{r}]$, Eq. (2.37b) requires $r_0 \Re\mathrm{e}[\boldsymbol{r}] = \Re\mathrm{e}[\boldsymbol{r}] \times \Im\mathrm{m}[\boldsymbol{r}]$, and we have two possibilities. If $r_0 = 0$ and, thus, $\Re\mathrm{e}[\boldsymbol{r}]$ is parallel to $\Im\mathrm{m}[\boldsymbol{r}]$, then $\boldsymbol{r} = e^{i\phi}\boldsymbol{v}$ with $\boldsymbol{v} \in \mathbb{R}^3$ and, being $\mathbf{M}$ unitary, we can simply write $\boldsymbol{r} = i\boldsymbol{v}$. The second possibility is $r_0 \neq 0$ and, in this case, $\Re\mathrm{e}[\boldsymbol{r}]$ should be parallel to $\Re\mathrm{e}[\boldsymbol{r}] \times \Im\mathrm{m}[\boldsymbol{r}]$. Therefore, $\Re\mathrm{e}[\boldsymbol{r}] = 0$ and, again, $\boldsymbol{r} = i\boldsymbol{v}$. Summarizing, for an unitary 2×2 matrix we have:

$$\mathbf{M} = r_0 \mathbb{1} + i\boldsymbol{v} \cdot \boldsymbol{\sigma}, \tag{2.38}$$

where $\boldsymbol{v} \in \mathbb{R}^3$. Furthermore, the condition in Eq. (2.37a) allows us to write:

$$\mathbf{M} = \cos\gamma\, \mathbb{1} + i \sin\gamma\, \boldsymbol{n} \cdot \boldsymbol{\sigma}, \tag{2.39}$$

with $\boldsymbol{n} = \boldsymbol{v}/\sqrt{\boldsymbol{v} \cdot \boldsymbol{v}}$. Finally, we have following useful identity:

$$\exp(i\gamma\, \boldsymbol{n} \cdot \boldsymbol{\sigma}) = \cos\gamma\, \mathbb{1} + i \sin\gamma\, \boldsymbol{n} \cdot \boldsymbol{\sigma}. \tag{2.40}$$

□ **– Exercise 2.5** *Prove Eq. (2.40) by using the expansion:*

$$\exp(i\gamma\, \boldsymbol{n} \cdot \boldsymbol{\sigma}) = \sum_{k=0}^{\infty} \frac{(i\gamma)^k}{k!} (\boldsymbol{n} \cdot \boldsymbol{\sigma})^k. \tag{2.41}$$

2.5.1 Linear transformations and Pauli matrices

The Pauli matrices introduced in Eqs. (1.27) are a basis for 2×2 matrices. Therefore we can write $\mathbf{M} = \sum_{k=0}^{3} M_k \sigma_k$, where $\sigma_0 = \mathbb{1}$ and $(\sigma_1, \sigma_2, \sigma_3) = (\sigma_x, \sigma_y, \sigma_z)$. Furthermore, by using the property $\mathrm{Tr}[\sigma_h \sigma_k] = 2\delta_{hk}$, we have:

$$\mathbf{M} = \frac{1}{2}\left\{ \mathrm{Tr}[\mathbf{M}]\mathbb{1} + \sum_k M_k \sigma_k \right\}, \tag{2.42}$$

that explicitly reads:

$$\mathbf{M} = \begin{pmatrix} m_{00} & m_{01} \\ m_{10} & m_{11} \end{pmatrix}, \tag{2.43}$$

$$= \frac{m_{00} + m_{11}}{2}\,\mathbb{1} + \frac{m_{01} + m_{10}}{2}\,\sigma_x + i\frac{m_{01} - m_{10}}{2}\,\sigma_y + \frac{m_{00} - m_{11}}{2}\,\sigma_z. \tag{2.44}$$

2.6 Quantum states, density operator and density matrix

Let us consider the following statistical ensemble $\{p_x, |\psi_x\rangle\}$, in which each state $|\psi_k\rangle$ is prepared with probability p_k. Given the observable $\hat{A}$ and the orthonormal basis $\{|\phi_s\rangle\}$ we have:

$$\begin{aligned}
\langle \hat{A} \rangle &= \sum_x p_x \, \langle \psi_x | \hat{A} | \psi_x \rangle \\
&= \sum_x p_x \, \langle \psi_x | \hat{A} \left(\sum_s |\phi_s\rangle\langle\phi_s| \right) |\psi_x\rangle \\
&= \sum_{x,s} p_x \, \langle \phi_s | \psi_x \rangle \langle \psi_x | \hat{A} | \phi_s \rangle \\
&= \sum_s \langle \phi_s | \underbrace{\left(\sum_x p_x \, |\psi_x\rangle\langle\psi_x| \right)}_{\hat{\varrho}} \hat{A} | \phi_s \rangle \\
&= \sum_s \langle \phi_s | \hat{\varrho} \hat{A} | \phi_s \rangle \equiv \mathrm{Tr}[\hat{\varrho}\,\hat{A}].
\end{aligned} \tag{2.45}$$

The linear operator $\hat{\varrho}$ is calles *density operator*. More in general a linear operator:

$$\hat{\varrho} = \sum_{n,m} \varrho_{n,m} |\phi_n\rangle\langle\phi_m|, \tag{2.46}$$

with $\varrho_{n,m} = \langle \phi_n | \hat{\varrho} | \phi_m \rangle$, is a density operator describing a physical system if $\hat{\varrho} = \hat{\varrho}^\dagger$, $\hat{\varrho} \geq 0$ and $\mathrm{Tr}[\hat{\varrho}] = 1$. The matrix ϱ of the coefficients $\varrho_{n,m}$ is the *density matrix* of the physical system. Of course, ϱ is diagonal if we write it in the basis of its eigenstates. For example, the two density operators:

$$\hat{\varrho}_a = \frac{1}{2}\left(|0\rangle\langle 0| + |0\rangle\langle 1| + |1\rangle\langle 0| + |1\rangle\langle 1| \right), \quad \text{and} \quad \hat{\varrho}_b = |+\rangle\langle +|, \tag{2.47}$$

with $|\pm\rangle = 2^{-1/2}(|0\rangle \pm |1\rangle)$, represent the *same* statistical ensemble written in different basis. In fact the two orthonormal states $|\pm\rangle$ are obtained by applying the Hadamard transformation, which is unitary, to the basis $\{|0\rangle, |1\rangle\}$.

□ **– Exercise 2.6** *Write the density matrices of the states in Eqs. (2.47) in the computational basis* $\{|0\rangle, |1\rangle\}$ *and in the transformed basis* $|\pm\rangle$.

□ **– Exercise 2.7** *Write the density operator and the density matrix of the state*

$$\hat{\varrho}_c = \frac{1}{2}\left(|+\rangle\langle+| + |-\rangle\langle-|\right), \tag{2.48}$$

in the computational basis $\{|0\rangle, |1\rangle\}$ *and in the transformed basis* $|\pm\rangle$.

2.6.1 Pure states and statistical mixtures

Note that $\hat{\varrho}_a^2 = \hat{\varrho}_a$ while $\hat{\varrho}_c^2 \neq \hat{\varrho}_c$, where $\hat{\varrho}_a$ and $\hat{\varrho}_c$ are given in Eqs. (2.47) and (2.48), respectively. Therefore we also have $\mathrm{Tr}[\hat{\varrho}_a] = \mathrm{Tr}[\hat{\varrho}_a^2] = 1$ but $\mathrm{Tr}[\hat{\varrho}_c^2] = 1/2 < 1$. Given a density operator $\hat{\varrho}$, in general one has:

$$\mu[\hat{\varrho}] = \mathrm{Tr}[\hat{\varrho}^2] \leq 1, \tag{2.49}$$

where the real, positive quantity $\mu[\hat{\varrho}]$ is the *purity* of the state $\hat{\varrho}$. In the case of a n-dimensional state we find:

$$\frac{1}{n} \leq \mu[\hat{\varrho}] \leq 1. \tag{2.50}$$

If $\mu[\hat{\varrho}] < 1$ then the state is a "statistical mixture", otherwise, i.e., if $\mu[\hat{\varrho}] = 1$, it is "pure". In fact, in the latter case, we can always write $\hat{\varrho} = |\psi\rangle\langle\psi|$. It is now clear that the state $\hat{\varrho}_c$ of Eq. (2.48) is the maximally mixed state for a qubit, i.e., a 2-dimensional state.

2.6.2 Density matrix of a single qubit

In the case of a single qubit the density matrix ϱ is a 2×2 matrix and, thus, by means of Eq. (2.42) we can write:

$$\varrho = \frac{1}{2}\left\{\mathrm{Tr}[\varrho]\,\mathbb{1} + \mathrm{Tr}[\varrho\,\sigma_x]\,\sigma_x + \mathrm{Tr}[\varrho\,\sigma_y]\,\sigma_y + \mathrm{Tr}[\varrho\,\sigma_z]\,\sigma_z\right\}. \tag{2.51}$$

A similar relation holds for the density operator:

$$\hat{\varrho} = \frac{1}{2}\left\{\mathrm{Tr}[\hat{\varrho}]\,\hat{\mathbb{1}} + \mathrm{Tr}[\hat{\varrho}\,\hat{\sigma}_x]\,\hat{\sigma}_x + \mathrm{Tr}[\hat{\varrho}\,\hat{\sigma}_y]\,\hat{\sigma}_y + \mathrm{Tr}[\hat{\varrho}\,\hat{\sigma}_z]\,\hat{\sigma}_z\right\}. \tag{2.52}$$

From now on, we can focus on the matrix representation of the operators, but we have the same result using the operator formalism. Since $\mathrm{Tr}[\hat{\varrho}] = 1$, we find:

$$\varrho = \frac{1}{2}\left(\mathbb{1} + \boldsymbol{r}\cdot\boldsymbol{\sigma}\right), \tag{2.53}$$

where we used the same formalism introduced in section 2.5. Note that, from the physical point of view, the elements of the Bloch vector are the expectations of the Pauli operators, namely, $r_k = \langle \hat{\sigma}_k \rangle = \mathrm{Tr}[\hat{\varrho}\,\hat{\sigma}_k]$, $k = x, y, z$.

Let us now consider ϱ^2, which explicitly reads:

$$\varrho^2 = \frac{1}{4}\left[\mathbb{1} + 2\boldsymbol{r}\cdot\boldsymbol{\sigma} + (\boldsymbol{r}\cdot\boldsymbol{\sigma})(\boldsymbol{r}\cdot\boldsymbol{\sigma})\right]. \tag{2.54}$$

Since $(\boldsymbol{r}\cdot\boldsymbol{\sigma})(\boldsymbol{r}\cdot\boldsymbol{\sigma}) = \boldsymbol{r}\cdot\boldsymbol{r}\mathbb{1} + i(\boldsymbol{r}\times\boldsymbol{r})\cdot\boldsymbol{\sigma} = |\boldsymbol{r}|^2\mathbb{1}$ we have the following expression for the purity:

$$\mu[\hat{\varrho}] = \frac{1}{2}\left(1 + |\boldsymbol{r}|^2\right), \tag{2.55}$$

and, being $\mu[\varrho] \leq 1$, we have the following condition on the Bloch vector $\boldsymbol{r}$:

$$|\boldsymbol{r}| \leq 1, \tag{2.56}$$

which is needed in order to represent a physical state.

2.7 The partial trace

Let $|\psi_{AB}\rangle \in \mathcal{H}_A \otimes \mathcal{H}_B$ and let us consider the measurement of the observable $\hat{A} = \sum_x a_x \hat{P}(a_x)$ on the system A. The overall observable measured on the global system A–B writes $\hat{A} \otimes \hat{\mathbb{1}}$ and we have the following probability for the outcome a_x (see the Postulate 2 in section 2.3):

$$p(a_x) = \mathrm{Tr}_{AB}\left[\hat{\varrho}_{AB}\,\hat{P}(a_x) \otimes \hat{\mathbb{1}}\right], \tag{2.57}$$

with $\hat{\varrho}_{AB} = |\psi_{AB}\rangle\langle\psi_{AB}|$. As a matter of fact, the Born rule should be valid also for the single system A, thus neglecting system B, namely, we can write:

$$p(a_x) = \mathrm{Tr}_A\left[\hat{\varrho}_A\,\hat{P}(a_x)\right], \tag{2.58}$$

where $\hat{\varrho}_A$ is the density operator describing the subsystem A. It is possible to show that the *unique map* $\hat{\varrho}_{AB} \to \hat{\varrho}_A$ that allows to maintain the Born rule at the level of the whole system and subsystem is the partial trace:

$$\hat{\varrho}_A = \mathrm{Tr}_B[\hat{\varrho}_{AB}]. \tag{2.59}$$

Note that $\mathrm{Tr}_A[\hat{\varrho}_A] = \mathrm{Tr}_{AB}[\hat{\varrho}_{AB}] = 1$. In fact, by introducing the orthonormal basis $\{|\phi_s^{(K)}\rangle\}$ of the system $K = A, B$, we have:

$$\begin{aligned}
p(a_x) &= \mathrm{Tr}_B \mathrm{Tr}_A \left[\hat{\varrho}_{AB}\, \hat{P}(a_x) \otimes \hat{\mathbb{I}}\right] \\
&= \sum_t \left\langle \phi_t^{(B)} \right| \underbrace{\sum_s \left\langle \phi_s^{(A)} \right| \hat{\varrho}_{AB}\, \hat{P}(a_x) \otimes \hat{\mathbb{I}} \left| \phi_s^{(A)} \right\rangle}_{\mathrm{Tr}_A[\hat{\varrho}_{AB}\, \hat{P}(a_x) \otimes \hat{\mathbb{I}}]} \left| \phi_t^{(B)} \right\rangle \\
&= \sum_s \left\langle \phi_s^{(A)} \right| \underbrace{\sum_t \left\langle \phi_t^{(B)} \right| \hat{\varrho}_{AB}\, \hat{P}(a_x) \otimes \hat{\mathbb{I}} \left| \phi_t^{(B)} \right\rangle}_{\mathrm{Tr}_B[\hat{\varrho}_{AB}\, \hat{P}(a_x) \otimes \hat{\mathbb{I}}]} \left| \phi_s^{(A)} \right\rangle \\
&= \sum_s \left\langle \phi_s^{(A)} \right| \underbrace{\sum_t \left\langle \phi_t^{(B)} \right| \hat{\varrho}_{AB}\, \hat{\mathbb{I}} \left| \phi_t^{(B)} \right\rangle}_{\hat{\varrho}_A \equiv \mathrm{Tr}_B[\hat{\varrho}_{AB}]} \hat{P}(a_x) \left| \phi_s^{(A)} \right\rangle \\
&= \sum_s \left\langle \phi_s^{(A)} \right| \hat{\varrho}_A\, \hat{P}(a_x) \left| \phi_s^{(A)} \right\rangle \equiv \mathrm{Tr}_A \left[\hat{\varrho}_A\, \hat{P}(a_x)\right] .
\end{aligned} \tag{2.60}$$

□ **– Exercise 2.8** *Given the density operator $\hat{\varrho}_{AB}$ describing the state of a bipartite system A–B and the observable $\hat{A} = \sum_x a_x\, \hat{P}(a_x)$ on the system A, show that $\langle \hat{A} \rangle = Tr_A \left[\hat{\varrho}_A\, \hat{A}\right]$, where $\hat{\varrho}_A = Tr_B[\hat{\varrho}_{AB}]$.*

2.7.1 Purification of mixed quantum states

Any quantum state $\hat{\varrho}_A$ can be written in the diagonal form choosing its eigenvectors $\left\{ \left| \psi_x^{(A)} \right\rangle \right\}$ as the basis for the corresponding Hilbert space $\mathcal{H}_A$, that is $\hat{\varrho}_A = \sum_x \lambda_x \left| \psi_x^{(A)} \right\rangle \left\langle \psi_x^{(A)} \right|$, where $\lambda_x \geq 0$ are the eigenvalues. Let us now consider another Hilbert space $\mathcal{H}_B$ with dimension at least equal to the number of nonzero eigenvalues λ_x and let $\left\{ \left| \theta_x^{(B)} \right\rangle \right\}$ a basis of $\mathcal{H}_B$. We have that the following *pure* state:

$$|\Psi_{AB}\rangle = \sum_x \sqrt{\lambda_x} \left| \psi_x^{(A)} \right\rangle \left| \theta_x^{(B)} \right\rangle, \tag{2.61}$$

is such that:

$$\mathrm{Tr}_B \left[|\Psi_{AB}\rangle\langle\Psi_{AB}| \right] = \sum_x \lambda_x \left| \psi_x^{(A)} \right\rangle \left\langle \psi_x^{(A)} \right| = \hat{\varrho}_A, \tag{2.62}$$

that is $|\Psi_{AB}\rangle$ is a *purification* of $\hat{\varrho}_A$.

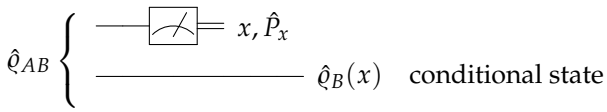

Figure 2.4: Conditional measurement performed on one qubit of a two-qubit state $\hat{\varrho}_{AB}$. See the text for details.

2.7.2 Conditional states

The figure 2.4 shows a *quantum circuit*[4] in which the qubit belonging to the system A of the input state $\hat{\varrho}_{AB}$ undergoes a projective measurement $\hat{P}_x$. Given the outcome x from the measurement, the conditional state of system B reads:

$$\hat{\varrho}_B(x) = \frac{\mathrm{Tr}_A \left[\hat{P}_x \otimes \hat{\mathbb{I}}\, \hat{\varrho}_{AB}\, \hat{P}_x \otimes \hat{\mathbb{I}}\right]}{p(x)} \tag{2.63}$$

with $p(x) = \mathrm{Tr}[\hat{\varrho}_{AB}\, \hat{P}_x \otimes \hat{\mathbb{I}}]$.

> □ **– Exercise 2.9** *Given the following 3-qubit state (the bit order 1-2-3 is from left to right as usual):*
>
> $$|\psi\rangle = \alpha|010\rangle - \beta|101\rangle + \gamma|110\rangle, \tag{2.64}$$
>
> *with $|\alpha|^2 + |\beta|^2 + |\gamma|^2 = 1$, write the conditional state of qubits 2 and 3 and the corresponding probability of obtaining it, when one performs a measurement involving only the qubit 1. (Note that the final state should be normalized!)*

2.8 Entanglement of two-qubit states

A pure state of two qubits belonging to the Hilbert space $\mathcal{H}_A \otimes \mathcal{H}_B$ which can be written as the tensor product of the two single-qubit states, namely, $|\psi_A\rangle|\phi_B\rangle$ is called *factorized* or *separable* state. A state which is not separable is called *entangled*, as the following state:

$$|\Psi_{AB}\rangle = \frac{|0_A\rangle|0_B\rangle + |1_A\rangle|1_B\rangle}{\sqrt{2}}, \tag{2.65}$$

which cannot be written as a tensor product of the two single-qubit states. In particular the state (2.65) is a maximally entangled state. Entanglement is a key ingredient in many quantum

[4] The representation of quantum evolution and measurement by means of quantum circuits will be discussed in the next chapter.

protocols and the characterization of entangled states as well the quantification of this resource is of extreme relevance. A measure $\mathcal{M}_E[\hat{\varrho}_{AB}]$ of the entanglement of the state $\hat{\varrho}_{AB}$ should satisfy the following two conditions:

- $\mathcal{M}_E[\hat{\varrho}_{AB}] = 0 \Leftrightarrow \hat{\varrho}_{AB} = \hat{\varrho}_A \otimes \hat{\varrho}_B$ (factorized state);
- given two local unitary operations $\hat{U}_A$ and $\hat{U}_B$ acting the sub-system A and B, respectively, $\mathcal{M}_E[\hat{U}_A \otimes \hat{U}_B \hat{\varrho}_{AB} \hat{U}_A^\dagger \otimes \hat{U}_B^\dagger] = \mathcal{M}_E[\hat{\varrho}_{AB}]$.

2.8.1 Entropy of entanglement

In the presence of pure states, the simplest measure of entanglement is given by the entropy of entanglement $E(\hat{\varrho}_{AB}) = \mathcal{S}[\hat{\varrho}_A] = \mathcal{S}[\hat{\varrho}_B]$, where

$$\mathcal{S}[\hat{\varrho}] = -\mathrm{Tr}[\hat{\varrho} \log_2 \hat{\varrho}] \tag{2.66}$$

is the von Neumann entropy. In the presence of a pure state $\hat{\varrho} = |\psi\rangle\langle\psi|$, one finds $\mathcal{S}[\hat{\varrho}] = 0$. On the other hand, given a N-level system the von Neumann entropy reaches its maximum $\mathcal{S}_{\max} = \log_2 N$ for $\varrho = N^{-1}\hat{\mathbb{I}}$, that is the maximally mixed state. Note that, because of the definition of the von Neumann entropy, this measure is independent of the Hilbert space basis and invariant under local unitary operations.

We focus on two two-level systems and start our analysis from the factorized state:

$$|\Psi_{AB}\rangle = \frac{1}{\sqrt{2}}\left(|0_A\rangle + |1_A\rangle\right) \otimes \frac{1}{\sqrt{2}}\left(|0_B\rangle + |1_B\rangle\right) = \frac{1}{2}\begin{pmatrix} 1 \\ 1 \\ 1 \\ 1 \end{pmatrix}. \tag{2.67}$$

Since the state (2.67) a tensor product of two pure states, its entropy of entanglement is null, namely $E(|\Psi_{AB}\rangle) = 0$. Now we consider the two-qubit unitary operation $\mathrm{CPh}(\varphi)$ associated with the following 4×4 matrix (we drop the null elements):

$$\mathrm{CPh}(\varphi) = \begin{pmatrix} 1 & & & \\ & 1 & & \\ & & \cos\varphi/2 & -\sin\varphi/2 \\ & & \sin\varphi/2 & \cos\varphi/2 \end{pmatrix}, \tag{2.68}$$

which corresponds to a controlled phase shift: a phase shift φ is applied to the qubit B is the qubit A is the state $|1_A\rangle$. If $\varphi = \pi$, the action of $\mathrm{CPh}(\pi)$ is similar to that of the CNOT, up to a phase [see Eq. (1.18)]. We have:

$$|\Phi_{AB}\rangle \equiv \mathrm{CPh}(\varphi)|\Psi_{AB}\rangle = \frac{1}{2}\begin{pmatrix} 1 \\ 1 \\ c_- \\ c_+ \end{pmatrix}, \tag{2.69}$$

where $c_\pm = \cos\varphi/2 \pm \sin\varphi/2$. The two sub-systems are described by the density matrices:

$$\varrho_A = \frac{1}{2}\begin{pmatrix} 1 & \cos\varphi/2 \\ \cos\varphi/2 & 1 \end{pmatrix}, \quad \text{and} \quad \varrho_B = \frac{1}{2}\begin{pmatrix} 1-\frac{1}{2}\sin\varphi & \cos^2\varphi/2 \\ \cos^2\varphi/2 & 1+\frac{1}{2}\sin\varphi \end{pmatrix}, \tag{2.70}$$

which both have the following eigenvalues: $\lambda_\pm = \frac{1}{2}(1 \pm \cos\varphi/2)$. The corresponding entropy of entanglement is:

$$\begin{aligned} E(|\Phi_{AB}\rangle) = &-\frac{1}{2}\left(1-\cos\frac{\varphi}{2}\right)\log_2\left[\frac{1}{2}\left(1-\cos\frac{\varphi}{2}\right)\right] \\ &-\frac{1}{2}\left(1+\cos\frac{\varphi}{2}\right)\log_2\left[\frac{1}{2}\left(1+\cos\frac{\varphi}{2}\right)\right], \end{aligned} \tag{2.71}$$

which vanishes for $\varphi = 0, 2\pi$ and reaches the maximum $E(|\Phi_{AB}\rangle) = \log_2 2 = 1$ for $\phi = \pi$. It is then clear that for $\varphi \neq 0, 2\pi$ the operation $\mathrm{CPh}(\varphi)$ is an *entangling gate*.

2.8.2 Concurrence

Another measure of entanglement is given by the concurrence. Given the two-qubit pure state:

$$|\psi_{AB}\rangle = \sum_{x,y} \alpha_{xy}|x_A\rangle|y_B\rangle, \tag{2.72}$$

with $\alpha_{xy} \in \mathbb{C}$, $x, y \in \{0,1\}$, and $\sum_{x,y}|\alpha_{xy}|^2 = 1$, the concurrence is defined as:

$$C(|\psi_{AB}\rangle) = 2|\alpha_{00}\alpha_{11} - \alpha_{01}\alpha_{10}|. \tag{2.73}$$

If $C = 0$, the state is factorized, whereas if $C > 0$, the state is entangled. Since:

$$\begin{aligned} 4|\alpha_{00}\alpha_{11} - \alpha_{01}\alpha_{10}|^2 &= 4\left[|\alpha_{00}\alpha_{11}|^2 + |\alpha_{01}\alpha_{10}|^2 - \alpha_{00}\alpha_{11}\alpha_{01}^*\alpha_{10}^* - \alpha_{00}^*\alpha_{11}^*\alpha_{01}\alpha_{10}\right] \\ &= 4\left\{\left(|\alpha_{00}|^2 + |\alpha_{01}|^2\right)\left(|\alpha_{10}|^2 + |\alpha_{11}|^2\right) - |\alpha_{00}\alpha_{01}^* + \alpha_{01}\alpha_{11}^*|^2\right\} \\ &\leq 4\left(|\alpha_{00}|^2 + |\alpha_{01}|^2\right)\left[1 - \left(|\alpha_{00}|^2 + |\alpha_{01}|^2\right)\right] \leq 1, \end{aligned} \tag{2.74}$$

we have $0 \leq C(|\psi_{AB}\rangle) \leq 1$.

The concurrence (2.73) can be written as a function of the purity of the sub-system states. For instance, the density matrix of the sub-system A of the state in Eq. (2.72) reads:

$$\varrho_A = \begin{pmatrix} |\alpha_{00}|^2 + |\alpha_{01}|^2 & \alpha_{00}\alpha_{01}^* + \alpha_{01}\alpha_{11}^* \\ \alpha_{00}^*\alpha_{01} + \alpha_{01}^*\alpha_{11} & |\alpha_{10}|^2 + |\alpha_{11}|^2 \end{pmatrix}, \tag{2.75}$$

therefore we have $C(|\psi_{AB}\rangle) = 2\sqrt{\det[\varrho_A]}$. Furthermore, using the results of section 2.6.2, we can write $\varrho_A = \frac{1}{2}(\mathbb{1} + \boldsymbol{r}_A \cdot \boldsymbol{\sigma})$, where $|\boldsymbol{r}_A|^2 = 2\mathrm{Tr}[\varrho_A^2] - 1$, and, thus, we obtain the following expression for the concurrence $C(|\psi_{AB}\rangle) = \sqrt{1 - |\boldsymbol{r}_A|^2}$.

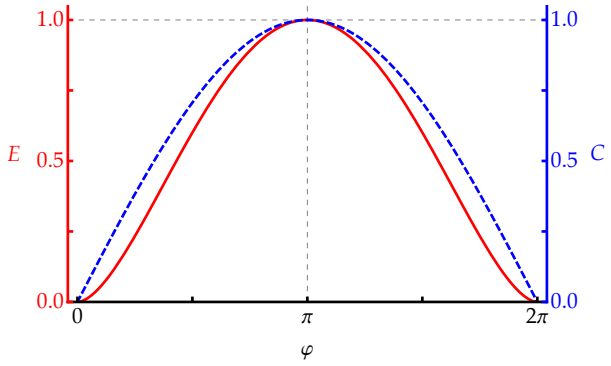

Figure 2.5: Plots of the entropy of entanglement E (red solid line) and concurrence C (blu dashed line) of the state $|\Phi_{AB}\rangle$ of Eq. (2.69).

In figure 2.5 we plot the entropy of entanglement and the concurrence of the state (2.69). It is clear that the numerical values of the two entanglement measures are different, but they reach the maximum ($E = C = 1$) in the presence of a maximally entangled state while they both vanish for a factorized state.

Though the entropy of entanglement is a good measure only in the presence of pure two-qubit states, the concurrence can be extended also to mixed states. In this case, given the two-qubit density operator $\hat{\varrho}_{AB}$, the concurrence is given by:

$$C(\hat{\varrho}_{AB}) = \max(0, \lambda_1 - \lambda_2 - \lambda_3 - \lambda_4), \tag{2.76}$$

where $\lambda_1 \geq \lambda_2 \geq \lambda_3 \geq \lambda_4$ are the eigenvalues of the operator:

$$\hat{R} = \sqrt{\sqrt{\hat{\varrho}_{AB}}\, \hat{\varrho}'_{AB} \sqrt{\hat{\varrho}_{AB}}}, \tag{2.77}$$

with $\hat{\varrho}'_{AB} = \hat{\sigma}_y \otimes \hat{\sigma}_y \hat{\varrho}^*_{AB} \hat{\sigma}_y \otimes \hat{\sigma}_y$.

2.9 Quantum measurements and POVMs

In the previous sections we have seen that a *projective* measurement with outcome x is described by the operators $\hat{P}_x = \hat{P}_x^2 \geq 0$, that is $\hat{P}_x$ is a positive operator. Given the state $\hat{\varrho}$, we have the following expressions for the probability of the outcome x and the corresponding conditional state $\hat{\varrho}_x$:

$$p(x) = \mathrm{Tr}\left[\hat{P}_x\, \hat{\varrho}\, \hat{P}_x\right] = \mathrm{Tr}\left[\hat{\varrho}\, \hat{P}_x^2\right] = \mathrm{Tr}\left[\hat{\varrho}\, \hat{P}_x\right], \tag{2.78}$$

and:

$$\hat{\varrho}_x = \frac{\hat{P}_x\, \hat{\varrho}\, \hat{P}_x}{p(x)}, \tag{2.79}$$

respectively.

A generalized measurement, not described by projectors, is a positive operator-valued measure (POVM), i.e., a set of positive operators $\{\hat{\Pi}_x\}$, $\hat{\Pi}_x \geq 0$, such that $\sum_x \hat{\Pi}_x = \hat{\mathbb{1}}$. In this case we can have $\hat{\Pi}_x^2 \neq \hat{\Pi}_x$ and the probability of the outcome x and the corresponding conditional state $\hat{\varrho}_x$ read:

$$p(x) = \mathrm{Tr}\left[\hat{\varrho}\,\hat{\Pi}_x\right] = \mathrm{Tr}\left[\hat{M}_x\,\hat{\varrho}\,\hat{M}_x^\dagger\right], \tag{2.80}$$

where $\hat{\Pi}_x = \hat{M}_x^\dagger \hat{M}_x$ or $\hat{M}_x = \sqrt{\hat{\Pi}_x}$, and:

$$\hat{\varrho}_x = \frac{\hat{M}_x\,\hat{\varrho}\,\hat{M}_x^\dagger}{p(x)}, \tag{2.81}$$

respectively.

Bibliography

- M. G. A. Paris, *The modern tools of quantum mechanics*, Eur. Phys. J. Special Topics **203**, 61-86 (2012).
- M. A. Nielsen and I. L. Chuang, *Quantum Computation and Quantum Information* (Cambridge University Press, 2010) – Chapter 2.
- S. Stenholm and K.-A. Suominen, *Quantum Approach to Informatics* (Wiley-Interscience, 2005) – Chapter 2.

Chapter 3

Quantum mechanics as computation

IN THIS CHAPTER we introduce the basic framework of quantum computation as an abstract extension of the classical logic. Quantum logic gates and their quantum circuit representations are given. Furthermore, we address the Deutsch, the Deutsch-Jozsa and the Bernstein-Vazirani algorithms.

3.1 Quantum logic gates

A quantum logic gate transforms an input qubit state as that given in Eq. (2.6) into an output state $|\psi'\rangle = \alpha'|0\rangle + \beta'|1\rangle$. Since the condition $|\alpha'|^2 + |\beta'|^2 = 1$ should be still satisfied, it is possible to show that the action of any quantum logic gate can be represented by a *linear unitary transformation* associated with the unitary operator $\hat{U}$, namely:

$$|\psi\rangle \rightarrow |\psi'\rangle \equiv \hat{U}|\psi\rangle, \tag{3.1}$$

where $\hat{U}^\dagger\hat{U} = \hat{U}\hat{U}^\dagger = \hat{\mathbb{1}}$. Being $\hat{U}$ unitary, not only the normalization of the qubit state is preserved during the transformation, but the operation is intrinsically *reversible*. In figure 3.1 the unitary transformation (3.1) is schematically represented by means of a *quantum circuit*: the horizontal lines are "wires" representing the time evolution (from left to right), and they connect the "gates", represented by means of boxes labeled by the corresponding unitary evolution.

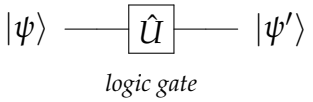

Figure 3.1: Example of a simple quantum circuit involving a single input qubit $|\psi\rangle$ and a unitary (quantum) logic gate U: $|\psi'\rangle$ correspond to the output state.

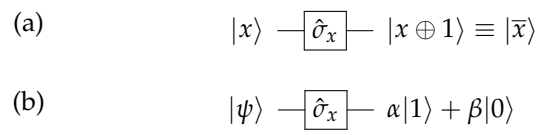

Figure 3.2: Quantum circuit for the NOT acting on: (a) the bit $|x\rangle$; (b) the qubit $|\psi\rangle = \alpha|0\rangle + \beta|1\rangle$.

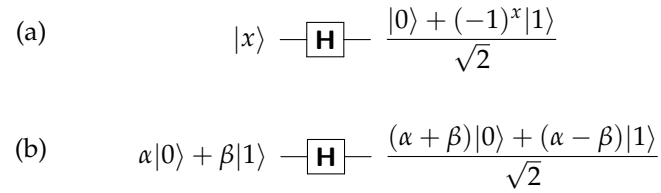

Figure 3.3: Quantum circuit for the Hadamard transformation: (a) action of **H** on a single bit $|x\rangle$; (b) action of **H** on the qubit $\alpha|0\rangle + \beta|1\rangle$.

3.1.1 Single qubit gates

In chapter 1 we explained that the only reversible classical operation is the NOT operation. In the quantum logic scenario it is represented by the Pauli matrix $\hat{\sigma}_x$ and the corresponding quantum circuit is sketched in figure 3.2. Note that due to the linearity of the transformation we have:

$$\hat{\sigma}_x(\alpha|0\rangle + \beta|1\rangle) = \alpha\hat{\sigma}_x|0\rangle + \beta\hat{\sigma}_x|1\rangle = \alpha|1\rangle + \beta|0\rangle, \tag{3.2}$$

as represented in figure 3.2 (b).

In general, a single qubit gate is a linear combination of the Pauli operators. Since any unitary transformation acting on a qubit can be seen as a quantum logic gate, we have infinite single-qubit gates!

Hadamard transformation – In particular, the gate associated with the Hadamard transformation $\mathbf{H} = \frac{1}{\sqrt{2}}(\hat{\sigma}_x + \hat{\sigma}_z)$ defined in Eq. (1.30) not only makes sense (now superpositions of qubit states are allowed!), but it transforms a bit $|x\rangle$ into a superposition and, as we will see, this is a key ingredient of many quantum algorithms. In figure 3.3 we can see the schematic representation of the action of **H** on a bit and on a qubit, respectively.

Phase shift gate – The Pauli operator $\hat{\sigma}_z$ adds a π phase shift between the computational states $|0\rangle$ and $|1\rangle$, since $\hat{\sigma}_z|x\rangle = \mathrm{e}^{-i\pi x}|x\rangle$. More in general, the phase shift gate acts as the phase shift operator:

$$\mathrm{e}^{-i\phi\hat{\sigma}_z} = \cos\phi\,\hat{\mathbb{I}} - i\sin\phi\,\hat{\sigma}_z \to \begin{pmatrix} \mathrm{e}^{-i\phi} & 0 \\ 0 & \mathrm{e}^{i\phi} \end{pmatrix} = \mathrm{e}^{-i\phi}\begin{pmatrix} 1 & 0 \\ 0 & \mathrm{e}^{i2\phi} \end{pmatrix}, \tag{3.3}$$

which adds a relative phase shift 2ϕ between the computational basis states. Note that in the last equality we can drop the *global* phase factor $\mathrm{e}^{-i\phi}$.

T gate or $\frac{\pi}{8}$ gate – This gate, usually referred to as T gate, represents the action of a phase shift gate with $\phi = \pi/8$, namely:

$$T = \begin{pmatrix} e^{-i\pi/8} & 0 \\ 0 & e^{i\pi/8} \end{pmatrix} \equiv \begin{pmatrix} 1 & 0 \\ 0 & e^{i\pi/4} \end{pmatrix}. \tag{3.4}$$

Phase gate – There are two important gates that can be built starting from the T gate, namely:

$$S = T^2 = \begin{pmatrix} 1 & 0 \\ 0 & i \end{pmatrix}, \quad \text{(phase gate)} \tag{3.5}$$

and:

$$T^4 = \begin{pmatrix} 1 & 0 \\ 0 & -1 \end{pmatrix} \to \hat{\sigma}_z. \tag{3.6}$$

The phase gate S, as a stand alone gate, is justified in order to implement fault-tolerant universal quantum computation.

3.1.2 Single qubit gates and Bloch sphere rotations

As a single-qubit pure state can be represented as point on they Bloch sphere (see section 2.2.1), the action of a quantum gate maps point to point and, thus, can be written as the unitary transformation $U = e^{i\alpha}\mathcal{R}_{\boldsymbol{n}}(\theta)$, where $\mathcal{R}_{\boldsymbol{n}}(\theta) = \exp(i\theta\boldsymbol{n}\cdot\boldsymbol{\sigma})$ is a rotation of 2θ around the unit vector $\boldsymbol{n}$. Due to the properties of the rotations, we can decompose $\mathcal{R}_{\boldsymbol{n}}(\theta)$ as the combination of rotations around the principal axes z and y axis (or, analogously, x and y). Therefore, the unitary transformation U can be written as:

$$U = e^{i\alpha}\,\mathcal{R}_z(\beta)\,\mathcal{R}_y(\gamma)\,\mathcal{R}_z(\delta), \tag{3.7}$$

where the values of the angles β, γ and δ depend on $\boldsymbol{n}$ and θ.

3.1.3 Two-qubit gates: the CNOT gate

In chapter 1 we have seen that any logical or arithmetical function can be computed from the composition of NOR or NAND two-bit gates, which are thus universal gates. However, these operators are not reversible and, thus, they cannot be represented by means of unitary operators. The irreversibility, in fact, can be seen as a loss of information.

The prototypical multiple qubit gate is the CNOT gate we introduced in section 1.4.2 and whose quantum circuit is shown in figure 3.4 for what concerns the action of $\mathbf{C}_{10}$ and in figure 3.5 for $\mathbf{C}_{01}$. In figure 3.6 we show the quantum circuit of a CNOT gate, which changes the value of the target if the control is in the state $|0\rangle$: in this case the full circle on the control wire is substituted by an open one. When we will refer to this gate we will use the symbol $\overline{\text{C}}$NOT to indicate that the control should be $|0\rangle$ to change the state of the target. Of course, the action of a

Figure 3.4: Two equivalent circuits representing the action of the CNOT gate $\mathbf{C}_{10}$. The filled circle is placed on the control qubit wire, while the XOR symbol $\oplus$ recall the action of the gate on the target qubit.

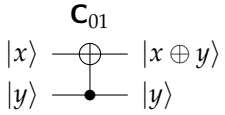

Figure 3.5: Circuit representing the action of the CNOT gate $\mathbf{C}_{01}$.

$\overline{\text{C}}$NOT can be represented as $\hat{\sigma}_x \otimes \mathbb{1}\, \mathbf{C}_{10}\, \hat{\sigma}_x \otimes \mathbb{1} \equiv \overline{\mathbf{C}}_{10}$ or $\mathbb{1} \otimes \hat{\sigma}_x\, \mathbf{C}_{01}\, \mathbb{1} \otimes \hat{\sigma}_x \equiv \overline{\mathbf{C}}_{01}$. It is worth noting that CNOT is a reversible operation on two qubits. In the next sections we will see how any multiple qubit gate may be composed from CNOT and single-qubit gates thus leading to the universal quantum computation. Figure 3.7 shows the quantum circuit of the SWAP operation and its equivalent realization based on three CNOT gates [see also Eq. (1.23)].

The unitary matrix associated with the CNOT (from now on we consider the first qubit as control) reads:

$$U_{\text{CNOT}} = \begin{pmatrix} \mathbb{1} & 0 \\ 0 & \sigma_x \end{pmatrix}. \tag{3.8}$$

More in general, the unitary matrix cU describing the conditional application of a unitary transformation U to a qubit, namely, $cU|x\rangle|y\rangle = \mathbb{1} \otimes U^x|x\rangle|y\rangle$ writes:

$$cU = \begin{pmatrix} \mathbb{1} & 0 \\ 0 & U \end{pmatrix}. \tag{3.9}$$

How can we implement the two-qubit gate cU with single-qubit gates and CNOT? We assume that U can be recast in the form (3.7) and introduce the three auxiliary unitary gates:

$$U_A = \mathcal{R}_z(\beta)\, \mathcal{R}_y\left(\frac{\gamma}{2}\right), \quad U_B = \mathcal{R}_y\left(-\frac{\gamma}{2}\right) \mathcal{R}_z\left(-\frac{\delta+\beta}{2}\right), \quad \text{and} \quad U_C = \mathcal{R}_z\left(\frac{\delta-\beta}{2}\right). \tag{3.10}$$

such that $U_A U_B U_C = \mathbb{1}$. Furthermore, since $\sigma_x \sigma_z \sigma_x = -\sigma_z$ and $\sigma_x, \sigma_y \sigma_z = -\sigma_y$, we also have:

$$\sigma_x U_B \sigma_x = \mathcal{R}_y\left(\frac{\gamma}{2}\right) \mathcal{R}_z\left(\frac{\delta+\beta}{2}\right), \tag{3.11}$$

and, thus, $U_A \sigma_x U_B \sigma_x U_C = \mathrm{e}^{-i\alpha} U$.

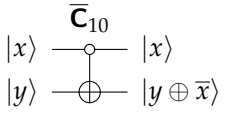

Figure 3.6: Circuit representing the action of a $\overline{\text{C}}$NOT gate $\overline{\mathbf{C}}_{10}$, namely a CNOT which changes the value of the target if the control is in the state $|0\rangle$.

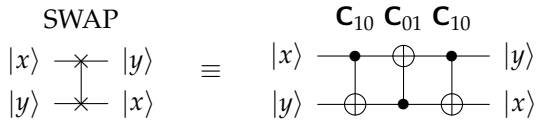

Figure 3.7: Quantum circuit representing the SWAP operation acting on two qubits composed from three CNOT gates.

3.2 Measurement on qubits

As we mentioned, the measurement is a critical point. As sketched in figure 3.9, the result of a measurement on the qubit (2.6) is a single bit $|0\rangle$ or $|1\rangle$ (the double line after the "meter" represents the classical wire carrying one bit of classical information) with a probability given by $|\alpha|^2$ and $|\beta|^2$, respectively. As a matter of fact, during the measurement process performed onto a qubit there is a (huge!) loss of information, which makes the measurement an irreversible process.

3.3 Application and examples

3.3.1 CNOT and No-cloning theorem

One of the peculiar aspect of quantum information is that an unknown quantum state cannot be perfectly cloned. This is a consequence of the linear nature of the operators acting on the quantum states.

In figure 3.10 it is shown how a CNOT gate can be used to clone a (classical) bit $|x\rangle$, $x = 0, 1$. In this case the state of the input bit $|0\rangle$ is converted into the state $|x\rangle$, so that the whole process can be summarized as $|x\rangle|0\rangle \to |x\rangle|x\rangle$: we end up with two copies of $|x\rangle$. However, if we try to

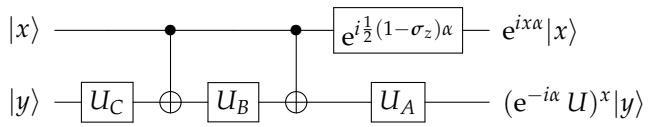

Figure 3.8: Quantum circuit acting as a cU, where $U_A\sigma_x U_B\sigma_x U_C = e^{-i\alpha}U$.

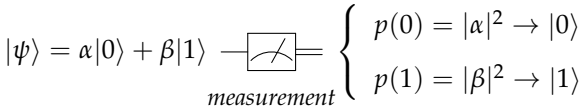

Figure 3.9: Circuit representing the measurement on the qubit $|\psi\rangle$: though the input is a superposition state, the outcome is either $|0\rangle$, with probability $p(0) = |\alpha|^2$, or $|1\rangle$, with probability $p(1) = |\beta|^2$.

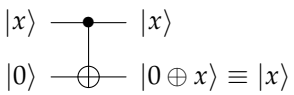

Figure 3.10: CNOT gate acting as a cloner of the classical bit $|x\rangle$.

use the same circuit to clone the qubit $|\psi\rangle$ of Eq. (2.6), we obtain:

$$\mathbf{C}_{10}|\psi\rangle|0\rangle = \alpha|0\rangle|0\rangle + \beta|1\rangle|1\rangle,$$

which is indeed different form the state $|\psi\rangle|\psi\rangle = \alpha^2|0\rangle|0\rangle + \alpha\beta(|0\rangle|1\rangle + |1\rangle|0\rangle) + \beta^2|1\rangle|1\rangle$, unless α or β vanishes, but this is exactly the classical case depicted in figure 3.10!

3.3.2 Bell states and Bell measurement

As we have seen in section 2.8 the pure state:

$$|\beta_{00}\rangle = \frac{|0\rangle|0\rangle + |1\rangle|1\rangle}{\sqrt{2}}, \tag{3.12}$$

is entangled since it cannot be written as a tensor product of the two single-qubit states. The state (3.12) is one of the four maximally entangled "Bell states":

$$|\beta_{xy}\rangle = \frac{|0\rangle|y\rangle + (-1)^x|1\rangle|\overline{y}\rangle}{\sqrt{2}}, \tag{3.13}$$

which can be produced starting from the separable state $|x\,y\rangle$ as depicted in figure 3.11. Note that the Bell states are a basis for the two-qubit space.

Indeed, the circuit to generate the Bell states is reversible and its inverse can be used to transform the Bell basis into the usual two-qubit computational basis $\{|0\rangle|0\rangle, |0\rangle|1\rangle, |1\rangle|0\rangle, |1\rangle|1\rangle\}$, as

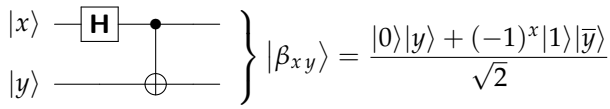

Figure 3.11: Quantum circuit to generate the Bell state $|\beta_{xy}\rangle$ from the separable state $|x\rangle|y\rangle$.

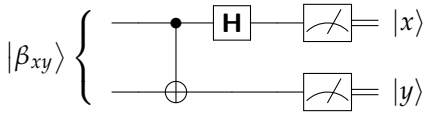

Figure 3.12: Quantum circuit to perform the Bell measurement: the maximally entangled state $|\beta_{xy}\rangle$ is transformed into the separable state $|x\,y\rangle$ and then measured.

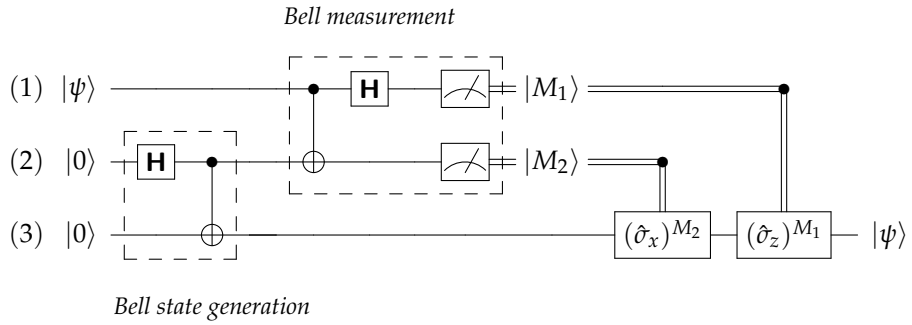

Figure 3.13: Quantum circuit to perform quantum teleportation.

sketched in figure 3.12. We can also expand the elements of the computational basis as a superposition of the Bell states, namely:

$$|x\rangle|y\rangle = \frac{1}{\sqrt{2}} \sum_{M=0,1} (\hat{\sigma}_z)^{Mx} \otimes \hat{\mathbb{I}} \, |\beta_{M\,x\oplus y}\rangle. \tag{3.14}$$

We use both the Bell generation and the Bell measurement in the next section to implement the so-called "quantum teleportation" protocol.

3.3.3 Quantum teleportation

As we pointed out, if we measure in the computational basis $\{|0\rangle, |1\rangle\}$ a qubit in a unknown quantum state, we will loose any information about it, obtaining as outcome just a classical bit $|x\rangle$ with a certain probability. However, it is sometimes necessary to *transfer* the state of a qubit from one part of a quantum computer to another. In this case, the state can be *teleported*, i.e., the unknown state $|\psi\rangle = \alpha|0\rangle + \beta|1\rangle$ of an input qubit can be reconstructed on a target qubit. The teleportation protocol requires two bits of classical information and a maximally entangled state.

In figure 3.13 we sketched the quantum circuit to implement quantum teleportation. The protocol takes as input the three-qubit state $|\psi\rangle|0\rangle|0\rangle$. The first step is to create an entangled state: following the procedure described in section 3.3.2, we create the Bell state $|\beta_{00}\rangle$ on the qubits 2 and 3 (see figure 3.13): this furnish the entanglement resource. At this stage the overall

three-qubit state reads:

$$|\psi\rangle|\beta_{00}\rangle = \frac{1}{\sqrt{2}}\left[\alpha|0\rangle|0\rangle|0\rangle + \beta|1\rangle|1\rangle|1\rangle + \alpha|0\rangle|1\rangle|1\rangle + \beta|1\rangle|0\rangle|0\rangle\right], \tag{3.15a}$$

$$= \frac{1}{\sqrt{2}}\left[|0\rangle|0\rangle\big(\alpha|0\rangle\big) + |1\rangle|1\rangle\big(\beta|1\rangle\big) + |0\rangle|1\rangle\big(\alpha\,\hat{\sigma}_x|0\rangle\big) + |1\rangle|0\rangle\big(\beta\,\hat{\sigma}_x|1\rangle\big)\right]. \tag{3.15b}$$

Now we should perform the Bell measurement (see again section 3.3.2) on qubits 1 and 2 by applying the gate $\mathbf{C}_{12}$ followed by $\mathbf{H}$ acting on qubit 1 and then measuring the two qubits in the computational basis. Since:

$$(\mathbf{H}\otimes\mathbb{1})\mathbf{C}_{12}|x\rangle|y\rangle = \frac{1}{\sqrt{2}}\sum_{M_1=0,1}(-1)^{M_1 x}|M_1\rangle|y\oplus x\rangle \tag{3.16a}$$

$$= \frac{1}{\sqrt{2}}\sum_{M_1=0,1}\left[(\hat{\sigma}_z)^{M_1 x}|M_1\rangle\right]|y\oplus x\rangle, \tag{3.16b}$$

after these transformations (but before the measurement!) the three-qubit state can be written in the following compact form:

$$(\mathbf{H}\otimes\mathbb{1})\mathbf{C}_{12}|\psi\rangle|\beta_{00}\rangle = \frac{1}{2}\sum_{M_1=0,1}\sum_{M_2=0,1}|M_1\rangle|M_2\rangle\otimes\left[(\hat{\sigma}_x)^{M_2}(\hat{\sigma}_z)^{M_1}(\alpha|0\rangle+\beta|1\rangle)\right], \tag{3.17}$$

where we used the identity (note the at the l.h.s. the operator $\hat{\sigma}_z$ act on the first qubit, whereas at the r.h.s. it acts on the third qubit):

$$\sum_{M_1=0,1}\left[(\hat{\sigma}_z)^{M_1}|M_1\rangle\right]|M_2\rangle\left[(\hat{\sigma}_x)^{M_2}|1\rangle\right] = \sum_{M_1=0,1}|M_1\rangle|M_2\rangle\left[(\hat{\sigma}_x)^{M_2}(\hat{\sigma}_z)^{M_1}|1\rangle\right], \tag{3.18}$$

with $M_2 = 0, 1$. It is now clear the a measurement carried out on qubits 1 and 2 with outcomes $|M_1\rangle$ and $|M_2\rangle$, respectively, leave the qubit 3 in the state:

$$(\hat{\sigma}_x)^{M_2}(\hat{\sigma}_z)^{M_1}(\alpha|0\rangle+\beta|1\rangle) \equiv (\hat{\sigma}_x)^{M_2}(\hat{\sigma}_z)^{M_1}|\psi\rangle. \tag{3.19}$$

Thus, in order to reconstruct the state of the input qubit onto the qubit 3 we should apply to Eq. (3.19) the unitary transformation $(\hat{\sigma}_x)^{M_2}(\hat{\sigma}_z)^{M_1}$.

It is worth noting that:

- only information is teleported, not matter;
- the input state is lost during the measurement (no-cloning theorem holds);
- no information about the input state is acquired through the measurement (the four outcomes $|M_1\,M_2\rangle$ do not contain any information about α an d β since they occur with the same probability, i.e., 25 %);
- the teleportation protocol is not instantaneous (one should send to the receiver by a classical channels the information about the two output classical bits $|M_1\rangle$ and $|M_2\rangle$);
- in order to reconstruct the state of a qubit we need two bits of classical information and the entanglement resource.

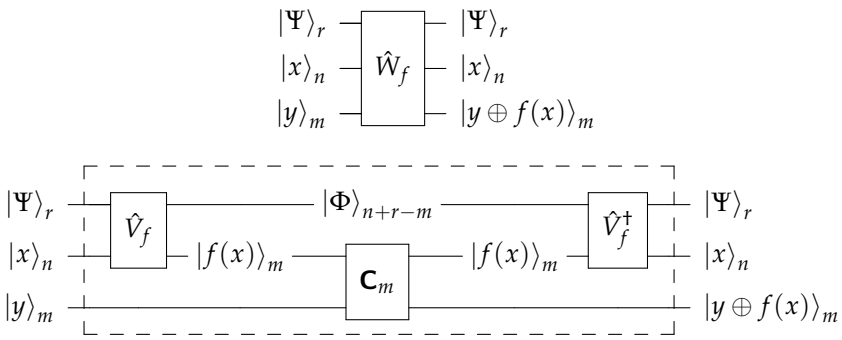

Figure 3.14: Realistic view of the structure of a unitary transformation $\hat{W}_f$ to carry out the calculation of $f(x)$. See the text for details.

3.4 The standard computational process

The goal of a computational process is to calculate the values $f(x)$ of some specified function f where x is encoded, with an accuracy which increases with n, in the computational-basis state of n qubits.

Since a quantum computer works with reversible operations, while $f(x)$ in general isn't, we should specify x and $f(x)$ as an n-bit and m-bit integers, respectively. Then we need at least $n+m$ qubits to perform the task. The set of n qubits, the *input register*, encodes x, the set of m-qubits, the *output register*, represents the value $f(x)$. Having separate registers for input and output is standard practice in the classical theory of reversible computation.

In order to perform the calculation of $f(x)$, we should apply a suitable unitary transformation $\hat{U}_f$ to our set of $n+m$ qubits. The standard computational protocol defines the action of $\hat{U}_f$ on every computational basis state $|x\rangle_n|y\rangle_m$ of the $n+m$ qubits making up the input and output registers as follows:

$$\hat{U}_f|x\rangle_n|y\rangle_m = |x\rangle_n|y \oplus f(x)\rangle_m, \tag{3.20}$$

where $\oplus$ can be seen as a generalized XOR acting on the single bits belonging to the two strings of bits y and $f(x)$. Indeed, $\hat{U}_f|x\rangle_n|0\rangle_m = |x\rangle_n|f(x)\rangle_m$: by initializing the starting output register to $|0\rangle_m$, after the computation it represents the actual value $f(x)$.

3.4.1 Realistic computation

The computation of $f(x)$ may require more than the $n+m$ qubit introduced in the section 3.4. In figure 3.14 it is sketched a more realistic quantum circuit to carry out the calculation of $f(x)$, where an additional register of r qubits and a unitary transformation $\hat{W}_f$ acting on $n+m+r$ qubit is used. As shown in the lower circuit of figure 3.14, the unitary $\hat{W}_f$ act as follows: the additional r-qubit state $|\Psi\rangle_r$ interact with the input register $|x\rangle_n$ through the unitary operation

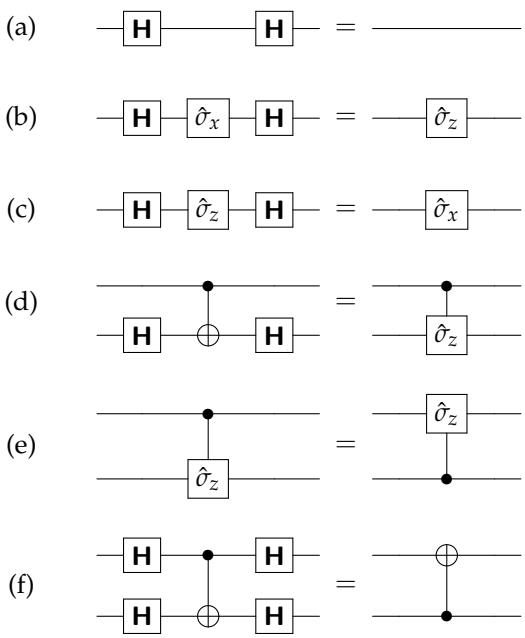

Figure 3.15: Useful circuit identities.

$\hat{V}_f$ obtaining the evolution:

$$\hat{V}_f|\Psi\rangle_r|x\rangle_n = |\Phi\rangle_{n+r-m}|f(x)\rangle_m. \tag{3.21}$$

Now, m controlled-NOT gates perform, bit by bit, the addition modulo 2 with the state of the output register (the control qubits are in the state $|f(x)\rangle_m$):

$$\mathbf{C}_m|f(x)\rangle_m|y\rangle_m = |f(x)\rangle_m|y \oplus f(x)\rangle_m. \tag{3.22}$$

A final unitary $\hat{V}_f^\dagger$ is used to obtain the transformation $\hat{V}_f^\dagger|\Phi\rangle_{n+r-m}|f(x)\rangle_m = |\Psi\rangle_r|x\rangle_n$.

3.5 Circuit identities

In figure 3.15 we report useful circuit identities that can be used to better understand the behavior of the quantum circuits described in the following sections. The reader can easily verify them. Here we explicitly consider the identity (f), namely, $\mathbf{H} \otimes \mathbf{H}\mathbf{C}_{10}\mathbf{H} \otimes \mathbf{H}$. Since $\mathbf{C}_{10} = \frac{1}{2}(\hat{\mathbb{I}} + \hat{\sigma}_z) \otimes \hat{\mathbb{I}} + \frac{1}{2}(\hat{\mathbb{I}} - \hat{\sigma}_z) \otimes \hat{\sigma}_x$ it is straightforward to verify that:

$$\mathbf{H} \otimes \mathbf{H}\mathbf{C}_{10}\mathbf{H} \otimes \mathbf{H} = \hat{\mathbb{I}} \otimes \frac{1}{2}(\hat{\mathbb{I}} + \hat{\sigma}_z) + \hat{\sigma}_x \otimes \frac{1}{2}(\hat{\mathbb{I}} - \hat{\sigma}_z) \equiv \mathbf{C}_{01}, \tag{3.23}$$

where we used the identities (b) and (c) of figure 3.15.

3.6 Introduction to quantum algorithms

As we have mentioned, a quantum algorithm involves two registers: the input register $|x\rangle_n$ and the output register $|y\rangle_m$. This is due to the reversibility of quantum operations: in general, a logical operation is not reversible, while the unitary operations indeed are. In this view, a quantum algorithm is similar to a classical reversible computation (of course, in the last case we cannot exploit the quantum features of qubits!).

We recall that the standard computational process that calculates $f(x)$, can be always represented as a suitable unitary operator $\hat{U}_f$ acting on the state $|x\rangle_n|y\rangle_m$, that is $\hat{U}_f|x\rangle_n|y\rangle_m = |x\rangle_n|y \oplus f(x)\rangle_m$.

Given a single qubit $|x\rangle$, $x = 0, 1$, the action of the Hadamard transformation $\mathbf{H}$ can be summarized as:

$$\mathbf{H}|x\rangle = \frac{|0\rangle + (-1)^x|1\rangle}{\sqrt{2}} \tag{3.24a}$$

$$= \frac{1}{\sqrt{2}} \sum_{z=0,1} (-1)^{xz}|z\rangle. \tag{3.24b}$$

Therefore, given an n-qubit state $|x\rangle_n$, with $0 \leq x < 2^n$ and $x = \sum_{k=0}^{n-1} x_k 2^k$ with $x_k \in \{0, 1\}$, we have:

$$\mathbf{H}^{\otimes n}|x\rangle_n = \left(\frac{|0\rangle + (-1)^{x_{n-1}}|1\rangle}{\sqrt{2}}\right) \otimes \cdots \otimes \left(\frac{|0\rangle + (-1)^{x_0}|1\rangle}{\sqrt{2}}\right) \tag{3.25a}$$

$$= \frac{1}{2^{n/2}} \sum_{z=0}^{2^n-1} (-1)^{x\cdot z}|z\rangle_n, \tag{3.25b}$$

where $x \cdot z = \oplus_{k=0}^{n-1} x_k z_k \pmod 2$.

It is also useful to note that if $f(x) \in \{0, 1\}$, then:

$$\hat{U}_f(\hat{\mathbb{I}} \otimes \mathbf{H})|x\rangle|1\rangle = |x\rangle \frac{|f(x)\rangle - |1 \oplus f(x)\rangle}{\sqrt{2}} \tag{3.26a}$$

$$= (-1)^{f(x)}|x\rangle \frac{|0\rangle - |1\rangle}{\sqrt{2}}. \tag{3.26b}$$

We will see that the factor $(-1)^{f(x)}$ is extremely important for quantum algorithms.

3.6.1 Deutsch algorithm

The first pedagogical algorithm we consider has been proposed to solve the so-called Deutsch problem. Given a function $f : \{0, 1\} \to \{0, 1\}$, suppose we are not interested in the *particular* values $f(0)$ and $f(1)$, but rather in a *relational* information, that is whether $f(0) = f(1)$ or $f(0) \neq f(1)$. Form the classical point of view, the only way to solve this problem is to evaluate

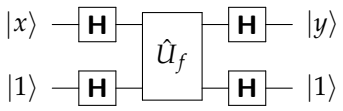

Figure 3.16: Quantum circuit to solve the Deutsch problem (Deutsch algorithm): if $f(0) = f(1)$ then $|y\rangle = |x\rangle$, otherwise $|y\rangle = |\overline{x}\rangle$, thus measuring the input register after the query we can discriminate between the two possible kind of functions.

$f(x)$ twice. We are going to show that a quantum algorithm can tell us the answer by using just one evaluation of the function. The circuit implementing the algorithm is shown in figure 3.16.

The first step of the algorithm is to apply the Hadamard transformations to the qubit initial states:

$$\mathbf{H} \otimes \mathbf{H}|x\rangle|1\rangle = \sum_z \frac{(-1)^{xz}}{\sqrt{2}}|z\rangle \left(\frac{|0\rangle - |1\rangle}{\sqrt{2}}\right) \tag{3.27}$$

where $z = 0, 1$. Now we apply $\hat{U}_f$:

$$\hat{U}_f \sum_z \frac{(-1)^{xz}}{\sqrt{2}}|z\rangle \left(\frac{|0\rangle - |1\rangle}{\sqrt{2}}\right) = \sum_z \frac{(-1)^{xz+f(z)}}{\sqrt{2}}|z\rangle \left(\frac{|0\rangle - |1\rangle}{\sqrt{2}}\right). \tag{3.28}$$

Finally, we apply again the Hadamard transformations, obtaining the following whole evolution:

$$(\mathbf{H} \otimes \mathbf{H})\, \hat{U}_f\, (\mathbf{H} \otimes \mathbf{H})|x\rangle|1\rangle = \sum_s c_f(x,s)|s\rangle|1\rangle, \tag{3.29}$$

where $s = 0, 1$, and we introduced the coefficients:

$$c_f(x,s) = \frac{1}{2}(-1)^{f(0)}\left[1 + (-1)^{x+s}(-1)^{f(1)-f(0)}\right]. \tag{3.30}$$

After the computation the output register has been left unchanged, since it is still in the state $|1\rangle$, while the input register has undergone the transformation:

$$|x\rangle \to \sum_s c_f(x,s)|s\rangle. \tag{3.31}$$

If $f(x) \in \{0,1\}$, then it is straightforward to verify that:

$$\begin{aligned} &- \text{if} \quad f(1) = f(0) \Rightarrow |c_f(x,x)|^2 = 1 \quad \text{and} \quad |c_f(x,\overline{x})|^2 = 0, \\ &- \text{if} \quad f(1) \neq f(0) \Rightarrow |c_f(x,x)|^2 = 0 \quad \text{and} \quad |c_f(x,\overline{x})|^2 = 1, \end{aligned}$$

therefore, if a measurement on the input register gives a result $|x\rangle$, we can conclude that $f(1) = f(0)$, if it leads to $|\overline{x}\rangle$, we have $f(1) \neq f(0)$. This happens after a single query of $\hat{U}_f$. Note that we do not know the actual value of $f(1)$ and $f(0)$: this is a typical quantum tradeoff that scarifies particular information to acquire relational information.

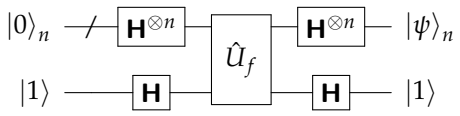

Figure 3.17: Quantum circuit to solve the Deutsch-Jozsa problem.

3.6.2 Deutsch-Jozsa algorithm

Now our function is $f : \{0,1\}^{\otimes n} \to \{0,1\}$, that is $f(x) \in \{0,1\}$ but $0 \leq x < 2^n$. We assume to know that f can only have the following two mutual exclusive properties:

- or f is *constant*: $f(x) = f(0), \forall x$;
- or f is *balanced*: $f(x) = 1$, for half of the possible 2^n values of x, otherwise $f(x) = 0$.

The problem is to decide if f is balanced.

In the best case a *deterministic* classical computer may solve the problem with just two queries [if $f(0) \neq f(1)$ then f is indeed balanced]. However in the worst case it could happen that the first $2^n/2 = 2^{n-1}$ queries give the same output, then we need one more query to answer the problem: if we have still the same result f is constant, otherwise it is balanced.

A classical *randomized* algorithm can indeed do better. This algorithm randomly chooses $m \leq 2^{n-1}$ values of x, obtaining the set $\{x^{(1)}, \ldots x^{(m)}\}$, and compare the value $f(x^{(k)})$ with that of $f(x^{(1)})$, $1 < k \leq m$. Given a balanced f and the value $f(x^{(1)})$, the probability that $f(x^{(k)}) = f(x^{(1)})$ is $1/2$. Therefore the *probability of failure*, that is the probability that $f(x^{(1)}) = f(x^{(k)})$, $\forall k$, is:

$$p_{\text{fail}}(m) = \underbrace{\frac{1}{2} \times \frac{1}{2} \times \ldots \times \frac{1}{2}}_{(m-1)\text{-times}} = \frac{1}{2^{m-1}}, \tag{3.32}$$

where we consider only $m-1$values of x because the first one is used as control. We thus obtain that after m queries, the probability of success, i.e., we find that f is balanced, is $p_{\text{succ}}(m) = 1 - p_{\text{fail}}(m)$.

In figure 3.17 we can see the quantum circuit to solve the Deutsch-Jozsa problem. The input states is the $n+1$ qubit state $|0\rangle_n|1\rangle$, and, after the application of the Hadamard transformations and the query of $\hat{U}_f$, we have:

$$\begin{aligned} \hat{U}_f(\mathbf{H}^{\otimes n} \otimes \mathbf{H})|0\rangle_n|1\rangle &= \hat{U}_f \left(\frac{1}{2^{n/2}} \sum_{x=0}^{2^n-1} |x\rangle_n \right) \left(\frac{|0\rangle - |1\rangle}{\sqrt{2}} \right) \\ &= \frac{1}{2^{n/2}} \sum_{x=0}^{2^n-1} (-1)^{f(x)} |x\rangle_n \left(\frac{|0\rangle - |1\rangle}{\sqrt{2}} \right). \end{aligned} \tag{3.33}$$

Now we should apply the Hadamard transformations:

$$(\mathbf{H}^{\otimes n} \otimes \mathbf{H})\,\hat{U}_f(\mathbf{H}^{\otimes n} \otimes \mathbf{H})|0\rangle_n|1\rangle = \frac{1}{2^n}\sum_{z=0}^{2^n-1}\sum_{x=0}^{2^n-1}(-1)^{z\cdot x+f(x)}|z\rangle_n|1\rangle \tag{3.34a}$$

$$= |\psi\rangle_n|1\rangle, \tag{3.34b}$$

where:

$$|\psi\rangle_n = \sum_{z=0}^{2^n-1} c_f(z)|z\rangle_n, \tag{3.35}$$

with

$$c_f(z) = \frac{1}{2^n}\sum_{x=0}^{2^n-1}(-1)^{z\cdot x+f(x)}. \tag{3.36}$$

We can focus on:

$$c_f(0) = \frac{1}{2^n}\sum_{x=0}^{2^n-1}(-1)^{f(x)}. \tag{3.37}$$

On the one hand, if $f(x)$ is *constant*, namely $f(x) = f(0)$, $\forall x$, we have $c_f(0) = (-1)^{f(0)}$, and, since $|\psi\rangle_n$ should be normalized, i.e., $\sum_z |c_f(z)|^2 = 1$, we obtain $c_f(z) = 0$, $\forall z \neq 0$. On the other hand, if $f(x)$ is *balanced* we get $c_f(0) = 0$, since the sum in Eq. (3.37) contains 2^{n-1} times the value "$+1$" and 2^{n-1} times the value "-1" and, thus, the corresponding state $|\psi\rangle_n$ does not contain $|0\rangle_n$.

Summarizing, the Deutsch-Jozsa algorithm leads to the following evolution of the n-qubit input register:

$$|0\rangle_n \rightarrow \begin{cases} |0\rangle_n & \text{if } f \text{ is constant,} \\ \sum_{z=1}^{2^n-1} c_f(z)|z\rangle_n & \text{if } f \text{ is balanced,} \end{cases} \tag{3.38}$$

therefore, just after a single call of U_f, a measurement of the evolved state of the input register allows us to decide if f is constant (we obtain $|0\rangle_n$) or balanced (in this last case we have $|x\rangle_n$, $x \neq 0$).

It is worth noting that: (i) there is not any known practical application of this kind of algorithm; (ii) the method used to evaluate $f(x)$ is different in the classical and in the quantum case; (iii) the probabilistic algoritms can find the solution of the Deutsch-Jozsa problem with high probability just after few (random) evaluations of $f(x)$.

□ **– Exercise 3.1** *Let us consider the Deutsch-Jozsa problem. Calculate the probability of finding a given $x \neq 0$ in the case of balanced f.*

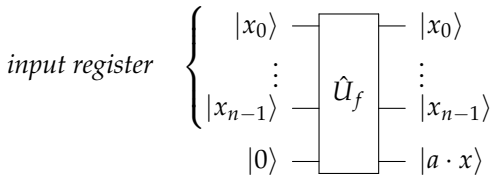

Figure 3.18: The Bernstein-Vazirani problem.

3.6.3 Bernstein-Vazirani algorithm

Let a be an unknown integer number, $0 \leq a < 2^n$ and consider the function:

$$f(x) = a \cdot x \equiv a_0 x_0 \oplus \cdots \oplus a_{n-1} x_{n-1}. \tag{3.39}$$

The problem is to find the unknown a given a subroutine that evaluates $f(x)$ for an integer $0 \leq x < 2^n$. Classically the only way to solve the problem is to evaluate $f(2^m) \equiv a_m$ for $m = 0, 1, \ldots, n-1$, which, thus, requires n evaluations of $f(x)$.

Figure 3.18 shows the quantum-circuit representation of the Bernstein-Vazirani problem. The input register encodes the n-qubit state $|x\rangle_n = |x_{n-1}\rangle \otimes \ldots \otimes |x_0\rangle$ while the output register, which is initialized to $|0\rangle$, after the evolution through the unitary operator $\hat{U}_f$ associated with the function defined in Eq. (3.39), becomes $|a \cdot x\rangle$.

The quantum circuit we need to solve the present problem with just one call of $\hat{U}_f$ is the same of the Deutsch-Jozsa problem (see figure 3.17). Since, now, the action of f is given in Eq. (3.39), the coefficients of the state in Eq. (3.35) read:

$$\begin{aligned} c_f(z) &= \frac{1}{2^n} \sum_{x=0}^{2^n-1} (-1)^{z \cdot x + a \cdot x} \\ &= \frac{1}{2^n} \prod_{k=0}^{n-1} \sum_{x_k=0,1} (-1)^{(z_k + a_k) x_k} \\ &= \frac{1}{2^n} \prod_{k=0}^{n-1} \left[1 + (-1)^{z_k + a_k} \right]. \end{aligned} \tag{3.40}$$

Form the last equality we conclude that if there exists k such that $z_k \neq a_k$, then $c_f(z) = 0$. Therefore we have:

$$c_f(z) \to \begin{cases} 0 & \text{if } z \neq a, \\ 1 & \text{if } z = a, \end{cases} \tag{3.41}$$

that is, the evolution of the input register can be summarized as:

$$|0\rangle_n \to |a\rangle_n, \tag{3.42}$$

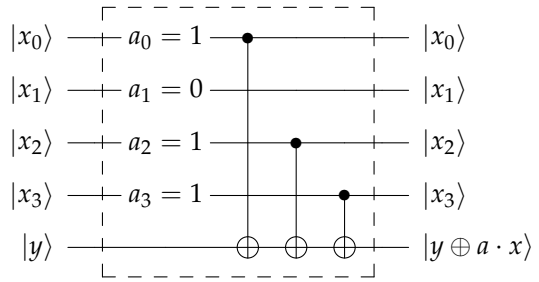

Figure 3.19: The quantum circuit to implement the Bernstein-Vazirani problem for $a = 1101$: if $a_k = 1$ then the bit k-th bit acts as control for the NOT operation on to the output register (lowest wire).

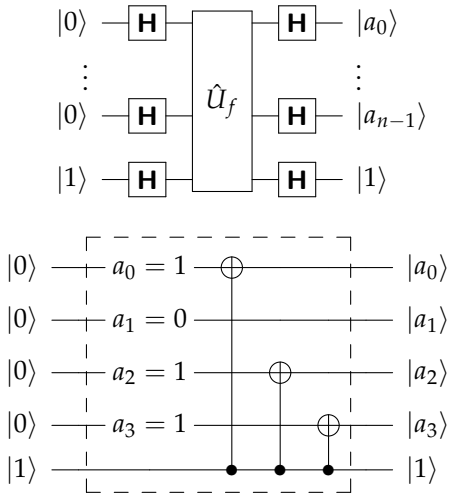

Figure 3.20: (Top) Quantum solution of the Bernstein-Vazirani problem. (Bottom) The equivalent quantum circuit to solve the problem for $a = 1101$: we used the identity $\mathbf{C}_{hk} = \mathbf{H}_h\mathbf{H}_k\mathbf{C}_{kh}\mathbf{H}_h\mathbf{H}_k$.

and the measurement of the evolved input register in the computational basis directly gives the unknown value of a.

A further investigation of the quantum circuit implementing $\hat{U}_f$ may explain the mechanism underling the Bernstein-Jozsa algorithm. In particular, in figure 3.19 we illustrate the quantum circuit, based on CNOT gates, used to calculate $f(x) = a \cdot x$ in the case of $n = 4$. It is clear that the value y of the output register is flipped only if a_k and x_k are both equal to 1, since the CNOT taking $|x_k\rangle$ as control bit is present in the circuit only if $a_k = 1$. As depicted in figure 3.20 (top), the solution of the problem consists in the application of the Hadamard transformation before and after the unitary U_f. But since $\mathbf{C}_{hk} = \mathbf{H}_h\mathbf{H}_k\mathbf{C}_{kh}\mathbf{H}_h\mathbf{H}_k$ (see exercise 1.7 and section 3.5), the resulting circuit is equivalent to the one depicted in figure 3.20 (bottom): it is now straightforward to see that by taking $|0\rangle_n$ and $|1\rangle$ as initial states of the input and output registers, respectively,

$\|x\rangle\|y\rangle\|z\rangle$	$\mathbf{T}\|x\rangle\|y\rangle\|z\rangle$
$\|0\rangle\|0\rangle\|0\rangle$	$\|0\rangle\|0\rangle\|0\rangle$
$\|0\rangle\|0\rangle\|1\rangle$	$\|0\rangle\|0\rangle\|1\rangle$
$\|0\rangle\|1\rangle\|0\rangle$	$\|0\rangle\|1\rangle\|0\rangle$
$\|0\rangle\|1\rangle\|1\rangle$	$\|0\rangle\|1\rangle\|1\rangle$
$\|1\rangle\|0\rangle\|0\rangle$	$\|1\rangle\|0\rangle\|0\rangle$
$\|1\rangle\|0\rangle\|1\rangle$	$\|1\rangle\|0\rangle\|1\rangle$
$\|1\rangle\|1\rangle\|0\rangle$	$\|1\rangle\|1\rangle\|1\rangle$
$\|1\rangle\|1\rangle\|1\rangle$	$\|1\rangle\|1\rangle\|0\rangle$

Table 3.1: The action of the Toffoli gate.

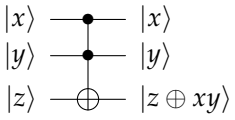

Figure 3.21: Quantum circuit for the Toffoli gate.

one has $|0\rangle_n \rightarrow |a\rangle_n$

3.7 Classical logic with quantum computers

3.7.1 The Toffoli gate

Any arithmetical operation can be built up on a reversible classical computer out of three-bit controlled-controlled-NOT (CCNOT) gates called Toffoli gates. The Toffoli gate, represented by the unitary operator $\mathbf{T}$, acts on a 3-bit state as follows:

$$\mathbf{T}|x\rangle|y\rangle|z\rangle = |x\rangle|y\rangle|z \oplus xy\rangle, \tag{3.43}$$

where xy corresponds to the arithmetical product between the values x and y. The action of the Toffoli gate onto the the computational basis is summarized in table 3.1. As one can see, $\mathbf{T}$ leaves unchanged the third bit, unless the state of the control bits are in the state $|1\rangle|1\rangle$, in this case the value of the target bit is flipped (see the last two lines of the table). Of course $\mathbf{T}$ is reversible and its action on the computational basis is a permutation. The quantum circuit for Toffoli gate is shown in figure 3.21.

As we mentioned in chapter 1, all the logical and, thus, arithmetical operations can be built up out of AND and NOT. By using the Toffoli gate one can calculate the logical AND of two

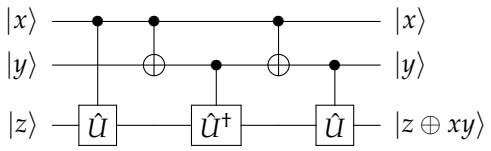

Figure 3.22: Quantum circuit acting as a CC-$\hat{U}^2$ gate based on CNOT and C-$\hat{U}$ gates. If we choose $\hat{U} = \sqrt{\hat{\sigma}_x}$ (the square root of NOT) we can reproduce the effect of the Toffoli gate.

bits, which corresponds to the product of their values, and the NOT, namely:

$$\text{AND} \rightarrow \mathbf{T}|x\rangle|y\rangle|0\rangle = |x\rangle|y\rangle|xy\rangle \equiv |x\rangle|y\rangle|x \wedge y\rangle, \tag{3.44a}$$

$$\text{NOT} \rightarrow \mathbf{T}|1\rangle|1\rangle|z\rangle = |1\rangle|y\rangle|z \oplus 1\rangle \equiv |1\rangle|1\rangle|\bar{z}\rangle, \tag{3.44b}$$

respectively. We demonstrated the universality of the Toffoli gate. Furthermore, we have:

$$\text{XOR} \rightarrow \mathbf{T}|1\rangle|y\rangle|z\rangle = |1\rangle|y\rangle|z \oplus y\rangle, \tag{3.45a}$$

$$\text{NAND} \rightarrow \mathbf{T}|x\rangle|y\rangle|1\rangle = |x\rangle|y\rangle|\overline{x \wedge y}\rangle, \tag{3.45b}$$

We can conclude that it is possible to do any computation reversibly.

We have seen the importance of the Toffoli gate. However, this gate cannot be realized by means of one- or two-bit classical gates. Fortunately, there exist quantum gates! In figure 3.22 is depicted a quantum circuit that acts as a controlled-controlled-$\hat{U}^2$ gate (a CC-$\hat{U}^2$), where $\hat{U}$ is a unitary operator ($\hat{U}\hat{U}^\dagger = \hat{U}^\dagger\hat{U} = \hat{\mathbb{I}}$), that involves only CNOT and controlled-$\hat{U}$ gates (C-$\hat{U}$). The reader can easily verify that the circuit applies the $\hat{U}^2$ operator to the state $|z\rangle$ of the output register only if the two-bit input register is $|x\rangle|y\rangle = |1\rangle|1\rangle$, namely:

$$|x\rangle|y\rangle|z\rangle \rightarrow \hat{\mathbb{I}} \otimes \hat{\mathbb{I}} \otimes \left[\hat{U}^y(\hat{U}^\dagger)^{x\oplus y}\hat{U}^x\right]|x\rangle|y\rangle|z\rangle. \tag{3.46}$$

If we now introduce the unitary operator:

$$\hat{U} = \sqrt{\hat{\sigma}_x} \rightarrow \frac{1}{1+i}\begin{pmatrix} 1 & i \\ i & 1 \end{pmatrix} \quad \text{(square root of NOT)} \tag{3.47}$$

such that $\hat{U}^2 = \sqrt{\hat{\sigma}_x}\sqrt{\hat{\sigma}_x} = \hat{\sigma}_x$, then the ccNOT can be obtained with the quantum circuit of figure 3.22. Note that $\sqrt{\hat{\sigma}_x}$ does not exist as a classical gate, but it exists as quantum gate, since:

$$\sqrt{\hat{\sigma}_x}|0\rangle = \frac{|0\rangle + i|1\rangle}{1+i}, \quad \text{and} \quad \sqrt{\hat{\sigma}_x}|1\rangle = \frac{i|0\rangle + |1\rangle}{1+i}. \tag{3.48}$$

3.7.2 The Fredkin gate

The Fredkin gate is another three-bit gate which can be used to build a universal set of gates. This gate has one control bit and two targets: when the control bit is 1 the targets are swapped,

$\lvert x\rangle\lvert y\rangle\lvert z\rangle$	$\mathbf{F}\lvert x\rangle\lvert y\rangle\lvert z\rangle$
$\lvert 0\rangle\lvert 0\rangle\lvert 0\rangle$	$\lvert 0\rangle\lvert 0\rangle\lvert 0\rangle$
$\lvert 0\rangle\lvert 0\rangle\lvert 1\rangle$	$\lvert 0\rangle\lvert 0\rangle\lvert 1\rangle$
$\lvert 0\rangle\lvert 1\rangle\lvert 0\rangle$	$\lvert 0\rangle\lvert 1\rangle\lvert 0\rangle$
$\lvert 0\rangle\lvert 1\rangle\lvert 1\rangle$	$\lvert 0\rangle\lvert 1\rangle\lvert 1\rangle$
$\lvert 1\rangle\lvert 0\rangle\lvert 0\rangle$	$\lvert 1\rangle\lvert 0\rangle\lvert 0\rangle$
$\lvert 1\rangle\lvert 0\rangle\lvert 1\rangle$	$\lvert 1\rangle\lvert 1\rangle\lvert 0\rangle$
$\lvert 1\rangle\lvert 1\rangle\lvert 0\rangle$	$\lvert 1\rangle\lvert 0\rangle\lvert 1\rangle$
$\lvert 1\rangle\lvert 1\rangle\lvert 1\rangle$	$\lvert 1\rangle\lvert 1\rangle\lvert 1\rangle$

Table 3.2: The action of the Fredkin gate.

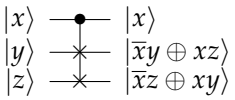

Figure 3.23: Quantum circuit for the Fredkin gate.

otherwise they are left unchanged. The action of the Fredkin gate, represented by the unitary operator $\mathbf{F}$, is summarized in table 3.2, whereas we show the corresponding quantum circuit in figure 3.23.

By suitably setting the input bits it is possible to implement any logical operation. For instance we have:

$$\text{AND} \to \mathbf{F}|x\rangle|y\rangle|0\rangle = |x\rangle|\overline{x} \wedge y\rangle|x \wedge y\rangle, \tag{3.49a}$$

$$\text{NOT} \to \mathbf{F}|x\rangle|0\rangle|1\rangle = |x\rangle|x\rangle|\overline{x}\rangle, \tag{3.49b}$$

therefore the Fredkin gate is universal. Note that in the last case we implemented both the COPY and the NOT operations at the same time.

3.8 Universal quantum gates

Universal quantum computation can be performed by means of any entangling interaction together with local unitaries, that is any unitary operator acting on a system of qubits can be reduced to a product of operators which entangle two qubits or act locally on a single qubit. In order to prove this claim, in this section first we show that any unitary acting on d levels can be decomposed in a product of unitaries acting at most on only two levels; then we prove that any two-level unitary can be implementsd by means of CNOT and single-qubit gates, the first ones being the entangling gates whereas the others perform local operations on the qubits.

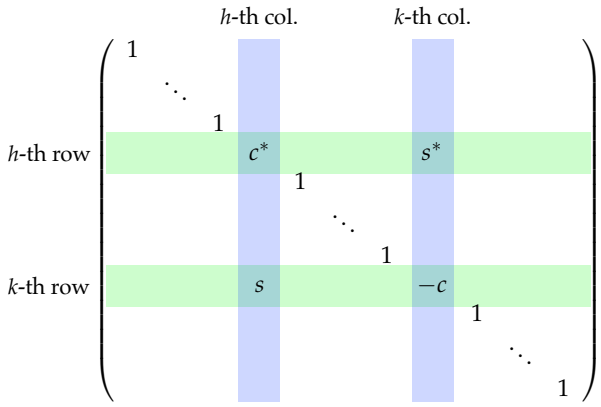

Figure 3.24: Matrix representation of the unitary transformation $\mathbf{G}(h,k)$.

3.8.1 Universality of two-level unitaries

Any unitary $\mathbf{U}$ acting on d levels can be decomposed in a product of two-level unitaries corresponding to suitable unitary transforms $\mathbf{G}(h,k)$, with $h < k$, acting on the levels h and k, $h,k \in \{1,\ldots,d\}$. The transformation $\mathbf{G}(h,k)$ can be seen as a $d \times d$ matrix whose elements are:

$$\begin{cases} g_{hh}(h,k) = c^*, \quad g_{kk}(h,k) = -c \\ g_{hk}(h,k) = s^*, \quad g_{kh}(h,k) = s \\ g_{pp}(h,k) = 1 \qquad\qquad\quad \text{if } p \neq h,k \\ g_{pq}(h,k) = 0 \qquad\qquad\quad \text{otherwise,} \end{cases} \tag{3.50}$$

where c and s are complex numbers (see figure 3.24). We will use this kind of transform to reduce $\mathbf{U}$ to a product of two-level unitaries, since when $\mathbf{G}(h,k)$ is applied to $\mathbf{U}$ it acts only on the two levels h and k.

In order to show how the method works, we focus on the simple three-level example (that is $d = 3$) and the reader will see that the extension to larger dimensions is straightforward. The basic idea is to exploit the transforms defined above to put equal to zero the matrix elements u_{p1} of the first column of $\mathbf{U}$, but u_{11} which is left equal to 1. We proceed as follows. If we choose $c = u_{11}/\mu$ and $s = u_{21}/\mu$, where $\mu = \sqrt{|u_{11}|^2 + |u_{21}|^2}$, we have (for the sake of clarity we focus on the first column only and use the symbol "$*$" for all the others):

$$\mathbf{G}(1,2)\,\mathbf{U} = \begin{pmatrix} \mu & * & * \\ 0 & * & * \\ u_{31} & * & * \end{pmatrix}. \tag{3.51}$$

It is clear that the action is to perform the transformation $u_{11} \to \mu$ and $u_{21} \to 0$ on the first column (as expected the element u_{31} is left unchanged). Now, acting in a similar way, we apply $\mathbf{G}(1,3)$ by setting $c = \mu/\mu'$ and $s = u_{31}/\mu'$, where $\mu' = \sqrt{\mu^2 + |u_{31}|^2} = 1$ (since $\mathbf{U}$ is unitary we

have $\sum_p |u_{p\tilde{q}}|^2 = \sum_q |u_{\tilde{p}q}|^2 = 1, \forall \tilde{p}, \tilde{q}$) and obtain:

$$\mathbf{G}(1,3)\,\mathbf{G}(1,2)\,\mathbf{U} = \begin{pmatrix} 1 & 0 & 0 \\ 0 & * & * \\ 0 & * & * \end{pmatrix} \equiv V_{2,3}. \tag{3.52}$$

Note that $V_{2,3}$ is a unitary operator acting on the two levels 2 and 3. Form Eq. (3.52) directly follows that $\mathbf{U}$ can be written as the product of the following two-levels unitary operators:

$$\mathbf{U} = V_{1,2} V_{1,3} V_{2,3}, \tag{3.53}$$

where $V_{1,2}^\dagger = G(1,2)$ and $V_{1,3}^\dagger = G(1,3)$.

For a generic dimension d, one should repeat the previous procedure to the other columns to obtain a final matrix of the form (only the non-zero elements are reported):

$$\begin{pmatrix} \mathbb{I}_{d-2} & & \\ & * & * \\ & * & * \end{pmatrix}, \tag{3.54}$$

which acts only on the last two levels. It is also possible to show that the number of needed two-level unitaries is at most $d(d-1)/2$. This concludes the proof of the universality of two-level unitaries.

It is worth noting that a system of n qubits encodes $d = 2^n$ levels, i.e., $|x\rangle_n = |x_{n-1}\rangle \dots |x_0\rangle$ with $x \in \{0, 1, \dots, 2^n - 1\}$ and $x_k \in \{0, 1\}$, and, thus, a two-level unitary may also couples two levels belonging to different qubits and the number of needed two-level unitaries is at most $2^n(2^{n-1} - 1)/2 \sim O(4^n)$. In the next section we will show that any two-level unitary can be implemented by using single-qubit and CNOT gates.

3.8.2 Universality of single-qubit and CNOT gates

For the sake of clarity (and simplicity!) here we focus on a system of three qubits, that is $d = 2^3 = 8$, spanned by the computational basis (levels):

$$\begin{aligned} &|0\rangle_3 = |0\rangle|0\rangle|0\rangle\,, \quad |1\rangle_3 = |0\rangle|0\rangle|1\rangle\,, \quad |2\rangle_3 = |0\rangle|1\rangle|0\rangle\,, \quad |3\rangle_3 = |0\rangle|1\rangle|1\rangle\,, \\ &|4\rangle_3 = |1\rangle|0\rangle|0\rangle\,, \quad |5\rangle_3 = |1\rangle|0\rangle|1\rangle\,, \quad |6\rangle_3 = |1\rangle|1\rangle|0\rangle\,, \quad |7\rangle_3 = |1\rangle|1\rangle|1\rangle\,. \end{aligned} \tag{3.55}$$

We consider a unitary matrix 8×8 matrix $\mathbf{U}$ acting only on the two levels $|x\rangle_3$ and $|y\rangle_3$, $x < y$, which has the following entries (see figure 3.25):

$$\begin{cases} u_{x+1\,x+1} = \alpha\,, & u_{x+1\,y+1} = \gamma\,, \\ u_{y+1\,x+1} = \beta\,, & u_{y+1\,y+1} = \zeta\,, \\ u_{pp} = 1 & \text{if } p \neq x+1, y+1 \\ u_{pq} = 0 & \text{otherwise,} \end{cases} \tag{3.56}$$

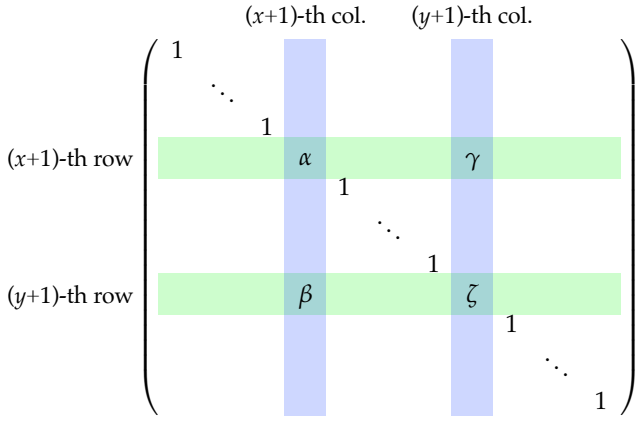

Figure 3.25: Matrix representation of the unitary $\mathbf{U}$.

which acts as follows:

$$\begin{cases} \mathbf{U}|x\rangle_3 = \alpha|x\rangle_3 + \beta|y\rangle_3\,, & \mathbf{U}|y\rangle_3 = \gamma|x\rangle_3 + \zeta|y\rangle_3\,, \\ \mathbf{U}|p\rangle_3 = |p\rangle_3 & \text{if } p \neq x, y. \end{cases} \tag{3.57}$$

We look for a quantum circuit implementing $\mathbf{U}$, built from single-qubit and CNOT gates. The trick is to use the so-called *Gray codes*: a Gray code connetting two binary number x and y is a sequence of m binary numbers $\{b_1, b_2, \dots b_m\}$ starting from $b_1 = x$ and arriving at $b_m = y$, such that adjacent numbers differ in exactly one bit.

As an example, we consider $x = 0$ and $y = 7$, that is, $|x\rangle_3 = |0\rangle|0\rangle|0\rangle$ and $|y\rangle_3 = |1\rangle|1\rangle|1\rangle$. The Gray code connecting the two numbers (or, equivalently, states), is (for the sake of clarity we added a subscript to identify the three qubits):

$$|0\rangle_3 = |0\rangle_A|0\rangle_B|0\rangle_C \tag{3.58a}$$
$$|0\rangle_A|0\rangle_B|1\rangle_C \tag{3.58b}$$
$$|0\rangle_A|1\rangle_B|1\rangle_C \tag{3.58c}$$
$$|1\rangle_A|1\rangle_B|1\rangle_C = |7\rangle_3\,. \tag{3.58d}$$

To pass from one element to the adjacent one, we can easily use CCNOT gates (NOT gates controlled by two qubits), which have as target the only different bit (here qubit A) and uses the values of the others as control (here B and C). We can use this strategy to connect step-wise $|x\rangle_3 = |0\rangle_A|0\rangle_B|0\rangle_C$ to $|0\rangle_A|1\rangle_B|1\rangle_C$, the element just before $|y\rangle_3 = |1\rangle_A|1\rangle_B|1\rangle_C$, and then act with a CC-$\mathbf{U}_{xy}$ *on the first qubit*, namely, the unitary operator $\mathbf{U}_{xy}$ defined as the 2×2 matrix:

$$\mathbf{U}_{xy} = \begin{pmatrix} \alpha & \gamma \\ \beta & \zeta \end{pmatrix} \tag{3.59}$$

is applied to qubit A only if the others are in the state $|1\rangle_B|1\rangle_C$. Finally, we apply the same CCNOT gates, but in the reversed order. The overall circuit is shown in figure 3.26. The action

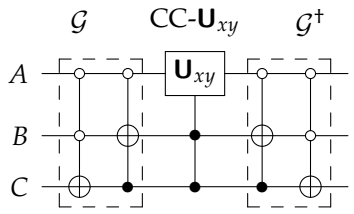

Figure 3.26: Quantum circuit implementing a unitary $\mathbf{U}_{xy}$ acting on the two levels (or states) $|x\rangle_3 = |0\rangle_A|0\rangle_B|0\rangle_C$ and $|y\rangle_3 = |1\rangle_A|1\rangle_B|1\rangle_C$.

of the first two gates can be summarized an operator G such that:

$$\mathcal{G}|0\rangle_3 = |0\rangle_A|1\rangle_B|1\rangle_C\,, \tag{3.60}$$

$$\mathcal{G}|7\rangle_3 = |1\rangle_A|1\rangle_B|1\rangle_C\,, \tag{3.61}$$

whereas when it is applied to the other states $|p\rangle_3$, with $p \neq 0, 7$, the final state of qubit B and C is $|0\rangle_B|0\rangle_C$ or $|b\rangle_B|c\rangle_C$, with $b \neq c$. Therefore, CC-$\mathbf{U}_{xy}$ can act non trivially only on the two states $|0\rangle_A|1\rangle_B|1\rangle_C$ and $|1\rangle_A|1\rangle_B|1\rangle_C$, that is:

$$\begin{aligned}\text{CC-}\mathbf{U}_{xy}\,\mathcal{G}|0\rangle_3 &= \text{CC-}\mathbf{U}_{xy}|0\rangle_A|1\rangle_B|1\rangle_C \\ &= \alpha|0\rangle_A|1\rangle_B|1\rangle_C + \beta|1\rangle_A|1\rangle_B|1\rangle_C\,,\end{aligned} \tag{3.62}$$

$$\begin{aligned}\text{CC-}\mathbf{U}_{xy}\,\mathcal{G}|7\rangle_3 &= \text{CC-}\mathbf{U}_{xy}|1\rangle_A|1\rangle_B|1\rangle_C \\ &= \gamma|0\rangle_A|1\rangle_B|1\rangle_C + \zeta|1\rangle_A|1\rangle_B|1\rangle_C\,,\end{aligned} \tag{3.63}$$

$$\text{CC-}\mathbf{U}_{xy}\,\mathcal{G}|p\rangle_3 = \mathcal{G}|p\rangle_3\,, \quad \text{if } |p\rangle_3 \neq |0\rangle_3, |7\rangle_3\,, \tag{3.64}$$

since $\mathbf{U}_{xy}|0\rangle_A = \alpha|0\rangle_A + \beta|1\rangle_A$ and $\mathbf{U}_{xy}|1\rangle_A = \gamma|0\rangle_A + \zeta|1\rangle_A$. Finally, the action of $\mathcal{G}^\dagger$ leads to the wanted transformation:

$$\begin{cases} \mathcal{G}^\dagger\,\text{CC-}\mathbf{U}_{xy}\,\mathcal{G}|0\rangle_3 = \alpha|0\rangle_3 + \beta|1\rangle_3\,, \\ \mathcal{G}^\dagger\,\text{CC-}\mathbf{U}_{xy}\,\mathcal{G}|7\rangle_3 = \gamma|0\rangle_3 + \zeta|1\rangle_3\,, \\ \mathcal{G}^\dagger\,\text{CC-}\mathbf{U}_{xy}\,\mathcal{G}|p\rangle_3 = |p\rangle_3\,, \qquad \text{if } |p\rangle_3 \neq |0\rangle_3, |7\rangle_3\,, \end{cases} \tag{3.65}$$

that is $\mathcal{G}^\dagger\,\text{CC-}\mathbf{U}_{xy}\,\mathcal{G} \equiv \mathbf{U}$, as one can also see from Eq. (3.57) with $x = 0$ and $y = 7$. We note that the controlled-controlled gates acting on the three qubits can be implemented using only CNOT and single-qubit gates (see figure 3.22).

In the general case of n qubits, where we have 2^n levels, one can extend the previous protocol based on Gray codes. If $|g_1\rangle_n, |g_2\rangle_n, \ldots, |g_m\rangle_n$ are the m elements of the Gray code connecting $|g_1\rangle_n = |x\rangle_n$ and $|g_m\rangle_n = |y\rangle_n$, we can always find a code such that $m \leq n+1$ (in fact $|x\rangle_n$ and $|y\rangle_n$ can differ in at most n locations). By using controlled gates we pass from $|g_1\rangle_n$ to $|g_{m-1}\rangle_n$, then we apply the controlled $\mathbf{U}_{xy}$ to the qubit located at the single bit where $|g_{m-1}\rangle_n$ and $|g_m\rangle_n$,

finally we undo the transformations of the first stage. Concerning the implementation, one can easily extend the scheme presented in figure 3.22 to system involving more than three qubits by suitably adding other CNOT and single-qubit gates. Therefore, thanks to the result obtained in the previous section (the universality of two-level unitaries), we have eventually proved also that CNOT and single-qubit gates are universal.

We note that the implementation of a unitary operation acting on n qubit requires a quantum circuit containing $O(n^2 4^n)$ single-qubit and CNOT gates. In fact, a two-level unitary requires $O(n^2)$ gates ($\mathcal{G}$ and the CC-$\mathbf{U}_{xy}$ both need $O(n)$ CNOT and single-qubit gates) and an arbitrary unitary requires $O(4^n)$ gates, as shown in the previous section. As a matter of fact, the approach followed in this universality construction does not provide efficient quantum circuits... In order to find fast algorithms one should use a different approach.

3.8.3 Hadamard, phase, CNOT and T gates are universal

We have shown that single-qubit and CNOT gates can be used to perform universal quantum computation. However, there isn't a straightforward method to implement all these to be resistant to errors. On the other hand, it is possible to find a discrete set of gates to *approximate* any unitary operation. The *standard set* of universal gates consists of the Hadamard, phase, CNOT and T (or $\frac{\pi}{8}$ gate), introduced in section 3.1. In reality Hadamard, CNOT and T gates may approximate a quantum circuit, but the presence of the phase gate, that is T^2, is justified since it allows to approximate the circuit fault-tolerantly.

Bibliography

- M. A. Nielsen and I. L. Chuang, *Quantum Computation and Quantum Information* (Cambridge University Press, 2010) – Chapter 1, Chapter 4.5.
- N. D. Mermin, *Quantum Computer Science* (Cambridge University Press, 2007) – Chapter 2.
- C.-K. Li, R. Roberts and X. Yin, *Decomposition of unitary matrices and quantum gates*, e-print arXiv:1210.7366 [quant-ph].

Chapter 4

Universal computers and computational complexity

IN THIS CHAPTER we (really) briefly describe two important examples of "universal computers": the *Turing machine* and its quantum counterpart, the *quantum Turing machine*. These "machines" are useful to check computability and efficiency of algorithms without specifying a particular hardware implementation, that is one of the main tasks of computer science. For the sake of completeness we also introduce the main complexity classes (P, NP and their quantum analogue BQP and QMA).

4.1 The Turing machine

The Turing machine is the simplest example for a *universal quantum computer*. We define the deterministic Turing machine as a discrete-time dynamical system, with an infinite input/output tape, a head to read and write symbols on the tape and a set of internal state. To these states belongs also the so-called "halt" state, in which the machine stops.

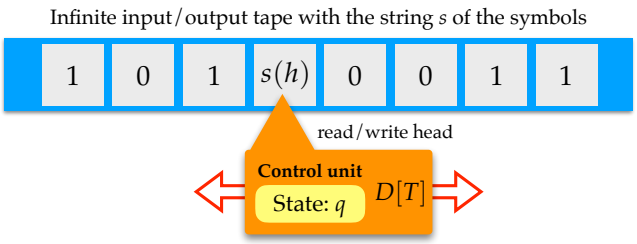

Figure 4.1: Schematic view of a Turing machine.

The configuration of a Turing machine can be defined as $C = (q_C, h_C, s_C)$, where q_C is the internal state of the machine, h_C the head position and s_C is the symbol on the tape. The particular symbol at position h on the tape, is given by $s(h)$ (see figure 4.1). The classical transition rules, given an internal state p and a read symbol σ, can be defined as $\delta_c(p, \sigma) = (\tau, q, d)$, namely, the machine writes the symbol τ on the tape, changes its internal state to q and moves the head position from h to $h + d$, where $d = +1$ ($d = -1$) corresponds to a step to the right (left). If, for instance, $\delta_c\big(q_C, s_C(h_C)\big) = (\tau, q, d)$, we have the transition:

$$(q_C, h_C, s_C) \to (q, h_C + d, s_C^\tau), \tag{4.1}$$

where $s_C^\tau(h_C) = \tau$ whereas $s_C^\tau(j) = s_C(j)$ for $j \neq h_C$. A computation is carried out by a suitable definition of the transition rules and the number of steps required to complete the computation is related to the complexity of the problem.

Though the Turing machine has no a practical interest, it is worth noting that every task that can be performed by a computer can be performed by a Turing machine. In fact, according to the Church-Turing thesis, *every function which would be naturally regarded as computable can be computed by the universal Turing machine* (there is also a strong Church-Turing thesis: *Any model of computation can he simulated on a probabilistic Turing machine with at most a polynomial increase in the number of elementary operations required*). A universal Turing machine T_U can simulate every Turing machine T given its description $D[T]$, namely, a binary number encoding the set of its transition rules. In particular, the number of steps used by T_U to simulate a given T is a polynomial function of the length of the number $D[T]$. If x is the input and $T(x)$ the output of the Turing machine T, then $T_U\big(D[T], x\big) = T(x)$.

4.2 The quantum Turing machine

The quantum version of the Turing machine, the quantum Turing machine, is characterized by a quantum state $|C\rangle$ corresponding to its configuration, that is a vector in a suitable Hilbert space. We can write the configuration as:

$$|C\rangle = |q_C\rangle|h_C\rangle|s_C\rangle. \tag{4.2}$$

The reader can see that the internal state, the head position and the symbol on the tape are now substituted by quantum states. The evolution, now, is not deterministic, but is described by a unitary U determined by the quantum transition function:

$$\delta(p, \sigma; \tau, q, d) \in \mathbb{C}, \tag{4.3}$$

that is the amplitude of the classical transition $(p, \sigma) \to (\tau, q, d)$. Therefore, we have:

$$U|C\rangle = \sum_{\tau,q,d} \delta\big(q_C, s_C(h_C); \tau, q, d\big)\, |q\rangle|h_C + d\rangle|s_C^\tau\rangle. \tag{4.4}$$

The result of the computation is obtained by measuring the tape... after the computation has been completed. And this is an issue, since the computation is completed when the internal state $|q\rangle$ is found the halt state, but to check it one should perform a measurement which may disturb (an usually it does) the computation itself. In order to solve the problem, Deutsch proposed to introduce an additional qubit, the *halt qubit*, and an observable $\hat{n}_0$ to monitor it. When the internal state is is different from the halt state, the halt qubit is $|0\rangle$, but in the presence of the halt state, its value is $|1\rangle$. Therefore, one initializes the halt qubit to $|0\rangle$ and a valid algorithm sets its value to $|1\rangle$ only at the end of the computation, without interacting with it otherwise. The observable $\hat{n}_0$, according to Deutsch, can be periodically observed from the outside, without affecting the operation of the machine.

4.3 Important classical and quantum complexity classes

In this section we focus on the so-called *decision problems*, namely, problems whose question can be posed as a yes-no question. Nevertheless, decision problems are closely related to *function problems*, where the problem is to compute the values of a given function. The space containing decision problems that can be solved by a Turing machine using a polynomial amount of space is called PSPACE.

In general, a computational problem can be classified according to several measures of complexity. The thorough analysis of complexity theory is beyond the scope of these notes and here we mention only some important classes (the interested interested reader can find a thorough analysis of the complexity classes zoo in the suggested Bibliography.).

Let us consider a task to be performed on an integer number x (the input of our computation). Depending on the particular task, a Turing machine will (hopefully) require a given number of steps s to solve it. As a matter of fact, s depends on x (for instance, factorizing a small integer requires less steps than the factorization of a 20-digit integer!). The computational complexity of the task characterizes how the number s increases with the number of bit needed to encode x, namely, $L = \log_2 x$. For instance, if the task is the calculation of x^2, we can find *an algorithm* such that, roughly, $s \propto L^2$. When s is a *polynomial* function of L, as in the latter case, we say that the problem belongs to the complexity class P (*polynomial in time*). If s rises exponentially with L, the problem is considered *hard*.

However, in many cases verify the solution is much easier than to find it. It is the case of the factorization of large integer: for the best algorithm we know (today...) we have $s \propto \exp\left(\sqrt[3]{\frac{64}{9} L \log L}\right)$. This kind of decision problems belong to the class NP, where NP means *nondeterministic polynomial*. A nondeterministic polynomial algorithm may at any step follows two different paths which are followed in parallel: one can perform an exponential number of calculations in polynomial time (at the expense of the computational capacity, that grows

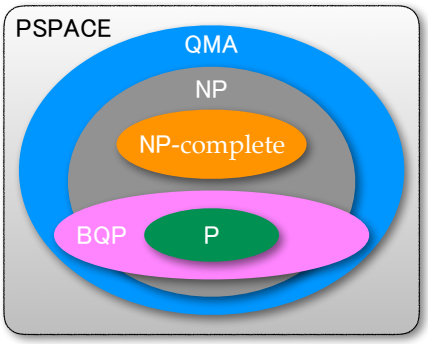

Figure 4.2: Relation between some important complexity classes discussed in the text.

exponentially...). In order to verify the solution one simply follows, in polynomial time, the right path of the tree-like algorithm.

Another important complexity class contains the so-called NP-complete problems. We recall that a problem P_2 is *reducible* or *polynomially reducible* to a problem P_1, if the solution of P_2 can be found by applying P_1 a polynomial number of times (one also say that "P_2 cannot be harder than P_1"). A problem is NP-complete if any NP problem can be reduced to it. A typical NP-complete problem is the *travelling salesman problem*: given a list of cities and the distances between each pair of them, find the shortest possible route that visits each city exactly once and returns to the origin city. More precisely, the class NP-complete corresponds to the intersection between the class NP and the class NP-hard, the latter being the set of problems (not only decision problems, but also optimization problems and so on). We can also say that a NP-hard problem is at least as hard as the hardest problems in NP. One of the most fundamental problems of theoretical quantum computer science is to find whether P and NP coincide: if somebody finds a polynomial solution for any NP-complete problem, then $\mathsf{P} = \mathsf{NP}$.

While the *travelling salesman problem* is an optimization problem belonging to both NP-hard and NP-complete, there are decision problems that are NP-hard but not NP-complete, for example the *halting problem*: suppose to have a Turing machine T with description $D[T]$, will the machine stop for a given input x? It is possible to show that NP-complete problems can be reduced to this problem; but it is also well-known that it is an example of *unsolvable* problem, thus, not complete! This can be proved by supposing that there exists a universal Turing machine T_H with description $D[T_H]$ such that "$T_H(D[T])$ halts iff $T(D[T])$ does not halt" (we are using as input for the machines binary number $D[T]$). But if we put now $T \equiv T_H$ we have the clear contradiction "$T_H(D[T_H])$ halts iff $T_H(D[T_H])$ does not halt"!! This is the argument used by the same Turing to prove that a general algorithm to decide whether a Turing machine stops does not exist.

In figure 4.2 we show a pictorial view of the relation between the complexity classes P, NP and NP-complete. In the same figure we also report the two most important quantum com-

plexity classes: the class BQP (*bound-error quantum polynomial time*) and the class QMA (*quantum Merlin Arthur*). The BQP is the class of decision problems which can be solved by a quantum computer in polynomial time, with an error probability of at most $1/3$ for all instances. To this class belongs, in particular, the Shor's factorization algorithm: it requires $s \propto L^2 \log L \log\log L$, this demonstrating that the integer factorization problem can be efficiently solved on a quantum computer and is thus in the complexity class BQP. The last class we mention is the QMA, the quantum analog of the class NP: it is related to BQP in the same way NP is related to P. Roughly speaking, the class QMA contains the decision problems for which the proofs (given by the oracle, Merlin, with infinite power) should be verifiable in polynomial time on a quantum computer: if the answer is positive, the verifier (Arthur) accepts a correct proof with probability greater than $2/3$, otherwise there is no proof which convinces the verifier to accept with probability greater than $1/3$.

Bibliography

- J. Stolze and D. Suter, *Quantum Computing: A Short Course from Theory to Experiment* (Wiley-VCH, 2004) – Chapter 3.3.
- M. Ozawa, *Quantum Nondemolition Monitoring of Universal Quantum Computers*, Phys. Rev. Lett. **80**, 631-634 (1998).
- D. Deutsch, *Quantum Theory, the Church-Turing Principle and the Universal Quantum Computer*, Proc. R. Soc. London A **400**, 97 (1985).
- J. Watrous, in *Meyers R. (eds) Encyclopedia of Complexity and Systems Science* (Springer, New York, NY, 2009).
- M. A. Nielsen and I. L. Chuang, *Quantum Computation and Quantum Information* (Cambridge University Press, 2010) – Chapter 3.2, Chapter 4.5.5.

Chapter 5

The Quantum Fourier Transform and the factoring algorithm

IN THIS CHAPTER we introduce the Quantum Fourier Transform (QFT) which is a key ingredient of many quantum protocols. We apply the QFT to the phase estimation problem and we address the factoring algorithm.

5.1 Discrete Fourier transform and QFT

The discrete Fourier transform maps a vector $(x_1, \ldots, x_N)$ of N complex numbers into a new vector $(y_1, \ldots, y_N)$, where:

$$y_h = \frac{1}{\sqrt{N}} \sum_{k=1}^{N} \exp\left(2\pi i \frac{h\,k}{N}\right) x_k\,. \tag{5.1}$$

In a similar way we can define the QFT. Given the n-qubit state $|x\rangle_n = \bigotimes_{m=0}^{n-1} |x_m\rangle = |x_{n-1}\rangle|x_{n-2}\rangle \ldots |x_0\rangle$, where x is an integer number, $0 \leq x < 2^n$, and $x_{n-1}x_{n-2}\ldots x_0$ is its binary representation, namely, $x = \sum_{k=0}^{n-1} x_k\, 2^k$, with $x_k \in \{0, 1\}$, we have:

$$\hat{F}_Q |x\rangle_n = \frac{1}{2^{n/2}} \sum_{y=0}^{2^n-1} \exp\left(2\pi i \frac{x\,y}{2^n}\right) |y\rangle_n. \tag{5.2}$$

Since $|y\rangle_n = \bigotimes_{m=0}^{n-1} |y_m\rangle$ and $y = \sum_{m=0}^{n-1} y_m\, 2^m$, we can write Eq. (5.2) as:

$$\hat{F}_Q |x\rangle_n = \frac{1}{2^{n/2}} \sum_{y_{n-1}=0}^{1} \cdots \sum_{y_0=0}^{1} \bigotimes_{m=0}^{n-1} \exp\left(2\pi i \frac{x\,y_m}{2^{n-m}}\right) |y_m\rangle \tag{5.3}$$

$$= \frac{1}{2^{n/2}} \bigotimes_{m=0}^{n-1} \left[|0_m\rangle + \exp\left(2\pi i \frac{x}{2^{n-m}}\right) |1_m\rangle\right] = \bigotimes_{m=0}^{n-1} |\psi_m\rangle, \tag{5.4}$$

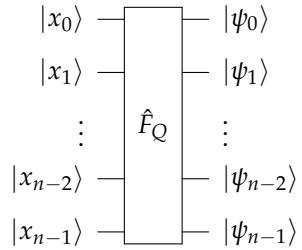

Figure 5.1: Quantum Fourier transform: the input n-qubit state $|x\rangle_n = \bigotimes_{k=0}^{n-1} |x_k\rangle = |x_{n-1}\rangle \dots |x_0\rangle$ is transformed into the output n-qubit state $\bigotimes_{k=0}^{n-1} |\psi_k\rangle = |\psi_{n-1}\rangle \dots |\psi_0\rangle$. See text for details.

where we defined:

$$|\psi_m\rangle = \frac{1}{\sqrt{2}} \left[|0_m\rangle + \exp\left(2\pi i \frac{x}{2^{n-m}}\right) |1_m\rangle \right].$$

In figure 5.1 we show the action of the QFT on the state $|x\rangle_n$.

In order to find the quantum circuit implementing the QFT, instead of the transformation (5.4) it is better to consider the following one (for the sake of simplicity we use the same symbol $\hat{F}_Q$ for both the operations):

$$\hat{F}_Q |x\rangle_n = \frac{1}{2^{n/2}} \bigotimes_{m=1}^{n} \left[|0_{n-m}\rangle + \exp\left(2\pi i \frac{x}{2^m}\right) |1_{n-m}\rangle \right], \tag{5.5a}$$

$$= \frac{1}{2^{n/2}} \bigotimes_{m=0}^{n-1} \left[|0_{n-m-1}\rangle + \exp\left(2\pi i \frac{x}{2^{m+1}}\right) |1_{n-m-1}\rangle \right] \tag{5.5b}$$

$$= \bigotimes_{m=0}^{n-1} |\psi_{n-m-1}\rangle. \tag{5.5c}$$

The subtle difference between (5.4) and (5.5a) is that the overall action of the first one can be summarized as:

$$\begin{aligned} |x_0\rangle &\rightarrow |\psi_0\rangle, \\ |x_1\rangle &\rightarrow |\psi_1\rangle, \\ &\vdots \\ |x_{n-1}\rangle &\rightarrow |\psi_{n-1}\rangle, \end{aligned}$$

while in the second case we have:

$$\begin{aligned} |x_0\rangle &\rightarrow |\psi_{n-1}\rangle, \\ |x_1\rangle &\rightarrow |\psi_{n-2}\rangle, \\ &\vdots \\ |x_{n-1}\rangle &\rightarrow |\psi_0\rangle, \end{aligned}$$

or, in a more compact form (for the sake of simplicity we drop the subscripts):

$$|x_m\rangle \rightarrow |\psi_{n-m-1}\rangle = \frac{1}{\sqrt{2}} \left[|0\rangle + \exp\left(2\pi i \frac{x}{2^{m+1}}\right) |1\rangle \right]. \tag{5.6}$$

Note that we can also write:

$$\exp\left(2\pi i\,\frac{x}{2^{m+1}}\right)=\prod_{k=0}^{n-1}\exp\left(2\pi i\,\frac{x_k 2^k}{2^{m+1}}\right), \tag{5.7}$$

where we used $x=\sum_{k=0}^{n-1}x_k 2^k$. By introducing the function:

$$f_m(z,k)=\begin{cases}\exp\left(2\pi i\,\frac{z}{2^{m-k+1}}\right) & \text{if } 0\leq k<m,\\ (-1)^z & \text{if } k=m,\\ 1 & \text{if } m<k<n,\end{cases} \tag{5.8}$$

with $z\in\{0,1\}$, we have:

$$\begin{aligned}|x_m\rangle &\to \frac{1}{\sqrt{2}}\left[|0\rangle+\prod_{k=0}^{n-1}f_m(x_k,k)\,|1\rangle\right]\\ &\to \frac{1}{\sqrt{2}}\left[|0\rangle+\prod_{k=0}^{m}f_m(x_k,k)\,|1\rangle\right].\end{aligned} \tag{5.9}$$

If we now define the operator $\hat{R}_h(z)$, such that:

$$\hat{R}_h(z)|0\rangle=|0\rangle,\quad\text{and}\quad\hat{R}_h(z)|1\rangle=\exp\left(2\pi i\,\frac{z}{2^h}\right)|1\rangle, \tag{5.10}$$

which corresponds to the 2×2 matrix:

$$\hat{R}_h(z)\to\begin{pmatrix}1 & 0\\ 0 & \exp\left(2\pi i\,\frac{z}{2^h}\right)\end{pmatrix}, \tag{5.11}$$

we can write (for $m>0$):

$$|x_m\rangle\to\frac{1}{\sqrt{2}}\left[|0\rangle+\prod_{k=0}^{m}f_m(x_k,k)\,|1\rangle\right]=\hat{R}_{m+1}(x_0)\,\hat{R}_m(x_1)\,\ldots\,\hat{R}_2(x_{m-1})\,\underbrace{\frac{|0\rangle+(-1)^{x_m}|1\rangle}{\sqrt{2}}}_{\mathbf{H}|x_m\rangle}, \tag{5.12}$$

where $\mathbf{H}$ is the Hadamard transformation (see Section 1.4.4). In order to be clearer, we can look at the evolution of the first three qubits:

$$\begin{aligned}|x_0\rangle &\to \frac{|0\rangle+f_1(x_0,0)|1\rangle}{\sqrt{2}}\equiv\mathbf{H}|x_0\rangle,\\ |x_1\rangle &\to \frac{|0\rangle+f_1(x_0,0)f_1(x_1,1)|1\rangle}{\sqrt{2}}=\frac{|0\rangle+\hat{R}_2(x_0)(-1)^{x_1}|1\rangle}{\sqrt{2}}\equiv\hat{R}_2(x_0)\mathbf{H}|x_1\rangle,\\ |x_2\rangle &\to \frac{|0\rangle+f_2(x_0,0)f_2(x_1,1)f_2(x_2,2)|1\rangle}{\sqrt{2}}=\frac{|0\rangle+\hat{R}_3(x_0)\hat{R}_2(x_1)(-1)^{x_2}|1\rangle}{\sqrt{2}}\\ &\qquad\equiv\hat{R}_3(x_0)\hat{R}_2(x_1)\mathbf{H}|x_2\rangle,\end{aligned}$$

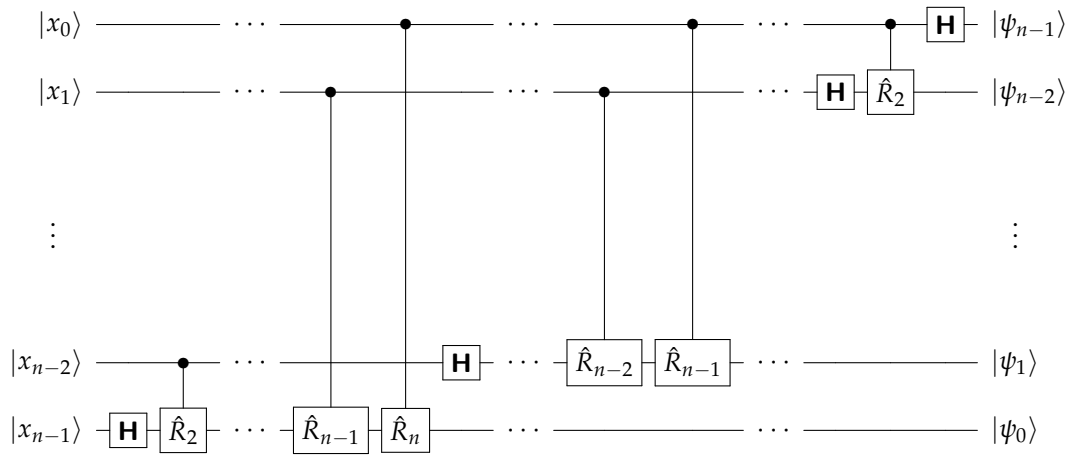

Figure 5.2: Quantum circuit implementing the QFT (we do not implement the final SWAP gates).

where we used Eq. (5.8). More in general, if $0 < m < n$ we have $|x_m\rangle \to \prod_{k=0}^{m-1} \hat{R}_{m-k+1}(x_k)\, \mathbf{H}|x_m\rangle$

As a matter of fact, $\hat{R}_h(0) = \hat{\mathbb{I}}$, thus we can see $\hat{R}_h(x_k)$ as a *controlled* gate, which applies a phase shift to the corresponding qubit only if the control qubit $|x_k\rangle$ assumes the value $x_k = 1$. Therefore, the corresponding quantum circuit involves single-qubit gates (Hadamard transformations) and two-qubit gates [controlled $\hat{R}_h \equiv \hat{R}_h(1)$], as depicted in figure 5.2.

In order to reverse the order of the outputs, one should apply at most $n/2$ SWAP gates (recall that three CNOT gates are needed to implement a single SWAP). Besides the SWAPs, the total number of gates involved in figure 5.2 is $n + (n-1) + \cdots + 1 = n(n+1)/2 \sim n^2$. Note that the classical Fast Fourier Transform algorithm needs $\sim n\, 2^n$ gates (since it ignores trivial operations such as the multiplication by 1), while the direct calculation of the discrete Fourier transform requires $\sim 2^{2n}$ gates! However, there are two main issues we should point out: (i) the final amplitudes cannot be accessed directly; (ii) there is not an efficient preparation of the initial state. Finding applications of the QFT is more subtle than one might hope...

5.2 The phase estimation protocol

The *phase estimation* procedure is a key ingredient for many quantum algorithms. Suppose that $\hat{U}$ is an unitary operator and $|u\rangle$ is one of its eigenvectors, such that:

$$\hat{U}|u\rangle = \exp(2\pi i\phi)\,|u\rangle, \tag{5.13}$$

where $\phi \in [0,1)$ is unknown. The binary representation of ϕ is given by $0.\varphi_1\varphi_2\varphi_3\ldots$, where $\varphi_k \in \{0,1\}$, and $\phi = \sum_k \varphi_k\, 2^{-k}$. Since ϕ is an overall phase, we cannot directly retrieve it. However, if we have "black boxes" (the *oracles*) capable of preparing $|u\rangle$ and of performing the

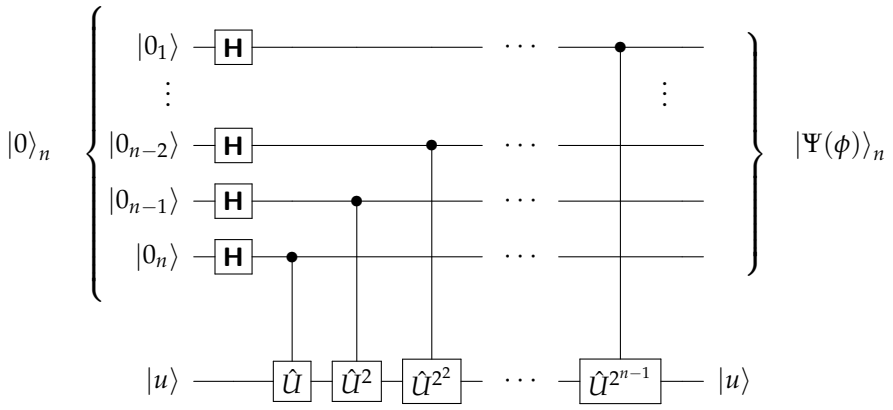

Figure 5.3: Quantum circuit representing the first step of the phase estimation procedure. The expression of the state $|\Psi(\phi)\rangle_n$ is given in Eq (5.16).

controlled-$\hat{U}^{2^{n-k}}$ operations, namely $c\hat{U}_k^{2^{n-k}}$, which use the k-th qubit as control, we can succeed in the estimation of ϕ. Note that since we cannot access $\hat{U}$ (for this reason it is represented as a "black box"), the phase estimation procedure is not a complete algorithm in its own right.

At first, we assume that ϕ can be exactly specified with n bits: in this case the estimation procedure allows us to obtain the actual value ϕ. The protocol uses two registers: the first one contains n qubits prepared in the initial state $|0\rangle_n$; the second one contains many qubit as is necessary to store $|u\rangle$ (without loss of generality we assume that only one qubit is needed). The first step of the procedure applies n Hadamard transformations to $|0\rangle_n$, generating a balanced superposition of all the states $|x\rangle_n$, $0 \leq x < 2^n$. Then we apply controlled-$\hat{U}^{2^k}$ to $|u\rangle$ with control qubit corresponding to the k-th qubit of the first register (see figure 5.3).

Since $c\hat{U}_k^{2^{n-k}}|x_k\rangle|u\rangle = \exp\left(2\pi i\phi\, x_k\, 2^{n-k}\right)|x_k\rangle|u\rangle$, we have (we write only the evolution of the k-th qubit of the first register and the second register):

$$c\hat{U}_k^{2^{n-k}}(\mathbf{H}\otimes\hat{\mathbb{I}})|0_k\rangle|u\rangle = \frac{1}{\sqrt{2}}\left[|0_k\rangle + \exp\left(2\pi i\, 2^{n-k}\phi\right)|1_k\rangle\right]|u\rangle \equiv |\psi_k\rangle|u\rangle. \tag{5.14}$$

Therefore, after the first step of the procedure, the first register evolves as follows (since the second register is left unchanged, we do not write it explicitly):

$$|0\rangle_n \to |\psi_n\rangle|\psi_{n-1}\rangle\ldots|\psi_1\rangle \equiv |\Psi(\phi)\rangle_n. \tag{5.15}$$

As in the case of Eq. (5.4), we can write:

$$|\Psi(\phi)\rangle_n = \frac{1}{2^{n/2}}\sum_{x=0}^{2^n-1}\exp\left(2\pi i\,\phi x\right)|x\rangle_n, \tag{5.16}$$

where it is worth noting that here $x = \sum_{k=1}^{n} x_k\, 2^{n-k}$. Now we apply the inverse of the QFT to

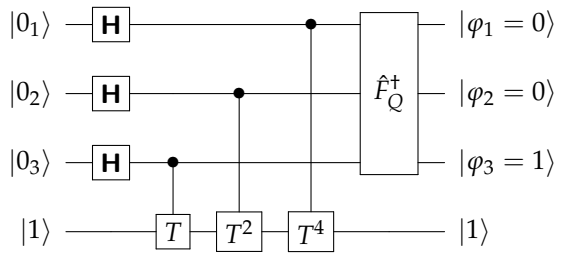

Figure 5.4: Phase estimation with the T or $\frac{\pi}{8}$ gate. See text for details.

$|\Psi(\phi)\rangle_n$:

$$\hat{F}_Q^\dagger |\Psi(\phi)\rangle_n = \frac{1}{2^n} \sum_{x=0}^{2^n-1} \exp\left(2\pi i\, \phi x\right) \sum_{y=0}^{2^n-1} \exp\left(-2\pi i\, \frac{yx}{2^n}\right) |y\rangle_n \tag{5.17a}$$

$$= \frac{1}{2^n} \sum_{y=0}^{2^n-1} \underbrace{\sum_{x=0}^{2^n-1} \exp\left[-2\pi i\, x\, \frac{(y - 2^n\phi)}{2^n}\right]}_{2^n\, \delta_{0,y-2^n\phi}} |y\rangle_n \tag{5.17b}$$

$$= |2^n\phi\rangle_n \equiv |\varphi\rangle_n \tag{5.17c}$$

where in Eq. (5.17b) we defined the *integer* number φ as:

$$2^n\phi = 2^n \sum_{m=1}^{n} \varphi_m 2^{-m} = \sum_{k=0}^{n-1} \varphi_{n-k} 2^k \equiv \varphi, \tag{5.18}$$

and we recall that both y and φ are integers less then 2^n [otherwise we don't have the Kronecker delta, see Eq. (5.21) below]. Finally, since (note the reversed order!):

$$|\varphi\rangle_n = |\varphi_n\rangle|\varphi_{n-1}\rangle \ldots |\varphi_1\rangle, \tag{5.19}$$

we can retrieve the value of each bit φ_k by measuring the corresponding qubit in the computational basis and obtain $\varphi = 0.\varphi_1\varphi_2\ldots\varphi_n$.

It this the following example, we consider the T gate defined in Eq. (3.4). It is straightforward to verify that $T|1\rangle = \mathrm{e}^{2\pi\phi}|1\rangle$ with $\phi = 1/8$ or, in binary notation, $\phi = 0.\varphi_1\varphi_2\varphi_3 = 0.001_2$ (where the subscript 2 refers to the chosen basis). The quantum circuit to implement the phase estimation is drawn in figure 5.4. The state of the input register after the inverse of the QFT reads (the proof is left to the reader):

$$\hat{F}_Q^\dagger |\Psi(\phi)\rangle_3 = \frac{1}{2^3} \sum_{y=0}^{7} \underbrace{\sum_{x=0}^{7} \exp\left[-2\pi i\, x\, \frac{y - 2^3\phi}{2^3}\right]}_{2^3\delta_{0,y-2^3\phi}} |y\rangle_3\,. \tag{5.20}$$

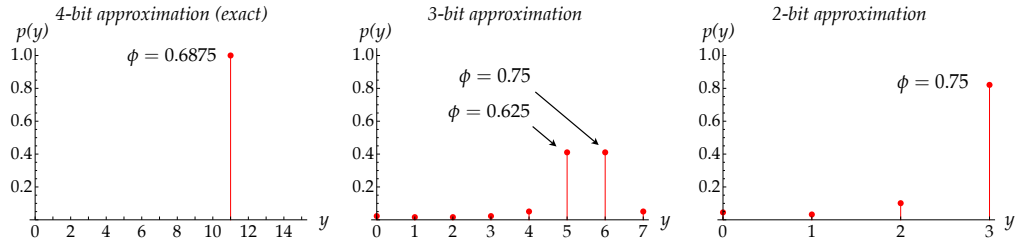

Figure 5.5: Plot of $p(y)$ given in Eq. (5.22) for the estimation of the phase $\phi^* = 0.6875$, that has the exact binary expansion 0.1011_2. We used a different number n of qubits for the input register, from left to right: $n = 4, 3$ and 2.

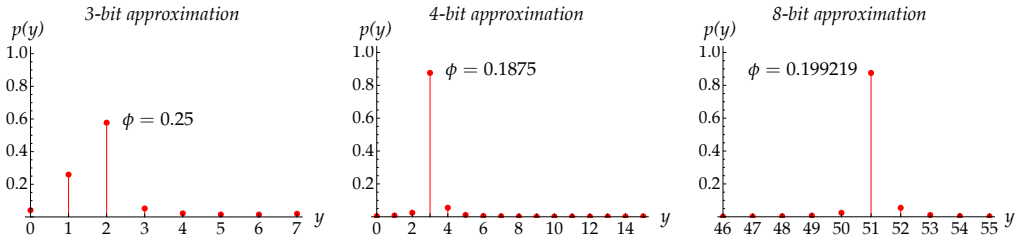

Figure 5.6: Plot of $p(y)$ given in Eq. (5.22) for the estimation of the phase $\phi^* = 0.2$, that does not have an exact binary expansion ($0.00110011\ldots_2$), using an increasing number n of qubits for the input register, from left to right $n = 3, 4$ and 8.

Since $2^3\phi = 1 = \varphi_1\varphi_2\varphi_3 = 001_2$, we obtain $\hat{F}_Q^\dagger|\Psi\rangle = |2^3\phi\rangle_3 = |\varphi_3\rangle|\varphi_2\rangle|\varphi_1\rangle = |1_3\rangle|0_2\rangle|0_1\rangle$ (note the reverse order!).

If the actual value of the phase, say ϕ^*, cannot be exactly written with an n-bit expression, then the estimation does not give its actual value, but just an approximation. In fact, in this case $2^n\phi^*$ is not an integer and Eq. (5.17b) becomes:

$$\begin{aligned}\hat{F}_Q^\dagger|\Psi(\phi)\rangle_n &= \sum_{y=0}^{2^n-1}\frac{1}{2^n}\frac{1-\exp\left[-2\pi i\left(y-2^n\phi^*\right)\right]}{1-\exp\left[-2\pi i\left(y-2^n\phi^*\right)2^{-n}\right]}|y\rangle_n,\\ &= \sum_{y=0}^{2^n-1} f_y(\phi^*;n)|y\rangle_n,\end{aligned} \tag{5.21}$$

that is a superposition of *all* the possible outcomes $|y\rangle_n$, each with probability:

$$p(y) = \left|f_y(\phi^*;n)\right|^2 = \frac{1}{2^{2n}}\frac{1-\cos\left[2\pi\left(y-2^n\phi^*\right)\right]}{1-\cos\left[2\pi\left(y-2^n\phi^*\right)2^{-n}\right]}. \tag{5.22}$$

The reader can check that $p(y) \geq 0$ and $\sum_{y=0}^{2^n-1} p(y) = 1$. In the figures 5.5 and 5.6 we plot the outcome probability $p(y)$ for two values of the unknown phase and a different number n of qubits of the input register.

Among the possible outcomes of the measurement there will be a particular integer $\varphi^{(b)}$, $0 \leq \varphi^{(b)} < 2^n$, such that $\phi^{(b)} = 2^{-n}\varphi^{(b)}$, is the best n-bit approximation of the actual value ϕ^*. Let us suppose that a measurement leads to the outcome φ corresponding to the phase $\phi = 2^{-n}\varphi$. One of the interesting features of the present phase-estimation procedure is that the probability that $|\varphi - \varphi^{(b)}| > t$, where the integer t represents the tolerance to error, decreases as t increases. Note that:

$$\left|\varphi - \varphi^{(b)}\right| > t \Rightarrow \left|\phi - \phi^{(b)}\right| > 2^{-n}t\,. \tag{5.23}$$

It is possible to show that this probability is given by:

$$p\left(\left|\varphi - \varphi^{(b)}\right| > t\right) \leq \frac{1}{2(t-1)} \tag{5.24}$$

and, thus, the *success probability* (the probability of getting an estimation of ϕ within the tolerance t) reads:

$$p\left(\left|\varphi - \varphi^{(b)}\right| \leq t\right) > 1 - \frac{1}{2(t-1)}. \tag{5.25}$$

This result allows to calculate the number of qubits n in order to achieve the phase estimation within a given accuracy. For instance, suppose we want to approximate ϕ to an accuracy 2^{-q}, $0 < q < n$, namely:

$$\left|\phi - \phi^{(b)}\right| < 2^{-q}, \tag{5.26}$$

or, equivalently, multiplying both sides by 2^n:

$$\left|\varphi - \varphi^{(b)}\right| \leq t = 2^{n-q} - 1, \tag{5.27}$$

(note that $2^{n-q} - 1$ corresponds to the maximum integer which can be encoded using only $n - q$ bits). If we require $p(|\varphi - \varphi^{(b)}| \leq t) = 1 - \varepsilon$, for a given $\varepsilon > 0$, then the number n of required qubits for the first register should be at least:

$$n = q + \left\lceil \log_2\left(2 + \frac{1}{2\varepsilon}\right)\right\rceil, \tag{5.28}$$

where $\lceil z \rceil$ is the ceiling function, which represents the smallest integer not less than $z \in \mathbb{R}$.

5.3 The factoring algorithm (Shor algorithm)

The aim of a factoring algorithm is to find the nontrivial factors of an integer N. In this section we show that the factoring problem turns out to be equivalent to the so-called *order-finding problem* we just studied, in the sense that a fast algorithm for order finding can easily be turned into a fast algorithm for factoring. The algorithm is essentially based on two theorems and it is useful to recall the following concepts. Given three integer numbers a, b and N, we have that:

$$a = b(\mathrm{mod}\, N) \Rightarrow \exists\, q \in \mathbb{Z} \text{ such that } a - b = q\,N. \tag{5.29}$$

Suppose, now, to have two integers, x and N, $x < N$, with *no common* factors. The *order* of $x(\mathrm{mod}\, N)$ is defined to be the least positive integer r such than $x^r(\mathrm{mod}\, N) = 1$. For instance, given $x = 5$ and $N = 21$, we have:

$$\begin{aligned} 5(\mathrm{mod}\, 21) &= 5, \quad & 5^4(\mathrm{mod}\, 21) &= 16, \\ 5^2(\mathrm{mod}\, 21) &= 4, \quad & 5^5(\mathrm{mod}\, 21) &= 17, \\ 5^3(\mathrm{mod}\, 21) &= 20, \quad & 5^6(\mathrm{mod}\, 21) &= 1. \end{aligned}$$

Therefore the order of $5(\mathrm{mod}\, 21)$ is $r = 6$. If we consider $x = 3$ and $N = 10$, we have:

$$\begin{aligned} 3(\mathrm{mod}\, 10) &= 3, \quad & 3^3(\mathrm{mod}\, 10) &= 7, \\ 3^2(\mathrm{mod}\, 10) &= 9, \quad & 3^4(\mathrm{mod}\, 10) &= 1, \end{aligned}$$

and the order of $3(\mathrm{mod}\, 10)$ is $r = 4$.

Note that if r is the order of x modulo N, then $x^{(r+s)}(\mathrm{mod}\, N) = x^s(\mathrm{mod}\, N)$, with $0 \leq s < r$.

□ **– Exercise 5.1** *Prove that given the integers x, y and N, one has:*

$$[x(\mathrm{mod}\, N)]\ [y(\mathrm{mod}\, N)] = [xy(\mathrm{mod}\, N)]\ . \tag{5.30}$$

We can now state the two theorems that are at the basis of the factoring algorithm:

Theorem 5.1 *Suppose N is an L-bit composite number, and x is a non-trivial solution to the equation $x^2 = 1(mod\, N)$ in the range $1 \leq x \leq N$, that is, $x \neq \pm 1(mod\, N)$. Then at least one of $gcd(x-1, N)$ and $gcd(x+1, N)$ is a non-trivial factor of N that can be computed using $O(L^3)$ operations.*

Note that if $x \in [1, N]$, then we have:

$$x \neq 1(\mathrm{mod}\, N) \Rightarrow x \neq 1, \quad \text{and} \quad x \neq -1(\mathrm{mod}\, N) \Rightarrow x \neq N-1.$$

The problem is thus reduced to find a non-trivial solution x to $x^2 = 1(\mathrm{mod}\, N)$. This second theorem can help us.

Theorem 5.2 *Suppose $N = p_1^{\alpha_1} \dots p_m^{\alpha_m}$ is the prime factorization of an odd composite positive integer. Let y be an integer chosen uniformly at random, subject to the requirements that $1 \leq y \leq N-1$ and y is co-prime to N, namely $gcd(y, N) = 1$. Let r be the order of y modulo N, that is the least positive integer such that $y^r(mod\, N) = 1$. Then the probability that r is even and $y^{r/2} \neq -1(mod\, N)$ satisfies:*

$$p\big(r \text{ even and } y^{r/2} \neq -1(mod\, N)\big) \geq 1 - \frac{1}{2^m}. \tag{5.31}$$

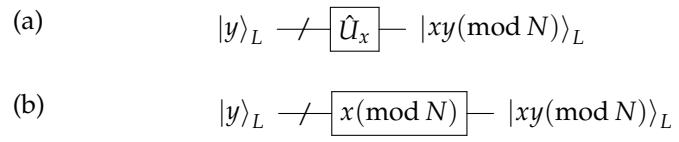

Figure 5.7: (a) Quantum circuit representing the action of the $\hat{U}_x$ gate acting on the input state $|y\rangle_L$ of L qubits. (b) For the sake of simplicity we can substitute to the symbol $\hat{U}_x$ the expression $x(\mathrm{mod}\, N)$.

Therefore, the factorizing problem is equivalent to find the order r of random number y modulo N [note that if $y = 1$, its order is $r = 1$, being $1^r(\mathrm{mod}\, N) = 1, \forall r > 0$]: if r is even and $x = y^{r/2}$ is not a trivial solution of $x^2 = 1(\mathrm{mod}\, N)$, and this is quite likely according to Theorem 5.2, then we can apply Theorem 5.1, that is, one of $\gcd(x-1, N)$ and $\gcd(x+1, N)$ is a non-trivial factor of N.

5.3.1 Order-finding protocol

To find the order of $x(\mathrm{mod}\, N)$ is a *hard problem* on a classical computer, since there is not an algorithm to solve this problem using resources polynomial in $O(L)$, where $L = \lceil \log_2 N \rceil$ is the number of bits needed to specify N. In the following we investigate the performance of a quantum algorithm.

We start from a unitary operator $\hat{U}_x$ such that:

$$\hat{U}_x |y\rangle_L = |xy(\mathrm{mod}\, N)\rangle_L, \tag{5.32}$$

where $0 \leq y < 2^L$. In figure 5.7 we report the quantum circuits representing the action of $\hat{U}_x$. Let us now consider the state:

$$|u_s(x,r)\rangle_L = \frac{1}{\sqrt{r}} \sum_{k=0}^{r-1} \exp\left(-2\pi i \frac{ks}{r}\right) \left|x^k(\mathrm{mod}\, N)\right\rangle_L \tag{5.33}$$

with $0 < s < r$ integer and r is the (unknown!) order of x modulo N, namely, $x^r(\mathrm{mod}\, N) = 1$. Note that ${}_L\langle u_t(x,r)|u_s(x,r)\rangle_L = \delta_{t,s}$. We have:

$$\hat{U}_x |u_s(x,r)\rangle_L = \frac{1}{\sqrt{r}} \sum_{k=0}^{r-1} \exp\left(-2\pi i \frac{ks}{r}\right) \left|x^{k+1}(\mathrm{mod}\, N)\right\rangle_L \tag{5.34}$$

$$= \frac{1}{\sqrt{r}} \sum_{k=1}^{r} \exp\left[-2\pi i \frac{(k-1)s}{r}\right] \left|x^k(\mathrm{mod}\, N)\right\rangle_L \tag{5.35}$$

$$= \exp\left(2\pi i \frac{s}{r}\right) \frac{1}{\sqrt{r}} \sum_{k=1}^{r} \exp\left(-2\pi i \frac{ks}{r}\right) \left|x^k(\mathrm{mod}\, N)\right\rangle_L. \tag{5.36}$$

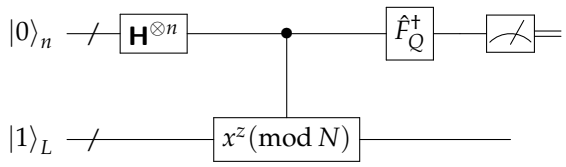

Figure 5.8: Quantum circuit implementing the order-finding procedure. After the Hadamard transformations the first register is $2^{-n/2}\sum_{z=0}^{2^n-1}|z\rangle_n$.

Since $|x^r \pmod N\rangle_L = |x^0 \pmod N\rangle_L = |1\rangle$ we can write the last equation as:

$$\hat{U}_x|u_s(x,r)\rangle_L = \exp\left(2\pi i\,\frac{s}{r}\right)\underbrace{\frac{1}{\sqrt{r}}\sum_{k=0}^{r-1}\exp\left(-2\pi i\,\frac{ks}{r}\right)\left|x^k \pmod N\right\rangle_L}_{|u_s(x,r)\rangle_L} \tag{5.37a}$$

$$= \exp\left(2\pi i\,\frac{s}{r}\right)|u_s(x,r)\rangle_L \tag{5.37b}$$

$$\equiv \exp\left[2\pi i\,\phi_s(r)\right]|u_s(x,r)\rangle_L \tag{5.37c}$$

where we introduced $\phi_s(r) = s/r$. It follows that $|u_s(x,r)\rangle_L$ is an eigenstate of $\hat{U}_x$ with eigenvalue $\exp\left(2\pi i\frac{s}{r}\right)$. Therefore, we can estimate the ratio $\phi_s(r) = s/r$ applying the phase-estimation procedure described in section 5.2. The quantum circuit implementing the order-finding procedure is sketched in figure 5.8.

Indeed, we should be able to implement the controlled-$\hat{U}^{2^k}$ gates, and this is fine. The issue could be the preparation of the eigenstate $|u_s(x,r)\rangle_L$. However we note that:

$$\frac{1}{\sqrt{r}}\sum_{s=0}^{r-1}|u_s(x,r)\rangle_L = \frac{1}{r}\sum_{k=0}^{r-1}\underbrace{\sum_{s=0}^{r-1}\exp\left(-2\pi i\,\frac{sk}{r}\right)}_{r\,\delta_{k,0}}\left|x^k \pmod N\right\rangle_L = |1\rangle_L. \tag{5.38}$$

Therefore, if we prepare the state $|1\rangle_L \equiv |1 \pmod N\rangle_L$, we are also preparing a balanced superposition of all the r states $|u_s(x,r)\rangle_L$, $0 \le s < r$, each with probability $1/r$. Let $1-\varepsilon$ be the success probability for the estimation of s/r for a given $|u_s(x,r)\rangle$, then the *overall* success probability (we do not know the actual value of s since we have a superposition) is $(1-\varepsilon)/r$.

Now we investigate how to implement a quantum circuit for the order-finding procedure. As for the usual phase-estimation protocol, we start from the input state $|0\rangle_n|1\rangle_L$ and apply $\mathbf{H}^{\otimes n}$ to the first register, that is to $|0\rangle_n$, obtaining the balanced superposition of all the integers from 0 to 2^n-1:

$$\frac{1}{2^{n/2}}\sum_{z=0}^{2^n-1}|z\rangle_n|1\rangle_L. \tag{5.39}$$

We can calculate the action of the controlled $U_x^{2^k}$, $k = 0,\ldots,n-1$, on $|1\rangle_L$, where, for a given

$|z\rangle_n = |z_{n-1}\rangle \dots |z_0\rangle$, $z = \sum_{h=0}^{n-1} z_h 2^h$, the control qubit is $|z_k\rangle$. In general we can write:

$$|z\rangle_n |1\rangle_L \longrightarrow |z\rangle_n \frac{1}{\sqrt{r}} \sum_{s=0}^{r-1} \hat{U}_x^{z_{n-1}2^{n-1}} \dots \hat{U}_x^{z_0 2^0} |u_s(x,r)\rangle_L \tag{5.40a}$$

$$|z\rangle_n \frac{1}{\sqrt{r}} \sum_{s=0}^{r-1} \exp\left[2\pi i \left(z_{n-1}2^{n-1} + \dots + z_0 2^0\right) \phi_s(r)\right] |u_s(x,r\rangle_L \tag{5.40b}$$

$$|z\rangle_n \frac{1}{\sqrt{r}} \sum_{s=0}^{r-1} \exp\left[2\pi i\, z\, \phi_s(r)\right] |u_s(x,r\rangle_L. \tag{5.40c}$$

Therefore, after the controlled-$\hat{U}_x^{2^k}$ we have the final state (before the inverse of QFT):

$$\frac{1}{\sqrt{r}} \sum_{s=0}^{r-1} \left\{ \frac{1}{2^{n/2}} \sum_{z=0}^{2^n-1} \exp\left[2\pi i\, z\, \phi_s(r)\right] |z\rangle_n \right\} |u_s(x,r\rangle_L. \tag{5.41}$$

Finally, we can rewrite the state (5.41) as follows:

$$\frac{1}{\sqrt{r}} \sum_{s=0}^{r-1} |\Psi[\phi_s(r)]\rangle_n |u_s(x,r)\rangle_L, \tag{5.42}$$

where :

$$|\Psi[\phi_s(r)]\rangle_n = \frac{1}{2^{n/2}} \sum_{z=0}^{2^n-1} \exp\left[2\pi i\, z\, \phi_s(r)\right] |z\rangle_n, \tag{5.43}$$

that has the same form as in Eq. (5.16). If we now suppose to measure (implicit measurement) the output register and to find as outcome the state $|u_s(x,r)\rangle_L$ (with probability $1/r$), then the input register is left in the state $|\Psi[\phi_s(r)]\rangle_n$. It is now clear that $\hat{F}_Q^\dagger |\Psi[\phi_s(r)]\rangle_n$ leads to an estimation of $\phi_s(r)$ as shown in the next section.

We have seen how the order-finding problem is reduced to a phase estimation process, where the unknown phase to be estimated is $\phi_s(r) = s/r$. Of course, at the end of the protocol we obtain an estimated value ϕ of $\phi_s(r)$, where both s and r are unknown, thus we should find a way to retrieve this information starting from ϕ. This will be shown in section 5.3.2.

5.3.2 Continued-fraction algorithm

First of all we recall that the continued-fraction algorithm describes a positive real number z in terms of positive integers $[a_0, a_1, \dots, a_M]$, where $a_0 \geq 0$ and $a_k > 0$, $k > 0$, namely:

$$z \to [a_0, a_1, \dots, a_M] = a_0 + \cfrac{1}{a_1 + \cfrac{1}{\dots + \cfrac{1}{a_M}}}. \tag{5.44}$$

The m-th convergent to the continued fraction $[a_0, a_1, \dots, a_M]$ is $[a_0, \dots, a_m]$, with $0 \leq m \leq M$. Furthermore, if $z = S/R$, where S and R are $L - bit$ integers, then the algorithm requires $O(L^3)$

operations. For instance, $z = 2.93 \rightarrow [2, 1, 13, 3, 2]$. It is also possible decomposing a fraction as a continued fraction, namely

$$z = \frac{31}{13} = 2.\overline{384615} \rightarrow [2, 2, 1, 1, 2].$$

In order to find the fraction s/r corresponding to the estimated phase ϕ of $\phi_s(r)$, we can use the following theorem:

Theorem 5.3 *If*

$$\left|\frac{s}{r} - \phi\right| \leq \frac{1}{2r^2} \tag{5.45}$$

then s/r is a convergent of the continued fraction for ϕ and can be computed with $O(L^3)$ operations using the continued-fraction algorithm.

In order to apply the Theorem 5.3 we should satisfy the condition in Eq. (5.45); in our case N is an L-bit integer, $r \leq N \leq 2^L$, and we, thus, have:

$$\frac{1}{2r^2} \geq \frac{1}{2^{2L+1}}. \tag{5.46}$$

Therefore, if we use $n = 2L + 1$ bits for the register involved in the estimation of $\phi_s(r)$, on the one hand the accuracy in the estimation of the best $\phi^{(b)}$ is $2^{-(2L+1)}$, that is:

$$\left|\phi^{(b)} - \phi\right| \leq \frac{1}{2^{2L+1}}, \tag{5.47}$$

and, on the other hand, Ineqs. (5.46) allow us to write:

$$\left|\phi^{(b)} - \phi\right| \leq \frac{1}{2r^2}, \tag{5.48}$$

and, thus, we can apply the Theorem 5.3 finding the two integers s and r such that:

$$\phi^{(b)} = \frac{s}{r}. \tag{5.49}$$

In particular we obtained the order r and we can check whether $x^r \pmod N = 1$.

5.3.3 The factoring algorithm

We can now summarize the procedure to factor an integer N:

1. If N is even, return the factor 2.
2. Determine whether $N = a^b$ for integers $a \geq 1$ and $b \geq 2$, and if so return the factor a (this can be done with a classical algorithm).
3. Randomly choose an integer $y \in [1, N-1]$. If $\gcd(y, N) > 1$ then return the factor $\gcd(y, N)$.

4. If $\gcd(y, N) = 1$, use the order-finding subroutine to find the order r of y modulo N (here quantum mechanics help us).

5. If r is even and $x = y^{r/2} \neq -1 (\mathrm{mod}\, N)$, then compute $\gcd(x-1, N)$ and $\gcd(x+1, N)$, and test to see if one of these is a non-trivial factor N, returning that factor if so (see Theorem 5.1). Otherwise, the algorithm fails.

5.3.4 Example: factorization of the number 15

The smallest integer number wich is not even or a power of some smaller integer is the number $N = 15$, thus we can apply the order-finding protocol in order to factorize it.

Since $N = 15$, we have $L = \lceil \log_2 15 \rceil = 4$. Therefore, if we require a success probability of at least $1 - \varepsilon = 3/4$, corresponding to an error probability of at most $\varepsilon = 1/4$, the number of qubits needed for the first register is:

$$n = 2L + 1 + \left\lceil \log_2 \left(2 + \frac{1}{2\varepsilon} \right) \right\rceil = 11, \tag{5.50}$$

where the term $2L + 1$ is needed to apply the continued-fraction algorithm (see section 5.3.2).

We proceeds as follows.

1. We generate the random number $y \in [1, N-1] \equiv [1, 14]$, for instance, we get $y = 7$.

2. We use the order-finding protocol to find the order r of $y (\mathrm{mod}\, N)$. The initial state is $|0\rangle_{11}|1\rangle_4$ and after the application of the Hadamard transformations and the controlled-$\hat{U}^{2^h}$ gates (but before the inverse of the QFT, see figure 5.8), we obtain the state:

$$\frac{1}{\sqrt{2048}} \sum_{z=0}^{2047} |z\rangle_{11} |y^z (\mathrm{mod}\, N)\rangle_4 \tag{5.51}$$

which explicitly writes:

$$\begin{aligned} \frac{1}{\sqrt{2048}} \Big(& |0\rangle_{11}|1\rangle_4 + |1\rangle_{11}|7\rangle_4 + |2\rangle_{11}|4\rangle_4 + |3\rangle_{11}|13\rangle_4 \\ & + |4\rangle_{11}|1\rangle_4 + |5\rangle_{11}|7\rangle_4 + |6\rangle_{11}|4\rangle_4 + |7\rangle_{11}|13\rangle_4 + \dots \Big). \end{aligned} \tag{5.52}$$

or, in a more compact form:

$$\frac{1}{\sqrt{512}} \sum_{k=0}^{511} \frac{1}{2} \left(|4k\rangle_{11}|1\rangle_4 + |1+4k\rangle_{11}|7\rangle_4 + |2+4k\rangle_{11}|4\rangle_4 + |3+4k\rangle_{11}|13\rangle_4 \right), \tag{5.53}$$

where we put in evidence four contributions. Now we should apply $\hat{F}_Q^\dagger$ to the first register. However, since the second register does not undergo further transformations, we can assume that it is measured before the application of the inverse of the QFT: this does not

affect the success of the protocol but simplifies the theoretical calculations. The measurement outcome will be one of the four possible states $|1\rangle_4$, $|7\rangle_4$, $|4\rangle_4$ or $|13\rangle_4$ with probability $1/4$. Suppose we get $|4\rangle_4$, thus the first register is left into the state (similar results follows from the other outcomes):

$$|\Psi[\phi_s(r)]\rangle_{11} = \frac{1}{\sqrt{512}} \sum_{k=0}^{511} |2+4k\rangle_{11}. \tag{5.54}$$

After the inverse of the QFT the previous state of the first register is transformed into the superposition:

$$\hat{F}_Q^\dagger |\Psi[\phi_s(r)]\rangle_{11} = \frac{1}{\sqrt{512}} \sum_{k=0}^{511} \frac{1}{\sqrt{2048}} \sum_{z=0}^{2047} \exp\left(-2\pi i\, z\, \frac{2+4k}{2048}\right) |z\rangle_{11} \tag{5.55}$$

$$= \sum_{z=0}^{2047} c_z |z\rangle_{11} = \frac{|0\rangle_{11} - |512\rangle_{11} + |1024\rangle_{11} - |1536\rangle_{11}}{2}. \tag{5.56}$$

where we introduced:

$$c_z = \frac{1}{1024} \sum_{k=0}^{511} \exp\left(-2\pi i\, z\, \frac{2+4k}{2048}\right) = \frac{e^{i\pi z}}{1024} \cos\left(\frac{\pi z}{512}\right) \frac{\sin(\pi z)}{\sin\left(\frac{\pi z}{512}\right)}, \tag{5.57}$$

which is non null only if z is an integer multiple of 512, namely, $z = 0, 512, 1024, 1536$. Therefore we have:

$$\hat{F}_Q^\dagger |\Psi[\phi_s(r)]\rangle_{11} = \frac{|0\rangle_{11} - |512\rangle_{11} + |1024\rangle_{11} - |1536\rangle_{11}}{2}. \tag{5.58}$$

The measurement on the first register gives with probability $1/4$ one of the four states and let's suppose that we obtain $|1536\rangle_{11}$ (similar results are obtained for $|512\rangle_{11}$). Since $2^{11} = 2048$, our outcome leads to the continued-fraction expansion $1536/2048 = 3/4$ and, therefore, the order of $y = 7$ modulo $N = 15$ is $r = 4$ (the denominator of the fraction), which is even!

3. Since the order r is even and $y^{r/2} = 7^2 = 49 \neq 14 \equiv -1 (\mathrm{mod}\, 15)$, $x = y^{r/2}$ is a solution of $x^2 = 1 (\mathrm{mod}\, N)$ and we can apply the Theorem 5.1 obtaining:

$$\gcd(x-1, N) = \gcd(48, 15) = 3, \tag{5.59a}$$

$$\gcd(x+1, N) = \gcd(50, 15) = 5. \tag{5.59b}$$

Finally: $15 = 3 \times 5$.

In the other two cases, namely, $|0\rangle_{11}$ and $|1024\rangle_{11}$, the algorithm fails. In fact, if $|0\rangle_{11}$ it is not possible to retrieve the information about r. In the case of $|1024\rangle_{11}$ we have the continued-fraction expansion $1024/2048 = 1/2$, therefore $r = 2$, that is even, $x = y^{r/2} = 7$ but $7^2 (\mathrm{mod}\, 15) = 4 \neq 1$ and the algorithm fails.

Bibliography

- M. A. Nielsen and I. L. Chuang, *Quantum Computation and Quantum Information* (Cambridge University Press, 2010) – Chapter 5.

Chapter 6

The quantum search algorithm

In this chapter we address the quantum solution to the search problem. In particular we focus on the search through a search space of $N = 2^n$ elements, where each element is identified by an integer index $x \in \Omega = \{0, 1, \ldots, N-1\}$ and, thus, by the state $|x\rangle_n$, and we assume that the search has M solutions. We can represent the instance of the search problem by means of a function $f : \{0, 1, \ldots, N-1\} \to \{0, 1\}$ such that:

$$f(x) = 0 \Rightarrow x \text{ is not a solution,} \tag{6.1a}$$

$$f(x) = 1 \Rightarrow x \text{ is a solution.} \tag{6.1b}$$

Indeed, we also need an oracle able to recognize the solutions to the search problem. As usual, we assume that the oracle acts as follows:

$$|x\rangle_n |q\rangle \xrightarrow{\hat{\mathcal{O}}} |x\rangle |q \oplus f(x)\rangle, \tag{6.2}$$

where $\hat{\mathcal{O}}$ is the quantum operator associated with the oracle and $|q\rangle$ is the oracle qubit, $q \in \{0, 1\}$. Note that $|q\rangle \to |\bar{q}\rangle$ only if $f(x) = 1$, namely, only if x is a solution. Due to the linearity, we also have:

$$|x\rangle_n \frac{|0\rangle - |1\rangle}{\sqrt{2}} \xrightarrow{\hat{\mathcal{O}}} |x\rangle_n \frac{|0 \oplus f(x)\rangle - |1 \oplus f(x)\rangle}{\sqrt{2}} \equiv (-1)^{f(x)} |x\rangle_n \frac{|0\rangle - |1\rangle}{\sqrt{2}}. \tag{6.3}$$

Since the state of the oracle qubit is left unchanged, we can focus only on the $|x\rangle$. We have:

$$|x\rangle_n \xrightarrow{\hat{\mathcal{O}}} |x\rangle_n \text{ if } x \text{ is not a solution,} \tag{6.4a}$$

$$|x\rangle_n \xrightarrow{\hat{\mathcal{O}}} -|x\rangle_n \text{ if } x \text{ is a solution,} \tag{6.4b}$$

that is, the oracle marks a solution x to the problem by shifting the phase of the corresponding qubit state $|x\rangle$. It is worth noting that the oracle does not know the solution: it is just able to recognize a solution.

6.1 Quantum search: the Grover operator

We start our search procedure with the n qubits prepared in the state $|0\rangle_n$ and, then, we apply n Hadamard transformations in order to generate a superposition of all the possible states:

$$\mathbf{H}^{\otimes n}|0\rangle_n = \frac{1}{2^{n/2}} \sum_{x=0}^{2^n-1} |x\rangle_n \equiv |\psi\rangle_n. \tag{6.5}$$

Now we apply the so-called *Grover iteration* or *Grover operator* $\hat{G}$ which consists in the following steps:

- apply the oracle (this needs also the additional oracle qubit that we do not consider explicitly): $|x\rangle_n \xrightarrow{\hat{\mathcal{O}}} (-1)^{f(x)}|x\rangle_n$;
- apply $\mathbf{H}^{\otimes n}$;
- apply the conditional shift $|x\rangle_n \to (-1)^{1+\delta_{x,0}}|x\rangle_n$, i.e., all the states but $|0\rangle_n$, which is left unchanged, undergo a phase shift;
- apply $\mathbf{H}^{\otimes n}$.

Note that the conditional phase shift can be described by the unitary operator $2|0\rangle_n\langle 0| - \hat{\mathbb{I}}$. Furthermore, we have:

$$\mathbf{H}^{\otimes n}(2|0\rangle_n\langle 0| - \hat{\mathbb{I}})\mathbf{H}^{\otimes n} = 2|\psi\rangle_n\langle\psi| - \hat{\mathbb{I}}, \tag{6.6}$$

therefore, the Grover operator can be written as:

$$\hat{G} = \left[(2|\psi\rangle_n\langle\psi| - \hat{\mathbb{I}}) \otimes \hat{\mathbb{I}}\right] \hat{\mathcal{O}}. \tag{6.7}$$

The action of the operator $2|\psi\rangle_n\langle\psi| - \hat{\mathbb{I}}$ is also referred to as "inversion by the mean". In fact, given the state $|\phi\rangle_n = \sum_{y=0}^{2^n-1} c_y|y\rangle_n$ with $\sum_{y=0}^{2^n-1} |c_y|^2 = 1$, we have

$$\begin{aligned}(2|\psi\rangle_n\langle\psi| - \hat{\mathbb{I}})\,|\phi\rangle_n &= 2\,\frac{1}{2^{n/2}} \sum_{y=0}^{2^n-1} \left(\frac{1}{2^{n/2}} \sum_{x=0}^{2^n-1} c_x\right) |y\rangle_n - |\phi\rangle_n \\ &= \sum_{x=0}^{2^n-1} (2\langle c\rangle - c_n)|y\rangle_n\,,\end{aligned} \tag{6.8}$$

where we defined the mean $\langle c\rangle = 2^{-n}\sum_{y=0}^{2^n-1} c_n$.

In the following we see that by applying $\hat{G}$ a certain number of times, one obtains a solution to the search problem with high probability.

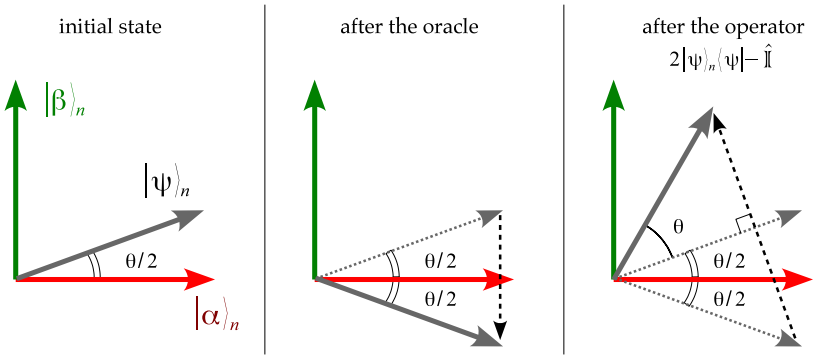

Figure 6.1: Geometric representation of the action of the Grover operator onto the state $|\psi\rangle_n$ (gray vector): (left) initial state; (center) after the oracle call the initial state is reflected across the direction of the $|\alpha\rangle_n$; (right) after the application of the operator $2|\psi\rangle_n\langle\psi| - \hat{\mathbb{I}}$ the final state is nearer to the vector of solution $|\beta\rangle_n$. The overall effect of a single application of the Grover operator is a counterclockwise rotation of amount θ applied to the initial state $|\psi\rangle_n$.

6.1.1 Geometric interpretation of the Grover operator

By definition, the state $|\psi\rangle_n$ is a superposition of *all* the possible states $|x\rangle_n$, $x \in \Omega$. However, we can introduce the two sets A and B, $A \cup B = \Omega$ and $A \cap B = \varnothing$, such that:

$$\text{if } x \in A \text{ then } f(x) = 0 \Rightarrow x \text{ is not a solution,}$$
$$\text{if } x \in B \text{ then } f(x) = 1 \Rightarrow x \text{ is a solution.}$$

Therefore we can define the two orthogonal sates:

$$|\alpha\rangle_n = \frac{1}{\sqrt{N-M}} \sum_{x \in A} |x\rangle_n, \quad \text{and} \quad |\beta\rangle_n = \frac{1}{\sqrt{M}} \sum_{w \in B} |w\rangle_n, \tag{6.9}$$

where $|\alpha\rangle_n$ represents the superposition of all the states $|x\rangle_n$ which are not solutions, while $|\beta\rangle_n$ is the superposition of all the states $|x\rangle_n$ which are solutions to the search problem. Of course we have:

$$|\psi\rangle_n = \sqrt{\frac{N-M}{N}} |\alpha\rangle_n + \sqrt{\frac{M}{N}} |\beta\rangle_n. \tag{6.10}$$

Since we reduced our N-dimensional system to a two-dimensional one, we can also introduce the following parameterization:

$$|\psi\rangle_n = \cos\frac{\theta}{2} |\alpha\rangle_n + \sin\frac{\theta}{2} |\beta\rangle_n, \tag{6.11}$$

with:

$$\cos\frac{\theta}{2} = \sqrt{\frac{N-M}{N}}, \quad \text{and} \quad \sin\frac{\theta}{2} = \sqrt{\frac{M}{N}}. \tag{6.12}$$

We can represent the states $|\alpha\rangle_n$, $|\beta\rangle_n$ and $|\psi\rangle_n$ in a two-dimensional (real) space, as shown in the left panel of figure 6.1. This allows us to obtain a geometrical interpretation of the action of

the Grover algorithm. After the query to the oracle we have $|\beta\rangle_n \to -|\beta\rangle_n$, therefore, the state $|\psi\rangle_n$ is reflected across the direction of the vector associated with $|\alpha\rangle_n$ (figure 6.1, center panel). Now we should apply $2|\psi\rangle_n\langle\psi| - \hat{\mathbb{I}}$, which corresponds to a reflection across the direction of the vector associated with $|\psi\rangle_n$ (right panel of figure 6.1). Overall, the action of $\hat{G}$ on $|\psi\rangle_n$ after a single iteration can be summarized as follows (recall that we are not explicitly considering the oracle qubit, which is indeed necessary to apply $\hat{\mathcal{O}}$):

$$|\psi\rangle_n = \cos\frac{\theta}{2}|\alpha\rangle_n + \sin\frac{\theta}{2}|\beta\rangle_n \xrightarrow{\hat{G}} \left|\psi^{(1)}\right\rangle_n = \cos\frac{3\theta}{2}|\alpha\rangle_n + \sin\frac{3\theta}{2}|\beta\rangle_n, \tag{6.13}$$

thus, from the geometrical point of view, the action of the Grover operator onto a state is a counterclockwise rotation of an amount θ, described by the matrix:

$$\hat{G} \to \begin{pmatrix} \cos\theta & -\sin\theta \\ \sin\theta & \cos\theta \end{pmatrix}. \tag{6.14}$$

After k iterations we find:

$$|\psi\rangle_n \xrightarrow{\hat{G}^k} \left|\psi^{(k)}\right\rangle_n = \cos\left(\frac{2k+1}{2}\theta\right)|\alpha\rangle_n + \sin\left(\frac{2k+1}{2}\theta\right)|\beta\rangle_n. \tag{6.15}$$

It is worth noting that θ is a function of both N, the total number of states, and of the number of solutions M.

□ **– Exercise 6.1** *By using the geometrical representation, prove that* $2|\psi\rangle_n\langle\psi| - \hat{\mathbb{I}}$ *corresponds to a reflection across the direction of the vector associated with* $|\psi\rangle_n$.

6.1.2 Number of iterations and error probability

As a matter of fact, we have a best number $\mathcal{R}$ of Grover iterations, which bring the initial state $|\psi\rangle_n$ as nearer as possible to the state $|\beta\rangle_n$: further iterations would drive the state away form $|\beta\rangle_n$. Thanks to the geometrical interpretation (see again the left panel of figure 6.1) we find that in order to obtain exactly $|\beta\rangle_n$ we should rotate $|\psi\rangle_n$ by an amount $\phi = \arccos\sqrt{M/N}$. Therefore the number of needed iterations is:

$$\mathcal{R} = \mathrm{CI}\left(\frac{\arccos\sqrt{M/N}}{\theta}\right), \tag{6.16}$$

where $\mathrm{CI}(z)$ corresponds to the closest integer to the real number z. After this number of iterations, one measures the final state in the computational basis and obtains a solution to the search problem with a high probability.

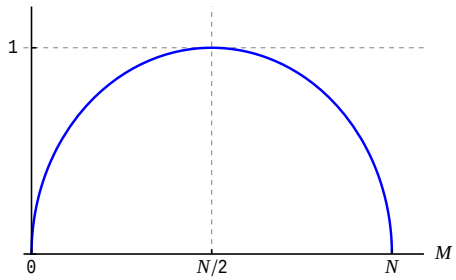

Figure 6.2: Plot of the r.h.s. of Eq. (6.20).

In particular, if $M \ll N$, we have that the angular error in the final state will be at most $\theta/2 \approx \sqrt{M/N}$, and the probability of error is thus given by:

$$P_{\text{err}} = \left|\sin\frac{\theta}{2}\right|^2 \approx \frac{M}{N} \ll 1. \tag{6.17}$$

Furthermore, since:

$$\mathcal{R} = \text{CI}\left(\frac{\arccos\sqrt{M/N}}{\theta}\right) \leq \left\lceil \frac{\pi}{2\theta} \right\rceil, \tag{6.18}$$

assuming $M \leq N/2$ we find $\theta/2 \geq \sin(\theta/2) = \sqrt{M/N}$ and we have the following bound on the best number of iterations, i.e.:

$$\mathcal{R} \leq \left\lceil \frac{\pi}{2\theta} \right\rceil \leq \left\lceil \frac{\pi}{4}\sqrt{\frac{N}{M}} \right\rceil, \tag{6.19}$$

that is $\mathcal{R} \sim O(\sqrt{N/M})$, while a classical algorithm would solve the search problem with $O(N)$ steps. It is worth noting that since:

$$\sin\theta = \frac{2\sqrt{M(N-M)}}{N}, \tag{6.20}$$

on the one hand if $M \leq N/2$, then θ grows with the number of solutions M, thus requiring less iterations; on the other hand, if $N/2 < M \leq N$, then θ decreases as M increases, namely, more iterations are required (see figure 6.2). This is a silly property of the quantum search algorithm, which can be solved by increasing the total number of state from $N = 2^n$ to $2N = 2^{n+1}$, that is , we just add one qubit.

6.1.3 Quantum counting

Up to now we addressed the search problem assuming that the number of solutions, and, thus, θ, was known. In general this is not the case. Nevertheless, it is possible to *estimate* both θ and M, and this allows us to find a solution quickly and also to decide whether or not a solution even exists!

In section 6.1.1 we have seen that in the space spanned by $|\alpha\rangle_n$ and $|\beta\rangle_n$, $\hat{G}$ behaves as a rotation described by the 2×2 matrix of Eq. (6.14). It is straightforward to see that $e^{i\theta}$ and $e^{i(2\pi-\theta)}$ are the eigenvalues of $\hat{G}$, therefore we can apply the phase estimation protocol described in section 5.2 in order to estimate θ and M. For ease the analysis, we double N by adding a qubit in order to be assured that the number of solution M is less then the half of the possible states, that is $2N$. Now, we have $\sin^2(\theta/2) = M/(2N)$.

Following section 5.2, if we want an accuracy to m bits, namely, $|\Delta\theta| \leq 2^{-m}$, with success probability $1-\varepsilon$, we need to use a register with at least a number of qubits given by Eq. (5.28). By using $\sin^2(\theta/2) = M/(2N)$ one can show that:

$$|\Delta M| < \left(2\sqrt{NM} + \frac{N}{2^{m+1}}\right) 2^{-m}. \tag{6.21}$$

6.1.4 Example of quantum search

As an example of quantum search we consider a 2-bit search space, that is $N = 2^2$ and we assume to know that there is only one solution to the problem, that is $x_0 \in \{0,1,2,3\}$. From the classical point of view one would need on average 2.25 oracle calls. What is the performance of the quantum algorithm?

We start, as usual, with the superposition:

$$|\psi\rangle_2 = \frac{1}{2}\sum_{x=0}^{3}|x\rangle_2 = \frac{\sqrt{3}}{2}|\alpha\rangle_2 + \frac{1}{2}|\beta\rangle_2, \tag{6.22}$$

where $|\alpha\rangle_2 = 3^{-1/2}\sum_{x\neq x_0}|x\rangle_2$ and $|\beta\rangle_2 = |x_0\rangle_2$. Since $\sin(\theta/2) = 1/2$, we have $\theta = \pi/3$, and, therefore, we need just one iteration of $\hat{G}$ with $\theta = \pi/3$. After the application of the oracle we have:

$$|\psi\rangle_2 \to \frac{1}{2}\sum_{x\neq x_0}|x\rangle_2 - \frac{1}{2}|x_0\rangle_2 = \sum_{x=0} 2^n - 1c_x|x\rangle_n \equiv |\phi\rangle_2\,. \tag{6.23}$$

According to Eq. (6.8), after the "inversion by the mean" we obtain:

$$|\phi\rangle_2 \to \sum_{x=0}^{3}(2\langle c\rangle - c_x)\,|x\rangle_2 = |x_0\rangle_2 \tag{6.24}$$

In summary, we have the following overall evolution:

$$|\psi\rangle_2 \xrightarrow{\hat{G}} |x_0\rangle_2. \tag{6.25}$$

We get the right solution with only one oracle call!

□ – **Exercise 6.2** *Draw the quantum circuit which implements the quantum search addressed in section 6.1.4.*

6.2 Quantum search and unitary evolution

Suppose that $x_0 \in \{0, 1, \ldots, 2^n - 1\}$ is the label of the only solution. We guess the Hamiltonian which solves the problem of $|\psi\rangle_n$ as initial state and $|x_0\rangle_n$ as solution. Formally, we want a Hamiltonian $\hat{H}$ such that (we use natural units, i.e., $\hbar \to 1$):

$$\exp\left(-i\hat{H}t\right)|\psi\rangle_n = |x_0\rangle_n, \tag{6.26}$$

after a certain time evolution t. As a matter of fact, $\hat{H}$ should depends on both $|\psi\rangle_n$ and $|x_0\rangle_n$. Therefore, the simplest Hamiltonian we can consider is:

$$\hat{H} = |x_0\rangle_n\langle x_0| + |\psi\rangle_n\langle\psi|. \tag{6.27}$$

For the sake of simplicity and to use the qubit formalism, we define the two following orthogonal states:

$$|0\rangle = |x_0\rangle_n, \quad \text{and} \quad |1\rangle = \frac{1}{\sqrt{N-1}} \sum_{x \neq x_0} |x\rangle_n, \tag{6.28}$$

and we write $|\psi\rangle_n = \alpha|0\rangle + \beta|1\rangle$, with $\alpha = \sqrt{(N-1)/N}$ and $\beta = \sqrt{1/N}$. We have:

$$\hat{H} = (\alpha^2 + 1)|0\rangle\langle 0| + \beta^2|1\rangle\langle 1| + \alpha\beta\left(|0\rangle\langle 1| + |1\rangle\langle 0|\right). \tag{6.29}$$

that is:

$$\hat{H} = \hat{\mathbb{I}} + \alpha(\beta\,\hat{\sigma}_x + \alpha\,\hat{\sigma}_z). \tag{6.30}$$

It follows that [see Eq. (2.40)]:

$$\exp\left(-i\hat{H}t\right) = \mathrm{e}^{-it}\left[\cos(\alpha t)\,\hat{\mathbb{I}} - i\sin(\alpha t)(\beta\,\hat{\sigma}_x + \alpha\,\hat{\sigma}_z)\right], \tag{6.31}$$

and we find the following evolution (we neglect the overall phase e^{-it}):

$$\exp\left(-i\hat{H}t\right)|\psi\rangle_n = \cos(\alpha t)\,|\psi\rangle_n - i\sin(\alpha t)\,|x_0\rangle_n. \tag{6.32}$$

By choosing $t = \pi/(2\alpha)$ we have, up to an overall phase, $|\psi\rangle_n \to |x_0\rangle_n$.

The Hamiltonian of Eq. (6.30) can be easily simulated using standard methods based on the result known as "Trotter formula":

Theorem 6.1 *Let $\hat{A}$ and $\hat{B}$ be Hermitian operators. Then for any real t we have:*

$$\lim_{k\to\infty}\left[\exp\left(i\hat{A}\frac{t}{k}\right)\exp\left(i\hat{B}\frac{t}{k}\right)\right]^k = \exp\left[i\left(\hat{A}+\hat{B}\right)t\right]. \tag{6.33}$$

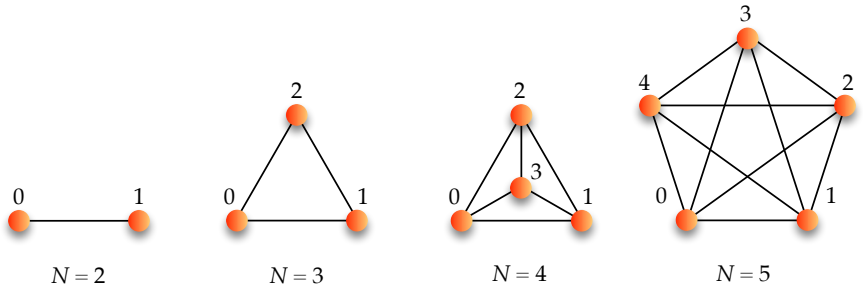

Figure 6.3: Examples of complete graphs with different values of N. The vertices are represented by the circles while the lines are the edges (the connections between the vertices).

6.3 Grover's algorithm and continuous-time quantum walks

The search problem investigated in the previous sections can be reformulated as a search on a complete graph of N vertices, that is a graph in which each vertex is connected with the other $N-1$ vertices (see figure 6.3). In this case, the vertices are associated with the entries of the search space, namely, $x \to |x\rangle_n$ with $x \in \Omega = \{0, 1, \ldots, N-1\}$, and the solutions are represented by marked vertices (whose actual positions on the graph are not known). The search is then pursued considering the so-called continuous-time quantum walk in a N-dimensional Hilbert space supported by the vertices of the graph.

In order to describe the dynamics of the quantum walk on the graph G, we should introduce the Laplacian $\boldsymbol{L} = \boldsymbol{A} - \boldsymbol{D}$ of G, where $\boldsymbol{A}$ is the *adjacency matrix* and $\boldsymbol{D}$ is a diagonal matrix such that D_{xx} is the number of edges that are incident to the vertex x, namely, the degree $\deg(x)$ of the vertex x. The adjacency matrix of an undirected graph is defined as

$$A_{x,y} = \begin{cases} 1 & (x,y) \in G, \\ 0 & \text{otherwise.} \end{cases} \tag{6.34}$$

As mentioned above, we associate the state $|x\rangle_n$ with the vertex x, thus the continuous-time quantum walk is defined by introducing the Hamiltonian $\hat{H}_{\text{qw}} = -\gamma \boldsymbol{L}$, where γ is the jumping rate to an adjacent vertex (for the sake of simplicity we consider $\hbar = 1$). Since here we consider only regular graphs $\boldsymbol{D}$ is independent of x and we can simply assume

$$\hat{H}_{\text{qw}} = -\gamma \boldsymbol{A}\,. \tag{6.35}$$

Following the formalism introduced in section 6.1.1, we should introduce the oracle Hamiltonian (the interested reader can find further details in the references proposed at the end of this chapter)

$$\hat{H}_{\text{sol}} = -\sum_{w \in B} |w\rangle_n \langle w|\,, \tag{6.36}$$

$w \in B$ being the solutions, whereas $x \in A$ are the entries which are not solutions, $A \cup B = \Omega$. Note that $\hat{H}_{\rm sol}$ has eigenvalues equal to zero for all the states but the ground states $|w\rangle_n$, $w \in B$, with eigenvalue -1.

To implement the search on the graph G, we define the Hamiltonian

$$\hat{H} = -\gamma \boldsymbol{A} + \hat{H}_{\rm sol}\,, \tag{6.37}$$

and we consider as initial state $|\psi_0\rangle = |\psi\rangle_n$ given in Eq. (6.5), that is the balanced superposition over the vertices. The evolution of the state at time t is the given by the Schrödinger equation

$$i\frac{\partial}{\partial t}|\psi_t\rangle = \hat{H}|\psi_t\rangle\,, \tag{6.38}$$

and the problem is to choose the transition rate γ in such a way that $|\psi_T\rangle$ approaches the superposition of the solution states $|\beta\rangle_n$, introduced in Eq. (6.9), for small a T as possible.

If we consider the Hilbert space spanned by the states $\{|\beta\rangle_n, |\alpha\rangle_n\}$, the Hamiltonian (6.37) can be written in the following matrix form:

$$\hat{H} = -\gamma \begin{pmatrix} M-1+\gamma^{-1} & \sqrt{M(N-M)} \\ \sqrt{M(N-M)} & N-M-1 \end{pmatrix}\,, \tag{6.39}$$

where

$$|\beta\rangle_n \to \begin{pmatrix} 1 \\ 0 \end{pmatrix} \quad \text{and} \quad |\alpha\rangle_n \to \begin{pmatrix} 0 \\ 1 \end{pmatrix}. \tag{6.40}$$

If we now set $\gamma = 1/N$, the eigenstates $\hat{H}|\Psi_\pm\rangle = E_\pm|\Psi_\pm\rangle$ read:

$$|\Psi_\pm\rangle = \frac{|\psi\rangle_n \mp |\beta\rangle_n}{\sqrt{\mathcal{N}_\pm}}\,, \tag{6.41}$$

with eigenvalues

$$E_\pm = \frac{1-N}{N} \pm \sqrt{\frac{M}{N}}\,. \tag{6.42}$$

Since from Eq. (6.41) we have

$$|\psi\rangle_n = \frac{\sqrt{\mathcal{N}_+}|\Psi_-\rangle + \sqrt{\mathcal{N}_-}|\Psi_+\rangle}{\sqrt{2}}\,, \tag{6.43}$$

we obtain

$$|\psi_t\rangle = e^{-i\hat{H}t}|\psi_0\rangle\,, \tag{6.44}$$

$$= \frac{\sqrt{\mathcal{N}_+}e^{-iE_-t}|\Psi_-\rangle + \sqrt{\mathcal{N}_-}e^{-iE_+t}|\Psi_+\rangle}{\sqrt{2}}\,, \tag{6.45}$$

or, up to a global phase:

$$|\psi_t\rangle = \cos\left(\frac{\Delta E\, t}{2}\right)|\psi\rangle_n - i\sin\left(\frac{\Delta E\, t}{2}\right)|\beta\rangle_n\,, \tag{6.46}$$

where $\Delta E = E_+ - E_- = 2\sqrt{M/N}$.

□ **– Exercise 6.3** *Prove that the Hamiltonian (6.37) can be written in the matrix form (6.39) and, in the case $\gamma = 1/N$, calculate the corresponding eigenvectors and eigenvalues.*

It is now clear that if we choose $t = T$ with

$$T = \frac{\pi}{\Delta E} \equiv \frac{\pi}{2}\sqrt{\frac{N}{M}} \tag{6.47}$$

we obtain (up to a global phase) $|\psi_T\rangle = |\beta\rangle_n$. It is worth noting that we obtained the same scaling $\sim O(\sqrt{N/M})$ found in section 6.1.2 in the case of the Grover's algorithm.

Bibliography

- M. A. Nielsen and I. L. Chuang, *Quantum Computation and Quantum Information* (Cambridge University Press, 2010) – Chapter 6.
- E. Farhi and S. Gutmann, *Analog analogue of a digital quantum computation*, Phys. Rev. A **57**, 2403–2406 (1998).
- A. M. Childs and J. Goldstone, *Spatial search by quantum walk*, Phys. Rev. A **70**, 022314 (2004).

Chapter 7

Quantum operations

THE QUANTUM OPERATION formalism allows us to describe the evolution of a quantum system in a wide variety of circumstances. In general, a quantum operation is a map $\mathcal{E}$ that transforms a quantum state described by a density operator $\hat{\varrho}$ into a new density operator $\hat{\varrho}'$, i.e.:

$$\mathcal{E}(\hat{\varrho}) = \hat{\varrho}'. \tag{7.1}$$

A quantum operation captures the dynamic change to a state which occurs as the result of some physical process. The simplest example of quantum operation is the evolution of a quantum state $\hat{\varrho}$ under a unitary operator $\hat{U}$, which can be written as $\mathcal{E}(\hat{\varrho}) \equiv \hat{U}\hat{\varrho}\,\hat{U}^\dagger$.

7.1 Environment and quantum operations

Suppose that we have a system S described by $\hat{\varrho}_S$ which interacts with another system E, which we call "environment", described by $\hat{\varrho}_E$. We assume also that the interaction is described by the unitary operator $\hat{U}$. Physically, this corresponds to describe the interaction by means of a Hamiltonian that couples the two systems, leading to their unitary evolution. If S and E are initially uncorrelated, and we are interested just in the evolution of the system, then its evolved state can be represented by the following map:

$$\hat{\varrho}_S \to \mathcal{E}(\hat{\varrho}_S) \equiv \mathrm{Tr}_E \left[\hat{U}\hat{\varrho}_S \otimes \hat{\varrho}_E\, \hat{U}^\dagger\right]. \tag{7.2}$$

Without lack of generality we assume that $\hat{\varrho}_E = |e_0\rangle\langle e_0|$, where $\{|e_k\rangle\}$ is an orthonormal basis of the Hilbert space associated with the environment. Now the quantum operation in

Eq. (7.2) can be written as:

$$\begin{aligned}\mathcal{E}(\hat{\varrho}_S) &= \mathrm{Tr}_E\left[\hat{U}\hat{\varrho}_S \otimes |e_0\rangle\langle e_0|\,\hat{U}^\dagger\right] \\ &= \sum_k \langle e_k|\hat{U}\hat{\varrho}_S \otimes |e_0\rangle\langle e_0|\,\hat{U}^\dagger|e_k\rangle \\ &= \sum_k \hat{E}_k\hat{\varrho}_S\,\hat{E}_k^\dagger, \qquad \text{(operator-sum representation)}\end{aligned} \tag{7.3}$$

where we introduced $\hat{E}_k = \langle e_k|\hat{U}|e_0\rangle$, that is a linear operator acting on the state space of the system S. Indeed, in order to have a quantum state we should require that $\forall\hat{\varrho}$, $\mathrm{Tr}_S[\hat{\varrho}] = 1$:

$$1 = \mathrm{Tr}_S\left[\mathcal{E}(\varrho)\right] = \mathrm{Tr}_S\left[\sum_k \hat{E}_k\hat{\varrho}\,\hat{E}_k^\dagger\right] = \sum_k \mathrm{Tr}_S\left[\hat{E}_k^\dagger\hat{E}_k\hat{\varrho}\right] = \mathrm{Tr}_S\left[\left(\sum_k \hat{E}_k^\dagger\hat{E}_k\right)\hat{\varrho}\right], \tag{7.4}$$

therefore one should have $\sum_k \hat{E}_k^\dagger\hat{E}_k = \hat{\mathbb{1}}$. More in general one may have $\sum_k \hat{E}_k^\dagger\hat{E}_k \leq \hat{\mathbb{1}}$, and when the inequality is saturated the map is referred to as *trace-preserving*.

7.2 Physical interpretation of quantum operations

Suppose we measure the environment in the basis $\{|e_k\rangle\}$. The conditional state $\hat{\varrho}_k$ of the system, corresponding to the outcome k from the measurement, is (we set $\hat{\varrho}_S = \hat{\varrho}$):

$$\begin{aligned}\hat{\varrho}_k &= \frac{1}{p_k}\,\mathrm{Tr}_E\left[\hat{U}\hat{\varrho}\otimes|e_0\rangle\langle e_0|\hat{U}^\dagger\,\hat{\mathbb{1}}\otimes\hat{P}_k\right] \\ &= \frac{1}{p_k}\,\langle e_k|\hat{U}\hat{\varrho}\otimes|e_0\rangle\langle e_0|\hat{U}^\dagger|e_k\rangle = \frac{1}{p_k}\,\hat{E}_k\hat{\varrho}\,\hat{E}_k^\dagger,\end{aligned} \tag{7.5}$$

where $\hat{P}_k = |e_k\rangle\langle e_k|$ and:

$$\begin{aligned}p_k &= \mathrm{Tr}_{SE}\left[\hat{U}\hat{\varrho}\otimes|e_0\rangle\langle e_0|\hat{U}^\dagger\,\hat{\mathbb{1}}\otimes\hat{P}_k\right], \\ &= \mathrm{Tr}_S\left[\hat{E}_k\hat{\varrho}\,\hat{E}_k^\dagger\right],\end{aligned} \tag{7.6}$$

is the probability of the outcome k. Therefore we have:

$$\mathcal{E}(\hat{\varrho}) = \sum_k \hat{E}_k\hat{\varrho}\,\hat{E}_k^\dagger \equiv \sum_k p_k\hat{\varrho}_k, \tag{7.7}$$

and the action of $\mathcal{E}$ is to replace $\hat{\varrho}$ with the conditional state $\hat{\varrho}_k$ with probability p_k.

7.3 Geometric picture of single-qubit operations

As we have seen in chapter 2, we can associate the density operator $\hat{\varrho}$ with a 2×2 density matrix ϱ, which can be written as:

$$\hat{\varrho} \to \varrho = \frac{1}{2}\left(\mathbb{1} + \boldsymbol{r}\cdot\boldsymbol{\sigma}\right) = \frac{1}{2}\begin{pmatrix} 1+r_z & r_x - ir_y \\ r_x + ir_y & 1-r_z \end{pmatrix}, \tag{7.8}$$

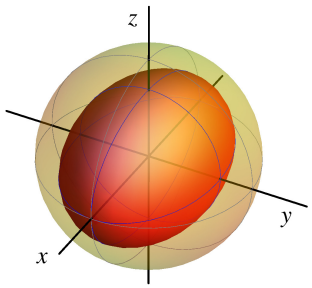

Figure 7.1: Effect of the bit flip operation on the Bloch sphere: we have a contraction of the z–y plane by a factor $1-2p$.

where $\boldsymbol{r} = (r_x, r_y, r_z)$, $\boldsymbol{\sigma} = (\sigma_x, \sigma_y, \sigma_z)$ are the Pauli matrices corresponding to the Pauli operators [see Eqs. (1.27)], and $\boldsymbol{r}\cdot\boldsymbol{\sigma} = r_x\sigma_x + r_y\sigma_y + r_z\sigma_z$. Therefore a trace-preserving quantum operation is equivalent to an affine map of the Bloch sphere into itself and can be written as $\boldsymbol{r} \to \boldsymbol{r}' = \mathbf{M}\boldsymbol{r} + \boldsymbol{v}$, $\mathbf{M}$ being a 3×3 real matrix and $\boldsymbol{v}$ a 3-dimensional real vector.

7.3.1 Bit flip operation

If p, with $0 \le p \le 1$, is the probability that a bit flip occurs to a qubit, that is $|0\rangle \to |1\rangle$ and $|1\rangle \to |0\rangle$, the corresponding quantum operation reads:

$$\mathcal{E}_{\rm bf}(\hat{\varrho}) = (1-p)\hat{\varrho} + p\hat{\sigma}_x\,\hat{\varrho}\,\hat{\sigma}_x, \tag{7.9}$$

and the corresponding elements of the operator-sum representation are:

$$\hat{E}_0 = \sqrt{1-p}\,\hat{\mathbb{1}}, \quad \text{and} \quad \hat{E}_1 = \sqrt{p}\,\hat{\sigma}_x. \tag{7.10}$$

The transformation of the vector $\boldsymbol{r}$ is (the proof is left to the reader):

$$\begin{cases} r_x & \to & r_x, \\ r_y & \to & (1-2p)\,r_y, \\ r_z & \to & (1-2p)\,r_z, \end{cases} \tag{7.11}$$

that is we have a contraction of the z–y plane by a factor $1-2p$, see figure 7.1.

7.3.2 Phase flip operation

The quantum operation corresponding to phase flip occurring with probability p is:

$$\mathcal{E}_{\rm pf}(\hat{\varrho}) = (1-p)\hat{\varrho} + p\hat{\sigma}_z\,\hat{\varrho}\,\hat{\sigma}_z, \tag{7.12}$$

and the corresponding elements of the operator-sum representation are:

$$\hat{E}_0 = \sqrt{1-p}\,\hat{\mathbb{1}}, \quad \text{and} \quad \hat{E}_1 = \sqrt{p}\,\hat{\sigma}_z. \tag{7.13}$$

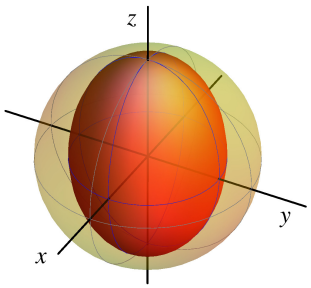

Figure 7.2: Effect of the phase flip operation on the Bloch sphere: we have a contraction of the x–y plane by a factor $1-2p$.

The transformation of the vector $\boldsymbol{r}$ is (the proof is left to the reader):

$$\begin{cases} r_x & \to & (1-2p)\, r_x, \\ r_y & \to & (1-2p)\, r_y, \\ r_z & \to & r_z, \end{cases} \tag{7.14}$$

now we have a contraction of the x–y plane by a factor $1-2p$, as shown in figure 7.2.

7.3.3 Bit-phase flip operation

When both bit flip and phase flip operations occur with probability p, the process is described by the quantum operation:

$$\mathcal{E}_{\text{bpf}}(\hat{\varrho}) = (1-p)\hat{\varrho} + p\hat{\sigma}_y\, \hat{\varrho}\, \hat{\sigma}_y, \tag{7.15}$$

and the elements of the operator-sum representation are:

$$\hat{E}_0 = \sqrt{1-p}\,\hat{\mathbb{I}}, \quad \text{and} \quad \hat{E}_1 = \sqrt{p}\,\hat{\sigma}_y. \tag{7.16}$$

The vector $\boldsymbol{r}$ trasforms as follows (the proof is left to the reader):

$$\begin{cases} r_x & \to & (1-2p)\, r_x, \\ r_y & \to & r_y, \\ r_z & \to & (1-2p)\, r_z, \end{cases} \tag{7.17}$$

and, thus, we have a contraction of the x–z plane by a factor $1-2p$, see figure 7.3.

7.3.4 Depolarizing channel

The so-called depolarizing channel describes a process in which $\hat{\varrho}$ is replaced by $\hat{\mathbb{I}}/2$, that is the maximally mixed state, with probability p, namely:

$$\mathcal{E}_{\text{dc}}(\hat{\varrho}) = (1-p)\hat{\varrho} + p\frac{\hat{\mathbb{I}}}{2}. \tag{7.18}$$

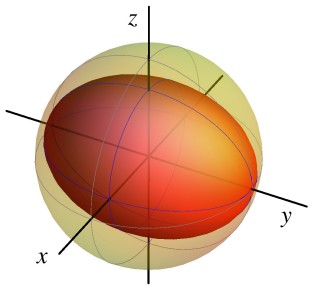

Figure 7.3: Effect of the bit-phase flip operation on the Bloch sphere: we have a contraction of the x–z plane by a factor $1-2p$.

In order to obtain the operator-sum representation of the depolarizing channel, we use the following identity (the proof his left to the reader):

$$\frac{\hat{\mathbb{I}}}{2} = \frac{1}{4}\left(\hat{\varrho} + \hat{\sigma}_x\,\hat{\varrho}\,\hat{\sigma}_x + \hat{\sigma}_y\,\hat{\varrho}\,\hat{\sigma}_y + \hat{\sigma}_z\,\hat{\varrho}\,\hat{\sigma}_z\right). \tag{7.19}$$

We find:

$$\mathcal{E}_{\rm dc}(\hat{\varrho}) = \left(1 - \frac{3p}{4}\right)\hat{\varrho} + \frac{p}{4}\sum_{k=x,y,z}\hat{\sigma}_k\,\hat{\varrho}\,\hat{\sigma}_k. \tag{7.20}$$

or:

$$\mathcal{E}_{\rm dc}(\hat{\varrho}) = (1-q)\,\hat{\varrho} + \frac{q}{3}\sum_{k=x,y,z}\hat{\sigma}_k\,\hat{\varrho}\,\hat{\sigma}_k, \tag{7.21}$$

with $q = 3p/4$, which tells us that the depolarizing channel leaves $\hat{\varrho}$ unchanged with probability $1-q$, while with probability $q/3$ one of the Pauli operators is applied to it. The vector $\boldsymbol{r}$ evolves as follows (the proof is left to the reader):

$$\begin{cases} r_x & \to & (1-p)\,r_x, \\ r_y & \to & (1-p)\,r_y, \\ r_z & \to & (1-p)\,r_z, \end{cases} \tag{7.22}$$

therefore, we have a contraction of the whole sphere by a factor $1-p$. Note that the maximally mixed state, in the Bloch sphere formalism, corresponds to the center of the sphere. Figure 7.4 shows the uniform contraction of the Bloch sphere under the effect of the depolarizing channel.

7.4 Amplitude damping channel

Amplitude damping describes the energy dissipation (e.g., an atom which emits a photon, losses during the propagation of light, a system approaching the thermal equilibrium). The map which describes this process is:

$$\mathcal{E}_{\rm ad}(\hat{\varrho}) = \hat{E}_0\hat{\varrho}\hat{E}_0^\dagger + \hat{E}_1\hat{\varrho}\hat{E}_1^\dagger, \tag{7.23}$$

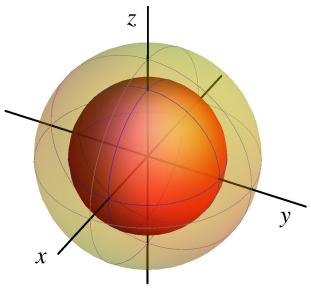

Figure 7.4: Effect of the depolarizing channel on the Bloch sphere: we have a uniform contraction by a factor $p-1$. The center of the sphere corresponds to the qubit maximally mixed state $\hat{\mathbb{I}}/2$.

with:

$$\hat{E}_0 = \frac{1}{2}\left[(1+\sqrt{1-\gamma})\,\hat{\mathbb{I}} + (1-\sqrt{1-\gamma})\,\hat{\sigma}_z\right] \to \begin{pmatrix} 1 & 0 \\ 0 & \sqrt{1-\gamma} \end{pmatrix}, \tag{7.24a}$$

$$\hat{E}_1 = \frac{\sqrt{\gamma}}{2}\,(\hat{\sigma}_x + i\hat{\sigma}_y) \to \begin{pmatrix} 0 & \sqrt{\gamma} \\ 0 & 0 \end{pmatrix}, \tag{7.24b}$$

$1 \leq \gamma \leq 0$. Note that we can also write $\sqrt{\gamma} = \sin\theta$ and $\sqrt{1-\gamma} = \cos\theta$.

> □ **– Exercise 7.1** *Write the amplitude damping map $\mathcal{E}_{\text{ad}}(\hat{\varrho})$ as a function of the Pauli operators.*

Since $\hat{E}_0 = |0\rangle\langle 0| + \sqrt{1-\gamma}\,|1\rangle\langle 1|$ and $\hat{E}_1 = \sqrt{\gamma}\,|0\rangle\langle 1|$, it is easy to verify that:

$$\hat{E}_0|0\rangle = |0\rangle, \quad \text{and} \quad \hat{E}_0|1\rangle = \sqrt{1-\gamma}|1\rangle, \tag{7.25}$$

and:

$$\hat{E}_1|0\rangle = 0, \quad \text{and} \quad \hat{E}_1|1\rangle = \sqrt{\gamma}|0\rangle, \tag{7.26}$$

therefore γ can be thought as the probability of loosing a quantum of energy. We have the following effect on the Bloch sphere:

$$\begin{cases} r_x & \to & \sqrt{1-\gamma}\,r_x, \\ r_y & \to & \sqrt{1-\gamma}\,r_y, \\ r_z & \to & \gamma + (1-\gamma)\,r_z. \end{cases} \tag{7.27}$$

In order to describe the dissipative dynamics affecting a qubit, we make the following substitution:

$$\gamma \to \gamma(t) = 1 - \mathrm{e}^{-t/\tau}, \tag{7.28}$$

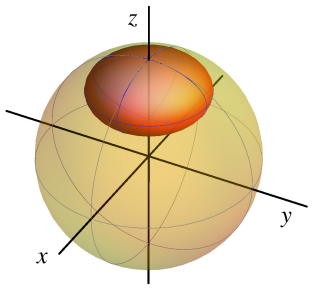

Figure 7.5: Effect of the amplitude damping channel on the Bloch sphere with $\hat{\varrho}_\infty = |0\rangle\langle 0|$, that is the north pole of the unit sphere.

where t is a parameter corresponding to the time evolution and τ is a characteristic time of the system (here we assume that $t = 0$ represents the initial time). Inserting $\gamma(t)$ into Eq. (7.23) we obtain a quantum operation describing a dissipative time evolution. In particular, since:

$$\lim_{t\to+\infty} \gamma(t) = 1, \tag{7.29}$$

as time increases the system evolves toward the state $|0\rangle$ (the north pole of the Bloch sphere), which is the lowest energy level of the qubit: we can now easily understand why the map of Eq. (7.23) represents dissipation... at least for a quantum system at zero temperature. Figure 7.5 shows the deformation of the Bloch sphere due to the amplitude damping channel (with asymptotic state $\hat{\varrho}_\infty = |0\rangle\langle 0|$).

7.5 Generalized amplitude damping channel

In general, quantum systems may have a nonzero temperature T and, in this case, the asymptotic state does not correspond to the lowest energy one. This fact is described by means of a *generalized* amplitude damping channel which involves the two operators $\hat{E}_0$ and $\hat{E}_1$ of Eqs. (7.24) and the following two further operators:

$$\hat{E}_2 = \frac{1}{2}\left[(1+\sqrt{1+\gamma})\,\hat{\mathbb{I}} - (1-\sqrt{1-\gamma})\,\hat{\sigma}_z\right] \to \begin{pmatrix} \sqrt{1-\gamma} & 0 \\ 0 & 1 \end{pmatrix}, \tag{7.30a}$$

$$\hat{E}_3 = \frac{\sqrt{\gamma}}{2}\left[\hat{\sigma}_x - i\hat{\sigma}_y\right] \to \begin{pmatrix} 0 & 0 \\ \sqrt{\gamma} & 0 \end{pmatrix}, \tag{7.30b}$$

which represent a *phase insensitive* amplification process. In fact, since $\hat{E}_2 = \sqrt{1-\gamma}\,|0\rangle\langle 0| + |1\rangle\langle 1|$ and $\hat{E}_3 = \sqrt{\gamma}\,|1\rangle\langle 0|$, it is easy to verify that:

$$\hat{E}_2|0\rangle = \sqrt{1-\gamma}|0\rangle, \quad \text{and} \quad \hat{E}_2|1\rangle = |1\rangle, \tag{7.31}$$

and:

$$\hat{E}_3|0\rangle = \sqrt{\gamma}|1\rangle, \quad \text{and} \quad \hat{E}_3|1\rangle = 0. \tag{7.32}$$

The whole map reads:

$$\mathcal{E}_{\text{gad}}(\hat{\varrho}) = p\,(\hat{E}_0\hat{\varrho}\hat{E}_0^\dagger + \hat{E}_1\hat{\varrho}\hat{E}_1^\dagger) + (1-p)\,(\hat{E}_2\hat{\varrho}\hat{E}_0^\dagger + \hat{E}_3\hat{\varrho}\hat{E}_1^\dagger), \tag{7.33}$$

where $0 \leq p \leq 1$. If we perform the same substitution given in Eq. (7.28), we find that the stationary state for $t \to +\infty$ is:

$$\hat{\varrho}_\infty = \frac{1}{2}\hat{\mathbb{I}} + \frac{2p-1}{2}\hat{\sigma}_z \to \begin{pmatrix} p & 0 \\ 0 & 1-p \end{pmatrix}. \tag{7.34}$$

□ **– Exercise 7.2** *Find the evolution of the vector* $\mathbf{r}$ *under the effect of the generalized amplitude damping channel.*

7.5.1 Approaching the thermal equilibrium

When the quantum operation of Eq. (7.33) describes the evolution of a qubit state toward the termal equilibrium, the probability p is a function of the temperature T. If $\mathscr{E}_x$ is the energy of the state $|x\rangle$, $x = 0, 1$, then one has that the state occupation probability is given by the Boltzmann distribution, namely:

$$p_x(T) = \frac{1}{\mathcal{Z}} \exp\left(-\frac{\mathscr{E}_x}{k_B T}\right), \tag{7.35}$$

where $\mathcal{Z} = p_0(T) + p_1(T)$ is the partition function and k_B is the Boltzmann constant. Therefore the stationary, equilibrium state writes:

$$\hat{\varrho}_\infty(T) \to \begin{pmatrix} p_0(T) & 0 \\ 0 & 1-p_0(T) \end{pmatrix} = \frac{1}{\mathcal{Z}} \begin{pmatrix} \exp\left[-\mathscr{E}_0/(k_B T)\right] & 0 \\ 0 & \exp\left[-\mathscr{E}_1/(k_B T)\right] \end{pmatrix}, \tag{7.36}$$

which represents the statistical mixture describing a two-level system at termal equilibrium at temperature T. The purity of the state $\hat{\varrho}_\infty(T)$ is:

$$\mu\left[\hat{\varrho}_\infty(T)\right] = 1 - 2p_0(T)\,p_1(T). \tag{7.37}$$

7.6 Phase damping channel

This kind of channel describes the loss of quantum information without loss of energy. We can derive the quantum operation of this channel addressing a single qubit system subjected to a

rotation around the z-axis of the Bloch sphere, namely:

$$\hat{R}_z(\vartheta) = \cos\vartheta\,\hat{\mathbb{I}} - i\sin\vartheta\,\hat{\sigma}_z \to \begin{pmatrix} \mathrm{e}^{-i\vartheta/2} & 0 \\ 0 & \mathrm{e}^{i\vartheta/2} \end{pmatrix}, \tag{7.38}$$

where ϑ is random (this is a random kick). We assume that ϑ is randomly distributed according to a Gaussian distribution with zero mean and variance $2\Delta^2$. We have the following evolution:

$$\hat{\varrho} \to \mathcal{E}_{\mathrm{pdc}}(\hat{\varrho}) = \int_{-\infty}^{+\infty} d\vartheta\, \frac{\exp\left(-\frac{\vartheta^2}{4\Delta^2}\right)}{\sqrt{4\pi\Delta^2}}\, \hat{R}_z(\vartheta)\,\hat{\varrho}\,\hat{R}_z(\vartheta)^\dagger \tag{7.39}$$

$$= \hat{E}_0\hat{\varrho}\hat{E}_0^\dagger + \hat{E}_0\hat{\varrho}\hat{E}_0^\dagger, \tag{7.40}$$

with:

$$\hat{E}_0 = \sqrt{\frac{1+\exp(-\Delta^2)}{2}}\,\hat{\mathbb{I}}, \quad \text{and} \quad \hat{E}_1 = \sqrt{\frac{1-\exp(-\Delta^2)}{2}}\,\hat{\sigma}_z. \tag{7.41}$$

It is worth noting that the quantum operation of Eq. (7.40) corresponds to the phase flip operation addressed in section 7.3.2 with $p = [1+\exp(-\Delta^2)]/2$. The effect on the Bloch sphere is analogous to that of the phase flip operation:

$$\begin{cases} r_x & \to & \mathrm{e}^{-\Delta^2}\, r_x, \\ r_y & \to & \mathrm{e}^{-\Delta^2}\, r_y, \\ r_z & \to & r_z. \end{cases} \tag{7.42}$$

Bibliography

- M. A. Nielsen and I. L. Chuang, *Quantum Computation and Quantum Information* (Cambridge University Press, 2010) – Chapter 8.2.

Chapter 8

Basics of quantum error correction

8.1 The binary symmetric channel

In a classical binary symmetric channel (BSC) the information is encoded into the bits $|0\rangle$ and $|1\rangle$ and we assume that a bit flip error may occurs with probability p. The probability of error, that is the probability that $|x\rangle \to |\overline{x}\rangle$, with $x = 0, 1$, is simply given by the bit flip probability, that is:

$$p_{\text{err}}^{(1)} = p, \tag{8.1}$$

where the superscript tell us we are using just one bit to encode the information.

8.1.1 The 3-bit code

One of the classical codes used to correct the bit flip error is the 3-bit code. Here the information is encoded onto three independent copies of the original bit and the correction strategy is based on the *majority voting*: if, among the received three bits, at least two have the same value x, then we decide that the sent bit value was x. Indeed, here we are also assuming that only one bit undergoes bit flip and, thus, we have the following error probability, which is the probability of having two or more bits flipped:

$$p_{\text{err}}^{(3)} \equiv p_{\geq 2} = p^3 + 3p^2(1-p) = 3p^2 - 2p^3. \tag{8.2}$$

As one can see from figure 8.1, we have that $p_{\text{err}}^{(3)} < p_{\text{err}}^{(1)}$ if $p < 1/2$.

8.2 Quantum error correction: the 3-qubit code

A quantum state cannot be cloned. Therefore we cannot have three identical copies of an unknown quantum state $|\psi\rangle$ (see section 3.3.1). Furthermore, in contrast to the classical case, we

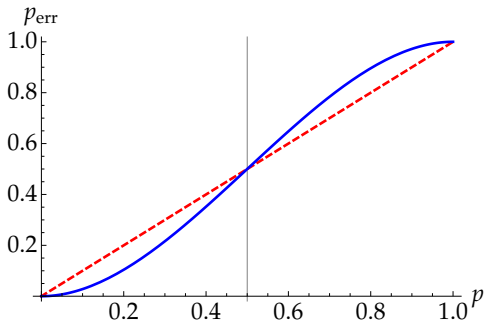

Figure 8.1: Plot of $p_{\text{err}}^{(1)}$ (dashed, red line) and $p_{\text{err}}^{(3)}$ (solid, blue line) as functions of the bit flip probability p. For values of p less than 0.5 the 3-bit code has a better performance with respect the single bit encoding.

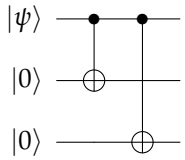

Figure 8.2: This quantum circuit implement the transformation $|\psi\rangle|0\rangle|0\rangle \rightarrow \alpha|000\rangle + \beta|111\rangle$, where $|\psi\rangle = \alpha|0\rangle + \beta|1\rangle$.

cannot measure the state in order to get information about the error, since the measurement destroys the quantum state... We should find a quantum circuit able to "detect" the eventual error (the bit flip) and to correct it *without destroying the quantum state*. The solution to this problem is given by the 3-qubit code, that is the analogous of the classical code

8.2.1 Correction of bit flip error

As we have seen in section 7.3.1, the evolution of a quantum state $\hat{\varrho}$ through a bit flip channel can be described by the quantum map:

$$\mathcal{E}(\hat{\varrho}) = (1-p)\,\hat{\varrho} + p\,\hat{\sigma}_x\,\hat{\varrho}\,\hat{\sigma}_x, \tag{8.3}$$

where, now, p is the bit flip probability. In the following we assume that the information is encoded in the qubit state $|\psi\rangle = \alpha|0\rangle + \beta|1\rangle$ and we also have $\hat{\sigma}_x|\psi\rangle = \alpha|1\rangle + \beta|0\rangle$. The basic idea of the 3-qubit code is to encode the information onto three qubits as follows:

$$|\psi\rangle \rightarrow |\Psi\rangle = \alpha|000\rangle + \beta|111\rangle, \tag{8.4}$$

where, as usual $|xyz\rangle = |x\rangle|y\rangle|z\rangle$. The reader can verify that this task is obtained by means of the quantum circuit of figure 8.2. It is worth noting that $|\Psi\rangle$ is an entangled state.

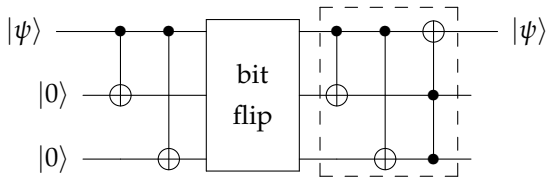

Figure 8.3: The dashed box encloses the quantum circuit implementing the 3-qubit code for quantum error correction against single bit flip operation.

As in the classical case, we let the bit flip channel affect *independently* each qubit (uncorrelated channels). After the noisy evolution we should implement the error diagnosis and correction: in figure 8.3 we can see the quantum circuit achieving this goal.

In order to understand how the 3-qubit code works, let us assume that after the bit flip channel the state is $|\Psi'\rangle = \hat{\sigma}_x \otimes \hat{\mathbb{I}} \otimes \hat{\mathbb{I}} |\Psi\rangle$, i.e., the first qubit has been flipped. The first CNOT gate performs the following transformation:

$$|\Psi'\rangle = \alpha|100\rangle + \beta|011\rangle \rightarrow \alpha|110\rangle + \beta|011\rangle, \tag{8.5}$$

thereafter, we have the second CNOT gate which leads to:

$$\alpha|110\rangle + \beta|011\rangle \rightarrow \alpha|111\rangle + \beta|011\rangle. \tag{8.6}$$

The last gate is a Toffoli gate which takes the second and third qubits as control and the first qubit as target, we obtain:

$$\alpha|111\rangle + \beta|011\rangle \rightarrow \alpha|011\rangle + \beta|111\rangle \equiv \underbrace{(\alpha|0\rangle + \beta|1\rangle)}_{|\psi\rangle}|11\rangle. \tag{8.7}$$

We conclude that the error has been corrected since the state of the first qubit is still $|\psi\rangle$.

□ **– Exercise 8.1** *Verify that the 3-qubit codes depicted in figure 8.3 works as follows:*

$$\begin{aligned}
\hat{\mathbb{I}} \otimes \hat{\mathbb{I}} \otimes \hat{\mathbb{I}} |\Psi\rangle &\rightarrow |\psi\rangle|00\rangle, \\
\hat{\sigma}_x \otimes \hat{\mathbb{I}} \otimes \hat{\mathbb{I}} |\Psi\rangle &\rightarrow |\psi\rangle|11\rangle, \\
\hat{\mathbb{I}} \otimes \hat{\sigma}_x \otimes \hat{\mathbb{I}} |\Psi\rangle &\rightarrow |\psi\rangle|10\rangle, \\
\hat{\mathbb{I}} \otimes \hat{\mathbb{I}} \otimes \hat{\sigma}_x |\Psi\rangle &\rightarrow |\psi\rangle|01\rangle.
\end{aligned}$$

The code may fails if more than one qubit is flipped. Since the probability that at most one bit is flipped reads:

$$p_{\leq 1} = (1-p)^3 + 3p\,(1-p)^2 = (1-p)^2(1+2p), \tag{8.8}$$

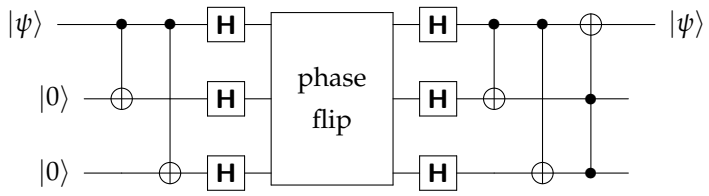

Figure 8.4: Quantum circuit describing the strategy to implement the 3-qubit code for quantum error correction against single phase flip operation.

we have the following probability of error at the output:

$$p_{\text{err,Q}}^{(3)} = 1 - p_{\leq 1} = 3p^2 - 2p^3, \tag{8.9}$$

the same obtained in the classical 3-bit code.

8.2.2 Correction of phase flip error

Phase flip error does not have classical analogue, since the transformation $|1\rangle \rightarrow -|1\rangle$ does not exist in classical logic. The quantum map describing a channel in which phase flip occurs with probability p reads (see also section 7.3.2):

$$\mathcal{E}(\hat{\varrho}) = (1-p)\,\hat{\varrho} + p\,\hat{\sigma}_z\,\hat{\varrho}\,\hat{\sigma}_z. \tag{8.10}$$

It is worth noting that since $\hat{\sigma}_z|x\rangle = (-1)^x|x\rangle$, we have:

$$\hat{\sigma}_z|\pm\rangle = |\mp\rangle, \tag{8.11}$$

where:

$$|\pm\rangle = \frac{|0\rangle \pm |1\rangle}{\sqrt{2}}, \tag{8.12}$$

and we conclude that the phase flip channel acts as a bit flip channel on the basis $|\pm\rangle$. Therefore, recalling the action of the Hadamard transformation on the computational basis $|0\rangle$ and $|1\rangle$, it is easy to prove that the quantum circuit represented in figure 8.4 corrects a single phase flip error. Actually, the first Hadamard transformations physically change the computational basis in order that the phase flip channel behaves like a bit flip channel; the second Hadamard transformations transform back to the original basis in order to apply the same correction code described in the previous section.

8.2.3 Correction of any error: the Shor code

As a matter of fact, in a realistic channel both bit and phase flip errors may take place. It is possible to protect the qubit against the effects of an *arbitrary* error by means of the Shor code,

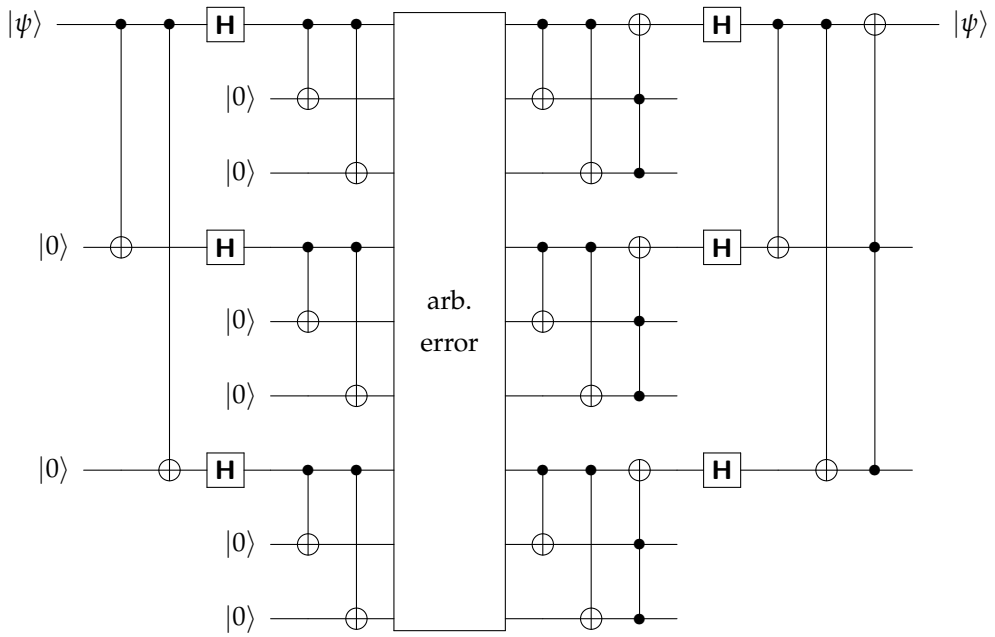

Figure 8.5: Quantum circuit implementing the Shor code to protect a qubit $|\psi\rangle$ against an arbitrary error.

which is a combination of the 3-qubit bit flip and phase flip error correction codes. In figure 8.5 we sketched the quantum circuit implementing the Shor code. The reader can investigate its action applying the results obtained in the previous sections.

Bibliography

- M. A. Nielsen and I. L. Chuang, *Quantum Computation and Quantum Information* (Cambridge University Press, 2010) – Chapter 10.

Chapter 9

Two-level systems and basics of QED

ANY TWO-LEVEL QUANTUM SYSTEM is associated with a Hilbert space spanned by two orthonormal states and , thus, can be seen as a qubit. In this chapter we will focus on $\frac{1}{2}$-spin particles and two-level atoms, which are the simplest example of qubits. We also explain how it is possible to manipulate spins and atoms in order to implement quantum logic gates.

9.1 Universal computation with spins

A typical two-level system is a $\frac{1}{2}$-spin particle which can be used as a qubit and manipulated by means of electromagnetic fields.

9.1.1 Interaction between a spin and a magnetic field

The operator associated with the spin magnetic moment of a $\frac{1}{2}$-spin particle is given by:

$$\hat{\boldsymbol{\mu}} = -\frac{gq}{2m}\,\hat{\mathbf{S}}, \tag{9.1}$$

where g is the gyromagnetic factor (for an electron $g \approx 2.002$), q and m are the charge and the mass of the particle, respectively, and $\hat{\mathbf{S}} = \frac{\hbar}{2}\,\hat{\boldsymbol{\sigma}}$, where $\hat{\boldsymbol{\sigma}} = (\hat{\sigma}_x, \hat{\sigma}_y, \hat{\sigma}_z)$ is, as usual, the vector of the Pauli operators.

The Hamiltonian describing the interaction between the $\frac{1}{2}$-spin particle and the (classical) static magnetic fiels $\boldsymbol{B} = (B_x, B_y, B_z)$ is:

$$\hat{H}_{\text{int}} = -\hat{\boldsymbol{\mu}} \cdot \boldsymbol{B} = \frac{gq}{2m}\,\frac{\hbar}{2}\,\hat{\boldsymbol{\sigma}} \cdot \boldsymbol{B}. \tag{9.2}$$

which can be written as:

$$\hat{H}_{\text{int}} = \frac{\hbar\omega}{2}\,\boldsymbol{n} \cdot \hat{\boldsymbol{\sigma}}, \tag{9.3}$$

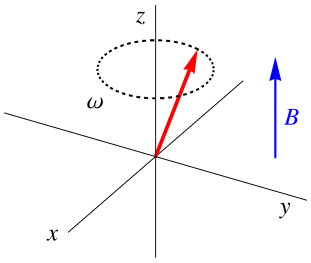

Figure 9.1: Precession of a spin (red arrow) under the effect of a magnetic field B directed along z-direction. The tip of the vector representing the spin rotate counterclockwise around the z-direction.

where we introduced the Larmor frequency $\omega = gq|\boldsymbol{B}|/(2m)$, and $\boldsymbol{n} = \boldsymbol{B}/|\boldsymbol{B}|$.

Without lack of generality, we assume $\boldsymbol{B} = (0, 0, B)$, that is we take the magnetic field along the z-direction and, accordingly, $\boldsymbol{n} \cdot \hat{\boldsymbol{\sigma}} = \hat{\sigma}_z$. Given the initial state (as we mentioned, any two-level system can be considered as a qubit, see section 2.2):

$$|\psi_0\rangle = \cos\frac{\theta}{2}\,|0\rangle + \sin\frac{\theta}{2}\,|1\rangle, \tag{9.4}$$

with $\hat{\sigma}_z|x\rangle = (-1)^x|x\rangle$, $x = 0, 1$, we have the following time evolution under the effect of $\hat{H}_{\text{int}}$:

$$\begin{aligned} |\psi_t\rangle &= \exp\left(-i\,\frac{\hat{H}_{\text{int}}}{\hbar}\,t\right)|\psi_0\rangle \\ &= \cos\frac{\theta}{2}\,\mathrm{e}^{-i\omega t/2}|0\rangle + \sin\frac{\theta}{2}\,\mathrm{e}^{i\omega/2t}|1\rangle \\ &= \mathrm{e}^{-i\omega t/2}\left(\cos\frac{\theta}{2}\,|0\rangle + \sin\frac{\theta}{2}\,\mathrm{e}^{i\omega t}|1\rangle\right), \end{aligned} \tag{9.5}$$

where, in the last equation, the overall phase $\mathrm{e}^{-i\omega t/2}$ can be neglected. Following section 2.2.1, the Bloch vector $\boldsymbol{r}_t$ associated with $|\psi_t\rangle$ reads:

$$\boldsymbol{r}_t = \begin{pmatrix} \sin\theta\,\cos\omega t \\ \sin\theta\,\sin\omega t \\ \cos\theta \end{pmatrix}, \tag{9.6}$$

that is we have the Larmor precession of the spin around the direction of the magnetic field (here the z-direction), as illustrated in figure 9.1.

More in general, the unitary evolution operator associated with the Hamiltonian (9.3) reads:

$$\exp\left(-i\,\frac{\hat{H}_{\text{int}}}{\hbar}\,t\right) = \cos\left(\frac{\omega t}{2}\right)\hat{\mathbb{1}} - i\,\sin\left(\frac{\omega t}{2}\right)\boldsymbol{n}\cdot\hat{\boldsymbol{\sigma}}, \tag{9.7}$$

and we can implement single qubit gates by suitably choosing the time t and the amplitude and orientation of the magnetic field $\boldsymbol{B}$.

9.1.2 Spin qubit and Hadamard transformation

If we orient the magnetic field along the x-z direction, i.e., $\boldsymbol{B} = B\,\boldsymbol{n}$ with $\boldsymbol{n} = 2^{-1/2}(1,0,1)$, and set the evolution time such that $\omega t = \pi$, form Eq. (9.7) we have:

$$\exp\left(-i\,\frac{\hat{H}_{\rm int}}{\hbar}\,t\right) \to -\frac{i}{\sqrt{2}}\,(\hat{\sigma}_x + \hat{\sigma}_z) \equiv -i\,\mathbf{H}, \tag{9.8}$$

that is, up to an overall phase factor "$-i$", we have the quantum operator describing the action of the Hadamard transformation introduced in section 1.4.4 [see Eq. (1.30)].

> □ **– Exercise 9.1** *Starting form Eq. (9.7), explain why it is possible to reproduce the action of any single-qubit gate by using a single spin and a suitably chosen classical magnetic field.*

9.1.3 How to realize a CNOT gate

The CNOT gate involves two qubits and the corresponding operator, taking qubits 1 and 2 as control and target, respectively, may be written as the following operator:

$$\mathbf{C}_{12} = \frac{1}{2}\left(\hat{\mathbb{I}} + \hat{\sigma}_z^{(1)} + \hat{\sigma}_x^{(2)} - \hat{\sigma}_z^{(1)}\hat{\sigma}_x^{(2)}\right), \tag{9.9}$$

where $\hat{\sigma}_k^{(h)}$, $k = x,y,z$ and $h = 1,2$, represent the Pauli operators acting on the h-th qubit (see section 1.4.2). However, as mentioned in section 3.5, $\hat{\sigma}_z = \mathbf{H}\,\hat{\sigma}_x\,\mathbf{H}$, therefore we can focus on the operator:

$$\mathbf{Z}_{12} = \left(\hat{\mathbb{I}} \otimes \mathbf{H}\right)\mathbf{C}_{12}\left(\hat{\mathbb{I}} \otimes \mathbf{H}\right) \tag{9.10a}$$

$$= \frac{1}{2}\left(\hat{\mathbb{I}} + \hat{\sigma}_z^{(1)} + \hat{\sigma}_z^{(2)} - \hat{\sigma}_z^{(1)}\hat{\sigma}_z^{(2)}\right), \tag{9.10b}$$

which is symmetric with respect the exchange of the two qubits. Since $(\mathbf{Z}_{12})^2 = \hat{\mathbb{I}}$ we have:

$$\exp\left(i\,\mathbf{Z}_{12}\,\theta\right) = \sum_{k=0}^{\infty}\frac{(i\theta)^k}{k!}(\mathbf{Z}_{12})^k \tag{9.11a}$$

$$= \cos\theta\,\hat{\mathbb{I}} + i\,\mathbf{Z}_{12}\,\sin\theta, \tag{9.11b}$$

and, setting $\theta = \pi/2$, we find:

$$\mathbf{Z}_{12} = -i\exp\left(i\,\mathbf{Z}_{12}\,\frac{\pi}{2}\right) \tag{9.12a}$$

$$= -i\exp\left[i\frac{\pi}{4}\left(\hat{\mathbb{I}} + \hat{\sigma}_z^{(1)} + \hat{\sigma}_z^{(2)} - \hat{\sigma}_z^{(1)}\hat{\sigma}_z^{(2)}\right)\right] \tag{9.12b}$$

$$= \exp\left(-i\frac{\pi}{4}\right)\exp\left[i\frac{\pi}{4}\left(\hat{\sigma}_z^{(1)} + \hat{\sigma}_z^{(2)} - \hat{\sigma}_z^{(1)}\hat{\sigma}_z^{(2)}\right)\right]. \tag{9.12c}$$

Therefore, we can implement the $\mathbf{Z}_{12}$ gate by letting the two qubits interact through the Hamiltonian:

$$\hat{H} \propto \hat{\sigma}_z^{(1)} + \hat{\sigma}_z^{(2)} - \hat{\sigma}_z^{(1)}\hat{\sigma}_z^{(2)}, \tag{9.13}$$

and by choosing a suitable time t for the corresponding unitary evolution. As we will see, the term $\hat{H}_0 \propto \hat{\sigma}_z^{(1)} + \hat{\sigma}_z^{(2)}$ is the free Hamiltonian of the system of the two qubits, while $\hat{\sigma}_z^{(1)}\hat{\sigma}_z^{(2)}$ represents a highly anisotropic interaction that couples the z-components of the qubits, known as *Ising interaction*.

Physically, the Hamiltonian $\hat{H}$ may be realized with $\frac{1}{2}$-spin particles. In this case the free Hamiltonian is $\hat{H}_0 = \frac{1}{2}\hbar\,(\hat{\sigma}_z^{(1)} + \hat{\sigma}_z^{(2)})$ and the interaction $\propto \hat{\sigma}_z^{(1)}\hat{\sigma}_z^{(2)}$ couples the spins along the z-direction subject to an uniform magnetic field, whose amplitude is proportional to the strength of their coupling. However, Ising interactions are hard to arrange and it is better to consider *exchange interactions* between spins. As we will see in chapter 9 (section 9.1.4), by applying suitable magnetic fields to the spins, with the same direction but different magnitudes and signs, we can build a $\mathbf{Z}_{12}$ gate.

□ **– Exercise 9.2** *Prove that the operators* $\mathbf{C}_{12}$ *and* $\mathbf{Z}_{12}$ *as defined in Eqs. (9.9) and (9.10b), respectively, act on* $|x\rangle|y\rangle$ *as a CNOT and a controlled-*$\mathbf{Z}$ *gates, where* $\hat{\sigma}_z|x\rangle = (-1)^x|x\rangle$ *and* $\hat{\sigma}_x|x\rangle = |\overline{x}\rangle$.

9.1.4 Exchange interactions and CNOT gate

In section 9.1.3 we have seen that CNOT may be implemented with two $\frac{1}{2}$-spins by using the Ising interaction, that is a kind of interaction which couples spin along z-direction. However, we pointed out that Ising interactions are hard to arrange and it is better to use *exchange interactions* between two spins, whose interaction Hamiltonian is:

$$\hat{H}_{\text{ex}} \propto \hat{\boldsymbol{\sigma}}^{(1)} \cdot \hat{\boldsymbol{\sigma}}^{(2)} = \hat{\sigma}_x^{(1)}\hat{\sigma}_x^{(2)} + \hat{\sigma}_y^{(1)}\hat{\sigma}_y^{(2)} + \hat{\sigma}_z^{(1)}\hat{\sigma}_z^{(2)}, \tag{9.14}$$

where $\hat{\boldsymbol{\sigma}}^{(k)} = (\hat{\sigma}_x^{(k)}, \hat{\sigma}_y^{(k)}, \hat{\sigma}_z^{(k)})$, $k = 1, 2$, is the vector of the Pauli operators acting on the Hilbert space $\mathcal{H}_k$ of the k-th spin.

The system we are considering here consists of two $\frac{1}{2}$-spins particles of mass m_k and charge q_k, $k = 1, 2$. We assume that each spin interacts with a magnetic field $\boldsymbol{B}_k$ whereas they are coupled through exchange interaction. The corresponding Hamiltonian reads (we use the same formalism introduced in the previous sections):

$$\hat{H} = \hbar\frac{\omega_1}{2}\,\boldsymbol{n}_1 \cdot \hat{\boldsymbol{\sigma}}^{(1)} + \hbar\frac{\omega_2}{2}\,\boldsymbol{n}_2 \cdot \hat{\boldsymbol{\sigma}}^{(2)} + \hbar J\,\hat{\boldsymbol{\sigma}}^{(1)} \cdot \hat{\boldsymbol{\sigma}}^{(2)}, \tag{9.15}$$

where ω_k are the corresponding Larmor frequencies and J is the strength of the exchange interaction. Note that if $J = 0$, then Eq. (9.15) reduces to the Hamiltonian of two uncoupled spins each interacting with the corresponding magnetic field, that is we have just two single-qubit gates.

Without lack of generality we can set $\boldsymbol{B}_k = (0, 0, B_k)$ and Eq. (9.15) becomes:

$$\hat{H} = \underbrace{\hbar\frac{\omega_1}{2}\,\hat{\sigma}_z^{(1)} + \hbar\frac{\omega_2}{2}\,\hat{\sigma}_z^{(2)}}_{\hat{H}_0} + \underbrace{\hbar J\,\hat{\boldsymbol{\sigma}}^{(1)}\cdot\hat{\boldsymbol{\sigma}}^{(2)}}_{\hat{H}_{\text{ex}}}, \tag{9.16}$$

where $\hat{H}_0$ is the free Hamiltonian of the two-spin system, while $\hat{H}_{\text{ex}}$ is the interaction Hamiltonian. In the following we show that, starting form the Hamiltonian in Eq. (9.16), we can build the two-qubit quantum gate $\mathbf{Z}_{12}$, that can be converted into a CNOT gate by means of Hadamard transformations realized through Eq. (9.8) (see section 9.1.3). In particular, we show that for a suitable choice of ω_k and t, given J, we may have $\mathbf{Z}_{12} = \exp(-i\,\hat{H}t/\hbar)$. First of all, we recall that:

$$\mathbf{Z}_{12} = \frac{1}{2}\left(\hat{\mathbb{I}} + \hat{\sigma}_z^{(1)} + \hat{\sigma}_z^{(2)} - \hat{\sigma}_z^{(1)}\hat{\sigma}_z^{(2)}\right), \tag{9.17}$$

and this is its action on the *triplet states* $|00\rangle$, $|11\rangle$ and $|\psi_+\rangle = 2^{-1/2}(|01\rangle + |10\rangle)$ and on the *singlet state* $|\psi_-\rangle = 2^{-1/2}(|01\rangle - |10\rangle)$:

$$\mathbf{Z}_{12}|00\rangle = |00\rangle, \qquad \mathbf{Z}_{12}|11\rangle = -|11\rangle, \tag{9.18a}$$

$$\mathbf{Z}_{12}|\psi_+\rangle = |\psi_+\rangle, \qquad \mathbf{Z}_{12}|\psi_-\rangle = |\psi_-\rangle. \tag{9.18b}$$

It is worth noting that the four states $\{|00\rangle, |11\rangle, |\psi_\pm\rangle\}$ form a basis of the Hilbert space $\mathcal{H}_1 \otimes \mathcal{H}_2$, $\mathcal{H}_k$ being the Hilbert space of the k-th spin. Therefore, it is enough to find the conditions on the involved parameters in order to have $\exp(-i\,\hat{H}t/\hbar)$ acting as $c\mathbf{Z}$ on such a basis.

The first step is to find the eigenvectors and eigenvalues of Eq. (9.16) and we proceed as follows. Since the SWAP operator may be written as $\mathbf{S} = \frac{1}{2}(\hat{\mathbb{I}} + \hat{\boldsymbol{\sigma}}^{(1)}\cdot\hat{\boldsymbol{\sigma}}^{(2)})$, therefore the following states are eigenstates of the operator $\hat{\boldsymbol{\sigma}}^{(1)}\cdot\hat{\boldsymbol{\sigma}}^{(2)}$, namely:

$$\hat{\boldsymbol{\sigma}}^{(1)}\cdot\hat{\boldsymbol{\sigma}}^{(2)}|00\rangle = |00\rangle, \qquad \hat{\boldsymbol{\sigma}}^{(1)}\cdot\hat{\boldsymbol{\sigma}}^{(2)}|11\rangle = |11\rangle, \tag{9.19a}$$

$$\hat{\boldsymbol{\sigma}}^{(1)}\cdot\hat{\boldsymbol{\sigma}}^{(2)}|\psi_+\rangle = |\psi_+\rangle, \qquad \hat{\boldsymbol{\sigma}}^{(1)}\cdot\hat{\boldsymbol{\sigma}}^{(2)}|\psi_-\rangle = -3\,|\psi_-\rangle. \tag{9.19b}$$

Furthermore, we can write:

$$\hat{H}_0 = \hbar\frac{\omega_+}{2}\left(\frac{\hat{\sigma}_z^{(1)} + \hat{\sigma}_z^{(2)}}{2}\right) + \hbar\frac{\omega_-}{2}\left(\frac{\hat{\sigma}_z^{(1)} - \hat{\sigma}_z^{(2)}}{2}\right), \tag{9.20}$$

with $\omega_\pm = \omega_1 \pm \omega_2$ and we find:

$$\frac{1}{2}\left(\hat{\sigma}_z^{(1)} + \hat{\sigma}_z^{(2)}\right)|00\rangle = |00\rangle, \qquad \frac{1}{2}\left(\hat{\sigma}_z^{(1)} - \hat{\sigma}_z^{(2)}\right)|00\rangle = 0, \tag{9.21a}$$

$$\frac{1}{2}\left(\hat{\sigma}_z^{(1)} + \hat{\sigma}_z^{(2)}\right)|11\rangle = -|11\rangle, \qquad \frac{1}{2}\left(\hat{\sigma}_z^{(1)} - \hat{\sigma}_z^{(2)}\right)|11\rangle = 0, \tag{9.21b}$$

$$\frac{1}{2}\left(\hat{\sigma}_z^{(1)} + \hat{\sigma}_z^{(2)}\right)|\psi_\pm\rangle = 0, \qquad \frac{1}{2}\left(\hat{\sigma}_z^{(1)} - \hat{\sigma}_z^{(2)}\right)|\psi_\pm\rangle = |\psi_\mp\rangle. \tag{9.21c}$$

Therefore we have:

$$\hat{H}|00\rangle = \hbar\left(J + \frac{\omega_+}{2}\right)|00\rangle, \qquad \hat{H}|11\rangle = \hbar\left(J - \frac{\omega_+}{2}\right)|11\rangle, \tag{9.22a}$$

$$\hat{H}|\psi_+\rangle = \hbar J|\psi_+\rangle + \hbar\frac{\omega_-}{2}|\psi_-\rangle, \qquad \hat{H}|\psi_-\rangle = -3\hbar J|\psi_-\rangle + \hbar\frac{\omega_-}{2}|\psi_+\rangle, \tag{9.22b}$$

that is $|00\rangle$ and $|11\rangle$ are eigenstates of $\hat{H}$, while $\hat{H}$ transforms $|\psi_\pm\rangle$ is a linear combination of $|\psi_+\rangle$ and $|\psi_-\rangle$. Thereafter, we have the following matrix representation of $\hat{H}$ in the chosen basis:

$$\hat{H} \to \hbar\begin{pmatrix} J + \frac{1}{2}\omega_+ & 0 & 0 & 0 \\ 0 & J - \frac{1}{2}\omega_+ & 0 & 0 \\ 0 & 0 & J & \frac{1}{2}\omega_- \\ 0 & 0 & \frac{1}{2}\omega_- & -3J \end{pmatrix}. \tag{9.23}$$

The matrix has a block-diagonal form and, to find its eigenvectors and eigenvalues we can consider only the 2×2 block [the other block is with eigenvectors and eigenvalues given in Eg. (9.22a)]:

$$\begin{pmatrix} J & \frac{1}{2}\omega_- \\ \frac{1}{2}\omega_- & -3J \end{pmatrix} \tag{9.24}$$

that has eigenvalues $-J \pm \sqrt{4J^2 + \frac{1}{4}\omega_-^2}$, corresponding to the eigenstates $|\Psi_\pm\rangle = \alpha_\pm|\psi_+\rangle + \beta_\pm|\psi_-\rangle$, where we do not explicitly calculate the expression of the coefficients $\alpha_\pm$ and $\beta_\pm$. Now, since $|\psi_\pm\rangle$ are eigenstates of $\mathbf{Z}_{12}$ with eigenvalue 1 [see Eq. (9.18b)], the states $|\Psi_\pm\rangle$ are still its eigenstates with the same eigenvalue. Therefore, we have found that the four states:

$$|00\rangle, \quad |11\rangle, \quad \text{and} \quad |\Psi_\pm\rangle, \tag{9.25}$$

are eigenstates of both $\mathbf{Z}_{12}$ and $\hat{H}$ and, thus, of the evolution operator $U_{\text{ex}}(t) = \exp(-i\hat{H}t/\hbar)$.

In order to have $\mathbf{Z}_{12} \equiv U_{\text{ex}}(t)$, their eigenstates should have the same eigenvalues, up to a

constant phase factor which should be the same for all the states, namely:

$$U_{\rm ex}(t)|00\rangle = \exp\left[-it\left(J+\frac{1}{2}\omega_+\right)\right]|00\rangle \qquad \leftrightarrow \qquad \mathbf{Z}_{12}|00\rangle = |00\rangle, \tag{9.26a}$$

$$U_{\rm ex}(t)|11\rangle = \exp\left[-it\left(J-\frac{1}{2}\omega_+\right)\right]|11\rangle \qquad \leftrightarrow \qquad \mathbf{Z}_{12}|11\rangle = -|11\rangle, \tag{9.26b}$$

$$U_{\rm ex}(t)|\Psi_+\rangle = \exp\left[-it\left(-J+\sqrt{4J^2+\frac{1}{4}\omega_-^2}\right)\right]|\Psi_+\rangle \qquad \leftrightarrow \qquad \mathbf{Z}_{12}|\Psi_+\rangle = |\Psi_+\rangle, \tag{9.26c}$$

$$U_{\rm ex}(t)|\Psi_-\rangle = \exp\left[-it\left(-J-\sqrt{4J^2+\frac{1}{4}\omega_-^2}\right)\right]|\Psi_-\rangle \qquad \leftrightarrow \qquad \mathbf{Z}_{12}|\Psi_-\rangle = |\Psi_-\rangle. \tag{9.26d}$$

This happens by setting $\omega_+ = 4J$, $\omega_- = 4\sqrt{3}J$ and $t = \pi/(4J)$, which also leads to the overall constant phase factor $\exp(-i\,3\pi/4)$ equal for all the states. Indeed, one can change the value of $\omega_\pm$ by changing the values of the two magnetic fields. In fact, the previous conditions are equivalent to require $\omega_1 = 2(1+\sqrt{3})J$ and $\omega_2 = 2(1-\sqrt{3})J$, and, thus, we find (for the sake of simplicity we assume the two $\frac{1}{2}$-spin particle to be of the same species, i.e., $m_k = m$, $g_k = g$ and $q_k = q$, $k = 1,2$):

$$B_1 = 4(\sqrt{3}+1)\frac{mJ}{gq}, \quad \text{and} \quad B_2 = -4(\sqrt{3}-1)\frac{mJ}{gq}, \tag{9.27}$$

Note that the two magnetic fields are directed along z-direction but have opposite sign; though $\mathbf{Z}_{12}$ is symmetric, its physical implementation by means of exchange interaction requires different magnetic fields acting on the two spins. However, if we set $\omega_1 = 2(1-\sqrt{3})J$ and $\omega_2 = 2(1+\sqrt{3})J$ we obtain the same result, that is, the symmetry is still present!

Let us now focus on the order of magnitude of the involved quantities. The Bohr magneton and the Nuclear magneton are:

$$\mu_{\rm B} = \frac{e\hbar}{2m_{\rm e}} = 9.27\times10^{-24}\ \frac{\rm J}{\rm T} \quad \text{and} \quad \mu_{\rm N} = \frac{e\hbar}{2m_{\rm p}} = 5.05\times10^{-27}\ \frac{\rm J}{\rm T} \tag{9.28}$$

respectively, where e is the charge of the electron while $m_{\rm e}$ and $m_{\rm p}$ are the masses of the electron and of the proton, respectively. Typical $\frac{1}{2}$-spin nuclei are ^{1}H, ^{13}C and ^{19}F and the J-coupling magnitudes are $J \sim 10^8$ Hz ($\sim$ 100 MHz). Since $\omega \sim 10^8$ Hz, we have that the involved magnetic field amplitudes are $\sim 10^{-2}$ T for the electronic spin and ~ 10 T for the nuclear spin, leading to a time-scale $t \sim 10^{-8}$ sec.

□ **– Exercise 9.3** *Draw the quantum circuit to implement the CNOT gate involving $\frac{1}{2}$-spin particles by using single-qubit gates and the two-qubit gate based on the exchange interaction. Explain how the involved magnetic fields should be directed, write their magnitude and the interaction time for each gate. Is it important to control the overall phases appearing on the quibit after the gates? Why?*

9.1.5 Further considerations

The exchange interaction Hamiltonians are typical of NMR systems and molecules. The interaction between the spins is an indirect interaction mediated by the electrons shared through a chemical bond. The magnetic field seen by the nucleus is perturbed by the state of the electronic cloud, which interacts with another nucleus through the overlap of the wave-function with the nucleus (Fermi contact interaction), that is a through-bond interaction.

The same Hamiltonian of Eq. (9.15) describe the excess of electron spins in pair of quantum dots, which are linked through a tunnel junction (Heisenberg Hamiltonian). This effective Hamiltonian can be derived from a microscopic model for electrons in coupled quantum dots.

9.2 Interaction between atoms and light: cavity QED

In this section we address a two-level atom, throughout the section $|g\rangle$ and $|e\rangle$ represent the states associated with the ground and the excited state, respectively. The free Hamiltonian of the two-level atom can be written by means of the Pauli operators as follows:

$$\hat{H}_{\mathrm{a}} = \hbar \frac{\omega_{eg}}{2} \hat{\sigma}_z, \tag{9.29}$$

where $\hbar\omega_{eg} = \hbar\omega_e - \hbar\omega_g$ is the energy difference between the two levels and we have the following association with the usual computational basis: $|e\rangle \to |0\rangle$ and $|g\rangle \to |1\rangle$.

In the two-level approximation, the electric-dipole moment operator of the atom can be written as:

$$\hat{\boldsymbol{D}} = d\left(\boldsymbol{\varepsilon}_{\mathrm{a}}\hat{\sigma}_- + \boldsymbol{\varepsilon}_{\mathrm{a}}^*\hat{\sigma}_+\right) \tag{9.30}$$

where we introduced $\hat{\sigma}_- = |g\rangle\langle e|$ and $\hat{\sigma}_+ = |e\rangle\langle g|$, the lowering and raising operators, d is the matrix element of the atomic transition and $\boldsymbol{\varepsilon}_{\mathrm{a}}$ is a complex vector which represents the atomic polarization transition. Note that $\hat{\sigma}_\pm = \frac{1}{2}(\hat{\sigma}_x \pm i\hat{\sigma}_y)$.

9.2.1 Interaction picture

Given a Hamiltonian $\hat{H} = \hat{H}_0 + \hat{H}_{\text{int}}$, $\hat{H}_0$ and $\hat{H}_{\text{int}}$ being the free and interaction Hamiltonian, respectively, it is sometime useful to use the so-called *interaction picture*. If $|\psi_t\rangle$ represents the state of the system at the time t, its evolution is governed by the Schrödingier equation:

$$i\hbar \frac{\partial}{\partial t}|\psi_t\rangle = \hat{H}|\psi_t\rangle \,. \tag{9.31}$$

Now, we apply the following unitary transformation:

$$|\psi_t\rangle \to |\psi'_t\rangle = \hat{U}_0(t)^\dagger |\psi_t\rangle \quad \Rightarrow \quad |\psi_t\rangle = \hat{U}_0(t)|\psi'_t\rangle \tag{9.32}$$

where $\hat{U}_0(t) = \exp(-i\hat{H}_0 t/\hbar)$. Substituting into the Schrödinger equation we have:

$$i\hbar \frac{\partial}{\partial t}\left[\hat{U}_0(t)|\psi'_t\rangle\right] = \left(\hat{H}_0 + \hat{H}_{\text{int}}\right)\hat{U}_0(t)|\psi'_t\rangle \tag{9.33a}$$

$$\hat{H}_0\hat{U}_0(t)|\psi'_t\rangle + i\hbar\hat{U}_0(t)\frac{\partial}{\partial t}|\psi'_t\rangle = \left(\hat{H}_0 + \hat{H}_{\text{int}}\right)\hat{U}_0(t)|\psi'_t\rangle \tag{9.33b}$$

and, after some algebra and applying $\hat{U}_0^\dagger(t)$ to both sides, we obtain:

$$i\hbar \frac{\partial}{\partial t}|\psi'_t\rangle = \hat{H}'_{\text{int}}(t)|\psi'_t\rangle \,, \tag{9.34}$$

where we introduced $\hat{H}'_{\text{int}}(t) = \hat{U}_0^\dagger(t)\hat{H}_{\text{int}}\hat{U}_0(t)$. Therefore, by using the interaction picture with respect to the free Hamiltonian[1] one can focus on the (transformed) interaction Hamiltonian: this is extremely useful in the presence of oscillatory terms as we will see in the next section where we will investigate the interaction of a two level atom with an oscillatory electric field.

9.2.2 Interaction between a two-level atom and a classical electric field

The interaction between a two-level atom and a classical electric field is formally equivalent to the interaction between a $\frac{1}{2}$-spin particle and a magnetic field discussed in the previous section. The quantum Hamiltonian describing the interaction between the atomic electric dipole moment and the classical field $\boldsymbol{E}(t) = i\,E_0\,(\boldsymbol{\varepsilon}_{\text{f}}\,\mathrm{e}^{-i\omega t - i\varphi} - \boldsymbol{\varepsilon}_{\text{f}}^*\,\mathrm{e}^{i\omega t + i\varphi})$ with real amplitude E_0, frequency ω and polarization $\boldsymbol{\varepsilon}_{\text{f}}$, is:

$$\hat{H}_{\text{int}} = -\hat{\boldsymbol{D}}\cdot\boldsymbol{E}(t), \tag{9.35}$$

and the whole hamiltonian is thus given by:

$$\hat{H}_{\text{tot}} = \hbar\frac{\omega_{eg}}{2}\,\hat{\sigma}_z - \hat{\boldsymbol{D}}\cdot\boldsymbol{E}(t)\,, \tag{9.36a}$$

$$= \hbar\frac{\Delta\omega}{2}\,\hat{\sigma}_z + \hbar\frac{\omega}{2}\,\hat{\sigma}_z - \hat{\boldsymbol{D}}\cdot\boldsymbol{E}(t)\,, \tag{9.36b}$$

[1] More in general, one can perform the interaction picture considering a different Hamiltonian which, in the case under investigation, allows to simplify the description of the system.

where $\Delta\omega = \omega_{eg} - \omega$ is the detuning between the two-level atom and the field. In order to focus on the interaction, we consider the interaction picture wither respect to the Hamiltonian $\hat{H}_0 = \hbar\omega\hat{\sigma}_z/2$ (note that here we use the frequency ω of the field). Following section 9.2.1 we have:

$$\hat{H}_{\text{tot}} \to \hat{H} = \hat{U}_0^\dagger(t)\hat{H}_{\text{tot}}\hat{U}_0(t) = \hbar\frac{\Delta\omega}{2}\hat{\sigma}_z - \hat{U}_0^\dagger(t)\hat{\boldsymbol{D}}\cdot\boldsymbol{E}(t)\hat{U}_0(t)\,. \tag{9.37}$$

Since $\hat{U}_0^\dagger(t)\hat{\sigma}_\pm\hat{U}_0(t) = \hat{\sigma}_\pm\,\mathrm{e}^{\pm i\omega t}$, the last term of Eq. (9.37) contains terms proportional to $\mathrm{e}^{\pm i\varphi}$ and to $\mathrm{e}^{\pm i2\omega t\pm i\varphi}$: these last terms are *fast rotating* and if we assume that the time-scale of the system is $1/\omega$, then their effect on the time evolution is negligible. This corresponds to perform the *rotating-wave approximation* (RWA) or *secular approximation*. Therefore, Eq. (9.36) reduces to (for the sake of simplicity we assume $\boldsymbol{\varepsilon}_\text{a}, \boldsymbol{\varepsilon}_\text{f} \in \mathbb{R}^3$):

$$\hat{H} = \hbar\frac{\Omega'}{2}\,\boldsymbol{n}\cdot\hat{\boldsymbol{\sigma}}, \tag{9.38}$$

where:

$$\boldsymbol{n} = \frac{1}{\Omega'}\,(-\Omega_0\sin\varphi, \Omega_0\cos\varphi, \Delta\omega). \tag{9.39}$$

with $\Omega' = \sqrt{(\Delta\omega)^2 + \Omega_0^2}$ and we introduced the *Rabi frequency*:

$$\Omega_0 = \frac{2d}{\hbar}\,E_0\,\boldsymbol{\varepsilon}_\text{a}\cdot\boldsymbol{\varepsilon}_\text{f}. \tag{9.40}$$

In the resonant case ($\Delta\omega = 0$) we have (we can assume $\Omega_0 \in \mathbb{R}$ and set $\varphi = 0$):

$$\hat{H} = \hbar\frac{\Omega_0}{2}\,\hat{\sigma}_y, \tag{9.41}$$

which has the following eigenstates $|\gamma_\pm\rangle = 2^{-1/2}(|0\rangle \pm i|1\rangle)$. More in general, if $\varphi \neq 0$, we obtain the following time evolution (still in the resonant case):

$$\begin{aligned}\hat{U}_\varphi(t) &= \exp\left(-i\frac{\Omega_0 t}{2}\,\boldsymbol{n}\cdot\hat{\boldsymbol{\sigma}}\right)\\ &= \cos\left(\frac{\Omega_0 t}{2}\right)\hat{\mathbb{I}} - i\sin\left(\frac{\Omega_0 t}{2}\right)\left[-\sin\varphi\,\hat{\sigma}_x + \cos\varphi\,\hat{\sigma}_y\right],\end{aligned} \tag{9.42}$$

and, by using the 2×2 matrix formalism (in the computational basis):

$$\hat{U}_\varphi(t) \to \begin{pmatrix} \cos\left(\frac{\Omega_0 t}{2}\right) & -\mathrm{e}^{-i\varphi}\sin\left(\frac{\Omega_0 t}{2}\right) \\ \mathrm{e}^{i\varphi}\sin\left(\frac{\Omega_0 t}{2}\right) & \cos\left(\frac{\Omega_0 t}{2}\right)\end{pmatrix}. \tag{9.43}$$

It is now straightforward to see that, in the interaction picture:

$$\hat{U}_\varphi(t)|e\rangle = \cos\left(\frac{\Omega_0 t}{2}\right)|e\rangle + \mathrm{e}^{i\varphi}\sin\left(\frac{\Omega_0 t}{2}\right)|g\rangle, \tag{9.44a}$$

$$\hat{U}_\varphi(t)|g\rangle = \cos\left(\frac{\Omega_0 t}{2}\right)|g\rangle - \mathrm{e}^{-i\varphi}\sin\left(\frac{\Omega_0 t}{2}\right)|e\rangle. \tag{9.44b}$$

We have three following relevant cases.

- $\frac{\pi}{2}$-pulse: in this case one sets $\Omega_0 t = \pi/2$ and we have the following evolution starting from $|g\rangle$ or $|e\rangle$:

$$|e\rangle \to 2^{-1/2}\left(|e\rangle + e^{i\varphi}|g\rangle\right), \quad \text{and} \quad |g\rangle \to 2^{-1/2}\left(|g\rangle - e^{-i\varphi}|e\rangle\right), \tag{9.45}$$

  and, for $\varphi = 0$, we obtain the Hadamard transformation.

- π-pulse: now $\Omega_0 t = \pi$ and we have:

$$|e\rangle \to e^{i\varphi}|g\rangle, \quad \text{and} \quad |g\rangle \to -e^{-i\varphi}|e\rangle, \tag{9.46}$$

  that is, besides and overall phase shift, the NOT gate.

- 2π-pulse: for $\Omega_0 t = 2\pi$ we get:

$$|e\rangle \to -|e\rangle, \quad \text{and} \quad |g\rangle \to -|g\rangle, \tag{9.47}$$

  i.e., we add a phase shift to the input state. This phase shift is a well-known properties of 2π-spin rotations.

□ **– Exercise 9.4** *Represent the evolution of the two-level atom interacting with a classical electric field by using the Bloch sphere formalism, in the case of $\frac{\pi}{2}$-pulse, π-pulse and 2π-pulse. Assume that the initial state is $|e\rangle$, that is the north pole of the unit sphere.*

9.3 The Fabry-Perot cavity

The main interaction between light and atoms in quantum electrodynamics (QED) is the dipolar interaction. On the one hand, the dipole moment is fixed by the nature of the atom: usually experimentalists use the Rydberg states (that is states with very high principal quantum number n in order to obtain a high electric dipole moment) of alkali atoms, such as Rb atoms. On the other hand, one can realize a very large electric field in a narrow band of frequencies and in a small volume of space by means of a Fabry-Perot cavity.

A Fabry-Perot cavity consists of two semi-reflecting mirrors with reflectivity R_1 and R_2, respectively. In order to find the field inside the cavity, we consider what happens when two classical fields $E_a^{(\text{in})}$ and $E_b^{(\text{in})}$ are mixed at a semi-reflecting mirror with reflectivity R (see figure 9.2). If we denote with $E_a^{(\text{out})}$ and $E_b^{(\text{out})}$ the output field, we have the following linear transformation:

$$\begin{pmatrix} E_a^{(\text{out})} \\ E_b^{(\text{out})} \end{pmatrix} = \begin{pmatrix} \sqrt{R} & \sqrt{1-R} \\ \sqrt{1-R} & -\sqrt{R} \end{pmatrix} \begin{pmatrix} E_a^{(\text{in})} \\ E_b^{(\text{in})} \end{pmatrix} \tag{9.48}$$

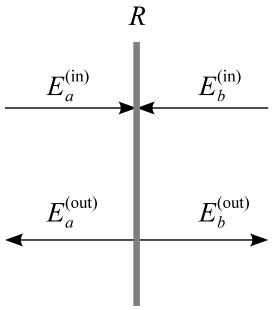

Figure 9.2: Input and output fields at a semi-reflecting mirror with reflectivity R.

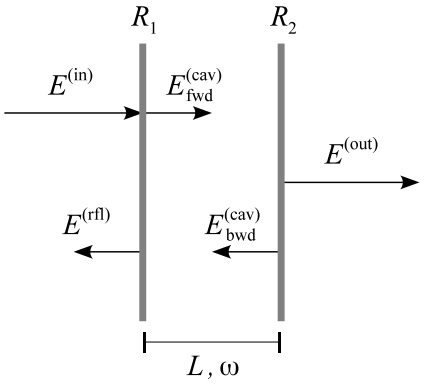

Figure 9.3: Scheme of Fabry-Perot cavity. See the text for details.

that is:

$$E_a^{(out)} = \sqrt{R}\, E_a^{(in)} + \sqrt{1-R}\, E_b^{(in)}, \tag{9.49}$$

$$E_b^{(out)} = -\sqrt{R}\, E_b^{(in)} + \sqrt{1-R}\, E_a^{(in)}. \tag{9.50}$$

The scheme of the Fabry-Perot cavity is sketched in figure 9.3: two mirrors with reflectivity R_1 and R_2, respectively, are placed at a distance L. The cavity is pumped with an input field $E^{(in)}$ of frequency ω, which impinges on the first mirror. The transmitted part undergoes multiple reflections between the two mirrors leading to an overall forward and backward field inside the cavity, $E_{fwd}^{(cav)}$ and $E_{bwd}^{(cav)}$, respectively, an overall transmitted field $E^{(out)}$ and an overall reflected field $E^{(rfl)}$, as depicted in figure 9.3. If we define $\phi = 2L\omega/c$, then we have:

$$E_{fwd}^{(cav)} = \frac{\sqrt{1-R_1}}{1+e^{i\phi}\sqrt{R_1 R_2}}\, E^{(in)}, \tag{9.51a}$$

$$E_{bwd}^{(cav)} = e^{i\phi/2}\sqrt{R_2}\, E_{fwd}^{(cav)}, \tag{9.51b}$$

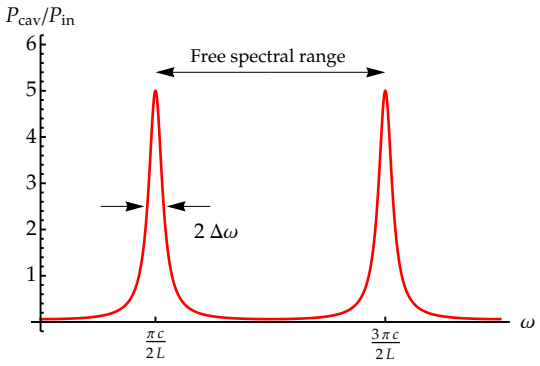

Figure 9.4: Ratio between the input power and the power of the field inside the cavity as a function of the input field frequency ω. We set $R_1 = R_2 = 0.8$. See the text for details.

and

$$E^{(\text{out})} = \mathrm{e}^{i\phi/2}\sqrt{1-R_2}\,E^{(\text{cav})}_{\text{fwd}}, \tag{9.52a}$$

$$E^{(\text{rfl})} = \mathrm{e}^{i\phi}\sqrt{(1-R_1)R_2}\,E^{(\text{cav})}_{\text{fwd}} + \sqrt{R_1}\,E^{(\text{in})}. \tag{9.52b}$$

In particular, if we assume $R_1 = R_2 = R$ and choose L such that $\phi = (2m+1)\pi$ (field-cavity resonance condition), $m \in \mathbb{N}$, we obtain:

$$E^{(\text{cav})}_{\text{fwd}} = \frac{E^{(\text{in})}}{\sqrt{1-R}}, \tag{9.53a}$$

$$E^{(\text{cav})}_{\text{bwd}} = i\,\frac{\sqrt{R}}{\sqrt{1-R}}\,E^{(\text{in})}, \tag{9.53b}$$

$$E^{(\text{out})} = i\,E^{(\text{in})}, \quad E^{(\text{rfl})} = 0. \tag{9.53c}$$

A quantity usually considered to investigate the behavior of the cavity is the ratio between the input field power and the forward cavity field power, namely:

$$\frac{P_{\text{cav}}}{P_{\text{in}}} = \left|\frac{E^{(\text{cav})}_{\text{fwd}}}{E^{(\text{in})}}\right|^2 = \frac{1-R_1}{1+R_1R_2+2\sqrt{R_1R_2}\,\cos\phi}. \tag{9.54}$$

In figure 9.4 we plot $P_{\text{cav}}/P_{\text{in}}$ as a function of the input field frequency: it is clear that near resonance we have a high field amplitude inside the cavity. In order to better understand the behavior of the ratio defined in Eq. (9.54) we introduce $\delta = \phi - \pi$, i.e., the resonance is obtained for $\delta = 0$, and consider the limit $\delta \ll 1$. We obtain the following expression for Eq. (9.54):

$$\frac{P_{\text{cav}}}{P_{\text{in}}} = \frac{1-R_1}{(1-\sqrt{R_1R_2})^2}\,\frac{\Delta^2(R_1,R_2)}{\delta^2+\Delta^2(R_1,R_2)} \tag{9.55}$$

that is a Lorentzian function where the half-width at half-maximum (HWHM) is:

$$\Delta^2(R_1, R_2) = \frac{(1 - \sqrt{R_1 R_2})^2}{\sqrt{R_1 R_2}}, \tag{9.56}$$

which, assuming $R_1 = R_2 = R$, reduces to:

$$\Delta(R) = \frac{1 - R}{\sqrt{R}}, \tag{9.57}$$

and corresponds to a spectral bandwidth HWHM:

$$\Delta\omega = \frac{c}{2L} \frac{1 - R}{\sqrt{R}}. \tag{9.58}$$

Finally, the cavity finesse is the ratio between the free spectral range, and the full-width half-maximum (FWHM) of Eq. (9.54) at resonance. In the present case the free spectral range is $2\pi c/(2L)$ (see figure 9.4), while the FWHM is $2\Delta\omega$, thus the cavity finess is given by:

$$\mathcal{F} = \frac{2\pi c}{2L} \frac{1}{2\Delta\omega} = \pi \frac{\sqrt{R}}{1 - R}. \tag{9.59}$$

The reader can obtain a quantitative analysis of the cavities involved in typical cavity QED experiments considering that $R \approx 1$ and $L \sim 1$ cm: this is why we have a very high field amplitude inside the cavity in the microwave domain, and, remarkably, microwaves are the characteristic transition frequencies of the Rydberg states involved in these experiments.

We now focus the attention on plain waves and assume that the axis of the cavity is aligned with the z-axis of a reference frame, where the mirrors are placed at $z = 0$ and $z = L$, respectively. In side the cavity we have two counter propagating waves [here we also assume to be at resonance and we use consider resonance and use Eqs. (9.53)]:

$$E^{(\mathrm{cav})}_{\mathrm{fwd}}(z, \omega) = \frac{E^{(\mathrm{in})}}{\sqrt{1 - R}} \cos(kz - \omega t), \tag{9.60a}$$

$$E^{(\mathrm{cav})}_{\mathrm{bwd}}(z, \omega) = -\frac{E^{(\mathrm{in})}\sqrt{R}}{\sqrt{1 - R}} \sin(kz + \omega t), \tag{9.60b}$$

therefore, inside the cavity we have the following wave:

$$E_{\mathrm{cav}}(z, \omega) = \frac{E^{(\mathrm{in})}}{\sqrt{1 - R}} \left[\cos(kz - \omega t) - \sqrt{R} \sin(kz + \omega t)\right]. \tag{9.61}$$

If we now perform the time average of the intensity of the field inside the cavity, we find:

$$\left\langle |E_{\mathrm{cav}}(z)|^2 \right\rangle \equiv \frac{\omega}{2\pi} \int_0^{2\pi/\omega} |E_{\mathrm{cav}}(z, \omega)|^2 \, dt = \frac{1 + R - 2\sqrt{R}\sin(2kz)}{2(1 - R)} \left|E^{(\mathrm{in})}\right|^2 \tag{9.62}$$

$$= \frac{1 + R - 2\sqrt{R}\sin\left[(2m + 1)\pi\frac{z}{L}\right]}{2(1 - R)} \left|E^{(\mathrm{in})}\right|^2, \tag{9.63}$$

where, in the last equality, we used the resonance condition for the wave vector $k = \omega/c$, namely $k = (2m+1)\pi/(2L)$. In the case of optical frequencies $m \approx 10^5$ and if we consider the average over the z direction we find:

$$\left\langle |E_{\text{cav}}|^2 \right\rangle \approx \frac{1+R}{2(1-R)} \left| E^{(\text{in})} \right|^2 . \tag{9.64}$$

9.4 The quantum description of light

The quantum Hamiltonian of the single-mode electromagnetic field in the cavity corresponds to that of a harmonic oscillator with the same frequency ω, namely:

$$\hat{H} = \frac{\hat{P}^2}{2} + \frac{1}{2}\omega^2 \hat{Q}^2 = \hbar\omega \left(\hat{a}^\dagger \hat{a} + \frac{1}{2} \right) \tag{9.65}$$

where we introduced the position- and momentum-like operators:

$$\hat{Q} = \sqrt{\frac{\hbar}{2\omega}} \left(\hat{a}^\dagger + \hat{a} \right), \quad \text{and} \quad \hat{P} = i\sqrt{\frac{\hbar\omega}{2}} \left(\hat{a}^\dagger - \hat{a} \right), \tag{9.66}$$

respectively, $\left[\hat{Q}, \hat{P}\right] = i\hbar\,\hat{\mathbb{I}}$, and:

$$\hat{a} = \sqrt{\frac{\omega}{2\hbar}} \left(\hat{Q} + i\frac{\hat{P}}{\omega} \right), \quad \text{and} \quad \hat{a}^\dagger = \sqrt{\frac{\omega}{2\hbar}} \left(\hat{Q} - i\frac{\hat{P}}{\omega} \right), \tag{9.67}$$

are the annihilation and creation bosonic field operators respectively. Note that $[\hat{a}, \hat{a}^\dagger] = \hat{\mathbb{I}}$. At each mode of the radiation field corresponds a bosonic field operator.

If we denote with $\{|n\rangle\}_{n\in\mathbb{N}}$ the set of the eigenvectors of the self-adjoint operator $\hat{N} = \hat{a}^\dagger\hat{a}$, namely, $\hat{N}|n\rangle = n|n\rangle$ we have:

$$\hat{a}|n\rangle = \sqrt{n}|n-1\rangle \quad \text{and} \quad \hat{a}^\dagger|n\rangle = \sqrt{n+1}|n+1\rangle, \tag{9.68}$$

and, thus:

$$|n\rangle = \frac{(\hat{a}^\dagger)^n}{\sqrt{n!}}|0\rangle, \tag{9.69}$$

where the state $|0\rangle$ represents the vacuum state. The set $\{|n\rangle\}_{n\in\mathbb{N}}$ is sometimes called Fock-state basis or photon-number basis.

9.5 The Jaynes-Cummings model

The full quantum model to describe the interaction between light and matter involves the quantum description of light. Now the classical electric field appearing in the interaction Hamiltonian of Eq. (9.35) is replaced by the corresponding quantum operator[2]:

$$\hat{\boldsymbol{E}} = iE_0 \left(\boldsymbol{\varepsilon}_{\text{f}} \hat{a} - \boldsymbol{\varepsilon}_{\text{f}}^* \hat{a}^\dagger \right), \tag{9.70}$$

[2]We consider a stationary, time-independent cavity field and, for the sake of simplicity, we also assume that the atom is placed at the center of the cavity.

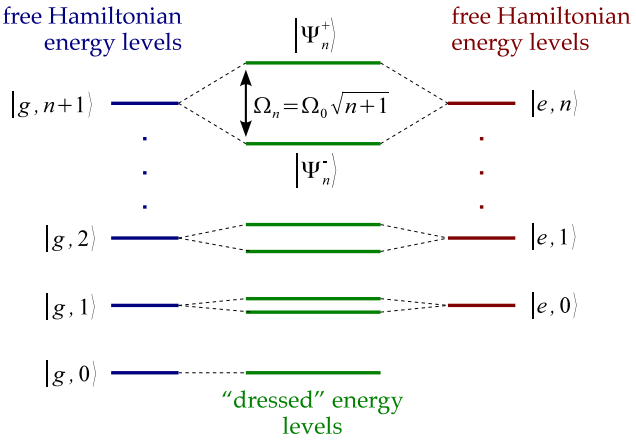

Figure 9.5: The blue and red lines refer to the energy levels corresponding to the eigenstates of the free Hamiltonian given in Eq. (9.71) with $\omega = \omega_{eg}$: it is clear that the states $|g, n+1\rangle$ and $|e, n\rangle$, with $n \geq 0$, are degenerate. The only non-degenerate level is the ground state $|g, 0\rangle$. The Jaynes-Cummings interaction removes degeneracy and couples the dressed states $|\Psi_n^{\pm}\rangle$, whose corresponding energy levels (green lines) have an energy difference equal to $\hbar\Omega_n = \hbar\Omega_0\sqrt{n+1}$.

where $\hat{a}$ and $\hat{a}^\dagger$ are the annihilation and creation field operators introduced in section 9.4 describing the stationary field inside the cavity (we assume the atom at the cavity center). The free Hamiltonian of the system reads:

$$\hat{H}_0 = \underbrace{\hbar\frac{\omega_{eg}}{2}\hat{\sigma}_z}_{\text{atom}} + \underbrace{\hbar\omega\left(\hat{a}^\dagger\hat{a} + \frac{1}{2}\right)}_{\text{field}}, \tag{9.71}$$

and we have the two families of eigenstates of $\hat{H}_0$, i.e.:

$$\hat{H}_0|g,n\rangle = \hbar\left[-\frac{\omega_{eg}}{2} + \omega\left(n + \frac{1}{2}\right)\right]|g,n\rangle, \tag{9.72a}$$

$$\hat{H}_0|e,n\rangle = \hbar\left[+\frac{\omega_{eg}}{2} + \omega\left(n + \frac{1}{2}\right)\right]|e,n\rangle, \tag{9.72b}$$

where $\{|e\rangle, |g\rangle\}$ are the eigenstates of $\hat{\sigma}_z$, $\{|n\rangle\}$ is the photon-number basis and $|x, y\rangle = |x\rangle|y\rangle$. As we can also see in figure 9.5, if $\omega = \omega_{eg}$ the states $|g, n+1\rangle$ and $|e, n\rangle$, with $n \geq 0$, are degenerate.

The interaction Hamiltonian reads:

$$H_{\text{int}} = -\hat{\boldsymbol{D}} \cdot \hat{\boldsymbol{E}}, \tag{9.73}$$

where $\hat{\boldsymbol{D}}$ is still given by Eq. (9.30). By performing the interaction picture with respect to the Hamiltonian $\hat{H}' = \hbar\omega(\hat{a}^\dagger\hat{a} + \frac{1}{2} + \frac{1}{2}\hat{\sigma}_z)$ and the RWA (see sections 9.2.1 and 9.2.2), we obtain the following interaction Hamiltonian:

$$\hat{H}_{\text{int}} = \hbar\frac{\delta}{2}\hat{\sigma}_z - i\hbar\frac{\Omega_0}{2}\left(\hat{\sigma}_+\,\hat{a} - \hat{\sigma}_-\,\hat{a}^\dagger\right), \qquad \text{(Jaynes-Cummings Hamiltonian)} \tag{9.74}$$

where Ω_0 is the Rabi frequency defined in Eq. (9.40) and $\delta = \omega_{eg} - \omega$ is the *detuning*. It is interesting to note that $\hat{H}_{\rm int}$ couples the two-dimensional manifold spanned by $\{|g, n+1\rangle, |e, n\rangle\}$, with $n > 0$. In fact, we have:

$$\left(\hat{\sigma}_+ \hat{a} - \hat{\sigma}_- \hat{a}^\dagger\right) |g, n+1\rangle = \sqrt{n+1}\, |e, n\rangle, \qquad \text{(absorption of one photon)} \tag{9.75}$$

$$\left(\hat{\sigma}_+ \hat{a} - \hat{\sigma}_- \hat{a}^\dagger\right) |e, n\rangle = -\sqrt{n+1}\, |g, n+1\rangle. \qquad \text{(emission of one photon)} \tag{9.76}$$

Note that the ground state of the free Hamiltonian, namely, $|g, 0\rangle$, is also an eigenstate of $\hat{H}_{\rm int}$.

Upon introducing the operator $\hat{\mathcal{N}} = \hat{a}^\dagger \hat{a} + \frac{1}{2} + \frac{1}{2}\hat{\sigma}_z$, the total Hamiltonian may be written as follows (after the RWA but not in the interaction picture):

$$\hat{H} = \hbar\omega\, \hat{\mathcal{N}} + \hbar \frac{\delta}{2} \hat{\sigma}_z - i\hbar \frac{\Omega_0}{2} \left(\hat{\sigma}_+ \hat{a} - \hat{\sigma}_- \hat{a}^\dagger\right). \tag{9.77}$$

If we focus on the resonant case $\delta = 0$, besides the ground state, we find the following eigenstates of the total Hamiltonian for $n \geq 0$:

$$\hat{H} \left|\Psi_n^\pm\right\rangle = \underbrace{\hbar \left[(n+1)\,\omega \pm \frac{1}{2}\Omega_n\right]}_{E_n^\pm} \left|\Psi_n^\pm\right\rangle, \tag{9.78}$$

where:

$$\left|\Psi_n^\pm\right\rangle = \frac{1}{\sqrt{2}} \left(|e, n\rangle \pm i|g, n+1\rangle\right), \tag{9.79}$$

and $\Omega_n = \Omega_0\sqrt{n+1}$ is the Rabi frequency for n photons. The states $|\Psi_n^\pm\rangle$ are called *dressed states* and $\Delta E_n = E_n^+ - E_n^- = \hbar\Omega_0\sqrt{n+1}$. Of course we can also write:

$$|e, n\rangle = \frac{1}{\sqrt{2}} \left(\left|\Psi_n^+\right\rangle + \left|\Psi_n^-\right\rangle\right), \quad \text{and} \quad |g, n+1\rangle = \frac{1}{i\sqrt{2}} \left(\left|\Psi_n^+\right\rangle - \left|\Psi_n^-\right\rangle\right). \tag{9.80}$$

> □ **– Exercise 9.5** *Assume that the system is initially prepared in the state $|e, n\rangle$, with $n \geq 0$. Find the probability to find the atom in the excited state after an interaction time t assuming $\delta = 0$.*

The physical meaning of the solution of the exercise 9.5 is that the atom and the field mode exchange one single photon with frequency Ω_n.

It is worth noting that the Jaynes-Cummings Hamiltonian of Eq. (9.74) can be also written as:

$$\hat{H}_{\rm int} = \hbar \frac{\Omega_0}{2} \left(\hat{\sigma}_+ \hat{a} + \hat{\sigma}_- \hat{a}^\dagger\right), \tag{9.81}$$

where we perform the following unitary transformation of mode $\hat{a} \to i\hat{a}$, which, of course, preserves the commutation relations, since $\left[(i\hat{a}), (i\hat{a})^\dagger\right] = \left[\hat{a}, \hat{a}^\dagger\right] = \hat{\mathbb{1}}$.

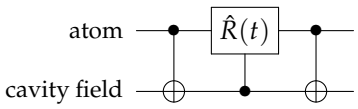

Figure 9.6: Quantum circuit implementing vacuum Rabi oscillations.

9.5.1 Vacuum Rabi oscillations: quantum circuit

If the atom is initially in the excited state $|e\rangle$ and the field is in the vacuum state $|0\rangle$, we have the *vacuum Rabi oscillations*. In particular we find:

- π-pulse ($\Omega_0 t = \pi$):
$$|e,0\rangle \to |g,1\rangle, \quad \text{and} \quad |g,1\rangle \to -|e,0\rangle; \tag{9.82}$$
- $\frac{\pi}{2}$-pulse ($\Omega_0 t = \pi/2$):
$$|e,0\rangle \to \frac{1}{\sqrt{2}}\left(|e,0\rangle + |g,1\rangle\right), \quad \text{and} \quad |g,1\rangle \to \frac{1}{\sqrt{2}}\left(|g,1\rangle - |e,0\rangle\right), \tag{9.83}$$
that are maximally entangled states of the atom and the cavity field.

□ **– Exercise 9.6** *Find the effect of a 2π-pulse ($\Omega_0 t = 2\pi$) on $|e,0\rangle$ and $|g,1\rangle$.*

The figure 9.6 shows how we can describe the vacuum Rabi oscillations by means of CNOT gates and controlled unitary operation:

$$\hat{R}(t) = \exp\left(-i\,\frac{\Omega_0 t}{2}\,\hat{\sigma}_y\right) = \cos\left(\frac{\Omega_0 t}{2}\right)\hat{\mathbb{I}} - i\sin\left(\frac{\Omega_0 t}{2}\right)\hat{\sigma}_y, \tag{9.84}$$

where we should use the following association between the physical states and the computational basis:

$$|g,0\rangle \leftrightarrow |00\rangle, \quad |g,1\rangle \leftrightarrow |01\rangle, \quad |e,0\rangle \leftrightarrow |10\rangle, \quad \text{and} \quad |e,1\rangle \leftrightarrow |11\rangle. \tag{9.85}$$

The reader can check that the quantum circuit of figure 9.6 acts on the computational basis as follows:

$$|00\rangle \to |00\rangle, \quad |11\rangle \to |11\rangle, \tag{9.86a}$$
$$|01\rangle \to \cos\left(\frac{\Omega_0 t}{2}\right)|01\rangle - \sin\left(\frac{\Omega_0 t}{2}\right)|10\rangle, \tag{9.86b}$$
$$|10\rangle \to \cos\left(\frac{\Omega_0 t}{2}\right)|10\rangle + \sin\left(\frac{\Omega_0 t}{2}\right)|01\rangle, \tag{9.86c}$$

that is the same evolution obtained with the Jaynes-Cummings Hamiltonian of Eq. (9.74), except for what concerns the state $|11\rangle = |e,1\rangle$, since, in this case, we have:

$$\exp\left(-i\frac{\hat{H}_{\text{int}}}{\hbar}\,t\right)\,|e,1\rangle = \cos\left(\frac{\Omega_1 t}{2}\right)|e,1\rangle + \sin\left(\frac{\Omega_1 t}{2}\right)|g,2\rangle. \tag{9.87}$$

As we have seen in the previous section, $\hat{H}_{\text{int}}$ couples the states $|e,1\rangle$ and $|g,2\rangle$, but $|g,2\rangle$ does not belong to the computational space spanned by the two qubits...

In order solve this problem, we should modify the evolution as follows:

$$\exp\left(-i\frac{\hat{H}_{\text{int}}}{\hbar}\,t\right) \to \exp\left(-i\frac{\hat{H}_{\text{int}}}{\hbar}\,t\right)\,\left[\hat{P}_q - |e,1\rangle\langle e,1|\right] + |e,1\rangle\langle e,1|, \tag{9.88}$$

where we introduced the projector operator $\hat{P}_q = \sum_{A=g,e}\sum_{F=0,1}|A,F\rangle\langle A,F|$, which projects the state onto the 4-dimensional space spanned by the 2-qubit computational basis.

We close this section showing how we can map an atomic superposition state $|\psi_A\rangle = c_e|e\rangle + c_g|g\rangle$ onto the cavity field state. To this aim it is enough to prepare the field in the vacuum state and then apply a π-pulse, namely (note that, here, 0 and 1 represent the number of photons):

$$(c_e|e\rangle + c_g|g\rangle)|0\rangle \xrightarrow{\pi\text{-pulse}} |g\rangle(c_e|1\rangle + c_g|0\rangle), \tag{9.89}$$

i.e., the atom is left in the ground state while the cavity is a superposition state with the same complex amplitudes of the input atomic state. On the other hand, when we try to map the state $|\psi_A\rangle = c_1|1\rangle + c_0|0\rangle$ of the field onto an atomic state, we obtain:

$$|g\rangle(c_1|1\rangle + c_0|0\rangle) \xrightarrow{\pi\text{-pulse}} (-c_1|e\rangle + c_0|g\rangle)|0\rangle, \tag{9.90}$$

i.e., we have a phase appearing in front of $|e\rangle$. It is worth noting that the field considered throughout this chapter is *inside* a cavity and, thus, is not directly accessible: one should measure the atom after the interaction in order to have some information about the cavity state!

Bibliography

- S. Haroche and J.-M. Raimond, *Exploring the Quantum: Atoms, Cavities, and Photons* (Oxford Graduate Texts, 2006) – Chapters 3, 5.
- M. A. Nielsen and I. L. Chuang, *Quantum Computation and Quantum Information* (Cambridge University Press, 2010) – Chapter 7.5, 7.7.
- G. Burkard *et al.*, *Physical optimization of quantum error correction circuits*, Phys. Rev. B **60**, 11404-11416 (1999).
- M. Bina, *The coherent interaction between matter and radiation*, Eur. Phys. J. Special Topics **203**, 163-183 (2012).

Chapter 10

Quantum computation with trapped ions

In chapter 9 we have seen how to manipulate a two-level atom by using oscillating electric field treated as classical or quantized entities. In that case the atoms usually move through a cavity which contains the field. A complementary approach consists in fixing the position of the atoms in the space and address suitably tuned laser beams in order to control their electronic levels and to perform quantum operations. In this last case, the atoms are ionized and *trapped* by using time-varying electric fields: now one can exploit the electronic levels of the ions to encode the qubits' state, but also their collective quantized motion, that allows to implement two-qubit gates.

In this chapter we review the basic working principle of a linear Paul trap, which is used to confine a chain of ions, and derive the quantum Hamiltonian describing their quantized motion of the ions and their manipulation through suitable classical laser pulses. We eventually show how to perform universal quantum computation with trapped ions.

10.1 The linear Paul trap (in brief)

The typical linear Paul trap used to implement quantum computation consists of four rod electrodes which confine the ions in the x-y plane, and two end-cap electrodes for the confinement along the z axis as depicted in figure 10.1. If we apply to one pair of the diagonally opposite electrodes a radio frequency (RF) voltage $V_1(t) = V\cos(\omega_{\mathrm{RF}})$ and to the other couple of rod electrodes the voltage $V_2(t) = -V\cos(\omega_{\mathrm{RF}})$, the time-varying potential along z axis (and near at the trap center) can be written as:

$$\Phi(x, y; t) = \phi_{\mathrm{s}}(x, y)\cos(\omega_{\mathrm{RF}} t)\,. \tag{10.1}$$

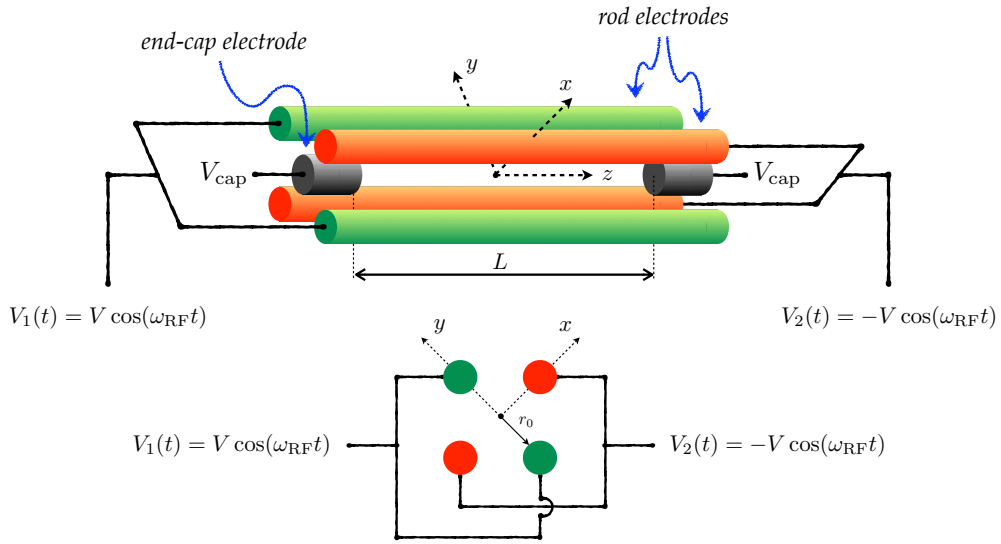

Figure 10.1: Scheme of a linear Paul trap with its main elements. On the bottom we show a side view of the trap (the end-cap electrodes are not depicted). See the text for details.

with

$$\phi_{\rm s}(x,y) = V\,\frac{x^2-y^2}{2r_0^2}\,, \tag{10.2}$$

where r_0 is the radial distance between the trap axis and the surface of one of the electrodes (see figure 10.1). This potential can be used to achieve radial confinement of charged particles.

If we consider a particle with mass m and charge Q, the classical equations of motion given the potential $\Phi(x,y;t)$ read:

$$\frac{d^2x}{d\zeta^2} = 2q\cos(2\zeta)\,x\,, \tag{10.3a}$$

$$\frac{d^2y}{d\zeta^2} = -2q\cos(2\zeta)\,y\,, \tag{10.3b}$$

$$\frac{d^2z}{d\zeta^2} = 0\,, \tag{10.3c}$$

where we introduced the following dimensionless quantities:

$$q = \frac{2QV}{mr_0^2\omega_{\rm RF}^2}\,, \qquad \text{and} \qquad \zeta = \frac{\omega_{\rm RF}t}{2}\,. \tag{10.4}$$

It is possible to show that the previous set of equations have *stable* solutions only if $0 < q < 0.908$: in this case the ion is confined radially, namely, in the x-y plane and can move freely along the z direction. If we consider on the x direction (an analoqgue result can be obtained for

the y direction), the approximate solution can be written as:

$$x(t) \approx \underbrace{\mathcal{A}_x \cos(\omega_r t)}_{\textit{secular motion}} \underbrace{\left[1 + \frac{q}{2}\cos(\omega_{\mathrm{RF}} t)\right]}_{\textit{micromotion}}, \tag{10.5}$$

where the parameter $\mathcal{A}_x$ depends on the boundary condition, while:

$$\omega_{r_0} \equiv \frac{q\,\omega_{\mathrm{RF}}}{2\sqrt{2}}\,. \tag{10.6}$$

The micromotion can be eliminated by adding further electrodes operating with compensation voltages, therefore one can consider only the secular motion.

In order to confine the charged particles also in the z direction it is necessary to add the so-called end-cap electrodes, to which the same voltages V_{cap} is applied. In figure 10.1 we represented these electrodes as two rods placed on the trap axis. However, there are other possible geometries, such as ring-shaped electrodes around the RF-rods. In the presence of the (DC) voltage V_{cap}, Eqs. (10.3a) become:

$$\frac{d^2x}{d\zeta^2} = 2q\cos(2\zeta)\,x - b\,, \tag{10.7a}$$

$$\frac{d^2y}{d\zeta^2} = -2q\cos(2\zeta)\,y - b\,, \tag{10.7b}$$

$$\frac{d^2z}{d\zeta^2} = -2bz\,, \tag{10.7c}$$

where we introduced the new dimensionless parameter

$$b = \alpha\,\frac{QV_{\mathrm{cap}}}{mL^2\omega_{\mathrm{RF}}^2}\,, \tag{10.8}$$

α being a parameter depending on the geometry of the trap and L is the distance between the end-cap electrodes (see figure 10.1). From Eq. (10.7c) it is clear that now the particle exhibits a harmonic motion along z axis with frequency:

$$\omega_z = \sqrt{\frac{b}{2}}\,\omega_{\mathrm{RF}}\,, \tag{10.9}$$

while in the regime $b, q \ll 1$ the motion along the x direction (and, analogously, along the y axis) is still given by Eq. (10.5) but now the *pure* radial frequency ω_{r_0} should be replaced by:

$$\omega_r \approx \frac{\omega_{\mathrm{RF}}}{2}\sqrt{\frac{q^2}{2} - b} \tag{10.10}$$

$$\approx \sqrt{\omega_{r_0}^2 - \frac{\omega_z^2}{2}}\,. \tag{10.11}$$

Therefore, we find a defocusing effect of the radial motion, due to the confinement along the trap axis. Nevertheless, in the cases of interest one chooses the regime $\omega_z \ll \omega_{r_0}$, thus the defocusing can be safely neglected.

Summarizing, all the above considerations allow us to describe the trapped ion as a charged particle confined in a 3-dimensional harmonic potential, namely:

$$\Xi_1(x,y,z) = \frac{m}{2}\left[\omega_r^2(x^2+y^2)+\omega_z^2 z^2\right], \tag{10.12}$$

where we assumed that the two radial frequencies are degenerate, namely, $\omega_x = \omega_y = \omega_r$.

In order to perform quantum information tasks, one should manipulate more than one ion at the time. Therefore, we should extend our analysis to N charged particles. In the following we assume that all the ions have the same mass m and charge Q and, taking into account the mutual Coloumb interactions, we obtain the following potential:

$$\Xi_N(x,y,z) = \frac{m}{2}\sum_{n=1}^{N}\left[\omega_r^2(x_n^2+y_n^2)+\omega_z^2 z_n^2\right] + \frac{Q^2}{8\pi\epsilon_0}\sum_{\substack{n,m=1\\ n\neq m}}^{N}\frac{1}{|\boldsymbol{r}_n-\boldsymbol{r}_m|}, \tag{10.13}$$

$\boldsymbol{r}_n = (x_n, y_n, z_n)$ being the position vector of the n-th ion.

If the radial confinement is stronger enough than the axial one and the number N is not too large, we obtain a linear ion chain configuration, in which the equilibrium positions of the ions are along the trap axis. This configuration is called ion crystal. In general, the distance between adjacent ions increases from the center to the outside of the string, and can be evaluated by numerical calculations. However, by increasing the number of ions we find a transition from the linear chain to the so-called zig-zag configuration (or other more complicated ones). The value of N, above which the transition occurs, has been investigated both numerically and experimentally and one finds the following condition

$$\mathcal{R} \equiv \left(\frac{\omega_z}{\omega_r}\right)^2 \lesssim 2.53\, N^{-1.73} \equiv \mathcal{R}_{\text{crit}}\,. \tag{10.14}$$

If $\mathcal{R} < \mathcal{R}_{\text{crit}}$ the zig-zag motion is suppressed and we can focus on the axial motion of the particles. Under this condition, we can study the dynamics of our system given the potential

$$\xi_N(z) = \frac{m}{2}\sum_{n=1}^{N}\omega_z^2 z_n^2 + \frac{Q^2}{8\pi\epsilon_0}\sum_{\substack{n,m=1\\ n\neq m}}^{N}\frac{1}{|z_n-z_m|}\,. \tag{10.15}$$

The thorough investigation of the dynamics of the N-ion chain is beyond the scope of this chapter. Here we recall that we can identify two main axial modes. The first mode corresponds to the center-of-mass (COM) axial mode, where all the ions moves along the z direction with the same amplitude and frequency ω_z. The second mode is the breathing mode: in this case the amplitude of oscillation of each ion increases as the distance from the center increases. In the following, we will assume that our system is excited in the COM axial mode and we can represent the position of the n-th ion as follows:

$$z_n(t) = \bar{z}_n + \Delta_n(t)\,, \tag{10.16}$$

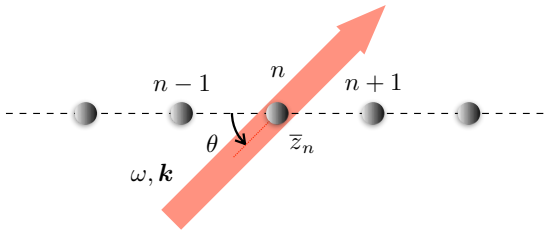

Figure 10.2: Sketch of the interaction of a laser beam with frequency ω and wave vector $\boldsymbol{k}$ with the n-th.

where $\bar{z}_n$ is its average equilibrium position and $\Delta_n(t)$ its time-dependent displacement. We note that it is possible to impose the normal oscillation modes by acting with an AC voltage on the end-cap electrodes. In the next section we will describe the motion of the ions as a *quantum* harmonic oscillator.

10.2 Quantum motion of the ion chain

If we consider just two electronic levels of each ion with transition frequency ω_{A} and assume the COM axial mode at frequency ω_z, the free quantum Hamiltonian of the system can be written as

$$\hat{H}_0 = \sum_{n=1}^{N} \frac{\hbar\omega_{\mathrm{A}}}{2}\,\hat{\sigma}_z^{(n)} + \hbar\omega_z\left(\hat{a}^\dagger\hat{a} + \frac{1}{2}\right), \tag{10.17}$$

where we introduced the annihilation, $\hat{a}$, and creation, $\hat{a}^\dagger$, operators of the harmonic oscillator, $[\hat{a}, \hat{a}^\dagger] = \hat{\mathbb{1}}$. The position z_n is then substituted by the operator

$$\hat{z}_n = \bar{z}_n + \frac{z_0}{\sqrt{N}}\left(\hat{a} + \hat{a}^\dagger\right), \tag{10.18}$$

with

$$z_0 = \sqrt{\frac{\hbar}{2m\omega_z}}\,. \tag{10.19}$$

In order to manipulate the internal levels of the n-th ion at position $\hat{\boldsymbol{r}}_n = (0, 0, \hat{z}_n)$, one should address on it a laser beam, whose electric filed can be written as (without loss of generality we assume a real polarization vector $\boldsymbol{\varepsilon}_{\mathrm{f}}$)

$$\boldsymbol{E}_n(t) = E_0\,\boldsymbol{\varepsilon}_{\mathrm{f}}\left[\mathrm{e}^{-i(\omega t - \boldsymbol{k}\cdot\boldsymbol{r}_n - \varphi)} + \mathrm{e}^{i(\omega_{\mathrm{L}} t - \boldsymbol{k}\cdot\boldsymbol{r}_n - \varphi)}\right], \tag{10.20}$$

ω, $\boldsymbol{k}$ and φ being the laser frequency, the wave vector and the phase of the electric field, respectively. The interaction Hamiltonian can be written in terms of both the dipole and quadrupole operators and can be written as

$$\hat{H}_{\mathrm{int}} = -\hat{\boldsymbol{D}}_n \cdot E_0\,\boldsymbol{\varepsilon}_{\mathrm{f}}\left\{e^{-i\left[\omega t - \eta(\hat{a}+\hat{a}^\dagger) - \varphi_n\right]} + e^{i\left[\omega t - \eta(\hat{a}+\hat{a}^\dagger) - \varphi_n\right]}\right\} \tag{10.21}$$

where $\hat{\boldsymbol{D}}_n = d_n \boldsymbol{\varepsilon}_\mathrm{a} \left(\hat{\sigma}_+^{(n)} + \hat{\sigma}_-^{(n)}\right)$ is the dipole moment operator of the n-th ion (we assume $\boldsymbol{\varepsilon}_\mathrm{a} \in \mathbb{R}^3$), $\hat{\sigma}_+^{(n)}$ and $\hat{\sigma}_-^{(n)}$ are its raising and lowering operators, respectively (see section 9.2), $\varphi_n = \varphi - |\boldsymbol{k}|\, \bar{z}_n \cos\theta$, θ being the angle between the wave vector $\boldsymbol{k}$ and the z axis (see figure 10.2), and we introduced the Lamb-Dicke parameter

$$\eta = \frac{1}{\sqrt{N}} |\boldsymbol{k}|\, z_0 \cos\theta \,. \tag{10.22}$$

Now we pass to the interaction picture with respect to the free Hamiltonian (10.17) and perform the RWA, obtaining the following Hamiltonian:

$$\hat{H}'_\mathrm{int} = \frac{\hbar\Omega_0}{2} \Bigg\{ \hat{\sigma}_+^{(n)} e^{-i\delta t} \exp\left[i\eta \left(\hat{a}\, e^{-i\omega_z t} + \hat{a}^\dagger e^{i\omega_z t} \right) + i\varphi_n \right] + \hat{\sigma}_-^{(n)} e^{i\delta t} \exp\left[-i\eta \left(\hat{a}\, e^{-i\omega_z t} + \hat{a}^\dagger e^{i\omega_z t} \right) - i\varphi_n \right] \Bigg\} , \tag{10.23}$$

where $\delta = \omega - \omega_\mathrm{A}$ is the laser-ion detuning and $\Omega_0 = 2 d_n E_0 \boldsymbol{\varepsilon}_\mathrm{a} \cdot \boldsymbol{\varepsilon}_\mathrm{f} / \hbar$ is the Rabi frequency. If we consider the so-called Lamb-Dicke regime, namely, $\eta^2 \langle (\hat{a} + \hat{a}^\dagger)^2 \rangle = \eta^2 (2\overline{n}) + 1) \ll 1$, where $\overline{n}$ is the average number of *phonons* and the expectation is calculated considering the COM mode state, we can expand $\hat{H}'_\mathrm{int}$ up to the first order in η, obtaining:

$$\hat{H}'_\mathrm{int} \approx \frac{\hbar\Omega_0}{2} \Bigg\{ \hat{\sigma}_+^{(n)} e^{-i\delta t + i\varphi_n} \left[1 + i\eta \left(\hat{a}\, e^{-i\omega_z t} + \hat{a}^\dagger e^{i\omega_z t} \right) \right] + \hat{\sigma}_-^{(n)} e^{i\delta t - i\varphi_n} \left[1 - i\eta \left(\hat{a}\, e^{-i\omega_z t} + \hat{a}^\dagger e^{i\omega_z t} \right) \right] \Bigg\} . \tag{10.24}$$

In order to perform universal quantum computation with the trapped ions we can choose three particular values of the detuning δ. If we we set $\delta = 0, \pm\omega_z$ and we neglect the oscillating terms $e^{\pm i\omega_z t}$ and $e^{\pm 2i\omega_z t}$, we obtain the following three Hamiltonians:

$$\hat{H}_\mathrm{C} = \frac{\hbar\Omega_0}{2} \left(\hat{\sigma}_+^{(n)} e^{i\varphi_n} + \hat{\sigma}_-^{(n)} e^{-i\varphi_n} \right) , \qquad (\delta = 0, \text{ carrier}) \tag{10.25a}$$

$$\hat{H}_\mathrm{B} = i\eta \frac{\hbar\Omega_0}{2} \left(\hat{\sigma}_+^{(n)} \hat{a}^\dagger e^{i\varphi_n} - \hat{\sigma}_-^{(n)} \hat{a}\, e^{-i\varphi_n} \right) , \qquad (\delta = +\omega_z, \text{ first blue sideband}) \tag{10.25b}$$

$$\hat{H}_\mathrm{R} = i\eta \frac{\hbar\Omega_0}{2} \left(\hat{\sigma}_+^{(n)} \hat{a}\, e^{i\varphi_n} - \hat{\sigma}_-^{(n)} \hat{a}^\dagger e^{-i\varphi_n} \right) . \qquad (\delta = -\omega_z, \text{ first red sideband}) \tag{10.25c}$$

In figure 10.3 we sketch the allowed transition in the presence of the three Hamiltonians (10.25). We can see that by suitably tuning the laser frequency ω one can obtain a transition between the electronic levels of the n-th ion preserving the phonon number state $|m\rangle$, namely:

$$|g_n\rangle |m\rangle \leftrightarrow |e_n\rangle |m\rangle \,, \qquad \text{(carrier transition)} \tag{10.26}$$

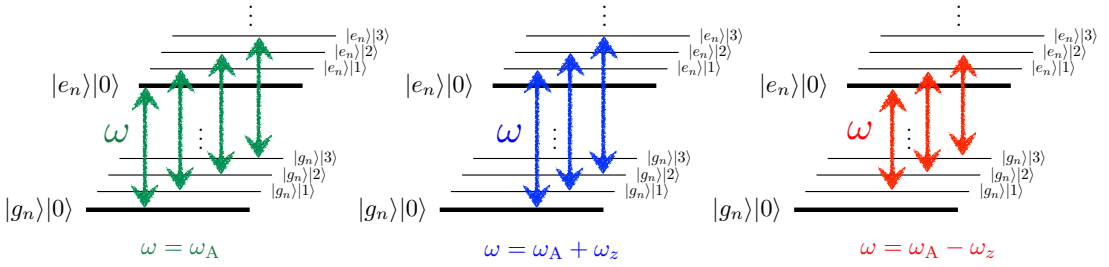

Carrier	First blue sideband	First red sideband
$\|g_n\rangle\|m\rangle \leftrightarrow \|e_n\rangle\|m\rangle$	$\|g_n\rangle\|m\rangle \leftrightarrow \|e_n\rangle\|m+1\rangle$	$\|g_n\rangle\|m+1\rangle \leftrightarrow \|e_n\rangle\|m\rangle$

Figure 10.3: Scheme of the allowed transition between the electronic ($|g_n\rangle$ and $|e_n\rangle$) and vibrational levels ($|m\rangle$) of the n-th ion in the presence of the carrier, first blue sideband and first red sideband transitions, respectively.

or change the internal level and adding one vibrational quantum:

$$|g_n\rangle|m\rangle \leftrightarrow |e_n\rangle|m+1\rangle\,, \qquad \text{(first blue sideband transition)} \tag{10.27}$$

or removing one vibrational quantum:

$$|g_n\rangle|m+1\rangle \leftrightarrow |e_n\rangle|m\rangle\,. \qquad \text{(first red sideband transition)} \tag{10.28}$$

In the next sections we will see that exploiting the three considered Hamiltonians it is possible to implement universal quantum computation with trapped ions. To this aim, the logical qubits are encoded into the electronic levels of the ions and the COM mode is used as a bus to perform multi-qubit conditional operations.

10.3 Single-qubit gates with trapped ions

If we identify the computational basis $|0\rangle$ and $|1\rangle$ with the level $|g_n\rangle$ and $|e_n\rangle$, of the n-th ion, respectively, we can implement single qubit gates exploiting the carrier transition and following the analysis given in section 9.2.2. The carrier Hamiltonian (10.25a) leads to the evolution operator (acting on the n-th ion):

$$\hat{C}_n(\theta,\phi) = \exp\left[-i\frac{\theta}{2}\left(\hat{\sigma}_+^{(n)}e^{i\varphi} + \hat{\sigma}_-^{(n)}e^{-i\varphi}\right)\right], \tag{10.29}$$

$$= \cos\left(\frac{\theta}{2}\right)\hat{\mathbb{1}} - i\sin\left(\frac{\theta}{2}\right)\left(\cos\varphi\,\hat{\sigma}_x^{(n)} - \sin\varphi\,\hat{\sigma}_y^{(n)}\right) \tag{10.30}$$

where $\theta = \Omega_0 t$ and we used $\hat{\sigma}_n^{(\pm)} = \frac{1}{2}\left(\hat{\sigma}_x^{(n)} \pm i\hat{\sigma}_y^{(n)}\right)$. In particular, we obtain the following relevant cases that will be used in the next section to implement the CNOT gate:

$$\hat{C}_n\left(\frac{\pi}{2},0\right)|g_n\rangle = \frac{|g_n\rangle - i|e_n\rangle}{\sqrt{2}}, \qquad \hat{C}_n\left(\frac{\pi}{2},0\right)|e_n\rangle = \frac{|e_n\rangle - i|g_n\rangle}{\sqrt{2}}, \tag{10.31a}$$

$$\hat{C}_n\left(\frac{\pi}{2},\pi\right)|g_n\rangle = \frac{|g_n\rangle + i|e_n\rangle}{\sqrt{2}}, \qquad \hat{C}_n\left(\frac{\pi}{2},\pi\right)|e_n\rangle = \frac{|e_n\rangle + i|g_n\rangle}{\sqrt{2}}. \tag{10.31b}$$

In order to achieve the universal quantum computation with trapped ions, we now need to build the CNOT operation, that will be the subject of the next section.

10.4 CNOT gate with trapped ions

In this section we will consider two particular ions of an ion chain, say ion 1 and ion 2, and we will exploit the common COM axial mode to change the electronic state of the ion 2 only if the ion 1 is in the excited state $|e_1\rangle$. Therefore, if we use as computational basis

$$|g_n\rangle \to |0_n\rangle, \quad \text{and} \quad |e_n\rangle \to |1_n\rangle, \tag{10.32}$$

the final result is the action of a CNOT gate (up to global phases), that is:

$$|g_1\rangle|g_2\rangle = |0_1\rangle|0_2\rangle \to |g_1\rangle|g_2\rangle = |0_1\rangle|0_2\rangle, \tag{10.33a}$$

$$|g_1\rangle|e_2\rangle = |0_1\rangle|1_2\rangle \to |g_1\rangle|e_2\rangle = |0_1\rangle|1_2\rangle, \tag{10.33b}$$

$$|e_1\rangle|g_2\rangle = |1_1\rangle|0_2\rangle \to |e_1\rangle|e_2\rangle = |1_1\rangle|1_2\rangle, \tag{10.33c}$$

$$|e_1\rangle|e_2\rangle = |1_1\rangle|1_2\rangle \to |e_1\rangle|g_2\rangle = |1_1\rangle|0_2\rangle. \tag{10.33d}$$

In order to implement the conditional operations needed to obtain the action of the CNOT gate, we will use the collective motion imposed by the COM mode by applying suitable carrier and first blue sideband pulses to the ions. For the sake of simplicity, we introduce the following evolution operator associated with the Hamiltonian (10.25b):

$$\hat{B}_n(\theta,\phi) = \exp\left[-i\frac{\theta}{2}\left(\hat{\sigma}_+^{(n)}\hat{a}^\dagger e^{i\varphi} + \hat{\sigma}_-^{(n)}\hat{a}\, e^{-i\varphi}\right)\right], \tag{10.34}$$

where $\theta = \eta\Omega_0 t$ and we applied the transformation $\hat{a} \to i\hat{a}$. As in the case of the Jaynes-Cummings model described in section 9.5, the operator $\left(\hat{\sigma}_+^{(n)}\hat{a}^\dagger e^{i\varphi} + \hat{\sigma}_-^{(n)}\hat{a}\, e^{-i\varphi}\right)$ has the following eigenvectors

$$|\Psi_n^{(\pm)}\rangle = \frac{|g_n\rangle|m\rangle \pm e^{i\varphi}|e_n\rangle|m+1\rangle}{\sqrt{2}}, \tag{10.35}$$

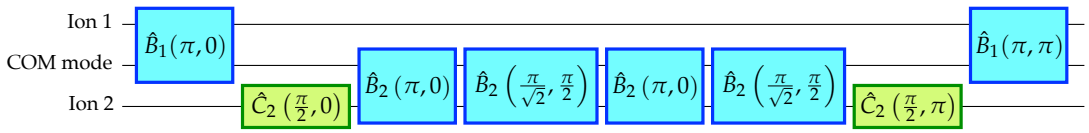

Figure 10.4: Quantum circuit used to implement a CNOT gate that changes the internal state of the ion 2 only if the ion 1 is in the excited state. The gates $\hat{C}_n(\theta,\phi)$ and $\hat{B}_n(\theta,\phi)$ refer to the carrier and to the first blue sideband pulses, respectively. The COM mode is used as a bus.

with eigenvalues $\pm\sqrt{m+1}$, $|m\rangle$ being the phonon Fock state, $\hat{a}^\dagger\hat{a}|m\rangle = m|m\rangle$. It is straightforward to show that:

$$\hat{B}_n(\theta,\phi)|g_n\rangle|m\rangle = \cos\left(\frac{\theta}{2}\sqrt{m+1}\right)|g_n\rangle|m\rangle - ie^{i\varphi}\sin\left(\frac{\theta}{2}\sqrt{m+1}\right)|e_n\rangle|m+1\rangle\,, \tag{10.36a}$$

$$\hat{B}_n(\theta,\phi)|e_n\rangle|m+1\rangle = \cos\left(\frac{\theta}{2}\sqrt{m+1}\right)|e_n\rangle|m+1\rangle - ie^{-i\varphi}\sin\left(\frac{\theta}{2}\sqrt{m+1}\right)|g_n\rangle|m\rangle\,. \tag{10.36b}$$

In figure 10.4 we show the quantum circuit to implement a CNOT gate with trapped ions, that is a suitable combination of carrier and first blue sideband pulses applied to the two involved ions. As one can see there are difference pulses which are required to control the phases raising from the first blue sideband gates. In the considered case, the CNOT gate uses the ion 1 as control qubit and changes the internal (electronic) state of ion 2, the target state, only in the presence of the state $|e_1\rangle$.

To understand the basic idea underlying the circuit of figure 10.4, we note that the first gate is $\hat{B}_n(\pi,0)$ applied to ion 1 affecting also the COM mode, maps the state of the first ion into the axial mode. In fact, if the starting state of the COM mode is $|0\rangle$, we have:

$$\hat{B}_1(\pi,0)|g_1\rangle|0\rangle = -i|e_1\rangle|1\rangle \quad \text{and} \quad \text{and} \quad \hat{B}_1(\pi,0)|e_1\rangle|0\rangle = |e_1\rangle|0\rangle\,, \tag{10.37}$$

and we can see how the state of the COM mode is changed to $|1\rangle$ only if the first ion is in its ground state $|g_1\rangle$. All the other $\hat{C}_2(\theta,\phi)$ and $\hat{B}_2(\theta,\phi)$ gates are used to change accordingly the state of the ion 2.

As an example, we consider the whole evolution of the state initial state

$$|e_1\rangle|e_2\rangle|0\rangle \equiv |1_1\rangle|1_2\rangle|0\rangle\,, \tag{10.38}$$

where we used both the physical basis (l.h.s.) and the computational basis (r.h.s.) for the ion states. Since, $\hat{B}_1(\pi,0)|e_1\rangle|0\rangle = |e_1\rangle|0\rangle$, we can focus on the evolution of $|e_2\rangle|0\rangle$. Following the

circuit in figure 10.4, we have:

$$|e_2\rangle|0\rangle \xrightarrow{\hat{C}_2(\frac{\pi}{2},0)} \frac{|e_2\rangle - i|g_2\rangle}{\sqrt{2}}|0\rangle \tag{10.39a}$$

$$\xrightarrow{\hat{B}_2(\pi,0)} |e_2\rangle\frac{|0\rangle - |1\rangle}{\sqrt{2}} \tag{10.39b}$$

$$\xrightarrow{\hat{B}_2(\frac{\pi}{\sqrt{2}},\frac{\pi}{2})} \frac{1}{\sqrt{2}}\left[|e_2\rangle|0\rangle - \cos\left(\frac{\pi}{2\sqrt{2}}\right)|e_2\rangle|1\rangle + \sin\left(\frac{\pi}{2\sqrt{2}}\right)|g_2\rangle|0\rangle\right] \tag{10.39c}$$

$$\xrightarrow{\hat{B}_2(\pi,0)} \frac{1}{\sqrt{2}}\left[|e_2\rangle|0\rangle + i\cos\left(\frac{\pi}{2\sqrt{2}}\right)|g_2\rangle|0\rangle - i\sin\left(\frac{\pi}{2\sqrt{2}}\right)|e_2\rangle|1\rangle\right] \tag{10.39d}$$

$$\xrightarrow{\hat{B}_2(\frac{\pi}{\sqrt{2}},\frac{\pi}{2})} \frac{|e_2\rangle + i|b_2\rangle}{\sqrt{2}}|0\rangle \tag{10.39e}$$

$$\xrightarrow{\hat{C}_2(\frac{\pi}{2},\pi)} i|g_2\rangle|0\rangle\,, \tag{10.39f}$$

and, thus, the output state after the whole circuit is (up to a global phase):

$$|e_1\rangle|g_2\rangle|0\rangle \equiv |1_1\rangle|0_2\rangle|0\rangle\,, \tag{10.40}$$

where we used $\hat{B}_1(\pi,\pi)|e_1\rangle|0\rangle = |e_1\rangle|0\rangle$. Therefore we obtained:

$$|1_1\rangle|1_2\rangle \to |1_1\rangle|0_2\rangle\,, \tag{10.41}$$

as expected. Analogous results can be obtained for the other two-ion states (see exercise 10.1).

In conclusion, we have shown the possibility to implement a CNOT gate. This result, together with the single ion operations described in section 10.3, proves that it is possible to perform universal quantum computation with trapped ions.

□ **– Exercise 10.1** *Prove that the quantum circuit represented in figure 10.4 acts a CNOT gate for the ion states (up to a global phase) and, in particular, one has:*

$$|g_1\rangle|g_2\rangle|0\rangle \to -|g_1\rangle|g_2\rangle|0\rangle\,, \tag{10.42a}$$

$$|g_1\rangle|e_2\rangle|0\rangle \to -|g_1\rangle|e_2\rangle|0\rangle\,, \tag{10.42b}$$

$$|e_1\rangle|g_2\rangle|0\rangle \to -i|e_1\rangle|e_2\rangle|0\rangle\,, \tag{10.42c}$$

$$|e_1\rangle|e_2\rangle|0\rangle \to i|e_1\rangle|g_2\rangle|0\rangle\,. \tag{10.42d}$$

10.5 Hyperfine and optical qubits

There are two possible ways to actually implement a qubit with trapped ions, which require different species of ions according to the presence or not of the nuclear angular momentum.

Ions such as $^{9}Be^{+}$, $^{43}Ca^{+}$ and $^{171}Yb^{+}$ exhibit non-zero nuclear angular momentum. Here the logical levels are the hyperfine structure of the ground state and the frequencies involved are of the order of GHz (microwaves).

In the case of ions with zero nuclear angular momentum, like $^{40}Ca^{+}$, $^{88}Sr^{+}$ and $^{174}Yb^{+}$, the logical levels are obtained within the fine structure and a metastable excited state. Now we have optical frequencies with quadrupole transition leading to a longer state's lifetime.

Bibliography

- D. Leibfried, R. Blatt, C. Monroe and D. Wineland, *Quantum dynamics of single trapped ions*, Rev. Mod. Phys. **75**, 281-324 (2003).
- S. Gulde, *Experimental realization of quantum gates and the Deutsch-Jozsa algorithm with trapped $^{40}Ca^{+}$ ions*, Ph.D. Thesis, Leopold-Franzens-Universität, Innsbruck (2003).
- L. Sanfilippo, *Implementation of quantum logic gates and quantum computation with trapped-ion systems*, Bachelor Thesis, University of Milan (2017).
- F. Schmidt-Kaler *et al.*, *Realization of the Cirac–Zoller controlled-NOT quantum gate*, Nature **422**, 408-411 (2003).

Chapter 11

Superconducting qubits: charge and transmon qubits

IN THIS CHAPTER we explain how it is possible to obtain a two-level system starting from superconducting circuits. In particular we consider the Josephson junction and the SQUID and we focus on the charge qubit and the transmon qubit. We also describe the coupling between a charge qubit and a 1-D transmission line resonator leading to a coupling Hamiltonian similar to that obtained in cavity QED experiments.

11.1 The LC circuit as a harmonic oscillator

We consider a circuit involving an inductor (with inductance L) and and a capacitor (with capacity C). If we indicate with V the voltage at the ends of the capacitor and with I the current flowing in the circuit, the energies stored in the capacitor and in the inductor are:

$$E_C = \frac{1}{2}CV^2 = \frac{Q^2}{2C}, \quad \text{and} \quad E_L = \frac{1}{2}LI^2 = \frac{\Phi^2}{2L}, \tag{11.1}$$

respectively, where $Q = CV$ is the charge of the capacitor and $\Phi = LI$ is the magnetic flux in the inductor. The classical Hamiltonian $H_{\text{cl}} = E_C + E_L$ is:

$$H_{\text{cl}} = \frac{Q^2}{2C} + \frac{\Phi^2}{2L}, \tag{11.2a}$$

$$= \frac{Q^2}{2C} + \frac{1}{2}C\omega_0^2\Phi^2, \tag{11.2b}$$

that is the classical Hamiltonian of a harmonic oscillator with "mass" C, momentum Q, position Φ and frequency $\omega_0 = 1/\sqrt{LC}$.

11.1.1 Quantization of the LC circuit

The quantization of H_{cl} is achieved by the substitution (see also section 9.4):

$$Q \to \hat{Q} = i\sqrt{\frac{\hbar}{2Z_0}}\left(\hat{a}^\dagger - \hat{a}\right), \quad \text{and} \quad \Phi \to \hat{\Phi} = \sqrt{\frac{\hbar Z_0}{2}}\left(\hat{a}^\dagger + \hat{a}\right), \tag{11.3}$$

where we introduced the impedance $Z_0 = \sqrt{L/C}$ and the annihilation and creation operators $\hat{a}$ and $\hat{a}^\dagger$, respectively, $[\hat{a}, \hat{a}^\dagger] = \hat{\mathbb{I}}$. Note that $\hat{\Phi}$ and $\hat{Q}$ are conjugated quantum variables, namely:

$$\left[\hat{\Phi}, \hat{Q}\right] = i\hbar\hat{\mathbb{I}}. \tag{11.4}$$

As usual, the quantum Hamiltonian reads:

$$\hat{H}_{LC} = \hbar\omega_0\left(\hat{a}^\dagger\hat{a} + \frac{1}{2}\right), \quad \hat{H}_{LC}|n\rangle = E_n|n\rangle, \tag{11.5}$$

where $|n\rangle$, $n \in \mathbb{N}$, are the corresponding eigenstates with eigenvalues $E_n = \hbar\omega_0(n + 1/2)$.

Since the difference between two levels $\Delta E = E_{n+1} - E_n = \hbar\omega_0$ is independent of n, we cannot select *only* two particular levels in order to obtain a qubit. To make the energies of the quantized levels different enough to obtain a two level system, we should introduce some nonlinearity, which leads to a nonlinear oscillator.

11.2 The Josephson junction and the SQUID

A Josephson junction consists of two superconductors connected via a tunnelling barrier. It can be described by its critical current I_c, and the *gauge invariant phase difference* φ across the junction. The actual value of the critical current depends on the superconducting material and the size of the junction. More in details, we can associate with each superconductor $k = 1, 2$ the wave function $\Psi_k = \sqrt{\varrho_k}\, e^{i\phi_k}$, where ϱ_k is the density of Cooper pairs of the k-th and ϕ_k its phase. The dynamics of the system is then described by the Schrödinger equations:

$$i\hbar\frac{\partial\Psi_1}{\partial t} = E_1\Psi_1 + \kappa\Psi_2\,, \tag{11.6a}$$

$$i\hbar\frac{\partial\Psi_2}{\partial t} = E_2\Psi_1 + \kappa\Psi_1\,, \tag{11.6b}$$

where E_1 and E_2 are the energies of the states and κ the coupling constant which measures the interaction of the two wave functions. By substituting the expression of Ψ_k into the Schrödinger equations we can obtain the following equations:

$$\hbar\frac{\partial\varrho_1}{\partial t} = 2\kappa\sqrt{\varrho_1\varrho_1}\sin\varphi\,, \tag{11.7a}$$

$$\hbar\frac{\partial\varrho_2}{\partial t} = -2\kappa\sqrt{\varrho_1\varrho_1}\sin\varphi\,, \tag{11.7b}$$

$$\hbar\frac{\partial\varphi}{\partial t} = E_2 - E_1\,. \tag{11.7c}$$

The derivatives $\partial_t \varrho_1 = -\partial_t \varrho_2$ are proportional to the so-called Josephson current I_J, while the quantity $2\kappa\sqrt{\varrho_1 \varrho_1}$ to critical current I_c mentioned above. Moreover, if we apply a voltage V to the junction, we have $E_2 - E_1 = 2eV$ and the previous equations can be rewritten as the two following *Josephson equations*:

$$I_J(t) = I_c \sin\varphi(t), \qquad (1^{\text{st}} \text{ Josephson equation}) \tag{11.8}$$

$$\frac{\partial\varphi(t)}{\partial t} = \frac{2\pi}{\Phi_0} V, \qquad (2^{\text{nd}} \text{ Josephson equation}) \tag{11.9}$$

that allow to describe the time evolution of the Josephson current I_J and of φ as a function of the applied voltage V. In Eq. (11.9) we introduced the *superconducting flux quantum* $\Phi_0 = h/(2e) = 2.07 \times 10^{-15}$ Wb, where $2e$ is the charge of a *Cooper pair*. The time derivative of Eq. (11.8) gives:

$$\dot{I}_J = I_c \cos\varphi \, \frac{\partial\varphi}{\partial t}, \tag{11.10}$$

and, using Eq. (11.9) and since $\dot{I} = V/L$, we can introduce the following *nonlinear inductance*:

$$L_J = \frac{1}{\cos\varphi} \frac{\Phi_0}{2\pi I_c}. \tag{11.11}$$

The energy associated with L_J is obtained as follows:

$$E_{J,L} = \int_0^t d\tau \, I_J(\tau) \, V = E_J(1 - \cos\varphi), \tag{11.12}$$

where:

$$E_J = \frac{\Phi_0 I_c}{2\pi} \tag{11.13}$$

is the Josephson energy, which is a measure of the coupling across the junction. Since a Josephson junction has also a capacitance C_J, we can calculate the corresponding energy:

$$E_{J,C} = \frac{Q^2}{2C_J}, \tag{11.14}$$

where Q is the charge of the junction.

The classical Hamiltonian of the Josephson junction can be written as (we neglect the constant term):

$$H_J = \frac{Q^2}{2C_J} - E_J \cos\varphi. \tag{11.15}$$

Since $Q = (2e)N$, where $N \in (-\infty, +\infty)$ is the *excess* of Cooper pair in the Junction, $N = N_1 - N_2$, where N_1 and N_2 represent the numbers of Cooper pairs present at each side of the junction, we can define the capacitive energy $E_c = e^2/(2C_J)$, and Eq. (11.15) becomes:

$$H_J = 4E_c N^2 - E_J \cos\varphi. \tag{11.16}$$

Instead of a single Josephson junction we can consider two Josephson junctions connected in parallel on a superconducting loop: this system is called SQUID (Superconducting QUantum

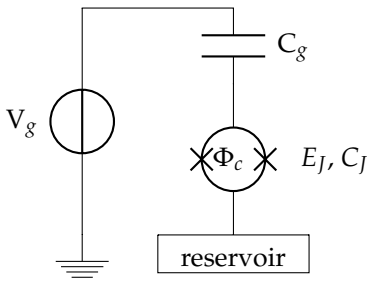

Figure 11.1: A SQUID embedded in a circuit with a gate voltage V_g.

Interference Device). If the inductance of the loop can be neglected, then the corresponding Hamiltonian is the same as in Eq. (11.16), but now:

$$C_J \to 2C_J^{(s)}, \quad E_J \to E_J(\Phi_c) = 2E_J^{(s)} \cos\left(\pi \frac{\Phi_c}{\Phi_0}\right), \tag{11.17}$$

where $C_J^{(s)}$ and $E_J^{(s)}$ are the single Josephson junction capacitance and energy, respectively, and Φ_c is the (eventual) external flux: changing Φ_c one can modify E_J.

From now on we assume that our system is a SQUID embedded in a circuit and a gate voltage V_g is applied through a capacitance C_g, as shown in figure 11.1. The presence of V_g simply shifts N in Eq. (11.16) by $N_g = C_g V_g/(2e)$, namely:

$$H = 4E_c(N - N_g)^2 - E_J \cos\varphi, \tag{11.18}$$

where, now:

$$E_c = \frac{e^2}{2(C_J + C_g)}. \tag{11.19}$$

If we associate $4E_c N^2$ with the kinetic energy and $-E_J \cos\varphi$ with the potential energy, then H represents the Hamiltonian of a nonlinear oscillator, where the conjugated variables are N (corresponding to the momentum) and φ (corresponding to the position).

11.2.1 Quantization of the Josephson junction and SQUID Hamiltonians

We can now obtain the quantum analogue of the Hamiltonian Eq. (11.18) associating with φ and N the corresponding quantum operators:

$$\varphi \to \hat{\varphi}, \quad N \to \hat{N}, \tag{11.20}$$

and the quantum Hamiltonian reads:

$$\hat{H} = 4E_c(\hat{N} - N_g)^2 - E_J \cos\hat{\varphi}. \tag{11.21}$$

It is worth noting that $\hat{N}$ is the operator associated with the excess of Cooper pairs N, where $N \in (-\infty, +\infty)$, and does not correspond to the *number operator* of the quantum harmonic oscillator, as the one considered for the electromagnetic field in section 9.4. We can write the relation between $\hat{\varphi}$ and $\hat{N}$ as:

$$e^{i\hat{\varphi}}\hat{N}e^{-i\hat{\varphi}} = \hat{N} - \hat{\mathbb{I}}. \tag{11.22}$$

However, since $\hat{\varphi}$ and $\hat{N}$ are conjugated variables, being $[\hat{\varphi}, \hat{N}] = i\hat{\mathbb{I}}$, in the basis of the eigenstates of $\hat{\varphi}$, we have the following association:

$$\hat{\varphi} \to \varphi, \quad \text{and} \quad \hat{N} \to -i\frac{\partial}{\partial\varphi}, \tag{11.23}$$

and the Hamiltonian rewrites:

$$\hat{H} = 4E_c\left(-i\frac{\partial}{\partial\varphi} - N_g\right)^2 - E_J\cos\varphi. \tag{11.24}$$

The solutions of the differential equation $\hat{H}\psi_m(\varphi) = E_m\psi_m(\varphi)$ are given in terms of the Floquet-type solutions $\mathrm{me}_\nu(q, x)$ as follows:

$$\psi_m(\varphi) = \frac{1}{\sqrt{2}}\,\mathrm{me}_{-2[N_g - f(m,N_g)]}\left(-\frac{E_J}{2E_c}, \frac{\varphi}{2}\right), \tag{11.25}$$

with:

$$\begin{aligned} f(m, N_g) = \sum_{k=\pm1} &[\mathrm{int}(2N_g + k/2) \bmod 2] \\ &\times \{\mathrm{int}(N_g) - k(-1)^m[(m+1)\,\mathrm{div}\,2 + m \bmod 2]\}, \end{aligned} \tag{11.26}$$

where $\mathrm{int}(x)$ rounds to the integer closest to x, $x \bmod y$ denotes the usual modulo operation, and $x \,\mathrm{div}\, y$ gives the integer quotient of x and y. The corresponding eigenvalues are:

$$E_m = E_c\, a_{-2[N_g - f(m,N_g)]}\left(-\frac{E_J}{2E_c}\right), \tag{11.27}$$

where $a_\nu(q)$ denotes Mathieu's characteristic value. In figure 11.2 we report the behavior of E_m, $m = 0, 1, 2$, and 3, as a function of N_g and normalized with respect to transition E_{01}, which is the minimum energy separation between the levels E_1 and E_0, for different values of the ratio E_J/E_c.

As shown in figure 11.3 we can identify two regimes: the *charge regime* ($E_c \gg E_J$) and the *transmon regime* ($E_c \ll E_J$). In each of these regimes we can define a two level system which can be used as a qubit.

11.3 The charge qubit

In the charge regime, $E_J \ll E_c$, our system can be seen as a Cooper pair box (CPB), that is sketched in figure 11.4. It consists in a superconducting electrode (the "island") in contact with a

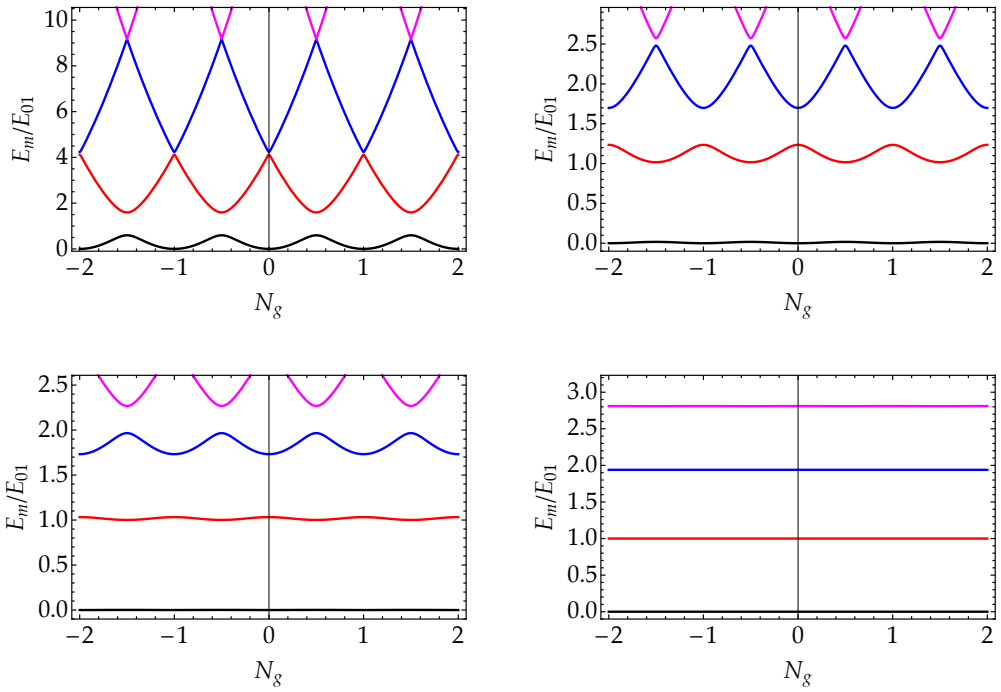

Figure 11.2: E_m as a function of N_g (in each plot, from bottom to top $m = 0, 1, 2$ and 3) normalized with respect to $E_{01} \equiv \min_{N_g}(E_1 - E_0)$ for different values of the ratio E_J/E_c. (Top left) $E_J/E_c = 1.0$; (top right) $E_J/E_c = 5.0$; (bottom left) $E_J/E_c = 10.0$; (bottom right) $E_J/E_c = 50.0$. The zero point of energy is chosen as the bottom of the $m = 0$ level.

superconducting reservoir though a tunnel junction (the grey zone in figure, which corresponds to a Josephson junction or to the two junctions of the SQUID) with capacitance C_J. Excess Cooper pairs may tunnel onto the island in response to an electric field applied by means of the gate capacitance C_g and voltage V_g.

In this case we have a well defined number N of tunneling Cooper pairs and, thus, of excess of Cooper pairs, and a strongly fluctuating phase. Therefore we can express the Hamiltonian (11.21) as a function of the eigenstates $|N\rangle$ of $\hat{N}$, that is, $\hat{N}|N\rangle = N|N\rangle$, $N \in \mathbb{Z}$; we have:

$$\hat{H}_{\text{CPB}} = \sum_{N=-\infty}^{+\infty} \left[4E_c(N - N_g)^2 |N\rangle\langle N| - \frac{1}{2} E_J(|N\rangle\langle N+1| + |N+1\rangle\langle N|) \right], \tag{11.28}$$

where the term $|N\rangle\langle N+1| + |N+1\rangle\langle N|$ describes the tunneling through the junction of a single Cooper pair. It is now clear that E_J represents a measure of the coupling across the junction. It is worth noting that the states:

$$|\varphi\rangle = \frac{1}{\sqrt{2\pi}} \sum_{N=-\infty}^{+\infty} \exp(iN\varphi)|N\rangle \tag{11.29}$$

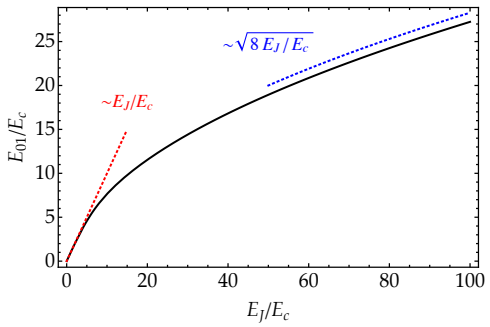

Figure 11.3: Plot of E_{01}/E_c as a function of the ratio E_J/E_c: for $E_c \gg E_J$ (charge regime) we have $E_{01} \sim E_J$; for $E_c \ll E_J$ (transmon regime) we have $E_{01} \sim \sqrt{8E_JE_c}$.

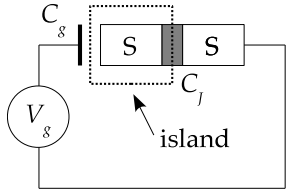

Figure 11.4: Schematics of the CPB. The dashed box encloses the superconducting island.

are eigenstates of the operator:

$$\hat{H}_{\text{tun}} = -\frac{1}{2}E_J \sum_{N=-\infty}^{+\infty} (|N\rangle\langle N+1| + |N+1\rangle\langle N|), \tag{11.30}$$

and $\hat{H}_{\text{tun}}|\varphi\rangle = -E_J \cos\varphi|\varphi\rangle$, that is we have the following expansion:

$$\cos\hat{\varphi} = \frac{1}{2} \sum_{N=-\infty}^{+\infty} (|N\rangle\langle N+1| + |N+1\rangle\langle N|). \tag{11.31}$$

□ **– Exercise 11.1** *Prove Eq. (11.31) by the explicit calculation of the matrix elements of* $\cos\hat{\varphi}$ *in the basis of the eigenstates* $|N\rangle$ *of* $\hat{N}$, $N \in \mathbb{Z}$.

If E_J is negligible, then $\hat{H}_{\text{CPB}}$ is just the sum of energies $4E_c(N - N_g)^2$ of the states $|N\rangle$ (see the left plot in figure 11.5): it is interesting to note that, for a particular choice of N_g, states with different number N may have the same energy (they are degenerate). In particular we can see that the two states $|N\rangle$ and $|N+1\rangle$ are degenerate if $N_g = (1+2N)/2$. As one may expect, the presence of the interaction, though weak but not negligible, breaks the degeneracy (see the right plot figure 11.5). In particular, an energy gap appears near degeneracy, which, for fixed N_g, allows us to identify two well defined energy levels whose energy difference is E_J (see the top

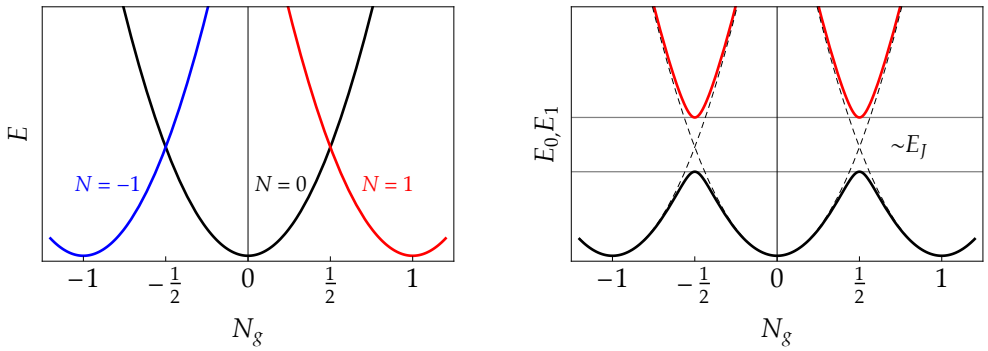

Figure 11.5: Left plot: energy levels of the states $|N\rangle$ without interaction ($E_J = 0$): note the degeneracy at $N_g = (1+2N)/2$. Right plot: as $E_J \neq 0$ the degeneracy is broken, and, if $E_J \ll E_c$, we can identify two levels, E_0 (black) and E_1 (red), whose energy difference at $N_g = (1+2N)/2$ is $\sim E_J$.

left plot in figure 11.2). In fact, for a fixed N, and considering $N_g \approx (1+2N)/2$, we can assume that only the two states $|N\rangle$ and $|N+1\rangle$ are coupled by the interaction (this can be shown more rigorously by considering the interaction picture and the RWA). The corresponding two-level Hamiltonian can be written as:

$$\hat{H}_{\mathrm{CPB}}(N_g, N) = 4E_c \left[(N - N_g)^2 |N\rangle\langle N| + (N+1-N_g)^2 |N+1\rangle\langle N+1|\right] - \frac{1}{2}E_J\left(|N\rangle\langle N+1| + |N+1\rangle\langle N|\right), \tag{11.32}$$

$$= 4E_c\left[(N_g - N) - \frac{1}{2}\right]\overline{\sigma}_z^{(N)} - \frac{1}{2}E_J\,\overline{\sigma}_x^{(N)} + 2E_c\left[(N-N_g)^2 + (N-N_g+1)^2\right]|N+1\rangle\langle N+1|, \tag{11.33}$$

where we introduced $\overline{\sigma}_z^{(N)} = |N\rangle\langle N| - |N+1\rangle\langle N+1|$ and $\overline{\sigma}_x^{(N)} = |N\rangle\langle N+1| + |N+1\rangle\langle N|$. The eigenvalues of $\hat{H}_{\mathrm{CPB}}(N_g, N)$ are:

$$E^{\pm}_{\mathrm{CPB}}(N_g, N) = 2E_c\left[(N-N_g)^2 + (N-N_g+1)^2\right] \pm \frac{1}{2}\sqrt{E_J^2 + 16E_c^2[1+2(N-N_g)]^2}.$$

Since at degeneracy $N - N_g = -1/2$, Eq. (11.32) rewrites (we neglect the constant term E_c):

$$\hat{H}_{\mathrm{CPB}} \equiv \hat{H}_{\mathrm{CPB}}(1/2, 0) = -\frac{1}{2}E_J\overline{\sigma}_x, \tag{11.34}$$

where $\overline{\sigma}_z = |0\rangle\langle 0| - |1\rangle\langle 1|$ and $\overline{\sigma}_x = |0\rangle\langle 1| + |1\rangle\langle 0|$. Since:

$$\hat{H}_{\mathrm{CPB}} \to \begin{pmatrix} 0 & -\frac{1}{2}E_J \\ -\frac{1}{2}E_J & 0 \end{pmatrix}, \tag{11.35}$$

it is straightforward to find the two eigenvalues:

$$E_{\pm} = \pm\frac{1}{2}E_J, \quad \text{with} \quad E_+ - E_- = E_J, \tag{11.36}$$

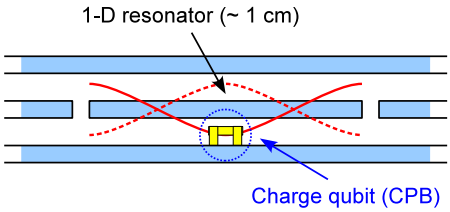

Figure 11.6: Sketch of a typical configuration to implement circuit QED. A superconducting qubit (a CPB, in yellow) is built inside a 1-D transmission line resonator. The final configuration is such that there is a maximum coupling between the qubit and resonator (the rms voltages reaches the maxima at the center of the conductor, see the red lines).

and the corresponding eigenstates:

$$|e\rangle = \frac{|1\rangle - |0\rangle}{\sqrt{2}}, \quad |g\rangle = \frac{|1\rangle + |0\rangle}{\sqrt{2}}, \tag{11.37}$$

with $\hat{H}_{\rm CPB}|e\rangle = E_+|e\rangle$ and $\hat{H}_{\rm CPB}|g\rangle = E_-|g\rangle$. Note that:

$$\overline{\sigma}_x = \underbrace{|g\rangle\langle g| - |e\rangle\langle e|}_{-\hat{\sigma}_z}, \quad \text{and} \quad \overline{\sigma}_z = \underbrace{|e\rangle\langle g| + |g\rangle\langle e|}_{\hat{\sigma}_x}, \tag{11.38}$$

where, as usual, $|e\rangle \to (1,0)^T$ and $|g\rangle \to (0,1)^T$. In the basis $\{|g\rangle, |e\rangle\}$, the Hamiltonian (11.34) simply reads (we neglect the constant term):

$$\hat{H}_{\rm CPB} = \hbar\frac{\Omega}{2}\hat{\sigma}_z, \tag{11.39}$$

with $\Omega = E_J/\hbar$, that is the Hamiltonian of an *artificial atom* which can be used as a qubit.

As a matter of fact, the charge qubit is very sensible to the fluctuations of N_g and, thus, of the gate voltage V_g. This problem can be solved considering the so-called transmon regime.

11.4 Charge qubit and capacitive coupling with a 1-D resonator

A 1-D transmission line resonator consists of a full-wave section of superconducting coplanar waveguide. If L_r and C_r are the effective inductance and capacitance of the resonator, respectively, then its characteristic frequency is $\omega_r = 1/\sqrt{L_r C_r}$ (typical values are $\omega_r \sim 10$ GHz). The quantum Hamiltonian of the resonator may be written as:

$$\hat{H}_r = \hbar\omega_r\left(\hat{a}^\dagger\hat{a} + \frac{1}{2}\right), \tag{11.40}$$

$\hat{a}$ being the annihilation operator, $[\hat{a}, \hat{a}^\dagger] = \hat{\mathbb{I}}$. The 1-D resonator plays the role of the cavity of a cavity QED experiment.

As depicted in figure 11.6, a superconducting qubit (here a CPB) is placed inside the 1-D resonator and it plays the role of the atom of the cavity QED setup. The system CPB+resonator are built is such a way that there is a maximum coupling between the qubit and resonator. As schematically shown in figure 11.6, the qubit couples with the mode 2 of the resonator (maxima at the center).

The *free* Hamiltonian of the system reads:

$$\hat{H}_0 = \hbar\omega_r \left(\hat{a}^\dagger \hat{a} + \frac{1}{2}\right) + 4E_c(\hat{N} - N_g)^2 - E_J \cos\hat{\varphi}, \tag{11.41}$$

where the the second and the third terms are the same as in Eq. (11.21).

The coupling between the resonator and the CPB is due to the presence of the quantum contribution to the voltage, which leads to the following substitution in Eq. (11.41):

$$N_g \to N_g + \hat{N}_r, \quad \text{with} \quad \hat{N}_r = \underbrace{\frac{C_g V_{\text{rms}}}{2e}}_{N_q} (\hat{a}^\dagger + \hat{a}), \tag{11.42}$$

where $V_{\text{rms}} = \sqrt{\hbar\omega_r/(2C_r)}$ is the rms voltage corresponding to the mode 2 of the resonator ($\omega_r \to \omega_r/2$) and C_g is the gate voltage. After the substitution we obtain the following Hamiltonian which describes also the coupling through the gate voltage (we neglect the constant term):

$$\hat{H} = \hbar\omega_r \hat{a}^\dagger \hat{a} + 4E_c \left[(\hat{N} - N_g) - N_q(\hat{a}^\dagger + \hat{a})\right]^2 - E_J \cos\hat{\varphi} \tag{11.43}$$

$$= \underbrace{\hbar\omega_r \hat{a}^\dagger \hat{a}}_{\text{resonator}} + \underbrace{4E_c(\hat{N} - N_g)^2 - E_J \cos\hat{\varphi}}_{\text{CPB}} - \underbrace{8E_c N_q(\hat{N} - N_g)(\hat{a}^\dagger + \hat{a})}_{\text{interaction}}, \tag{11.44}$$

where we neglected the terms proportional to N_q^2 (note that $V_{\text{rms}} \sim \mu$V).

In the charge regime, $E_c \gg E_J$, and, as shown in section 11.3, we can expand the Hamiltonian in the eigenstates $|N\rangle$ of $\hat{N}$. For the sake of simplicity, we consider only the two states $|0\rangle$ and $|1\rangle$. By introducing $\overline{\sigma}_z = |0\rangle\langle 0| - |1\rangle\langle 1|$, we have the following identities:

$$(\hat{N} - N_g) = \frac{1}{2}\left(\hat{\mathbb{1}} - \overline{\sigma}_z\right) - N_g, \tag{11.45a}$$

$$(\hat{N} - N_g)^2 = \left(N_g^2 - N_g + \frac{1}{2}\right) - (1 - 2N_g)\overline{\sigma}_z, \tag{11.45b}$$

$$(\hat{a}^\dagger + \hat{a})(\hat{N} - N_g) = \frac{1}{2}(\hat{a}^\dagger + \hat{a})\left[(1 - 2N_g)\hat{\mathbb{1}} - \overline{\sigma}_z\right]. \tag{11.45c}$$

If we now use the basis $\{|e\rangle, |g\rangle\}$ introduced in section 11.3, we have:

$$\overline{\sigma}_z = \hat{\sigma}_x = \hat{\sigma}_+ + \hat{\sigma}_-, \tag{11.46}$$

where $\hat{\sigma}_+ = |e\rangle\langle g|$ and $\hat{\sigma}_- = |g\rangle\langle e|$; finally we obtain (at the degeneracy point $N_g = \frac{1}{2}$):

$$\hat{H} = \hbar\omega_r \hat{a}^\dagger \hat{a} + \hbar\frac{\Omega}{2}\hat{\sigma}_z + 4E_c N_q(\hat{a}^\dagger + \hat{a})(\hat{\sigma}_+ + \hat{\sigma}_-), \tag{11.47}$$

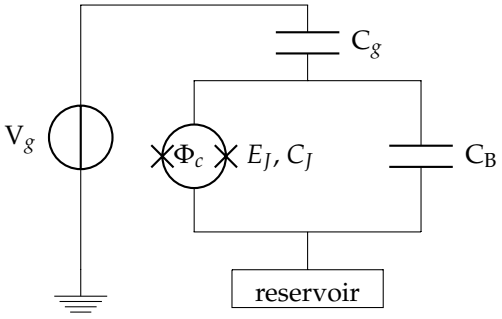

Figure 11.7: The transmon qubit: a SQUID shunted by a large capacitance C_B, that reduces the fluctuations of the gate voltage by reducing E_c.

where $\Omega = E_J/\hbar$ and the last term corresponds to the interaction between the artificial atom and the resonator, which is the same interaction addressed in section 9.5.

Indeed, it is also possible to couple the transmon qubit with the 1-D resonator. However, the theoretical description of the interaction requires advanced methods of quantum optics and it is left to the interested readers.

11.5 The transmon qubit

Let us focus the attention on figure 11.2: as the ratio E_J/E_c increases, the energy levels E_m can be approximated by the oscillating functions:

$$E_m(N_g) \approx E_m(N_g = 1/4) + \frac{\varepsilon_m}{2}\cos(2\pi N_g), \tag{11.48}$$

where:

$$\varepsilon_m \approx (-1)^m E_c \frac{2^{4m+5}}{m!}\sqrt{\frac{2}{\pi}}\left(\frac{E_J}{2E_c}\right)^{\frac{m}{2}+\frac{3}{4}} e^{-\sqrt{8E_J/E_c}}. \tag{11.49}$$

Therefore, in the limit $E_J \gg E_c$ they become almost independent of N_g (see the bottom right plot of figure 11.2), and we reach the *transmon* regime, where "transmon" refers to "transmission line shunted plasma oscillation qubit" (this is related to the physical implementation to achieve $E_J \gg E_c$). This regime is achieved by using the same configuration of the charge qubit (a dc SQUID coupled to a gate voltage V_g via the gate capacitance C_g) but now the SQUID is shunted by a large capacitance C_B, as depicted in figure 11.7. For this system one has (see the references at the end of this chapter for further details):

$$E_c = \frac{e^2}{2(C_J + C_g + C_B)}, \tag{11.50}$$

therefore, by increasing C_B it is possible to decrease E_c in order to obtain the regime $E_c \ll E_J$. In this way the fluctuations of the gate voltage are also reduced.

Since $E_J \gg E_c$, we can expand up to the 4-th order the cos $\hat{\varphi}$ in Eq. (11.21), obtaining (since the energy levels are independent of N_g, this quantity does not appear explicitly):

$$\hat{H}_{\text{Tr}} = 4E_c\hat{N}^2 + \frac{1}{2}E_J\hat{\varphi}^2 - \frac{1}{24}E_J\hat{\varphi}^4 \tag{11.51}$$

where we can easily identify the Hamiltonian $\hat{H}_0 = 4E_c\hat{N}^2 + \frac{1}{2}E_J\hat{\varphi}^2$, that represents a harmonic oscillator and the nonlinear term $\hat{H}_1 = -\frac{1}{24}E_J\hat{\varphi}^4$. In the following, we show that the presence of $\hat{H}_1$ is what we need to make the energy levels different enough in order to select a well defined two-level system.

Equation (11.51) represents the Hamiltonian of a nonlinear oscillator, therefore we can introduce the bosonic field annihilation, $\hat{b}$ and creation, $\hat{b}^\dagger$, operators, respectively, with $[\hat{b}, \hat{b}^\dagger] = \hat{\mathbb{1}}$, and put:

$$\hat{\varphi} = \left(\frac{2E_c}{E_J}\right)^{\frac{1}{4}}\left(\hat{b}^\dagger + \hat{b}\right) = 2\sqrt{\frac{E_c}{\hbar\omega_p}}\left(\hat{b}^\dagger + \hat{b}\right), \tag{11.52}$$

$$\hat{N} = i\left(\frac{E_J}{32E_c}\right)^{\frac{1}{4}}\left(\hat{b}^\dagger - \hat{b}\right) = \frac{i}{4}\sqrt{\frac{\hbar\omega_p}{E_c}}\left(\hat{b}^\dagger - \hat{b}\right), \tag{11.53}$$

where we introduced the *Josephson plasma frequency*:

$$\omega_p = \frac{\sqrt{8E_JE_c}}{\hbar}. \tag{11.54}$$

It is easy to show that $[\hat{\varphi}, \hat{N}] = i\hat{\mathbb{1}}$ and that Eq. (11.51) becomes:

$$\hat{H}_{\text{Tr}} = \underbrace{\hbar\omega_p\left(\hat{b}^\dagger\hat{b} + \frac{1}{2}\right)}_{\hat{H}_0} - \frac{1}{12}E_c\left(\hat{b}^\dagger + \hat{b}\right)^4, \tag{11.55}$$

and $\hbar\omega_p = \sqrt{8E_JE_c}$. Since $E_c \ll E_J$, in order to calculate the eigenvalues of Eq. (11.55) we can apply the first order perturbation theory. The unperturbed eigenvalues of $\hat{H}_{\text{Tr}}$ are:

$$E_n^{(0)} = \hbar\omega_p\left(n + \frac{1}{2}\right), \tag{11.56}$$

where $\hat{H}_0|n\rangle = E_n^{(0)}|n\rangle$. The first order correction to $E_n^{(0)}$ is given by:

$$\begin{aligned} E_n^{(1)} &= -\langle n|\left[\frac{1}{12}E_c\left(\hat{b}^\dagger + \hat{b}\right)^4\right]|n\rangle \\ &= -\frac{1}{12}E_c\langle n|\left[12\,\hat{b}^\dagger\hat{b} + 6(\hat{b}^\dagger)^2\hat{b}^2 + 3 + (\text{terms s.t. } \langle n|\cdots|n\rangle = 0)\right]|n\rangle \\ &= -E_cn - \frac{1}{2}E_cn(n-1) - \frac{1}{4}E_c. \end{aligned} \tag{11.57}$$

Therefore, neglecting the constant term, the perturbed energy levels are:

$$E_n = \left(\sqrt{8E_JE_c} - E_c\right)n - \frac{1}{2}E_cn(n-1). \tag{11.58}$$

It is worth noting that, due to the nonlinearity, the difference between adjacent levels is now dependent on n, namely:

$$\Delta E_{n,n+1} \equiv E_{n+1} - E_n = \left(\sqrt{8E_J E_c} - E_c\right) - E_c n. \tag{11.59}$$

In particular, we have:

$$\Delta E_{0,1} = \sqrt{8E_J E_c} - E_c, \tag{11.60}$$

$$\Delta E_{1,2} = \Delta E_{0,1} - E_c. \tag{11.61}$$

Since typical values of the involved quantities are $E_J/\hbar \approx 2$ GHz ad $E_c/\hbar \approx 400$ MHz (usually, $C_J \approx 10^{-12}$ F), it is possible to experimentally select only the transition between the levels E_0 and E_1, thus obtaining the so-called transmon qubit.

It is worth noting that the gain in charge-noise insensitivity as E_J/E_c increases, leads also to a loss in anharmonicity. In order to reduce a many-level system to a qubit, that is a system with two well-defined levels, a sufficient anharmonicity is required. Form the experimental point of view this sets a lower bound on the duration of control pulses to implement the quantum logic gates. However it is possible to show that the energy ratio should satisfy $20 \lesssim E_J/E_c \ll 5 \cdot 10^4$, opening up a large range with exponentially decreased sensitivity to charge noise and yet sufficiently large anharmonicity for qubit operations. The interested reader can find further details in the references cited in the Bibliography.

Bibliography

- V. Bouchiat *et al.*, *Quantum coherence with a single Cooper pair*, Phys. Scr. **T76**, 165–170 (1998).
- A. Blais *et al.*, *Cavity quantum electrodynamics for superconducting electrical circuits: An architecture for quantum computation*, Phys. Rev. A **69**, 062320 (14 pages) (2004).
- J. Koch *et al.*, *Charge-insensitive qubit design derived from the Cooper pair box*, Phys. Rev. A **76**, 042319 (19 pages) (2007).
- M. Devoret, S. Girvin and R. Schoelkopf, *Circuit-QED: How strong can the coupling between a Josephson junction atom and a transmission line resonator be?*, Ann. Phys. **16**, 767–779 (2007).

Chapter 12

Quantum computation and adiabatic evolution

IN THE PREVIOUS CHAPTERS we addressed quantum computation considering the quantum circuit model, where the information, encoded into qubits, is processed by means of quantum gates implementing a well defined algorithm. In this chapter we introduce a different approach to quantum computation, based on the adiabatic evolution. Here the problem is encoded into a given *problem Hamiltonian* and the solution is given by the *ground state* of the Hamiltonian itself. In order to find the solution, one starts form the ground state of an initial Hamiltonian which is then adiabatically transformed into the problem Hamiltonian. If the requirement of the so-called adiabatic theorem are satisfied, during the dynamics the system remains into the ground state of the *instantaneous* Hamiltonian and, thus, we finally end up in the ground state of the problem Hamiltonian.

12.1 Clauses and instances of satisfiability

In our context, a *clause* C is a boolean expression which can be *true* or *false* according to the values of the involved bits. For example, the two-bit clause

$$x_1 \wedge x_2 \,, \tag{12.1}$$

where $x_k \in \{0, 1\}$, is *true*, that is $x_1 \wedge x_2 = 1$, only if $x_1 = x_2 = 1$. We can also write the formal identity

$$x_1 \wedge x_2 = x_1 x_2 \,, \tag{12.2}$$

where at the r.h.s. we have the mathematical product of the bit values.

It is possible to associate a two-qubit Hamiltonian with the clause (12.1) whose ground state is the searched solution. In fact, recalling that $\hat{\sigma}_z|x\rangle = (-1)^x|x\rangle$, we can write

$$\frac{1}{2}\left(\hat{\mathbb{I}} - \hat{\sigma}_z\right)|x\rangle = x|x\rangle\,, \tag{12.3a}$$

$$\frac{1}{2}\left(\hat{\mathbb{I}} + \hat{\sigma}_z\right)|x\rangle = \overline{x}|x\rangle\,, \tag{12.3b}$$

and it is straightforward to check that the ground state $|x_1\rangle|x_2\rangle = |1\rangle|1\rangle$ of the Hamiltonian (for the sake of simplicity in this chapter we assume that all the quantities are dimensionless, namely, we set $\hbar = 1$):

$$\hat{H}_{x_1 \wedge x_2} = \hat{\mathbb{I}} - \frac{1}{2}\left(\hat{\mathbb{I}} - \hat{\sigma}_z^{(1)}\right) \otimes \frac{1}{2}\left(\hat{\mathbb{I}} - \hat{\sigma}_z^{(2)}\right)\,, \tag{12.4}$$

just encodes the solution of the clause (12.1). A similar result can be obtained for the clause

$$x_1 \wedge \overline{x}_2 = x_1\overline{x}_2\,, \tag{12.5}$$

and the corresponding Hamiltonian:

$$\hat{H}_{x_1 \wedge \overline{x}_2} = \hat{\mathbb{I}} - \frac{1}{2}\left(\hat{\mathbb{I}} - \hat{\sigma}_z^{(1)}\right) \otimes \frac{1}{2}\left(\hat{\mathbb{I}} + \hat{\sigma}_z^{(2)}\right)\,, \tag{12.6}$$

whose ground state is $|1\rangle|0\rangle$.

Up to now we considered the AND operation. However, exploiting the logical identity $x_1 \vee x_2 = \mathrm{NOT}(\overline{x}_1 \wedge \overline{x}_2)$, we can see that the Hamiltonian "solving" the clause $x_1 \vee x_2$ reads:

$$\hat{H}_{x_1 \vee x_2} = \frac{1}{2}\left(\hat{\mathbb{I}} + \hat{\sigma}_z^{(1)}\right) \otimes \frac{1}{2}\left(\hat{\mathbb{I}} + \hat{\sigma}_z^{(2)}\right)\,, \tag{12.7}$$

that has the three degenerate ground states $|1\rangle|0\rangle$, $|0\rangle|1\rangle$ and $|1\rangle|1\rangle$.

As a last example, we consider a clause involving tree bits, an example of the so-called 3-SAT problem in which each clause involves just three bits, *e.g.*:

$$x_1 \vee x_2 \vee \overline{x}_3 \equiv \mathrm{NOT}(\overline{x}_1 \wedge \overline{x}_2 \wedge x_3)\,. \tag{12.8}$$

The reader can find that the Hamiltonian encoding the solution 001 in its ground state is

$$\hat{H}_{x_1 \vee x_2 \vee \overline{x}_3} = \frac{1}{2}\left(\hat{\mathbb{I}} + \hat{\sigma}_z^{(1)}\right) \otimes \frac{1}{2}\left(\hat{\mathbb{I}} + \hat{\sigma}_z^{(2)}\right) \otimes \frac{1}{2}\left(\hat{\mathbb{I}} - \hat{\sigma}_z^{(3)}\right)\,. \tag{12.9}$$

Inspecting the previous examples, it is easy finding the general rule to associate a suitable Hamiltonian with a logical clause. On the other hand, if writing that Hamiltonian is quite straightforward, retrieving the actual ground state cannot be easy at all... For example, an n-bit instance of satisfiability is a logical expression

$$C_1 \wedge C_2 \wedge \cdots \wedge C_M\,, \tag{12.10}$$

where C_k is a particular instance depending on the values of some subset of n bits. Finding a solution of a single clause could be simple but retrieving the solution of the whole instance (if it exists!) can be quite difficult. Nevertheless, it is clear that we can associate a Hamiltonian $\hat{H}_k$, whose ground state is its specific solution, with any single clause C_k . Therefore, the total Hamiltonian:

$$\hat{H} = \hat{H}_1 + \hat{H}_2 + \cdots + \hat{H}_M \equiv \sum_{k=1}^{M} \hat{H}_k \,, \tag{12.11}$$

encodes in its ground state the solution of the instance (12.10) by construction. Notice that, for the sake of simplicity, we considered a scenario in which the ground state has zero energy.

Of course, now the problem is to find the ground state of the Hamiltonian (12.11) and, here, quantum mechanics can help.

12.2 The adiabatic theorem

In the previous section we have seen that we can associate a Hamiltonian $\hat{H}_\mathrm{p}$ with a satisfiability problem in such a way that its ground state $|\Psi_\mathrm{p}\rangle$ encodes the solution. In general finding the ground state of $\hat{H}_\mathrm{p}$ can be a hard problem. Nevertheless, we can find it by applying the *adiabatic theorem*. In the following we will see the main ingredients of this theorem and its application to our purposes.

First of all we consider a Hamiltonian $\hat{H}_0$ whose ground state $|\Psi_0\rangle$ is easy to prepare and, then, we assume to have also a slowly-varying time-dependent *interpolating* Hamiltonian $\hat{H}(t)$ such that $\hat{H}(0) \equiv \hat{H}_0$ and $\hat{H}(T) \equiv \hat{H}_\mathrm{p}$. Indeed, the time evolution of the state $|\psi(t)\rangle$ of the system is given a s usual by the Schrödinger equation:

$$i\frac{d}{dt}|\psi(t)\rangle = \hat{H}(t)|\psi(t)\rangle \,. \tag{12.12}$$

If we define the parameter $s = t/T$, we can focus our analysis on the one-parameter family of Hamiltonians $\tilde{H}(s = t/T) \equiv \hat{H}(t)$ with $0 \leq s \leq 1$: the role of T is to control the rate at which $\hat{H}(t)$ changes, the longer T the slower the rate. Now we introduce the instantaneous eigenstates and eigenvalues of $\tilde{H}(s)$, namely:

$$\tilde{H}(s)|\phi_n(s)\rangle = E_n(s)|\phi_n(s)\rangle \tag{12.13}$$

where

$$E_0(s) \leq E_1(s) \leq \cdots \leq E_{N-1}(s) \,, \tag{12.14}$$

N being the actual dimension of the Hilbert space of the system. According to the adiabatic theorem, if $E_1(s) - E_0(s) > 0$, $\forall s \in [0,1]$, we have:

$$\lim_{T\to\infty} |\langle\phi_0(1)|\psi(T)\rangle| = 1 \,, \tag{12.15}$$

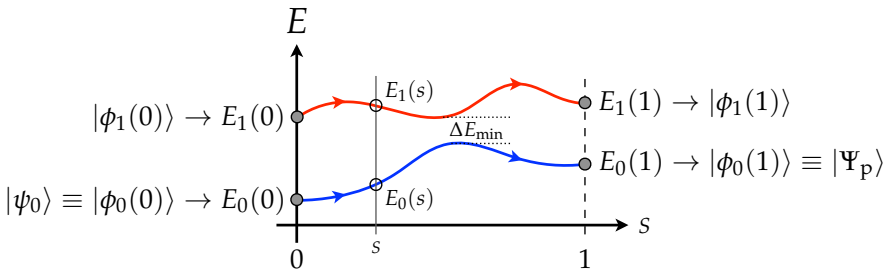

Figure 12.1: In this plot we summarize the working principle of quantum computation assisted by the adiabatic evolution. In particular we plot two energy levels $E_0(s)$ and $E_1(s)$ as functions of $s = t/T$ assuming that they satisfy the adiabatic theorem: if the time T is large enough, the systems remains in its ground state during the whole evolution. See the text for details.

namely, during the evolution the state $|\psi(t)\rangle$ of the system remains very close to the instantaneous ground state of the Hamiltonian $\hat{H}(t)$, $\forall t \in [0, T]$, if T is large enough. More in details, the adiabatic theorem states that if

$$T \gg \frac{\Gamma_{\max}}{(\Delta E_{\min})^2} \tag{12.16}$$

where

$$\Gamma_{\max} = \max_{s\in[0,1]} \left| \left\langle \phi_1(s) \left| \frac{d\tilde{H}(s)}{ds} \right| \phi_0(s) \right\rangle \right| , \tag{12.17}$$

and

$$\Delta E_{\min} = \min_{s\in[0,1]} \left[E_1(s) - E_0(s) \right] , \tag{12.18}$$

then $|\langle \phi_0(1)|\psi(T)\rangle| \to 1$.

We are ready to apply the adiabatic theorem to the satisfiability problems.

12.3 Finding the solutions through the adiabatic evolution

The simplest interpolating, time-dependent Hamiltonian $\hat{H}(t)$ such that $\hat{H}(0) = \hat{H}_0$ and $\hat{H}(T) = \hat{H}_p$, the problem Hamiltonian, is:

$$\hat{H}(t) = \left(1 - \frac{t}{T}\right) \hat{H}_0 + \frac{t}{T} \hat{H}_p , \qquad t \in [0, T] , \tag{12.19}$$

or, equivalently,

$$\tilde{H}(s) = (1 - s) \hat{H}_0 + s \hat{H}_p , \qquad s \in [0, 1] . \tag{12.20}$$

More in general, one can also use more sophisticated Hamiltonians substituting to the parameter s some other functions of the ratio t/T. It is clear that if we suitably choose T in order to satisfy the conditions of the adiabatic theorem, then we can let our system evolve from the initial ground state $|\psi_0\rangle \equiv |\phi_0(0)\rangle$ of the beginning Hamiltonian $\hat{H}_0$ and reach the ground state

$|\Psi_{\rm p}\rangle \equiv |\phi_0(1)\rangle$ of the problem Hamiltonian $\hat{H}_{\rm p}$, as sketched in figure 12.1. If, however, the evolution is "too fast", then it is possible to obtain a final state at time $t = T$, *i.e.* $s = 1$, that is a linear combination of others energy eigenstates, thus finding, with a given probability, a wrong solution to the problem ...

As a matter of fact, the beginning Hamiltonian should not be diagonal in the same basis of the problem one, otherwise the systems will always remain in the initial eigenstate, that, in general, is not the instantaneous ground state of the interpolating Hamiltonian, as we will see in the next section. Since, as we have mentioned in section 12.1, at least in our cases the problem Hamiltonian in the presence of n qubits can be written as a function of the Pauli matrices $\hat{\sigma}_z^{(k)}$, $k = 1, \ldots, N$, a good choice for the starting Hamiltonian is

$$\hat{H}_0 = \sum_{k=1}^{N} \hat{H}_0^{(k)} \tag{12.21}$$

with

$$\hat{H}_0^{(k)} = \frac{1}{2}\left(\hat{\mathbb{I}} - \hat{\sigma}_x^{(k)}\right) . \tag{12.22}$$

It is worth noting that the corresponding ground state is (using the computational basis, namely, the eigenstates of $\hat{\sigma}_z^{(k)}$):

$$|\psi_0\rangle \equiv |\psi_0(s)\rangle = \frac{1}{2^{n/2}} \sum_{z=0}^{2^n-1} |z\rangle_n , \tag{12.23}$$

that is the balanced superposition of all the possible inputs. In the next section we will see a simple example based on a single qubit in order to see adiabatic computation at work. The interested reader can find more complex examples in the references proposed at the end of this chapter.

12.4 One-qubit example of adiabatic quantum computation

Though this example is almost useless, we can use it to check the requirements of the adiabatic theorem and to follow the the whole protocol analytically.

Here, we assume that our clause involves only one bit and it is simply:

$$C = z , \tag{12.24}$$

that is satisfied when $z = 1$ (of course!). The corresponding problem Hamiltonian reads (we still use dimensionless quantities):

$$\hat{H}_{\rm p} = \frac{1}{2}\left(\hat{\mathbb{I}} + \hat{\sigma}_z\right) , \tag{12.25}$$

and, as mentioned above, we use the following beginning Hamiltonian:

$$\hat{H}_0 = \frac{1}{2}\left(\hat{\mathbb{I}} - \hat{\sigma}_x\right) , \tag{12.26}$$

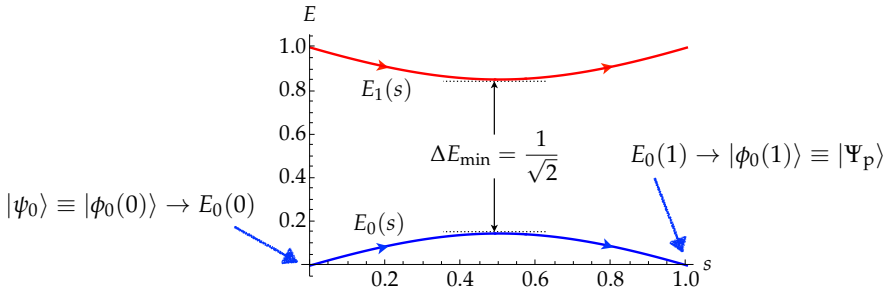

Figure 12.2: Plot of the two eigenvalues of the Hamiltonian (12.27) as functions of s. We have explicitly highlighted the instantaneous eigenstates corresponding to the lowest eigenvalues at $s = 0$ and $s = 1$.

whose ground states is $|\psi_0\rangle = 2^{-1/2}\left(|0\rangle + |1\rangle\right)$.

The time-dependent Hamiltonian follows from Eq. (12.20) and, in the matrix representation, reads:

$$\tilde{H}(s) = \frac{1}{2}\begin{pmatrix} 1+s & s-1 \\ s-1 & 1-s \end{pmatrix}, \tag{12.27}$$

whose two eigenvalues

$$E_0(s) = \frac{1}{2}\left(1 - \sqrt{2s^2 - 2s + 1}\right), \tag{12.28a}$$

$$E_1(s) = \frac{1}{2}\left(1 + \sqrt{2s^2 - 2s + 1}\right), \tag{12.28b}$$

are plotted in figure 12.2. We can see that the two levels are well-separated with $\Delta E_{\min} = 1/\sqrt{2}$, thus, the adiabatic theorem can be applied and, after the evolution, the final state corresponds to the ground state of $\hat{H}_p$.

Starting from Eq. (12.17) we also find $\Gamma_{\max} = 1/\sqrt{2}$ and, by using Eq. (12.16), we obtain $T \gg \sqrt{2}$ to achieve the adiabatic evolution. In order to assess the "success" of the computation, we introduce the *fidelity* between the final state $|\psi(T)\rangle$ and the instantaneous eigenstate $|\phi_0(s)\rangle$, namely

$$F(s) = |\langle\phi_0(s)|\psi(T)\rangle|^2. \tag{12.29}$$

In figure 12.3 we plot $F(s)$ as a function of $s = t/T$ for different values of T: we can see that, as T increases, the fidelity at $s = 1$ or, equivalently, at $t = T$, approaches 1, that is the state $|\psi(T)\rangle$ comes to coincide with the ground state of the Hamiltonian $\hat{H}(T) = \hat{H}_p$.

If we had chosen as starting Hamiltonian

$$\hat{H}_0' = \frac{1}{2}\left(\hat{\mathbb{I}} - \hat{\sigma}_z\right), \tag{12.30}$$

which clearly commutes with $\hat{H}_p$, then we would have

$$\tilde{H}'(s) = \begin{pmatrix} s & 0 \\ 0 & 1-s \end{pmatrix}, \tag{12.31}$$

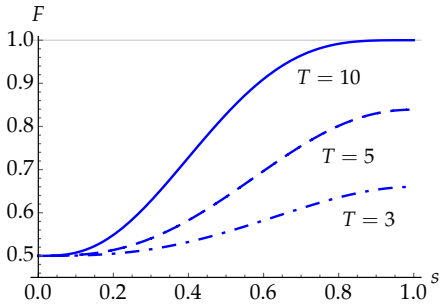

Figure 12.3: Plot of the fidelity $F(s)$, with $s = t/T$, between the instantaneous eigenstate $|\phi_0(s)\rangle$, corresponding to the lowest eigenvalue of the Hamiltonian (12.27), and the evolved state $|\psi(T)\rangle$. The curves refer to different values of T: in the present case, the adiabatic theorem requires $T \gg \sqrt{2} \approx 1.41$. See the text for details.

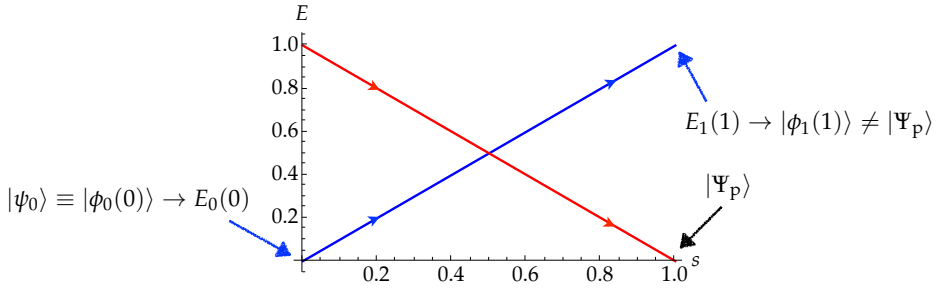

Figure 12.4: Plot of the two eigenvalues of the Hamiltonian (12.31) as functions of s. Note that the lowest eigenvalue at $s = 0$ in transformed during the evolution in to the highest eigenvalue at $s = 1$. Since $\Delta E_{\min} = 0$, the adiabatic theorem cannot be applied.

whose two eigenvalues becomes equal at $s = 1/2$ (see figure 12.4). In this case we can see that at the end of the evolution the system passed from the state ground state of $\hat{H}_0$ to the excited state of $\hat{H}_p$: remarkably, they formally coincide, since the initial state is an eigenvector of $\tilde{H}'(s)$ and, thus, it is left unchanged during the whole evolution, up to a global phase.

It is interesting to note that in order to remove the leveldegeneracy it is enough to add a perturbation to starting Hamiltonian, in such a way that the resulting one does no longer commute with H_p. In particular, if we consider

$$\hat{H}_0' = \frac{1}{2}\left(\hat{\mathbb{I}} - \hat{\sigma}_z\right) + \varepsilon\,\hat{\sigma}_x\,, \tag{12.32}$$

with $0 < \varepsilon \ll 1$, we have

$$\tilde{H}'(s) = \begin{pmatrix} s & \varepsilon(1-s) \\ \varepsilon(1-s) & 1-s \end{pmatrix}, \tag{12.33}$$

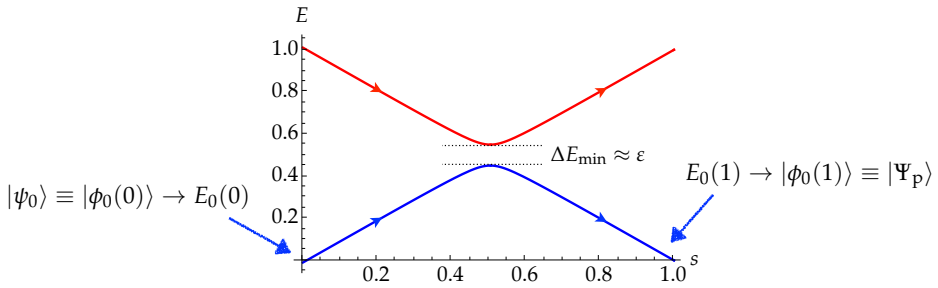

Figure 12.5: Plot of the two eigenvalues of the Hamiltonian (12.31) as functions of s. We have explicitly highlighted the instantaneous eigenstates corresponding to the lowest eigenvalues at $s = 0$ and $s = 1$.

and the two corresponding eigenvalues read

$$E_0(s) = \frac{1}{2}\left[1 - \sqrt{(2s-1)^2 + 4\varepsilon^2(1-s)^2}\right], \tag{12.34a}$$

$$E_1(s) = \frac{1}{2}\left[1 + \sqrt{(2s-1)^2 + 4\varepsilon^2(1-s)^2}\right], \tag{12.34b}$$

which are plotted in figure 12.5. Now, the degeneracy at $s = 1/2$ is broken and, by suitably choosing T, the adiabatic theorem can be applied. Note that, in this particular case we have

$$\Delta E_{\min} = \frac{\varepsilon}{\sqrt{1+\varepsilon^2}} \approx \varepsilon\,, \tag{12.35}$$

occurring at

$$s_{\min} = \frac{1+2\varepsilon^2}{2(1+\varepsilon^2)} \approx \frac{1}{2}\,. \tag{12.36}$$

12.5 Factorization with adiabatic evolution

In section 5.3 we discussed the Shor algorithm for factorization of integer numbers. That algorithm is based on the circuit model of quantum computation. However, it has been proved that the adiabatic model of quantum computation and the circuit model are equivalent. In the following we will describe a factoring algorithm based on the adiabatic evolution that has been also experimentally implemented using nuclear magnetic resonance (see the Bibliography at the end of the chapter for further details).

The problem we address is to find the *two integer prime factors* p and q of an integer number N encoded into $L = \lceil \log_2 N \rceil$ bits. It is worth noting that we are assuming from the beginning that there are *only two factors*. In order to solve our problem by adiabatic evolution, we should turn it into a problem of optimization, that will allow us to define the beginning and problem Hamiltonian.

First of all, we introduce the function

$$f(x,y) = (N - xy)^2\,, \tag{12.37}$$

and it is clear that $f(x,y) \geq 0$ and $f(x,y) \geq 0$ only if $xy = pq \equiv N$. The problem Hamiltonian can be introduced assuming that $f(x,y)$ are its eigenvalues, namely

$$\hat{H}_{\rm p} = \sum_{x,y} f(x,y)\, |x,y\rangle\langle x,y|\,, \tag{12.38}$$

where $|x,y\rangle = |x\rangle|y\rangle$, $|x\rangle = |x\rangle_X$ and $|y\rangle = |y\rangle_Y$ encoding the two factors x and y, respectively, where X and Y are the numbers of qubits used.

At this point we make two reasonable assumptions to simplify the problem:

(a) N is odd, otherwise one factor is the number 2. Therefore, we know that x and y should be odd and we save one bit, since if $|x\rangle = |x_{X-1}\rangle \cdots |x_0\rangle$ with binary expansion $x = \sum_{k=0}^{X-1} 2^k x_k$, we have $x_0 \equiv 1$.

(b) $x < y$, that is we can take $3 \leq x \leq \sqrt{N}$ and $\sqrt{N} \leq y \leq N/3$.

These assumptions allow us evaluating the effective number of qubits n_x and n_y needed to encode the factors, namely:

$$n_x \leq \left\lfloor \frac{L+1}{2} \right\rfloor \quad \text{and} \quad n_y \leq L-1\,. \tag{12.39}$$

We can conclude that the total number $n = n_x + n_y$ of qubits scales as $n \sim O(\frac{3}{2}L)$. Here we recall that, in the case of the Shor algorithm, the number of needed bits is $n = 2L + 1 + \lceil \log\left[2 + (2\varepsilon)^{-1}\right] \rceil$, ε being the failure probability (see section 5.3).

We now turn the attention to the problem Hamiltonian. Since the two factors are odd, we actually need $(n_x - 1) + (n_y - 1) = n - 2$ qubits (we exclude from the count the last qubit of each factor which is always 1). Following the method introduced in section 12.1, the Hamiltonian can be written as:

$$\begin{aligned}\hat{H}_{\rm p} = \Bigg[N\hat{\mathbb{I}} - \left(2^{n_x-1} \frac{\hat{\mathbb{I}} - \hat{\sigma}_z^{(1)}}{2} + \cdots 2^1 \frac{\hat{\mathbb{I}} - \hat{\sigma}_z^{(n_x-1)}}{2} + 2^0 \hat{\mathbb{I}} \right) \\ \otimes \left(2^{n_y-1} \frac{\hat{\mathbb{I}} - \hat{\sigma}_z^{(n_x)}}{2} + \cdots 2^1 \frac{\hat{\mathbb{I}} - \hat{\sigma}_z^{(n-2)}}{2} + 2^0 \hat{\mathbb{I}} \right) \Bigg]^2 \end{aligned} \tag{12.40}$$

which acts on the states:

$$|x\rangle_{n_x-1}|y\rangle_{n_y-1} = |x_{n_x-1}\rangle \cdots |x_1\rangle |y_{n_y-1}\rangle \cdots |y_1\rangle\,, \tag{12.41}$$

$$= \underbrace{|z_1\rangle \cdots |z_{n_x-1}\rangle}_{n_x-1} \underbrace{|z_{n_x}\rangle \cdots |z_{n-2}\rangle}_{n_y-1} \equiv |z\rangle_{n-2} \tag{12.42}$$

Note that $\sum_{k=1}^{n_x-1} 2^k x_k = 2\sum_{k=0}^{n_x-2} 2^k x_{k+1} = 2x$ and $\sum_{k=1}^{n_y-1} 2^k y_k = 2\sum_{k=0}^{n_y-2} 2^k y_{k+1} = 2y$, where x

and y are encoded into $n_x - 1$ and $n_y - 1$ bits, respectively. Therefore we have:

$$\hat{H}_{\mathrm{p}}|z\rangle_{n-2} = \left[N - \left(2^{n_x-1}z_1 + \cdots + 2^1 z_{n_x-1} + 1\right)\left(2^{n_y-1}z_{n_x} + \cdots + 2^1 z_{n-2} + 1\right)\right]^2 |z\rangle_{n-2}\,, \tag{12.43a}$$

$$= \left[N - (2x+1)(2y+1)\right]^2 |z\rangle_{n-2}\,. \tag{12.43b}$$

The lowest eigenvalue of H_{p} is 0 corresponding to the state $|p'\rangle_{n_x-1}|q'\rangle_{n_y-1}$, which encodes the two numbers $p = 2p' + 1$ and $q = 2q' + 1$, that is the solution of our problem.

As beginning Hamiltonian we can choose, for instance,

$$\hat{H}_0 = \gamma \sum_{k=1}^{n-2} \hat{\sigma}_x^{(k)} \tag{12.44}$$

with ground state

$$|\psi_0\rangle_{n-2} = \frac{1}{2^{(n-2)/2}} \sum_{z=1}^{2^{n-2}-1} (-1)^{\Pi(z)} |z\rangle_{n-2} \tag{12.45}$$

where $\Pi(z)$ is the parity of the number z, that is the number of 1s in the binary representation modulo 2. Interestingly, the Hamiltonian (12.44) describes a system, in which all the spins interact with the same magnetic field oriented along the x direction, γ being the coupling strength.

As a matter of fact, in order to eventually apply the adiabatic theorem, one should verify whether the conditions underlaying it are satisfied and this requires to choose a particular N and to study the corresponding problem Hamiltonian. The adiabatic protocol has been experimentally applied to the factorization of $N = 21$ by using nuclear magnetic resonance and the interested reader can find further details about the experiment in the Bibliography at the end of this chapter.

Bibliography

- E. Messiah, *Quantum Mechanics*, Volume II (Holland Publishing Company, 1965) – Chapter XVII, §13.
- E. Farhi, J. Goldstone, S. Gutmann and M. Sipser, *Quantum Computation by Adiabatic Evolution*, MIT-CTP-2936, e-print arXiv:quant-ph/0001106.
- X. Peng *et al.*, *A Quantum Adiabatic Algorithm for Factorization and Its Experimental Implementation*, Phys. Rev. Lett. **101**, 220405 (2008).